AD 273 818

RADC-TDR-62-41
ASTIA Document No. AD _____
Code 25500

9 January 1962
Copy No. 42

FINAL REPORT:

ELECTRONIC CORRELATION TECHNIQUES FOR TARGET RECOGNITION

Goodyear Aircraft Corporation

Akron 15, Ohio

GER-10449

CONTRACT NO. AF30(602)-2459

PROJECT NO. 6244

TASK NO. 624408

PREPARED FOR

Rome Air Development Center
Air Research and Development Command
United States Air Force
Griffiss Air Force Base
New York

RADC-TDR-62-41
ASTIA Document No. AD _____
Code 25500

9 January 1962
Copy No. 42

FINAL REPORT:

ELECTRONIC CORRELATION TECHNIQUES

FOR TARGET RECOGNITION

GOODYEAR AIRCRAFT CORPORATION

AKRON 15, OHIO

GER-10449

CONTRACT NO. AF30(602)-2459
PROJECT NO. 6244
TASK NO. 624408

PREPARED FOR

ROME AIR DEVELOPMENT CENTER
AIR RESEARCH AND DEVELOPMENT COMMAND
UNITED STATES AIR FORCE
GRIFFISS AIR FORCE BASE
NEW YORK

ABSTRACT

Under Contract AF30(602)-2459, Goodyear Aircraft Corporation (GAC) conducted a study that approached the target recognition problem analytically, experimentally, and through photographic examination of target attributes.

Aerial photographs of runways, petroleum refineries, and industrial complexes provided attribute data on which part of the analytical and experimental studies were based. The detection of petroleum refineries in the spatial frequency domain and of industrial complexes in the time domain were investigated analytically.

Correlation surfaces of targets and a slit template were studied experimentally. Further development of this effort demonstrated that the second derivative of the correlation function is a reliable attribute for the detection of such straight-line patterns as runways, roads, and ships. A width-gating device was constructed and the extraction of straight-line patterns from their backgrounds on the basis of the width attribute was demonstrated.

Three suggested systems for the detection of straight-line patterns and the recognition of runways are described, and a system for the detection of irregular pattern areas is defined. GAC recommends that several of these systems be assembled and their screening ability evaluated. Methods of automatic threshold compensation for variations in photographic parameters should be examined, and attributes and attribute-measuring techniques should be studied for other target patterns not considered in this report.

AIR FORCE FOREWORD

This study was initiated by the Reconnaissance Charting and Interpretation Branch of the Information Processing Laboratory as a part of the Air Force program to develop an interpretation capability compatible with future reconnaissance systems. Specifically, the purpose of this study was to investigate the value of electronic correlation techniques for the automatic and semi-automatic detection and recognition of targets on aerial reconnaissance photography.

This study has investigated both analytically and experimentally several possible techniques. These include the spatial and time domain analysis of the original imagery, the analysis of correlation surfaces generated by optical correlation between imagery and templets, and the analysis of target signatures generated by the measurement of various attributes of the imagery.

Extensive analyses of these techniques were performed and some of the analytical conclusions were validated empirically. Current and programmed work will validate further the analytical portion of the work.

On the basis of the extensive analytical and empirical analyses, the report presents several suggested target recognition systems. Three of the systems are straight-line pattern analyzers while the fourth is a pattern and detector that would be designed to detect pattern with specific dimensions and length-to-width ratios. It is possible to make use of the techniques developed during the study through the breadboarding of these suggested configurations.

The study has generated ideas and techniques that may be of immediate interest to help solve some existing problems, such as detection of clouds, water, and rural areas or the detection of indicators of human activity. However, the work also has a more long range application. As "perceptive" and "cognitive" devices are applied towards some of the photo interpretation tasks, techniques such as those developed by Goodyear Aircraft Corporation will be required to reduce the complex aerial photograph to a simpler and more usable form.

This document presents the results of a scientific investigation. It is hoped that it will stimulate interest in the problem and will serve as an indication of our interest. Comments on this work, scientific or philosophical, are invited and should be addressed to the contract scientist.

LYNWOOD D. SINNAMON, Jr.
Physical Scientist
ATTN: RAWICC
Rome Air Development Center
Griffiss Air Force Base, New York
March 1962

PREFACE

This report was prepared by Goodyear Aircraft Corporation, Akron, Ohio, under Air Force Contract AF30(602)-2459. It describes studies begun in March 1961 and concluded in December 1961.

The study personnel were members the Advanced Avionics Systems Engineering Department of Goodyear Aircraft Corporation. The chief contributors and their fields of participation were: R. S. Bachtell, project engineer; M. Hansburg and J. N. Burns, correlation techniques; C. Leontis and T. V. Link, experimental evaluation; R. H. Smith, system design; and J. F. Simpson, target attribute studies.

TABLE OF CONTENTS

LIST OF ILLUSTRATIONS

LIST OF TABLES

LIST OF APPENDIXES

SECTION I - INTRODUCTION

1. GENERAL

Goodyear Aircraft Corporation (GAC), under Contract AF30(602)-2459,[1,a] conducted a program to make possible the recognition of target patterns in aerial photographs by electronic correlation techniques. The results of that program are reported herein.

2. STATEMENT OF PROBLEM

a. General

The problem of pattern recognition has two major parts.

First, target patterns must be classified a priori according to some measurable characteristics or attributes. Three different levels of pattern classification by attributes are detection, recognition, and identification. Patterns that are detected can be subdivided into patterns that are recognized and, further, patterns that are identified. For example, straight-line patterns can be detected, runways recognized, and specific airports identified. (Since "recognition" cannot be precisely defined, it will be used herein as the subclass of those patterns that are detected.)

Second, the desired target patterns must be automatically detected, and the pattern attributes must be automatically measured and compared with the values of the a priori selected attributes.

b. Target Classification

The target classification most amenable to automatic recognition is attributes, or characteristics, of the target. The attributes can be

[a]Superior numbers in the text refer to items in the List of References, p. 207.

geometrical, such as linear dimensions or shape, and can be related to the reflectivity of the target, such as the texture of a runway or the shadows at the edges of a building, or they can result from some linear or nonlinear filtering operation on the photograph. For example, various characteristics of the correlation function or of spectral energy in the spatial frequency domain may represent usable attributes.

Many targets are classified both by target attributes and by inference from nearby objects. Much recognition by photographic interpreters is of this type. For example, a pattern can be classified as a building by its shape and background contrast and can be further classified by inference as an industrial plant by the presence of a large parking lot filled with automobiles. However, this program did not deal with inference as an aid to classification.

The usual classification of targets is verbal, which may have no relation to attributes but be based on function only. In some cases, all the individual targets that comprise a verbal class may have similar attributes, but this is not generally true. A verbal class such as "missile launch sites" can possibly be subdivided into verbal categories that have similar attributes, such as surface-to-surface or surface-to-air. However, if they do not have similar attributes, they must then be subdivided into still finer categories, so that instead of one recognition problem, many emerge.

In other cases, individual targets of a verbal class may have similar attributes but other verbal classes may have the same attributes and hence no distribution between the classes is possible. For example, the verbal class "steel fabrication plant" has no special attributes (at least for automatic recognition) that could distinguish it from many other industrial classes.

Third, the first part of the recognition problem is the a priori selection of measurable attributes that will classify the target pattern. The study of runways, petroleum refineries, and industrial complexes

described in Section II had as its objective the a priori selection of geometrical attributes.

One objective at the analytical study of correlation techniques described in Section III was the examination and selection of nongeometrical attributes; i.e., attributes of the correlation function or of spectral energy.

c. Automatic Detection and Classification of Target Patterns

The second part of the recognition problem is complicated by several factors.

First, the target location is not known a priori, which, although obvious, is a major part of the classification or recognition problem since a target must somehow be detected or located before it can be classified. (In some cases detection and classification occur simultaneously.)

Second, the target orientation and possible scale are not known a priori. This means that either the detection and classification technique must be independent of these factors or the photograph must be examined over a wide range of orientation and scales.

Third, the target is surrounded by a background that may confuse or interfere with the detection and classification phase. The contrast between target and background may be so low that only the most careful examination will reveal its presence. The background also may contain nearby patterns that could be counted as part of the target and hence could confuse the classification.

The measurement of attributes may be either in sequence or in parallel. There are justifications for both methods. Comparisons of measured attributes with the a priori attributes would probably be statistical. An example of runway recognition using statistical decision theory is given in Section II.

The second part of the recognition problem is then to develop correlation techniques that will:

1. Detect the pattern regardless of scale, orientation, and position.
2. Measure the pattern attributes and ignore undesirable background attributes.
3. Determine whether or not the combination of measured attributes is similar enough to the combination of a priori attributes.

Section IV describes the laboratory study of correlation techniques for the automatic detection and measurement of pattern attributes.

SECTION II - PHOTOGRAPHIC EXAMINATION OF PATTERN ATTRIBUTES

1. GENERAL

Attribute studies were made for runways and industrial complexes. Two classes of industrial complexes were considered: those that contain circular patterns and those that contain rectangular and polyrectangular patterns.

At the beginning of the study period, considerable work had already been completed for runways. Those studies showed that successful recognition of runways could possibly be based on the identification of rectangular patterns in terms of two parameters, width and length. The feasibility of this concept was further determined through a statistical examination of runways and typical nontargets of the northeastern United States.

A preliminary attribute study of industrial complexes was made to determine the usefulness of individual circular or noncircular patterns in recognizing a given complex. Separate studies made for the circular and noncircular patterns provided statistical descriptions of the dimensions, spacings, and edge gradients for each pattern class. Additional useful industrial attributes were found, such as the parallelism and straightness of a high-frequency activity.

2. STATISTICAL EXPERIMENT IN RUNWAY RECOGNITION

a. General

The purpose of the statistical experiment in runway recognition was to demonstrate the feasibility of identifying airfield runways in a heterogeneous background typical of the northeastern U.S.

The differentiation of runways (the "targets" in the statistical experiment) from nonrunway ("nontarget") patterns was based on identifying

rectangular patterns and evaluating the two parameters, width and length.

The statistical analysis indicated the probabilities of correct and incorrect identification of targets and nontargets and provided evidence of the reliability of runway identification.

b. Target and Nontarget Data

Targets sought in the statistical experiment were the type of runways found at military airfields or at civilian airfields with military facilities. Every fourth airfield listed in Reference 2 was tabulated. A total of 22 airfields with 61 total runways was included. The runway widths (a) and lengths (b) together with their respective conditional probability distributions P(a|t) and P(b|t) are given in Table I.

TABLE I - DISTRIBUTION AND PROBABILITY OF TARGET AND NONTARGET ATTRIBUTES

Attribute	Targets		Nontargets		Probability ratio
Width, a (ft)	Number	P(a|t)	Number	P(a|nt)	P(a|t)/P(a|nt)
75-124	5	0.082	42	0.140	0.579
125-174	45	0.735	48	0.160	4.590
175-224	7	0.114	50	0.167	0.683
225-274	0	0	49	0.163	0
275-324	4	0.065	46	0.153	0.378
325-374	0	0	38	0.126	0
375-425	0	0	27	0.090	0
Length, b (ft)	Number	P(b|t)	Number	P(b|nt)	P(b|t)/P(b|nt)
0-499	0	0	48	0.160	0
500-999	0	0	85	0.283	0
1,000-1,499	0	0	108	0.360	0
1,500-1,999	0	0	34	0.113	0
2,000-2,499	0	0	13	0.043	0

TABLE I - DISTRIBUTION AND PROBABILITY OF TARGET AND NONTARGET ATTRIBUTES (Continued)

Attribute	Targets		Nontargets		Probability ratio
Length, b (ft)	Number	P(b|t)	Number	P(b|nt)	P(b|t)/P(b|nt)
2,500-2,999	0	0	10	0.033	0
3,000-3,499	0	0	0	0	0
3,500-3,999	6	0.098	0	0	∞
4,000-4,499	5	0.082	0	0	∞
4,500-4,999	5	0.082	0	0	∞
5,000-5,499	13	0.213	0	0	∞
5,500-5,999	4	0.065	0	0	∞
6,000-6,499	4	0.065	0	0	∞
6,500-6,999	4	0.065	0	0	∞
7,000-7,499	9	0.148	0	0	∞
7,500-7,999	0	0	0	0	0
8,000-8,499	4	0.065	2	0.006	10.41
8,500-8,999	0	0	0	0	0
9,000-9,499	2	0.033	0	0	∞
9,500-9,999	1	0.016	0	0	∞
10,000-10,499	0	0	0	0	0
10,500-10,999	0	0	0	0	0
11,000-11,499	1	0.016	0	0	∞
11,500-11,999	1	0.016	0	0	∞
12,000-12,499	2	0.033	0	0	∞

Nontargets were selected in an area of 138 sq naut mi in Lucas County in north central Ohio. This area was chosen because it encompasses farm land, urban and industrial areas, a coastline and port, a navigable river, railroads and railroad yards, and turnpike-type highways. In addition, the topography is essentially flat and therefore suitable for runways or other long, man-made features. The area

has been surveyed on a basis of one-square-mile sections. Therefore, the property boundaries and roads have a high degree of linearity and 90-deg conjunctions, which provides a greater opportunity for confusion of targets and nontargets than in areas of nonrectangular surveys. Thus, the sample area chosen is believed to represent the most difficult assemblage of patterns that could be anticipated in the northeastern U.S. A total of 300 nontargets was measured; their lengths, widths, and probability distributions are also given in Table I.

c. Statistical Evaluation of Attribute Data

A statistical analysis was made of the probability of correct discrimination between targets and nontargets together with proper identification of targets. The factors of probability dealt with are defined as:

$P(nt|t)$ = conditional probability of a nontarget decision when a target is present (incorrect decision)

$P(t|nt)$ = conditional probability of a target decision when a nontarget is present (incorrect decision)

$P(t|t)$ = conditional probability of a target detection when a target is present (correct decision)

$P(nt|nt)$ = conditional probability of a nontarget detection when a nontarget is present (correct decision)

$P(a|t)$ = conditional probability of width a when the pattern is a target

$P(a|nt)$ = conditional probability of width a when the pattern is a nontarget

The correct decision probabilities were computed by first calculating the incorrect decision probabilities and then using the following relationships:

$$P(nt|nt) + P(t|nt) = 1$$

$$P(t|t) + P(nt|t) = 1$$

The conditional probability $P(nt|t)$ of a nontarget decision when a

target exists, for a single attribute (in this case width, a), is expressed by

$$P(nt|t) = \sum_{A_{nt}} P(a|t) , \tag{1}$$

where A_{nt} is a set of values of the width a that satisfies the condition of a nontarget decision, and

$$L \frac{P(a|t)}{P(a|nt)} < 1 , \tag{2}$$

where L is a loss-ratio constant assumed in this case to be unity.

The conditional probability $P(t|nt)$ of a target decision if a nontarget is present, for the same single parameter, can be calculated from

$$P(t|nt) = \sum_{A_t} P(a|nt) , \tag{3}$$

where A_t is a set of values of width a that satisfies the condition of a target decision, and

$$L \frac{P(a|t)}{P(a|nt)} > 1 . \tag{4}$$

$P(a|t)$ and $P(a|nt)$ are given in Table I with the ratio $P(a|t)/P(a|nt)$. Thus,

$$P(nt|t) = 0.254,$$

$$P(t|nt) = 0.160,$$

$$P(t|t) = 1 - 0.254$$

$$= 0.746,$$

and

$$P(nt|nt) = 1 - 0.160$$

$$= 0.84.$$

Similar calculations were made for the other parameter, length b. The results are given in Table II.

TABLE II - DECISION PROBABILITIES FOR LENGTH AND WIDTH PARAMETERS

	Incorrect decision probabilities		Correct decision probabilities	
Parameter	P(nt|t)	P(t|nt)	(Pt|t)	P(nt|nt)
Width, a	0.254	0.160	0.746	0.84
Length, b	0	0.006	1.00	0.994

d. Results

The large values (see Table II) obtained in the statistical experiment for the correct decision probabilities, P(t|t) and P(nt|nt), and the small values obtained for the incorrect decision probabilities, P(nt|t) and P(t|nt), indicate that the parameters of width and particularly of length are valid criteria for the recognition and discrimination of airfield runways in the northeastern U.S. Therefore, there is a high probability of success for a runway recognition process that utilizes (1) pattern widths to separate the targets from their background and (2) pattern lengths to render the final target decisions.

3. CHARACTERISTICS OF INDUSTRIAL COMPLEXES

a. General

Aerial photographs were examined to determine proper attribute descriptions for industrial complexes of Toledo, Ohio, and Dallas, Texas. In Toledo 25 complexes were studied; in Dallas, 19. The frequency distribution of the areal sizes of these complexes is given graphically in Figure 1.

Two distinct pattern classes exist within the Toledo and Dallas

Figure 1 - Distribution of Sizes of Industrial Complexes

complexes: circles (usually oil tanks) and the more common rectangular or polyrectangular pattern. (See Figure 2.) The polyrectangular patterns are discussed in item 4, below, while the Toledo-Dallas and other circular patterns are considered in item 5.

b. Pattern Contrast

For the attributes of a given pattern to be determined in an automatic recognition device, there must be sufficient contrast between the pattern and its background. For this study, the contrast has been measured in terms of the number of equivalent density steps in a standard density wedge, in which the ratio of transmissivities between sucessive steps is two. The distribution of these density-step contrast values for the examined patterns is given in Figure 3.

Although most of these patterns exhibit contrast values greater than one density step and therefore are readily analyzed with proper readout equipment, some patterns do have contrast values of less than one step.

c. Miscellaneous Industrial Complex Attributes

For industrial complexes the following general characteristics are important sources of recognition information.

The parallelism of the patterns, i.e., the tendency of the major axes of the patterns within a given complex to be either parallel to each other or perpendicular, is a useful characteristic. Of the 44 complexes studied, only 32 percent had any acute angles in the arrangement of the included patterns, and these deviations were generally for only a small portion of the patterns within the complex.

The extent of the background adjoining the complex (i.e., the relative isolation of the complex) is important in recognition systems that examine the complex as an entity. Complexes were subjectively judged to be either "isolated" or "contiguous" in relation to adjacent buildings. These decisions were made as follows:

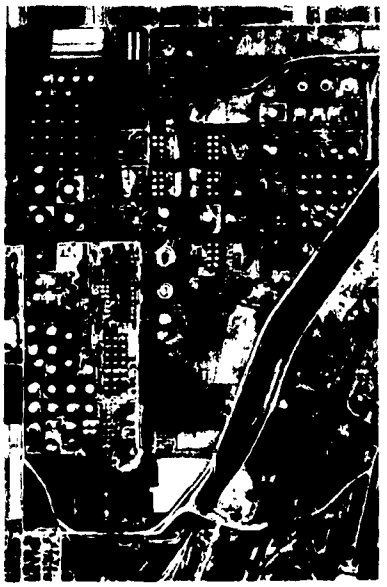

CIRCULAR PATTERN

POLYRECTANGULAR PATTERN

POLYRECTANGULAR PATTERN

POLYRECTANGULAR PATTERN

Figure 2 - Representative Circular and Polyrectangular Industrial Patterns

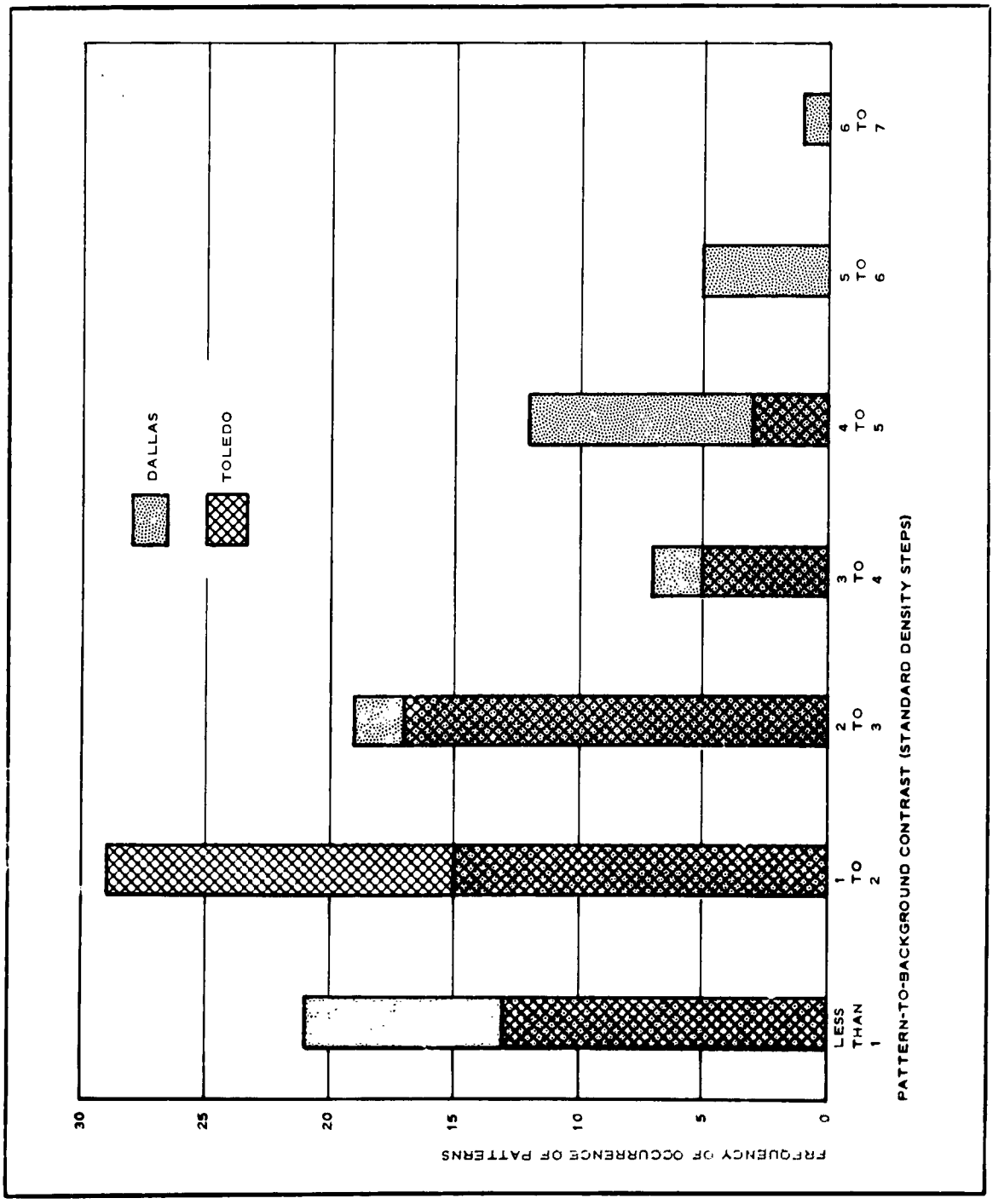

Figure 3 - Distribution of Pattern Contrasts

	Dallas	Toledo
Isolated	7	10
Intermediate	7	2
Contiguous	5	13

Another important recognition characteristic of an industrial complex is the accompanying high-frequency activity. For example, parked cars, the spaces between factory buildings, skylights, interconnecting roads, and paths provide a high-frequency activity, most of which is in the form of parallel, straight lines of restricted lengths that can be readily detected with a line correlator. (See Section V.) Examples of such high-frequency activity are given in Figure 2.

4. ATTRIBUTE DESCRIPTION OF POLYRECTANGULAR PATTERNS

The polyrectangular patterns were subdivided into rectangles for more convenient handling, and the widths and lengths of the individual rectangles were measured. The distributions of these lengths and widths are given in Figures 4 and 5, respectively.

The dimensions of a pattern do not by themselves determine the pattern; analytical time-domain and frequency-domain pattern identification studies (see Section III) showed that the pattern spacing or the extent of a pattern's adjoining background is equally important. The distribution of the spacing of these patterns is given in Figure 6.

5. ATTRIBUTE CLASSIFICATION OF PETROLEUM REFINERIES (CIRCULAR PATTERNS)

a. Statement of Problem

(1) General

Recognition of a class of patterns by attribute measurement requires a unique combination of attributes. A series of photographs of petroleum refineries and similar complexes was interpreted

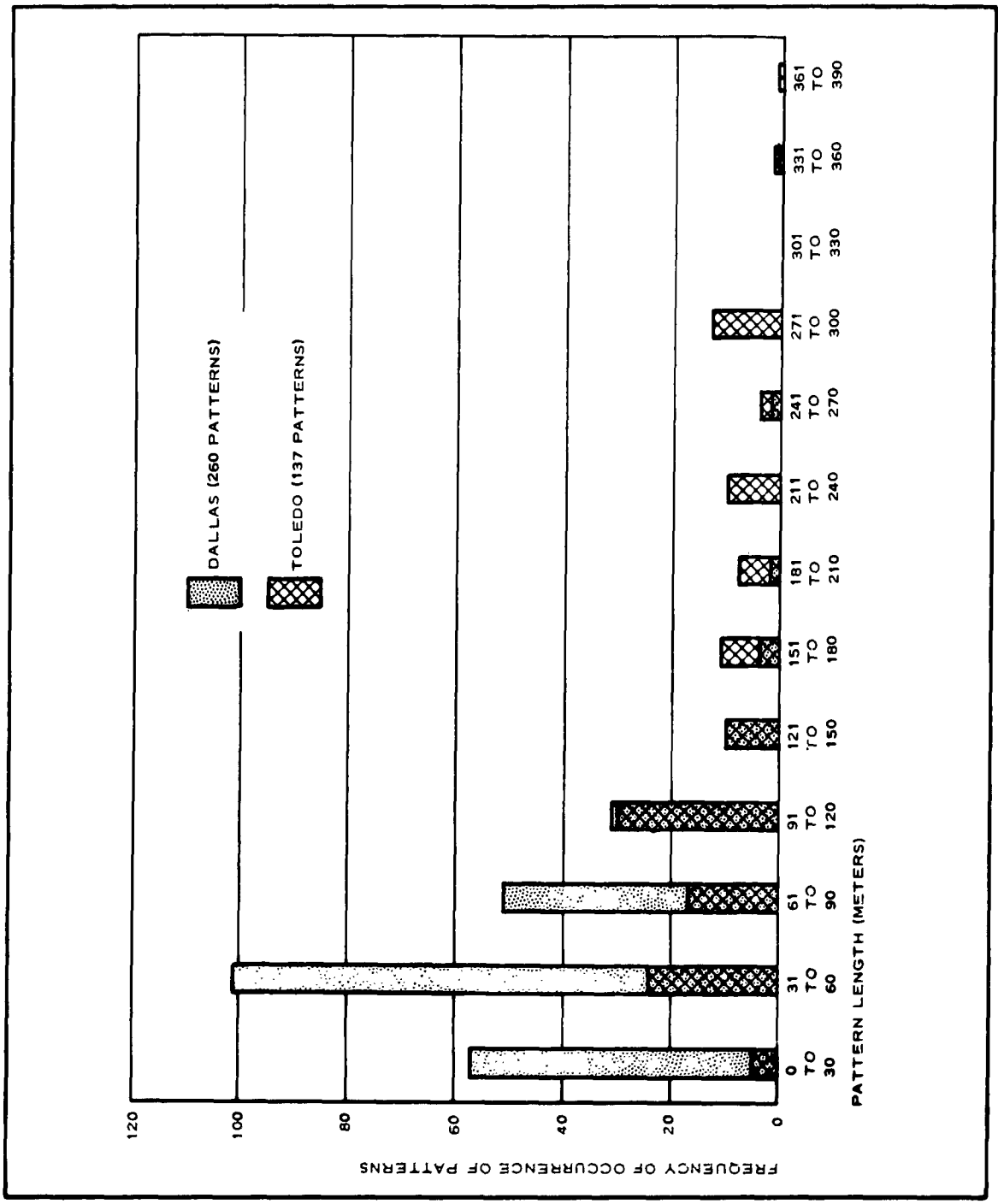

Figure 4 - Distribution of Lengths of Industrial Rectangular Subpatterns

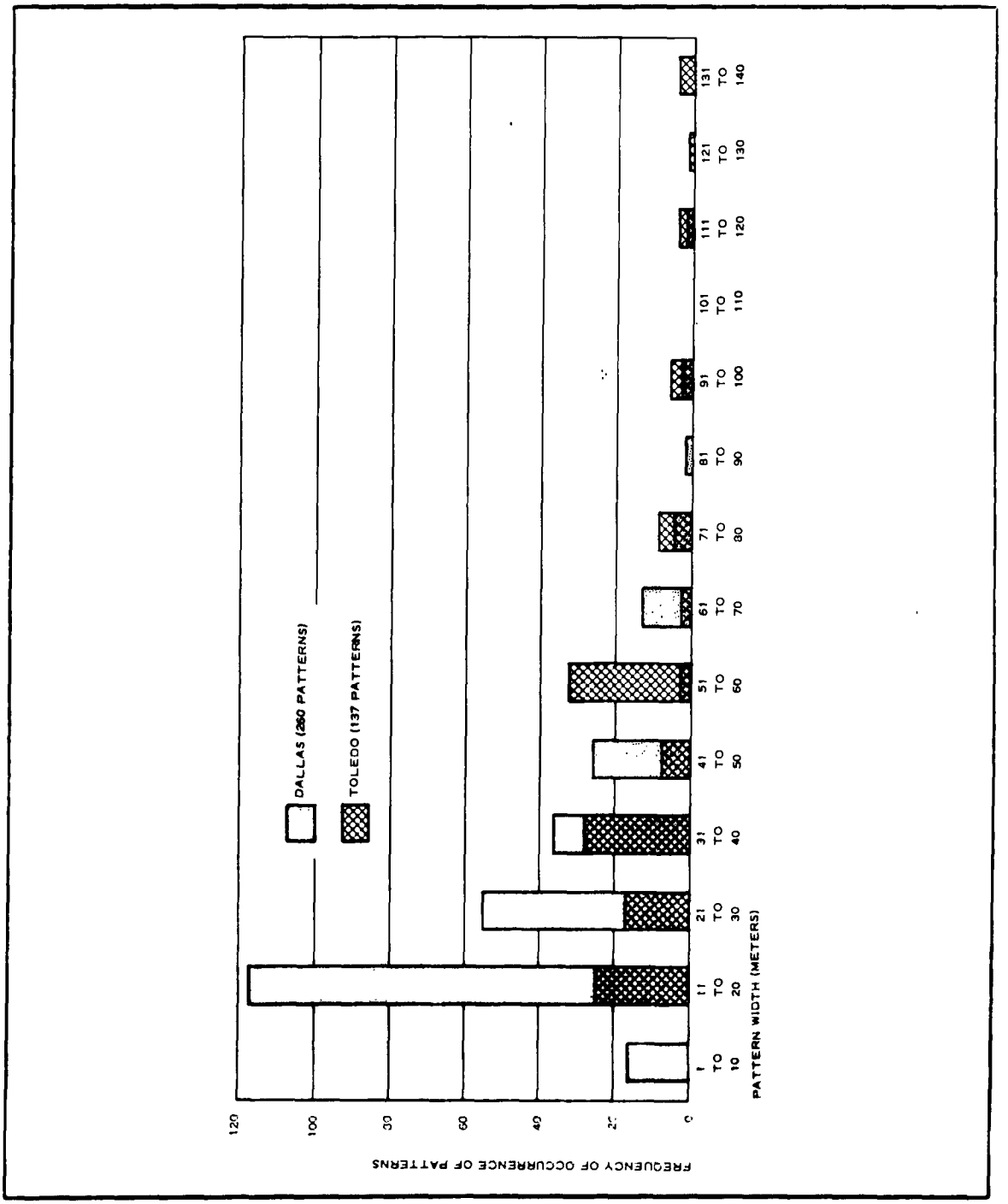

Figure 5 - Distribution of Widths of Industrial Rectangular Subpatterns

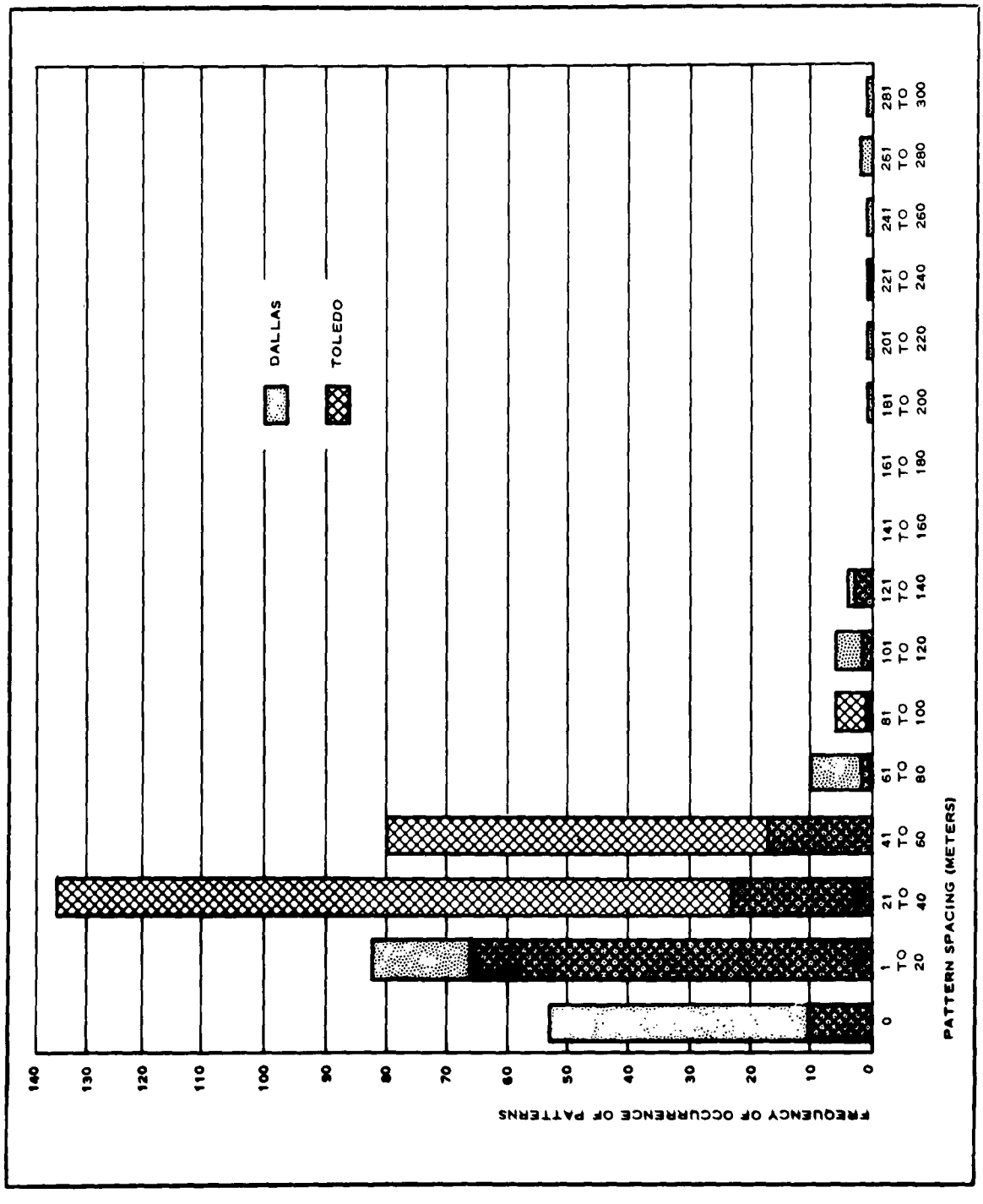

Figure 6 - Distribution of Spacings for Industrial Subpatterns

to collect data describing the geometry of the storage tanks and to determine whether or not a unique set of attributes exists.

(2) Experimental Approach

Various target complexes containing circular patterns were examined and subdivided into groups of equal-size circular patterns. Each group was measured to determine (1) the number of tanks, (2) tank diameters, (3) the number of rows, (4) the number of columns, (5) spacing along the rows, (6) spacing along the columns, (7) the polarity of tanks versus backgrounds, and (8) the density increment between tanks and backgrounds. The critical factors were then analyzed and presented in graph form.

(3) Sample Areas and Samples

Eleven refineries were studied. Three were in Toledo; one near Cincinnati, Ohio; two near Dallas; four near New Orleans, La.; and one near Shreveport, La. These refineries contained a total of 951 tanks.

Six nonrefineary complexes were studied. Four were in the Dallas area and two were in the New Orleans area. These nonrefinery complexes contained a total of 174 circular patterns.

b. Results of Refinery Analysis

The frequency distribution of the 951 tank diameters in the refinery complexes is shown graphically in Figure 7, which indicates a high frequency for tanks between 5 and 20 m and between 36 and 40 m in diameter.

Figure 8 shows the frequency distribution for the number of tanks contained in each of 118 groups of equal-diameter tanks. The number of groups at each of the 11 refineries studied was as follows, with a standard deviation of 6.16:

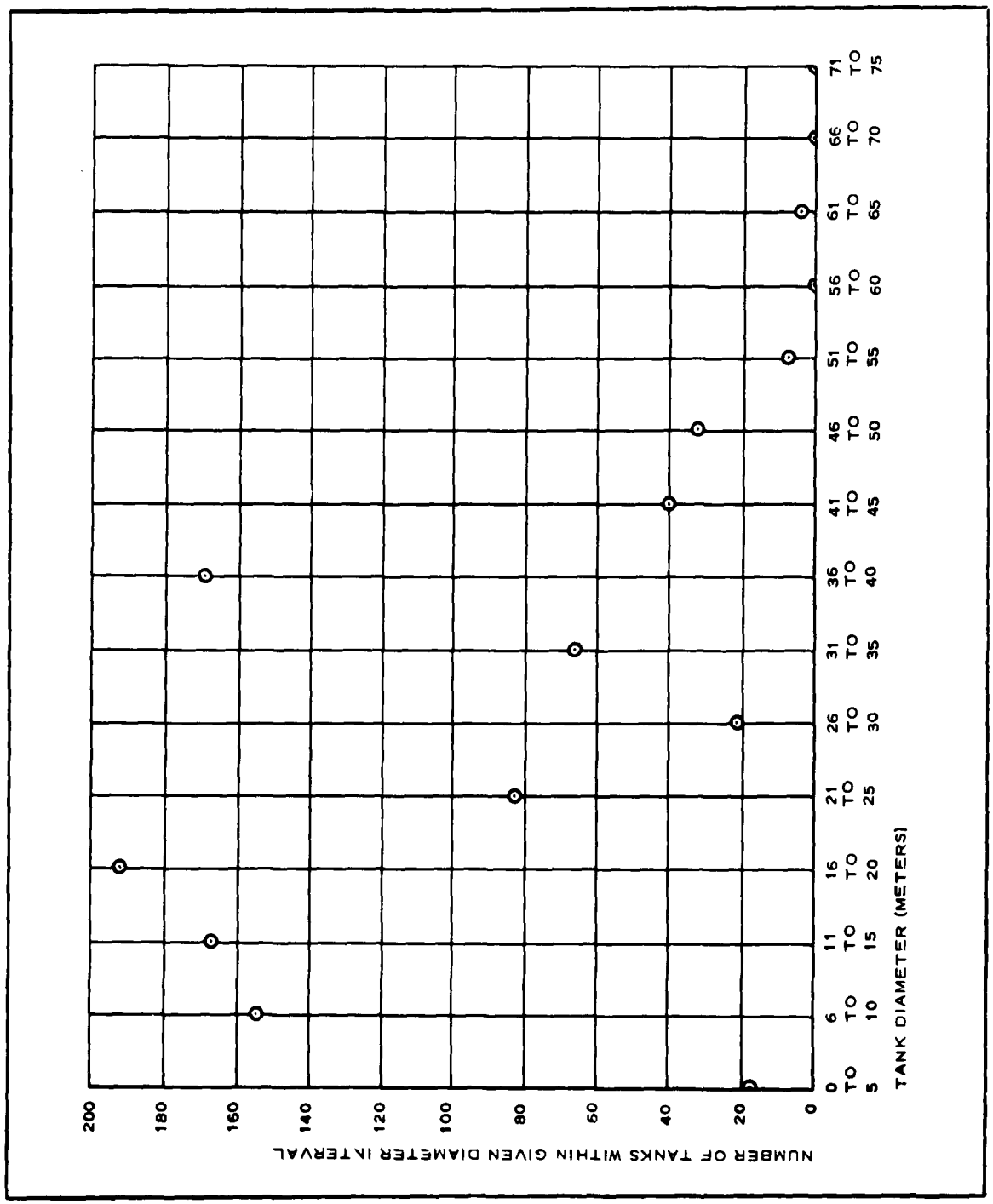

Figure 7 - Frequency Distributon of Tank Diameters

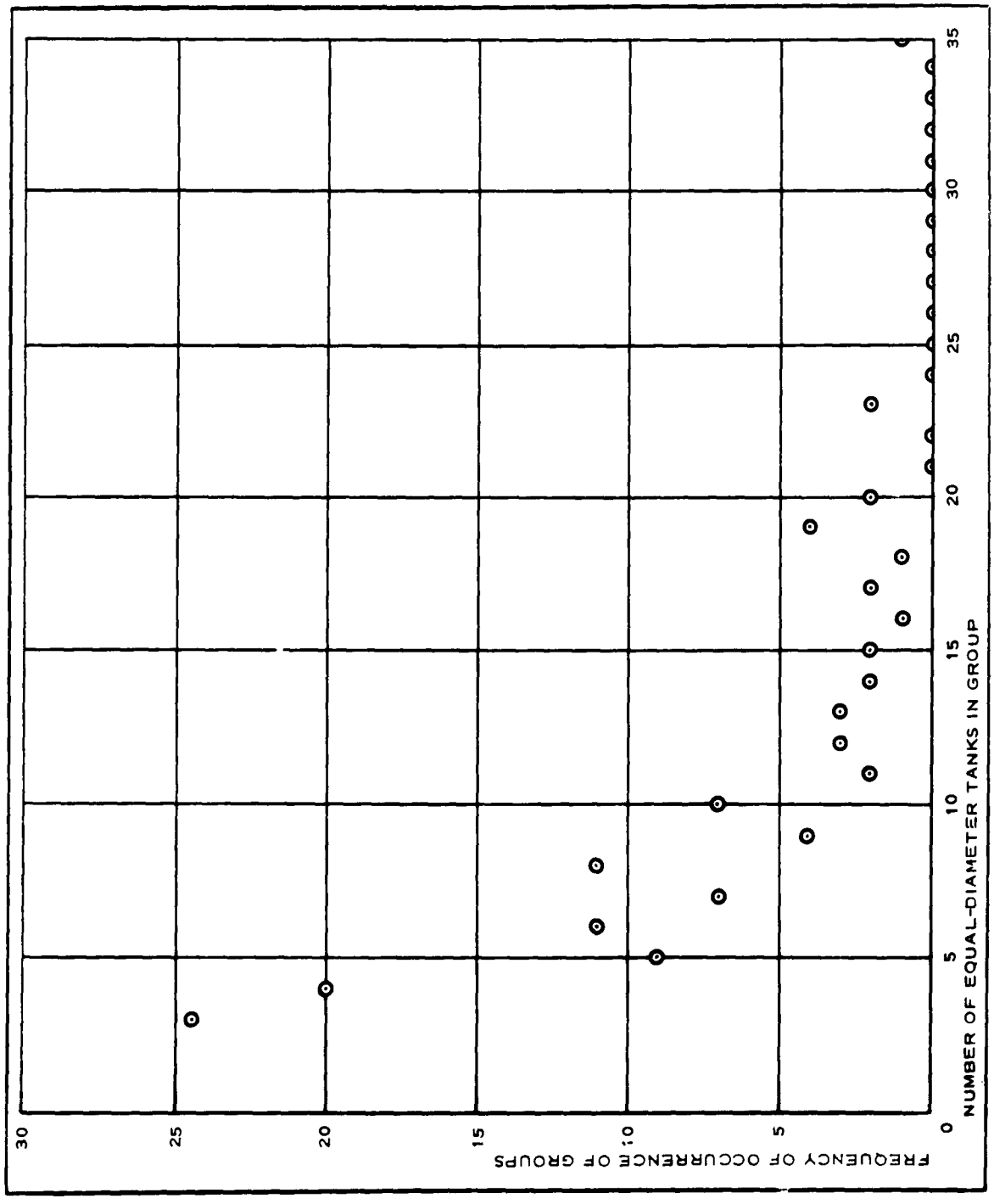

Figure 8 - Number of Tanks in Group of Equal-Diameter Tanks

Refinery	Number of groups
I	14
II	13
III	25
IV	11
V	5
VI	10
VII	6
VIII	3
IX	5
X	11
XI	18
Average	11

Table III indicates the occurrence of groups of tanks of equal diameters for the 11 refineries. An "X" indicates that at least one group of tanks of a given diameter was present at a given refinery.

Figure 9 shows the frequency of occurrence of various groups of tanks of a given equal diameter. The average group had a diameter of 21 to 25 m and the standard deviation was 13.4 m.

Figure 10 shows the average spacing of rows and columns between refinery tanks. The ratio of spacing to tank diameter was approximately 1.5 to 1, which corresponds to a tank duty cycle of 0.4 for most of the tanks. The triangles that bracket the average points in Figure 10 indicate the limits of ±1 standard deviation.

The polarity of refinery tanks against backgrounds was predominantly (94.3 percent) light on dark. The degree of this contrast was determined in terms of an arbitrary density wedge that contained six steps from 0 (white) to 6 (black). The frequency of tank occurrence for a given contrast per number of steps is shown in Figure 11. Reliable readout can be obtained for contrasts of one or more density steps.

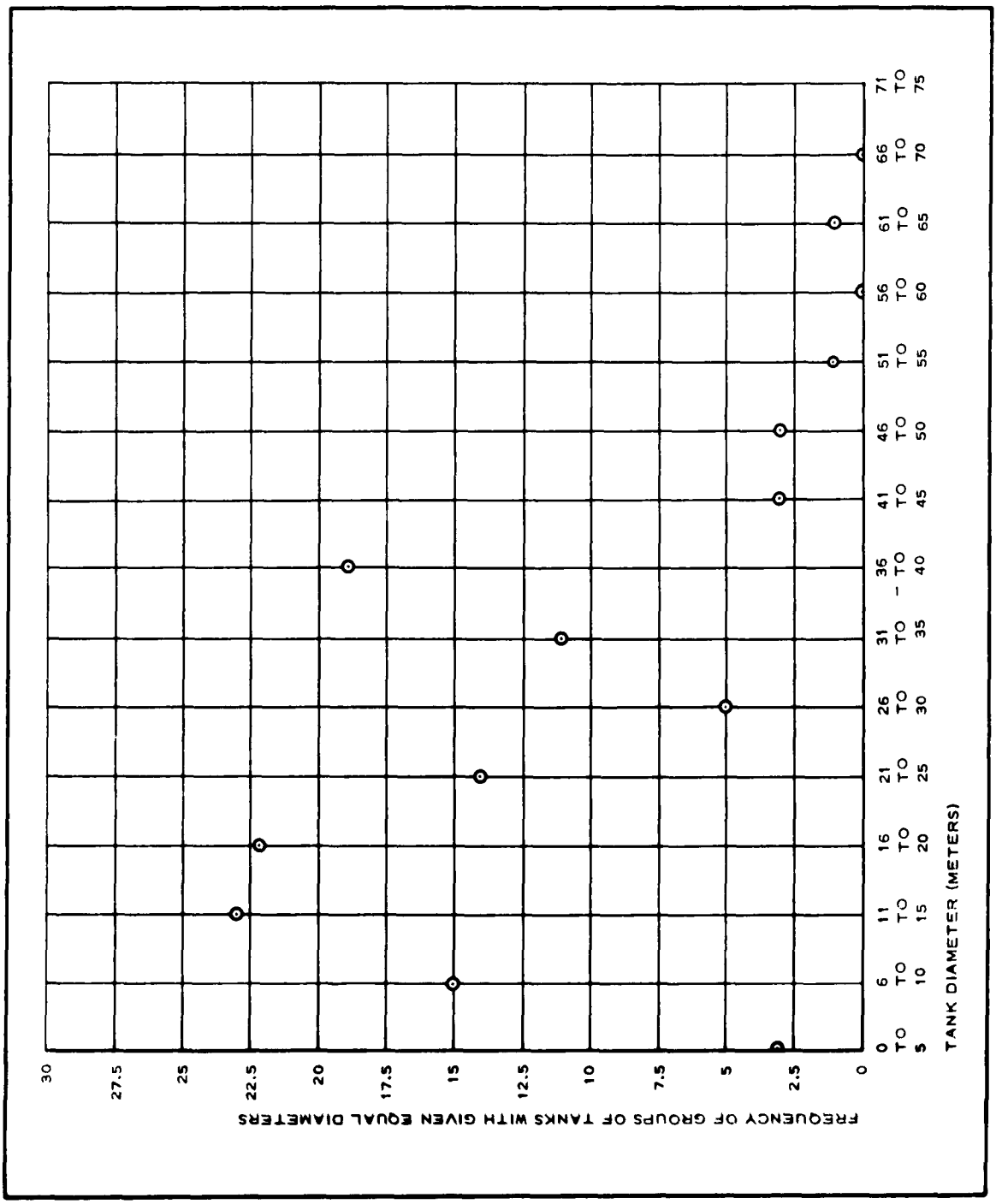

Figure 9 - Frequency Distribution of Groups of Tanks of Equal Diameters

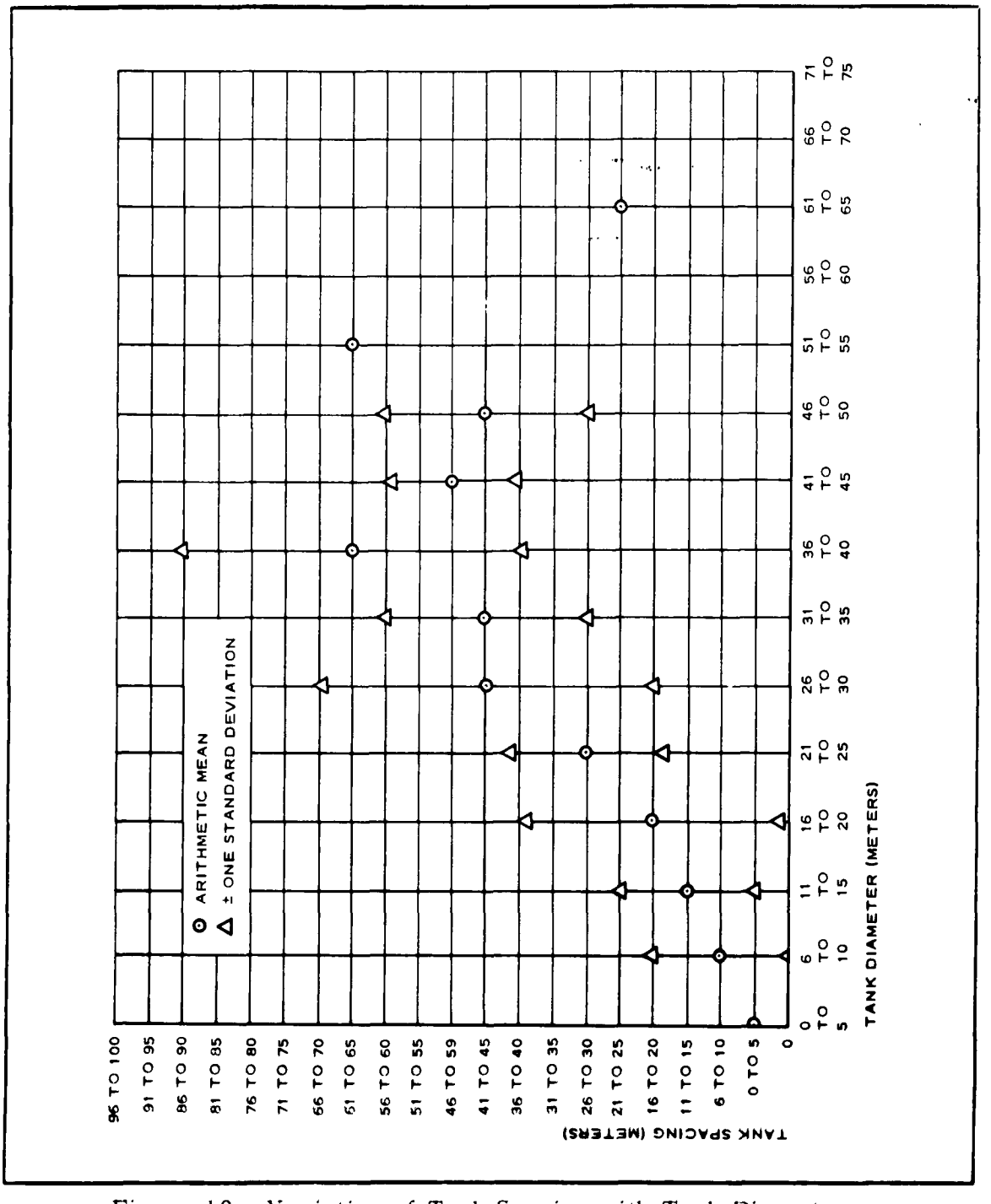

Figure 10 - Variation of Tank Spacing with Tank Diameters

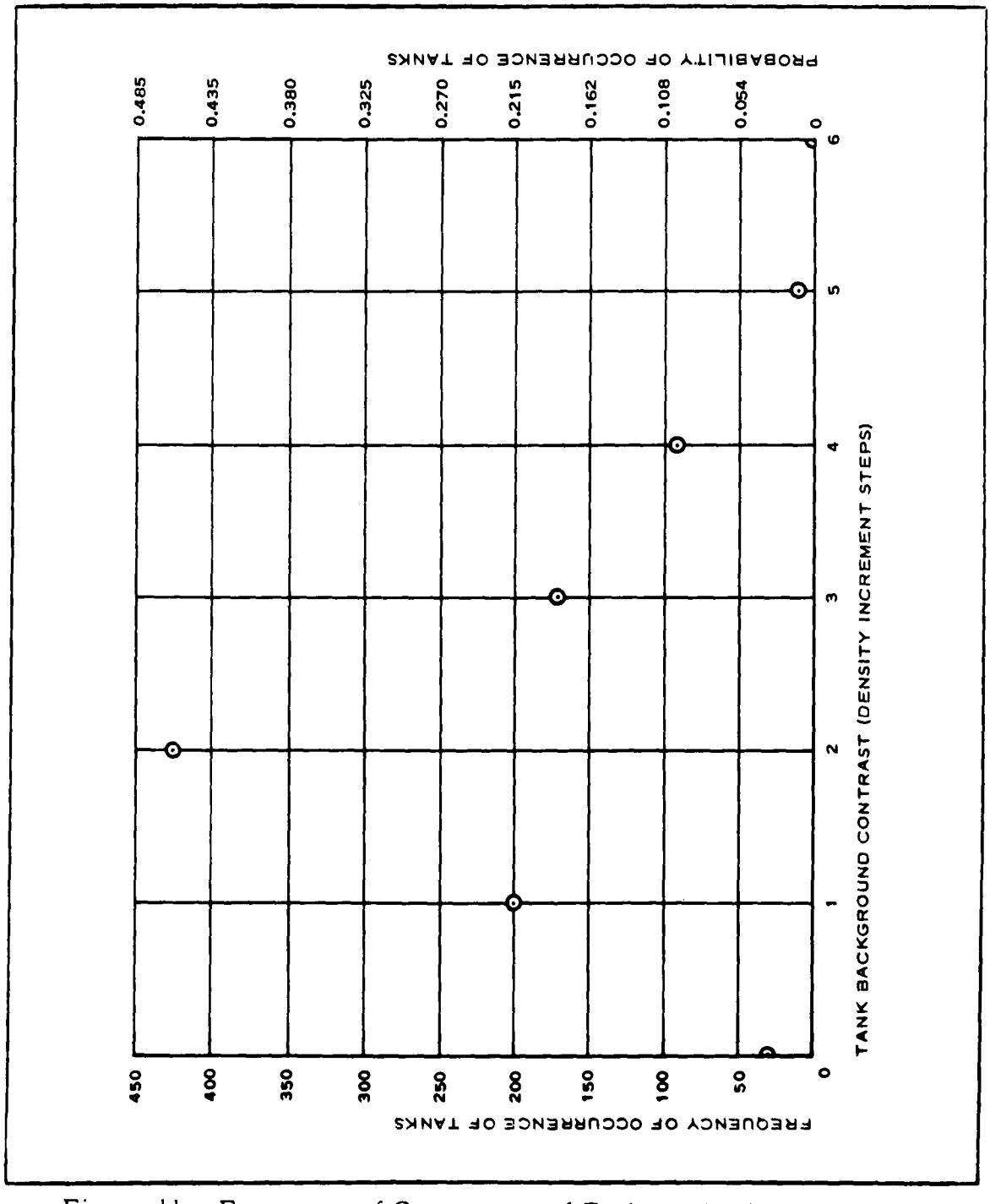

Figure 11 - Frequency of Occurrence of Tanks with Given Contrast

TABLE III - OCCURRENCE OF EQUAL-DIAMETER TANK GROUPS WITHIN A GIVEN REFINERY

Tank diameter (meters)	Refinery										
	I	II	III	IV	V	VI	VII	VIII	IX	X	XI
0 to 5		X									
6 to 10	X		X	X	X	X				X	X
11 to 15	X	X	X	X	X	X		X	X	X	X
16 to 20	X	X	X	X	X	X			X		X
21 to 25	X		X	X		X	X		X	X	X
26 to 30		X	X	X							X
31 to 35	X	X		X	X					X	X
36 to 40	X	X	X	X		X	X	X	X		X
41 to 45							X			X	X
46 to 50							X				X
51 to 55							X				
56 to 60											
61 to 65										X	

c. Results of Nonrefinery Analysis

Figure 12 shows the frequency distributon of diameters of circular patterns in nonrefinery complexes. Three diameter ranges having a high frequency were 0 to 5, 36 to 40, and 46 to 50 m.

Figure 13 is a plot of diameter versus spacing of nonrefinery patterns. Spacing appeared to be constant at about 0 to 5 m for diameters of less than 25 m, and increased irregularly beyond that diameter. However, the ratio of spacing to diameter was never greater than 0.5 to 1 and differed from the ratio of 1.5 to 1 for oil tanks.

d. Conclusions

Contrast of tanks (Figure 11) was sufficient to permit high readout reliability. Groups of tanks between 5 and 40 m in diameter can be

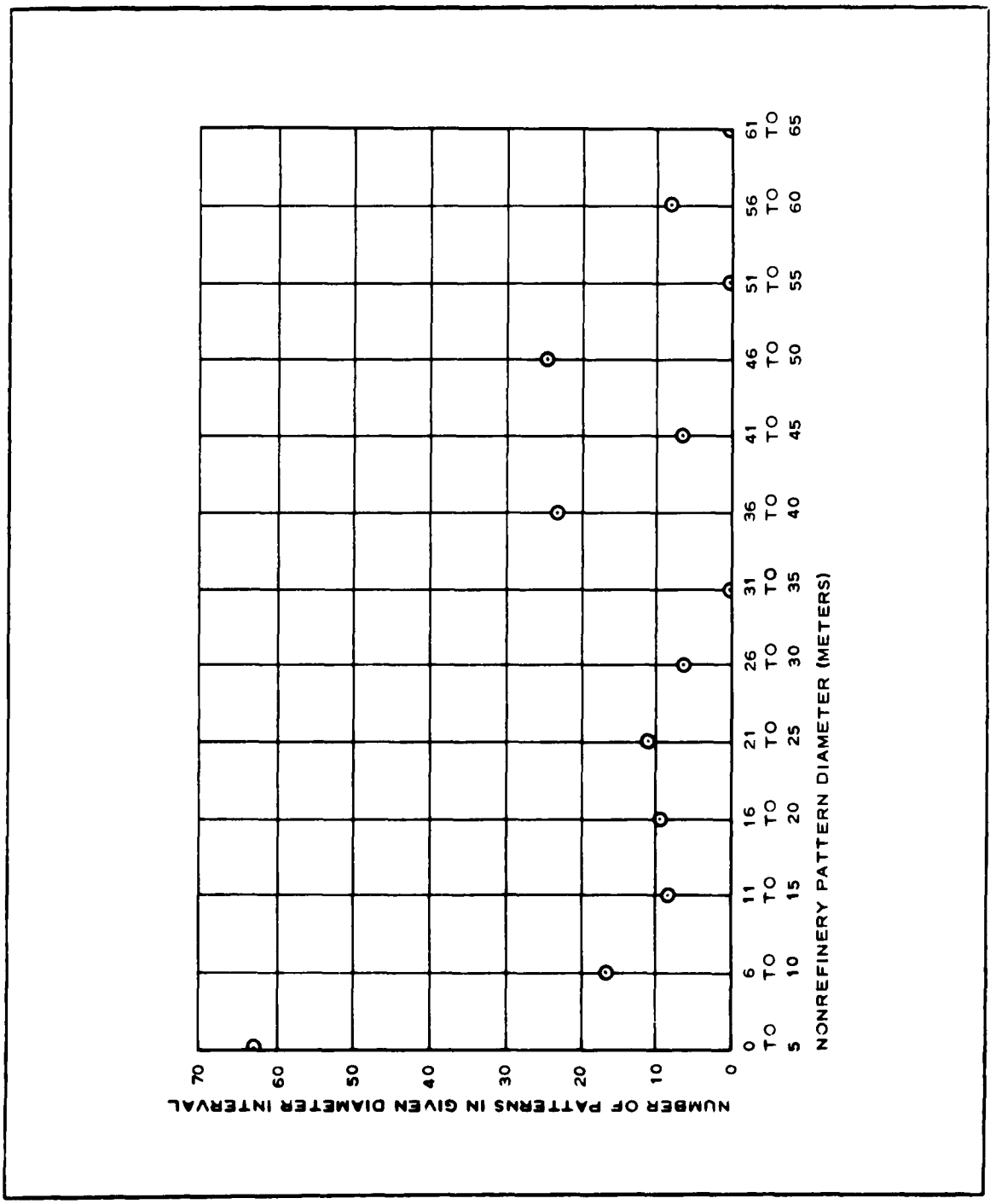

Figure 12 - Frequency Distribution of Diameters of Nonrefinery Tanks

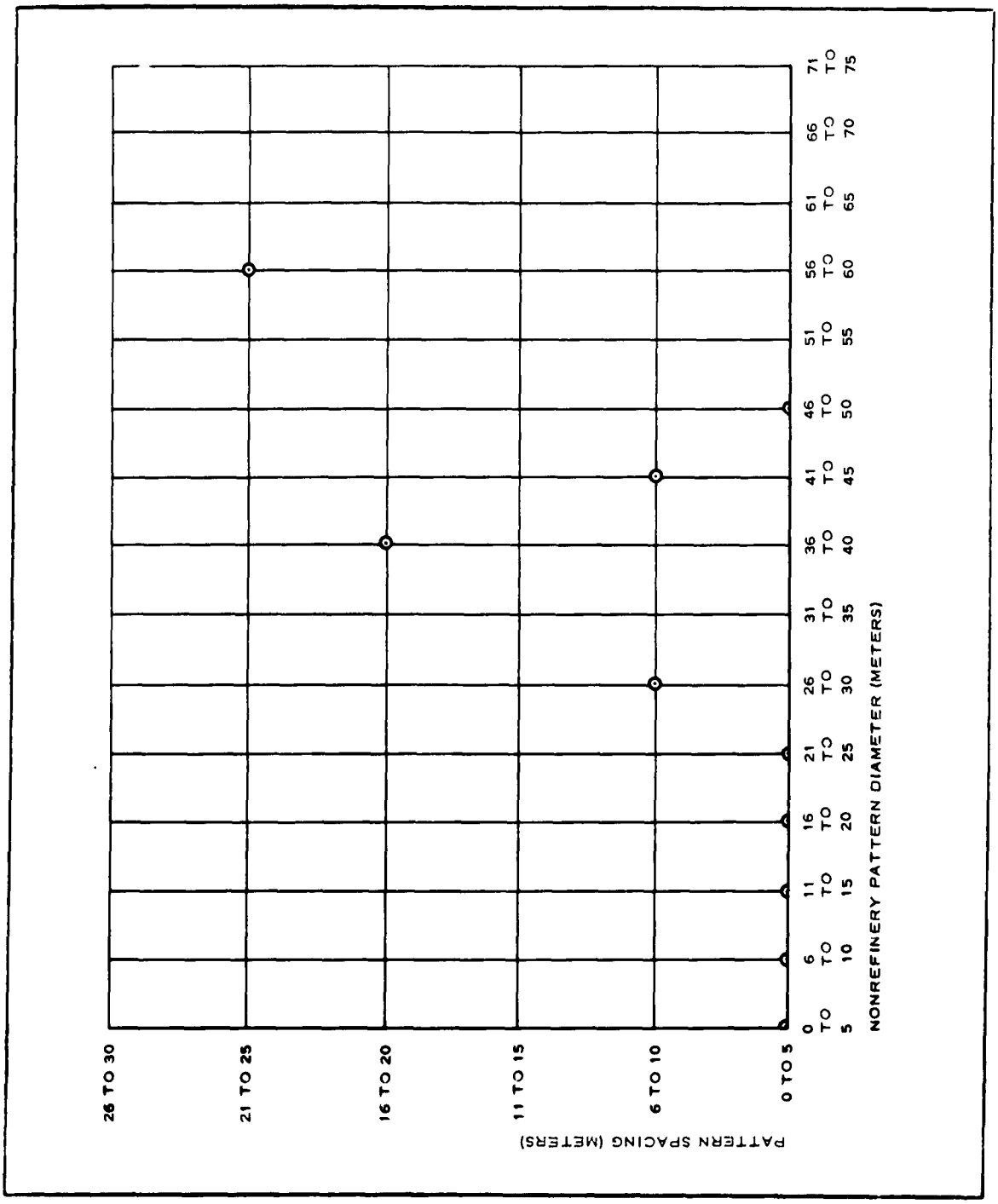

Figure 13 - Nonrefinery Pattern Spacing vs Diameter

anticipated with high probability in refinery complexes. Refinery tanks are ordinarily spaced so that the ratio of spacing to diameter is 1.5 to 1.

Thus, it appears that a pattern recognition device designed to measure these parameters will be successful in recognizing petroleum refineries.

6. CONCLUSIONS

The attributes of runways, petroleum refineries, and more general industrial complexes were analyzed through careful examination of selected photographs. The following conclusions can be drawn from the study.

A high probability for the successful recognition of runways is obtained through the detection of rectangular patterns that lie within given intervals of width (125 to 325 ft) and length (3500 to 12,500 ft) for the northeastern U.S. This conclusion is substantiated by the high values for the correct-decision probabilities and the low values for the incorrect-decision probabilities (Table II).

The following attributes give oil tanks a unique spectral distribution that can be used in their recognition and therefore in the recognition of refineries. Tanks are usually light in a dark background and have sufficient contrast (see Figure 11) for reliable readout. Equally spaced tanks of equal diameter exist in repetitive groups in which the ratio of tank spacing to tank diameter is approximately 1.5 to 1, which is equivalent to a duty cycle of 0.4. Each refinery is almost certain to contain some such groups of tanks with diameters between 5 and 40 m.

Recognition of general industrial complexes is more difficult because the complexes cannot be classified by any reasonably simple set of geometrical attributes. However, they do contain, among other things, rectangular or polyrectangular patterns and parallel, straight, and very narrow strips that appear between the individual buildings, skylights, parked cars, interconnecting walks, and driveways. Although in some cases the complexes

can be classified from geometrical attributes alone, it seems necessary to examine other attributes for a general solution. (See Section III.)

SECTION III - ANALYTICAL STUDY OF PATTERN ATTRIBUTES

Subsection One - General

Two general methods of correlation can be utilized to achieve pattern recognition. One method correlates a reference template (a representation of the desired pattern) with the actual photographic scene. The other method uses correlation of the scene with a spot, an expanding spot, a line, or some other elementary pattern to obtain information concerning the unique attributes of the pattern; this information then yields pattern recognition.

The first method, template matching, requires proper target-template correspondence in orientation, scale, and signal polarity before a suitable peak correlation is obtained. However, even if such correspondence is achieved - and it is a difficult problem - the correlation peak obtained is not highly reliable.

The second correlation method, which recognizes targets through their attributes, is simpler and more successful. A quantitative photograph study of some of the unique attributes that are characteristic of runways and industrial complexes is described in Section II.

The recognition of the rectangular pattern of a runway is accomplished through attributes that define the pattern edges, the straightness of the edges, and the pattern length and width. The correlators used are (1) the width-sifter, which correlates the scene with a spot to determine the pattern edges and widths, and (2) the straight-line detector (see Section V), which uses the correlation of a line to determine pattern edge straightness and length.

The recognition of industrial complexes, on the other hand, requires that many attributes be measured before recognition can be considered reliable. Therefore, an analytical study of the other attributes that can be used to achieve a

more reliable recognition of industrial complexes is described in this section. However, a more important contribution of such a study is the sets of restricting requirements generated for each attribute that define the applicability of the attribute to the recognition of a given target class.

Because of the parallel or perpendicular orientation of industrial patterns and especially because of the periodicity of the circular patterns, the uniqueness of the spectral energy distributions of such patterns was investigated. Unique spectral attributes amenable to filtering were found mainly in target patterns that have a repetitive sequence of at least two patterns and approximately equal target length and spacing.

A frequency domain "oil tank" filter for use in a coherent optical channel was designed to take advantage of these spectral requirements. Such a filter permits simple experimental verification of the frequency domain study and comparison of the frequency and time domain correlation efforts.

A time domain method, the expanding-spot scanner, for the identification of irregular patterns was studied. Such a scanner utilizes the correlation of an expanding spot to overcome some of the frequency domain restrictions: i.e., pattern recurrence, approximately equal target length and spacing, and positive target polarity (white on black background). A quantitative analysis was also made of the action of the expanding spot.

SECTION III - ANALYTICAL STUDY OF PATTERN ATTRIBUTES

Subsection Two - Frequency Domain Analysis of Industrial Patterns

1. GENERAL

The distribution of spectral energy for single pulses, pulse pairs (doublets), and recurrent sequences that can be used to simulate photographic patterns of varying complexity were studied and are discussed in the following paragraphs. The energy associated with the principal spectral loops, or maxima, of recurrent spectrums are useful in pattern recognition because of the uniqueness of such energy distributions. A quantitative description is given of the relative energy content of the first few spectral loops as a function of the duty cycle and the number of pulses of a recurrent sequence.

2. SPECTRAL DENSITY AND ENERGY OF SIMULATED INDUSTRIAL PATTERNS

The buildings and spacings for most industrial sites can be simulated by single pulses, pulse pairs, or sequences of repetitive pulses. To simplify the mathematics in this first preliminary investigation, spectral calculations were carried out in only one dimension, although it is recognized that the buildings and the spacings are actually two-dimensional. However, if the x and y dimensions of a pattern are independent of each other, as in a rectangle that is aligned with the coordinate system, the two-dimensional spectrum is the product of two one-dimensional spectrums.

The three signals chosen to simulate industrial patterns are shown in Figure 14. The pulses, which simulate the buildings, have an amplitude $\sqrt{A_h}$ and a width of 2a m, while the pulse or building spacings are at zero level and 2b m wide.

A preliminary statistical study (see Section II, item 4) of the industrial

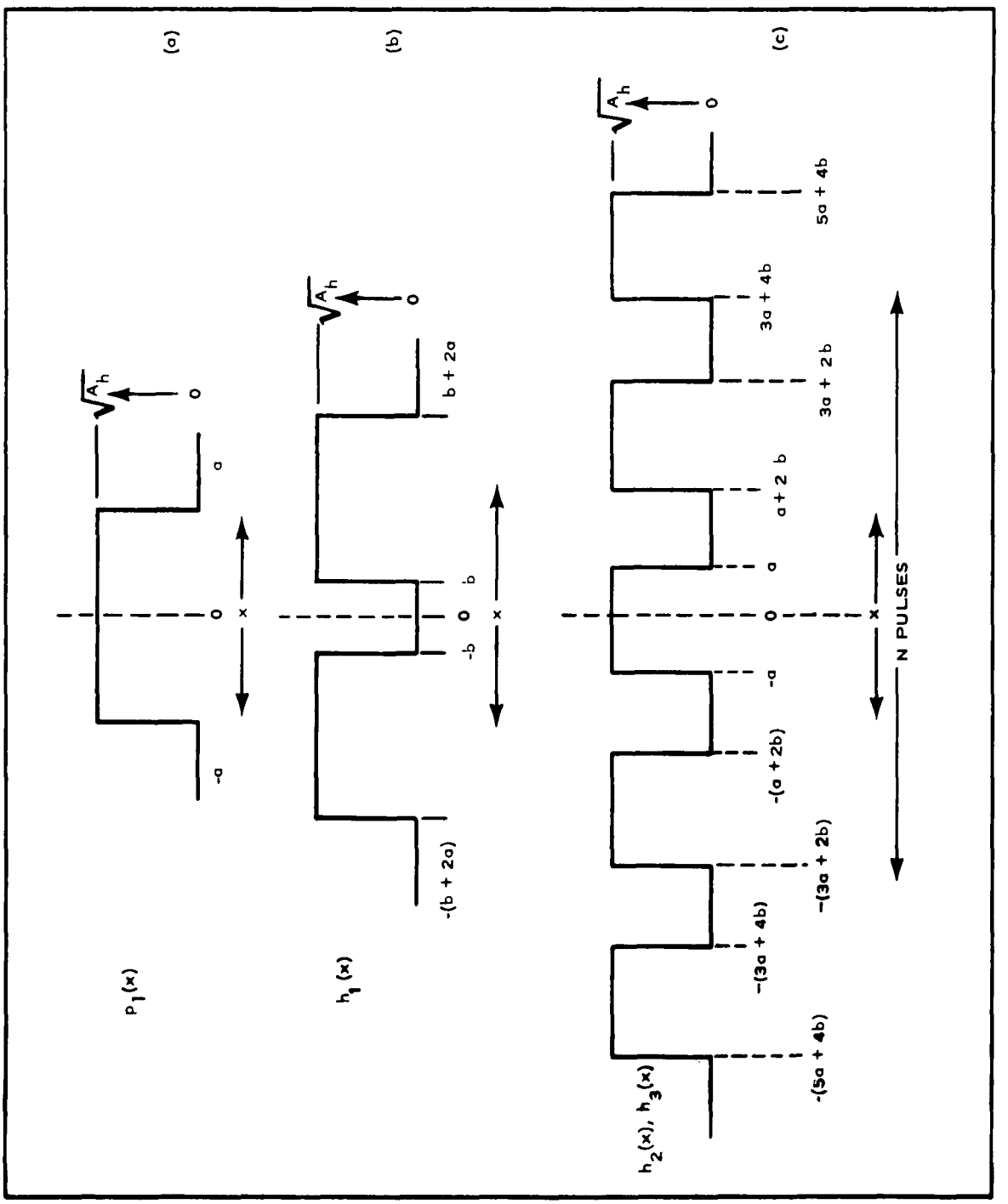

Figure 14 - Simulation of Industrial Signals

buildings of Toledo and Dallas indicates a spread in lengths (2a) of 10 to 400 m and in spacings (2b) of 10 to 300 m.

The spectral energy contents of the three signals are presented below. The expressions for the spectrums of the pulse, double pulse, and recurrent pulses can be obtained from the Fraunhofer diffraction patterns of a slit, dual slit, and grating, respectively. Such patterns are given in Reference 3 as a function of the ray angle, θ, and of the wave length, λ, of the coherent light source. These expressions can be converted to the desired spectral equation with the following relationship between the radial frequency, ω, and the diffraction parameters:

$$\omega = \frac{2\pi \sin \theta}{\lambda} \quad . \tag{5}$$

(The deviation of Equation 5 is given in Reference 4.)

The single pulse $p_1(x)$ (see Figure 14), representing an industrial site with a single large factory building, has the following energy spectrum, $\left|P_1(f)\right|^2$:

$$\left|P_1(f)\right|^2 = A_h 4a^2 \left(\frac{\sin a\omega}{a\omega}\right)^2 \quad . \tag{6}$$

The dual pulse $h_1(x)$ (Figure 14), representing the next order of industrial site complexity, has the following energy spectrum, $\left|H_1(f)\right|^2$:

$$\left|H_1(f)\right|^2 = A_h 16a^2 \left(\frac{\sin \omega a}{\omega a}\right)^2 \cos^2 \omega(a + b) \quad . \tag{7}$$

Sequences of repetitive pulses $h_2(x)$, $h_3(x)$ (Figure 14) are characteristic of such industrial complexes as oil refineries, warehouses, and railroad yards, and of other area complexes such as military barracks and urban developments. The energy spectrums, $\left|H_2(f)\right|^2$, for a repetitive sequence of N patterns are defined by

$$\left|H_2(f)\right|^2 = 4A_h a^2 \frac{(\sin^2 \omega a)\left|\sin^2[(N\omega)(a + b)]\right|}{(\omega a)^2 \left|\sin^2[(\omega)(a + b)]\right|} \quad . \tag{8}$$

The dual pulse spectrums are a special case of the above spectrums and and can be obtained by substituting N = 2 in Equation 8.

Representative spectrums, in square meters, of these types of signals are plotted in Figure 15 as a function of the radial frequency, ω, in radians per meter. The ω scale is defined in terms of an integer, n, and a unit radian measure (0.00362 radians per meter), which is comparable to a spatial wave length of 1735 m.

The curves labeled $|P_1(f)|^2$ and $|H_1(f)|^2$ represent, respectively, a single pulse of length 2a = 580 m and a pulse pair in which 2a = 290 m and 2b = 70 m. The pulse pair represents a pair of acceptable industrial buildings; while the single target, since its length exceeds that of an industrial building, represents a noisy background signal with a total energy content equal to that of the pair of industrial buildings. Comparison of the two spectrums indicates that little difference exists except at the second loop, $3 \leq n < 6$, and that this difference represents a small portion of the total energy of each spectrum.

The other pair of spectral curves in Figure 15 represents two sets of recurrent pulses; one has an equal pulse and spacing length of 25 m, and the other has a pulse and spacing length of 40 m and 10 m, respectively. Such recurrent spectrums display main loops or principal maxima of energy at

$$\omega = 0, \frac{\pi}{a+b}, \frac{2\pi}{a+b}, \ldots, \frac{k\pi}{a+b} .$$

The first central energy loops for each of the two recurrent spectrums are shown in Figure 15.

A more useful measure of the discrimination between the spectrums of targets and nontargets is the cumulative integral, with respect to ω, of the spectral energy: i.e., the total energy within a given load pass. From such data, the discriminatory effectiveness of a given band pass filter can be obtained by noting the percent of signal energy passed by the filter. The cumulative spectral energy, E(H), for a given signal spectrum, $|H(f)|^2$, is

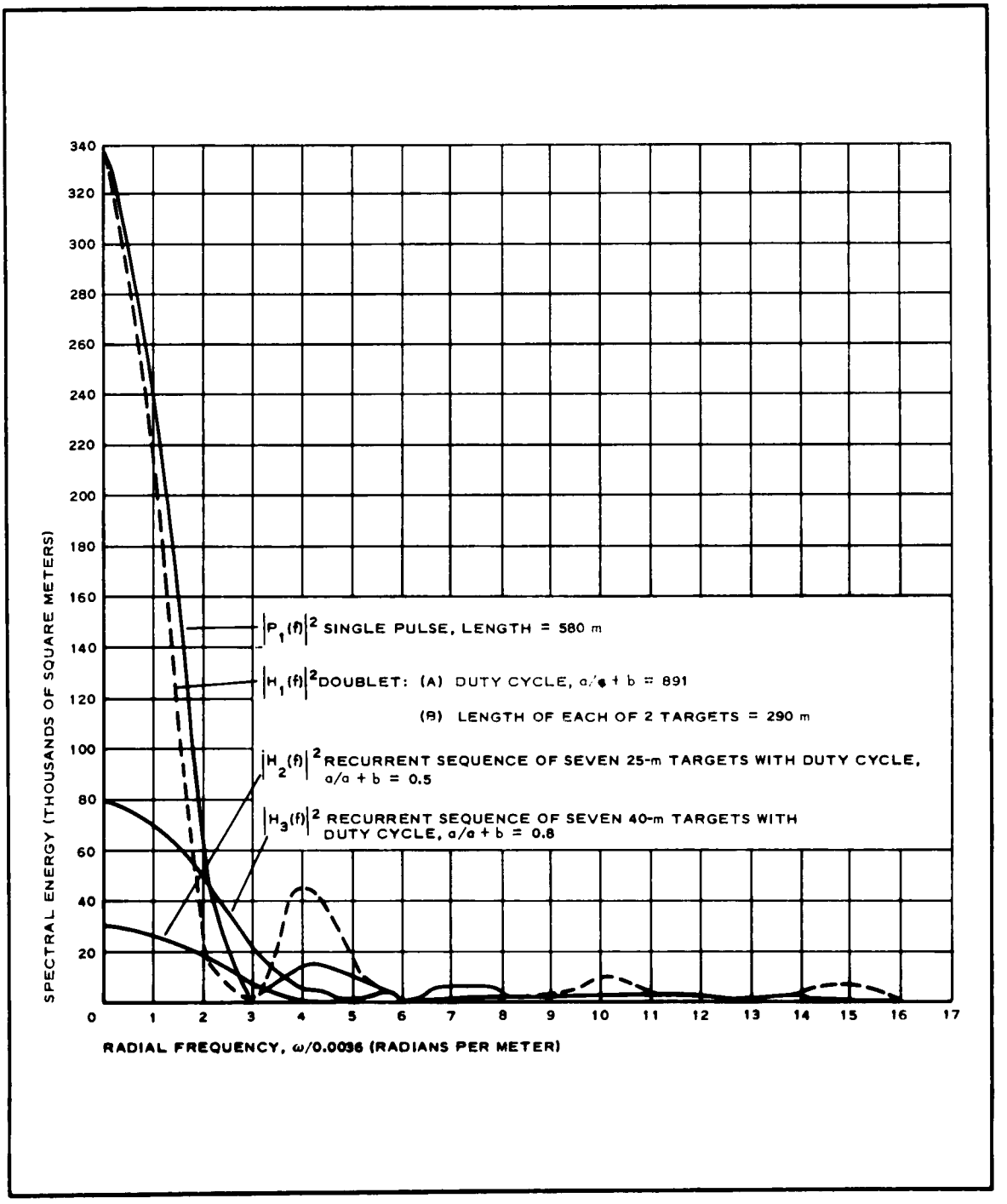

Figure 15 - Energy Spectrums for Simulated Industrial Signals

$$E(H) = \frac{1}{\pi}\int_0^{\omega} \left|H(f)\right|^2 d\omega \quad .$$

The integrals of the spectrums from Equations 6 and 8 were computed numerically with Simpson's rule and are plotted in Figure 16 in terms of the percentage of the original energy content, E_o, available from

$$E_o = \int_{-\infty}^{+\infty} h(x)^2 \, dx \quad . \tag{9}$$

Again for the pulse and for the pulse pair, little of the signal energy exists outside the central loop; i.e., at frequencies higher than n = 3 (this value of n is equal to $\omega a \cong \pi$, in which 2a is the width of the pulse in each case). The slightly larger amount of high-frequency energy associated with the pulse pair (22 percent versus 9.5 percent), due primarily to the small spacing between the two pulses, is not sufficient to provide a reliable discrimination between the target and nontarget signals.

A different situation exists with the cumulative energies of the recurrent spectrums, $\left|H_2(f)\right|^2$ and $\left|H_3(f)\right|^2$; in this case the higher frequencies contain a greater portion of the energy. This is especially true as the pulse and spacing lengths approach equality; it should be noted that the signal spectrums $\left|H_2(f)\right|^2$, in which the seven pulses and spacings are each 25 m, has more than 50 percent of its energy associated with frequencies outside its first central loop. Such an energy distribution is amenable to filtering and is considered in the following paragraphs, in which the relative distribution of energy between the central spectral loop and the higher-frequency principal spectral loops that lie outside the central loop is evaluated.

3. DISTRIBUTION OF SPECTRAL ENERGY AMONG PRINCIPAL SPECTRAL LOOPS

The recurrent spectrums $\left|H_2(f)\right|^2$ of N patterns, (N > 1), described by

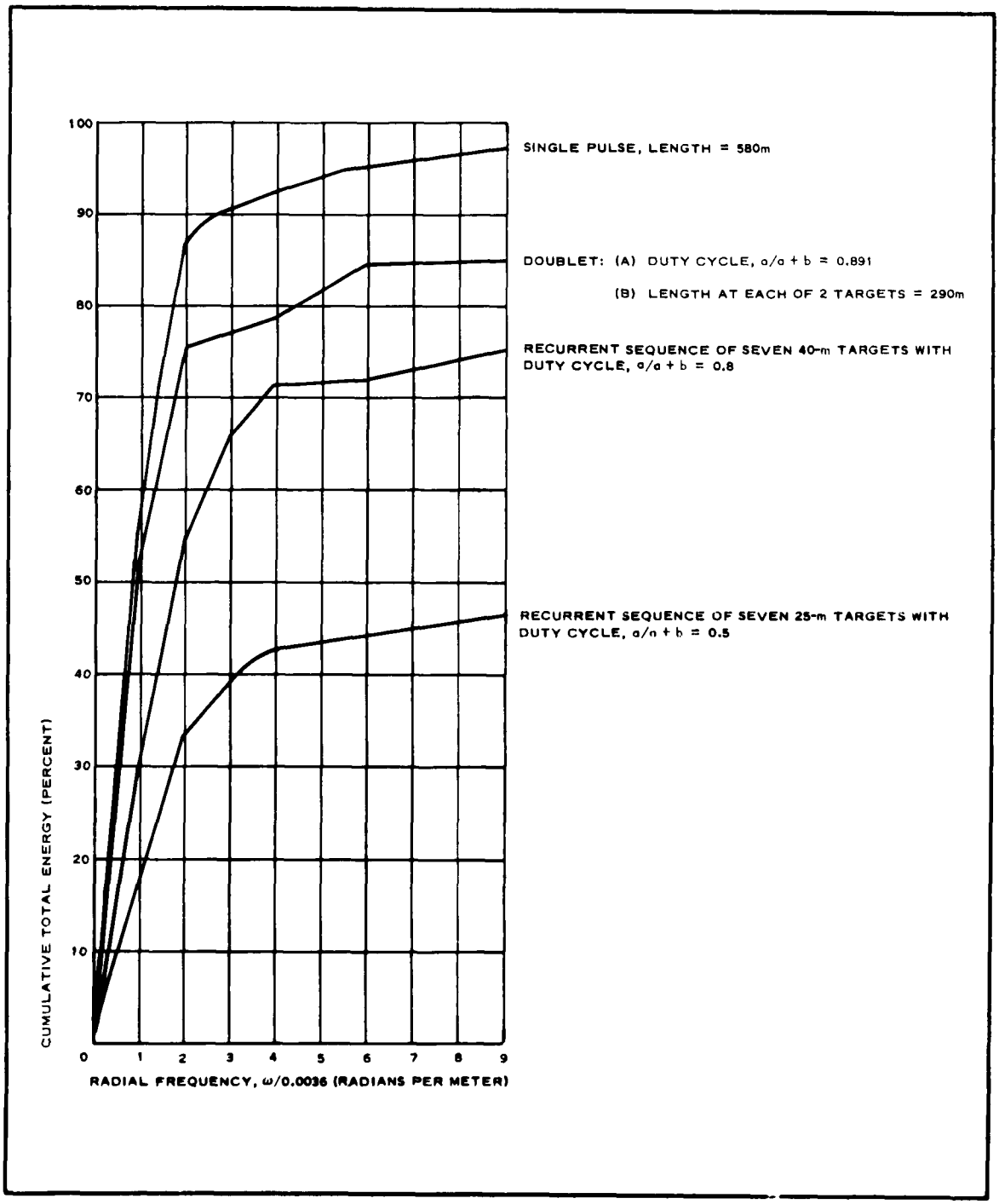

Figure 16 - Cumulative Percent of Spectral Energy vs Radial Frequency

Equation 8, exhibit spectral loops whose peaks occur at radial frequencies ω_k, so that the last term is

$$\left\{\frac{\sin\left[(N)(\omega_k)(a+b)\right]}{\sin\left[(\omega_k)(a+b)\right]}\right\}^2 = N^2 \quad . \tag{10}$$

The various values for these radial frequencies, ω_k, which define each of the k spectral loops, are inversely proportional to the periodic width, a + b, or

$$\omega_k = \frac{(k-1)(\pi)}{a+b} \quad . \tag{11}$$

The spectral widths of the loops are defined by the radial frequencies ω_{ka} and ω_{kb}, which mark, respectively, the first zeros that precede and follow the peak and are

$$\omega_{ka} = \left(k - 1 - \frac{1}{N}\right)\left(\frac{\pi}{a+b}\right) \tag{12}$$

and

$$\omega_{kb} = \left(k - 1 + \frac{1}{N}\right)\left(\frac{\pi}{a+b}\right) . \tag{13}$$

The energy, E_k, contained in a given k spectral loop is obtained by integrating the spectrum, $\left|H_2(f)\right|^2$ (Equation 8) between the two zeros ω_{ka} and ω_{kb} defined by Equations 12 and 13 above, or

$$E_k = \frac{4a^2 A_h}{\pi} \int_{\omega_{ka}}^{\omega_{kb}} \left(\frac{\sin \omega a}{\omega a}\right)^2 \left\{\frac{\sin\left[(N\omega)(a+b)\right]}{\sin\left[(\omega)(a+b)\right]}\right\}^2 d\omega \quad . \tag{14}$$

(E_k represents the combined energy of both the positive and negative frequency portions of the k^{th} loop.)

A more convenient representation of the loop energy is R_k, the percent of the total signal energy, obtained as a ratio of the integral of Equation 14

to E_o of Equation 9. The percent of signal energy contained in the k^{th} loop, in which $k > 1$, becomes approximately (see Appendix A)

$$R_k \cong \frac{a}{a+b}\left(C_0 + \frac{C_2}{N^2} + \frac{C_4}{N^4} \cdots\right) . \tag{15}$$

The terms, C_0, C_2, and C_4, which are functions of the duty cycle or of the pulse-width-to-period ratio, $a/a+b$, and of the loop number, k, are evaluated in Appendix A. The values of $a/a+b$ and k are restricted so that

$$\left(\frac{a}{a+b}\right)\left(k - 1 + \frac{1}{N}\right) \leq 1 .$$

When $N > 5$ an alternate and less restrictive representation of the loop energy percentage, R_k, is obtained (see Appendix A):

$$R_k \cong \left(\frac{a}{a+b}\right)(1.85)\frac{\left\{\sin^2\left[\left(\pi\frac{a}{a+b}\right)(k-1)\right]\right\}}{\left[\left(\frac{\pi a}{a+b}\right)(k-1)\right]^2} . \tag{16}$$

Finally, the percent of spectral energy, R_1, in the central loop has the following approximate value (see item 2, Appendix A) and is plotted in Figure 17:

$$R_1 \cong \frac{a}{a+b}\left\{0.925 + \frac{0.33\left[1 - \left(\frac{a}{a+b}\right)\right]^2}{N^2} + \frac{0.0779\left[1 - \left(\frac{a}{a+b}\right)^2\right]^2}{N^4} \cdots\right\} . \tag{17}$$

The constant term, 0.925, represents the percent of energy present in the central loop of the "sin x over x" spectrum of a single target pulse and indicates the change of a recurrent sequence into a single target as the ratio $a/a+b$ approaches one.

Figure 17 provides a measure of the spectral distribution of energy among the first three loops for recurrent sequences of N pulses, for $N > 1$, with

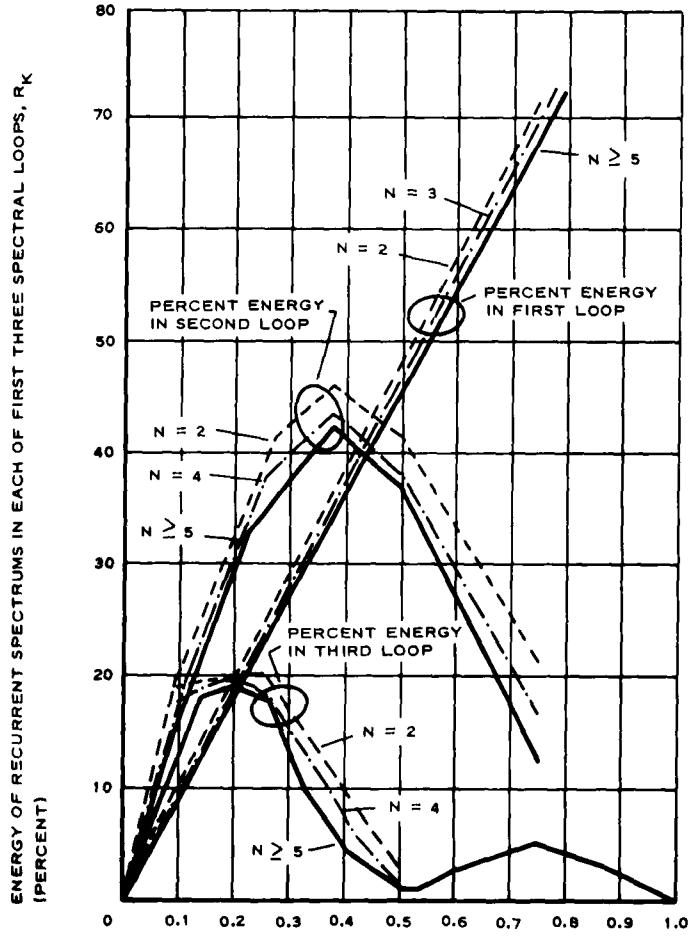

LOOP*	LOCATION OF PEAK, ω_o	UPPER CUTOFF, ω_b	LOWER CUTOFF, ω_a
1	0	$+\pi/N(a+b)$	$-\pi/N(a+b)$
2	$+\pi/a+b$	$\pm(1+1/N)(\pi/a+b)$	$\pm(1-1/N)(\pi/a+b)$
3	$+2\pi/a+b$	$\pm(2+1/N)(\pi/a+b)$	$\pm(2-1/N)(\pi/a+b)$

*THE ENERGIES PLOTTED REFER TO THE SUM OF BOTH THE POSITIVE AND NEGATIVE FREQUENCY LOOPS IN EACH CASE.

Figure 17 - Percent of Signal Energy vs Ratio of Pulse to Period Width

a given duty cycle or pulse-to-period-width ratio of a/a + b. Signals that have a low duty cycle, a/a + b < 0.1, have their energy distributed rather evenly among the first three loops and substantial amounts of energy associated with the remaining higher order loops. However, as the targets increase in size and as spacings decrease to render a/a + b larger, an increasing amount of energy is accounted for by the first few loops; at a/a + b = 0.2 almost 70 percent is associated with the first three loops, at a/a + b = 0.4 almost 78 percent of the energy is contained in the first two loops, and at a/a + b = 0.8 over 70 percent of the energy is in the first loop alone. It should be noted that number of pulses, N, has a small effect (a difference of less than 5 percent) on the spectral distribution.

4. CONCLUSIONS

The spectral energy distributions of pulses, doublets, and recurrent sequences indicate that:

1. If the duty cycle of doublets or recurrent sequences approach unity - that is, if the targets are larger than their separation - the spectrums of such signals cannot be reliably used in pattern recognition since the recurrent spectrums in these cases are too much like the spectrums of those single noise pulses that are equal to the size of the sequences.

2. As the duty cycle is decreased so that it lies between 0.3 and 0.5, most of the spectral energy of doublets and recurrent sequences are associated with the first two spectral loops; sufficient spectral uniqueness exists to permit the isolation of such target classes.

3. Since the energy is divided among many spectral loops, the spectral distribution associated with a low duty cycle (i.e., less than 0.2), is best processed through a

comb-type filter that will pass only the several principal spectral loops.

The most effective filtering is obtained for those repetitive signals that have most of their energy concentrated in a second spectral loop that is sufficiently removed from the low frequencies of the central loop. A frequency domain design of a suitable recognition filter for such signals is discussed in the following paragraphs.

SECTION III - ANALYTICAL STUDY OF PATTERN ATTRIBUTES

Subsection Three - Frequency Domain Filtering

1. GENERAL

A method for utilizing spectral attributes in a recognition process requires the original data to be passed through a filter that is designed to maximize the spectral discrimination between the desirable targets and the background noise. Examination of the relative amount of original target and nontarget energy passed by the filter, in conjunction with other attributes, will permit recognition of the desirable patterns. The target signals must not only have the proper spectral characteristics but must provide a proper polarity signal energy, that is, a white intensity in a black background.

Two filtering methods are available for the processing of the spectral attributes. One is carried out in the frequency domain through use of a coherent optical channel; the other, carried out in the space domain, utilizes the correlation of an expanding spot in a modified flying-spot scanner (fss). (The second method, the expanding-spot scanner, is discussed in Subsection Four, this section.)

Frequency domain filtering is suggested for two reasons: first, a coherent optical channel is available that permits experimental verification of the frequency domain analysis with minimum effort; and second, a comparison of the results of frequency and time domain filtering can be made.

2. FILTER DESIGN

The filter in the coherent optical channel is a two-dimensional transmissivity plot on film of the frequencies to be passed. The resulting film is placed at the frequency transform plane of the coherent optical channel;

the output at the image plane is an intensity plot of the input energy allowed to pass through the filter.

One approach to the design of the filter, maximizing the signal-to-noise ratio without regard for signal fidelity,[5] requires a single average spectrum for the background noise and one for the desirable signals. Such average spectrums can be computed in each case from the experimentally obtained probability distributions of the various parameters that affect the spectrums. If, for example, the background noise is random and has a flat spectrum, the required filter is matched; i.e., it has a spectrum exactly like that of the average signal spectrum. Such a complex function would be extremely difficult to reproduce on film for use in the coherent channel and would be almost impossible to incorporate into a time domain fss filter. Furthermore, certain of the actual signal spectrums would deviate from this average value and caution must be used to ensure that these spectrums will not be penalized too severely by the action of this "average" filter.

An alternate and simpler approach is to consider a two-level omnidirectional band pass filter (see Figure 18), which can be described completely

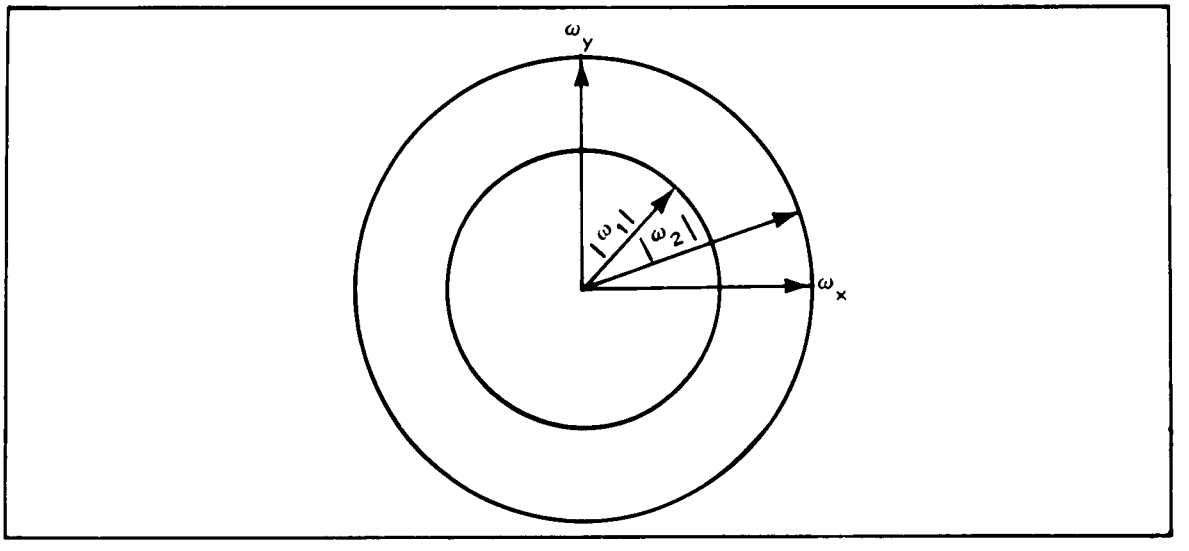

Figure 18 - Omnidirectional Band Pass Filter

by the upper and lower corner frequencies, ω_2 and ω_1, respectively, and can be readily made for a coherent channel. Optimum values for the corner frequencies can be obtained by maximizing the signal-to-noise ratio. The calculations for a maximal signal-to-noise discrimination in this case can be carried out separately for each of the corner frequencies with boundary values for the high- and low-frequency signals and with an average noise spectrum. For example, the proper values for the filter's corner frequencies ω_1 and ω_2 will satisfy the following equations for the maximums of the signal-to-noise ratios, or

$$\frac{\partial}{\partial \omega_1}\left(\frac{S}{T}\right)_1 = 0 \tag{18}$$

and

$$\frac{\partial}{\partial \omega_2}\left(\frac{S}{T}\right)_2 = 0 \ . \tag{19}$$

The calculation for the lower cutoff frequency, ω_1 from Equation 18, utilizes low-frequency signal spectrums $(S)_1$; that for ω_2 uses high-frequency spectrums $(S)_2$. In each case T represents the average noise spectrums.

An example of a two-dimensional recurrent signal spectrum is associated with the matrix of oil tanks, which are characteristic of an oil refinery. If a symmetrical N × N arrangement of N^2 tanks is assumed, the two-dimensional spectrum becomes the product of the two single-dimensional spectrums, or

$$\left|H(\omega_x \omega_y)\right|^2 = \left(A_h 16a^4\right)\left(\frac{\sin \omega_x a}{\omega_x a}\right)^2\left[\frac{\sin (\omega_y a)}{\omega_y a}\right]^2 \times \left[\frac{\sin N\omega_x(a+b)}{\sin \omega_x(a+b)}\right]^2\left[\frac{\sin (N\omega_y)(a+b)}{\sin (\omega_y)(a+b)}\right]^2 \ , \tag{20}$$

which assumes that the individual tanks of widths 2a are square when actually they are round. This discrepancy in the equation is reflected in the

first two "sin x over x" terms, and is not excessive (see pages 302 and 303 of Reference 3); furthermore, the last two terms, which are not affected by this error, are much more effective in determining the energy contents of the several recurrent spectral loops upon which the filtering action depends.

The main energy loops of the two-dimensional recurrent spectrums, as defined by Equation 20, are plotted schematically as an intensity function of ω_x and ω_y in Figure 19. The relative energy content R_{ij} of a given i, j loop can be determined from Figure 17, in which the plotted energies for the second and third loops refer to the combined energy of both the positive and negative loops, so that the individual loop energy is one half of the plotted figure. For example, if a/a + b = 1/2 and N = 2, from Figure 17 the energy of loop 1, 2 is

$$R_{1,2} = \frac{(0.41)}{2}(0.48)$$

$$= 0.0984 .$$

If it is assumed that the two dotted circles define the unity band pass of a two-level filter, the spectral loops (1, 2), (2, 1), (1, -2), and (-2, 1) are passed (see Figure 19). The combined relative energy R_T of these four loops under the conditions a/a + b = 1/2 and N = 2 is

$$R_T = 4\left[\left(\frac{0.41}{2}\right)(0.48)\right]$$

$$= 0.394 .$$

Thus, 39.4 percent of the input recurrent pattern energy is passed by a two-level filter whose corner frequencies correspond to the boundary frequencies required for the second spectral loop (see Figure 17 and Equations 12 and 13). Such a filter will be designed in accordance with the maximal methods given in Equations 18 and 19. Since the two corner frequencies of the filter depend mainly on the frequencies associated with the one-dimensional second loop, the filter design is carried out with respect to this loop.

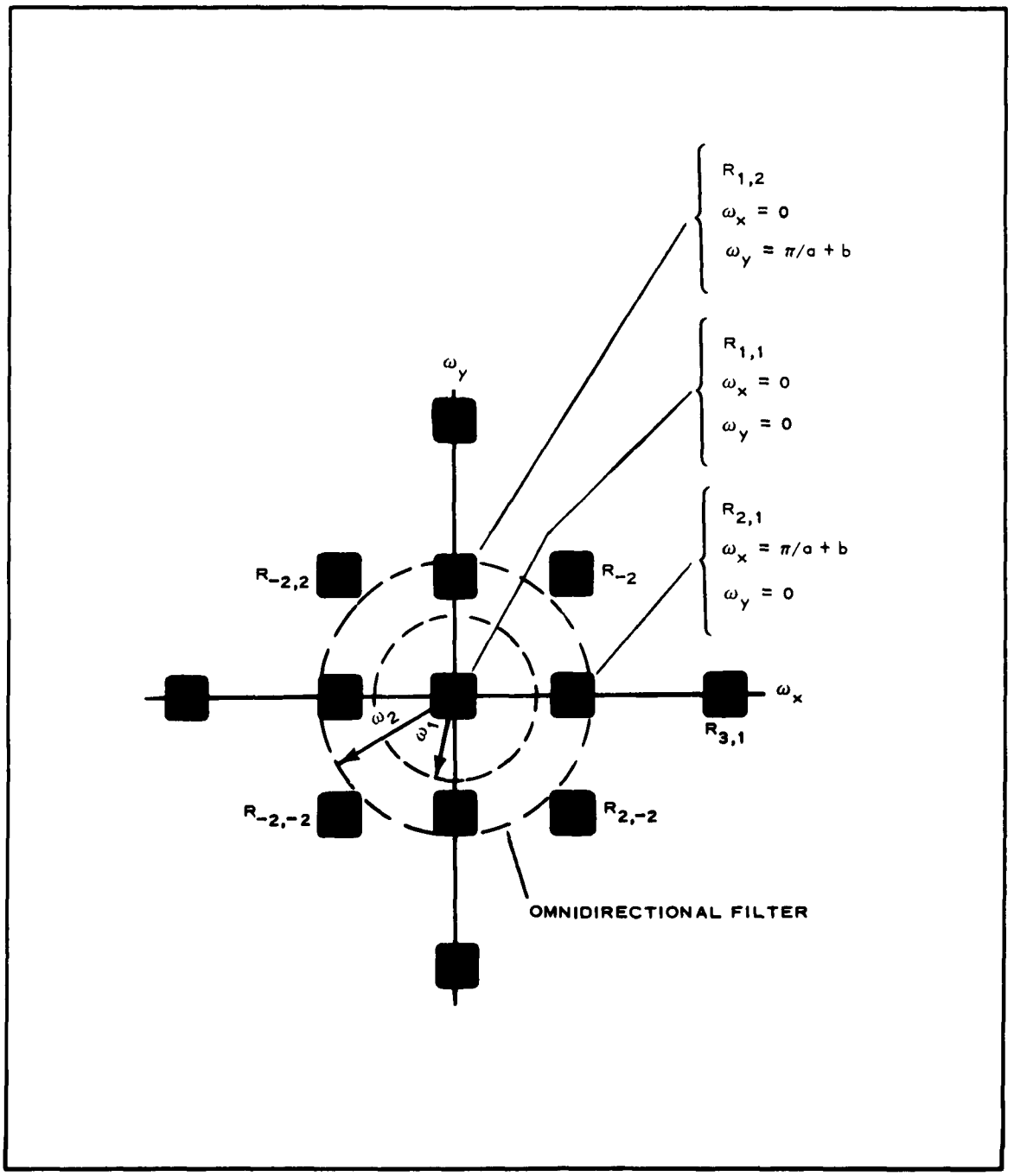

Figure 19 - Spectral Energy of Two-Dimensional Repetitive Pattern and Two-Level Omnidirectional Filter

The evaluation of the signal (S) and noise (T) energies and the solution of the filter design expressions (Equations 18 and 19) are given in Appendix B.

3. EVALUATION OF TWO CORNER FREQUENCIES ω_1 AND ω_2

The general solutions developed in Appendix B provide values of α as a function of the number of pulses, N, and of the minimum and maximum one-half-period lengths (i.e., the combined half-lengths of target plus spacing) that occur in a given input ensemble of repetitive signals. The term α refers to the percentage of the second spectral loop energy, of a given extreme upper or lower frequency input signal, that is passed by the filter; it is related to the lower and upper corner frequencies, ω_1 and ω_2, respectively, as follows:

$$\omega_1 = \left(\frac{\pi}{A}\right)\left(1 - \frac{\alpha}{N}\right) \tag{21}$$

and

$$\omega_2 = \left(\frac{\pi}{B}\right)\left(1 + \frac{\alpha}{N}\right) , \tag{22}$$

where A and B are, respectively, the maximum and minimum one-half-period lengths associated with the input ensemble of target signals.

The solutions of Equation B-12 of Appendix B in terms of α_1 and Equation 21 in terms of ω_1 for several values of the number of sequence pulses and the ratio $\pi/\omega_2 A$ are given in Table IV; $\pi/\omega_2 A$ has approximately the same value as the ratio B/A of the minimum and maximum one-half-period lengths. The relative insensitivity of the solutions of α_1 to various values of N and of the ratio $\pi/\omega_2 A$ is apparent. The linear relationship that exists between the number of pulses, N, and the portion of the loop, α, that is to be passed by the filter is offset by the fact that the spectral width of the second spectral loop (see Equations 12 and 13) varies inversely with N. A relatively constant value for ω_1 thus results.

Table V gives a similar compilation of values for α_2 from Equation B-13

TABLE IV - SOLUTIONS OF EQUATION B-13 FOR α_1 AND EQUATION 21 FOR ω_1

Number of sequence pulses, N	$\frac{\pi}{\omega_2 A} \cong \frac{B}{A}$	Solution of Equation B-13 for α_1	Solution of Equation 21 for ω_1
2	1/2	0.3	$\frac{\pi}{A}$ (0.85)
2	1/3	0.35	$\frac{\pi}{A}$ (0.825)
3	1/2	0.40	$\frac{\pi}{A}$ (0.87)
3	1/3	0.45	$\frac{\pi}{A}$ (0.85)
3	1/10	0.5	$\frac{\pi}{A}$ (0.84)
5	1/2	0.55	$\frac{\pi}{A}$ (0.89)
5	1/3	0.60	$\frac{\pi}{A}$ (0.87)

TABLE V - SOLUTIONS OF EQUATION B-14 FOR α_2 AND EQUATION 22 FOR ω_2

Number of sequence pulses, N	$\frac{\pi}{\omega_1 B} \cong \frac{A}{B}$	Solution of Equation B-14 for α_2	Solution of Equation 22 for ω_2
2	3	0.68	$\frac{\pi}{B}$ (1.34)
3	2	0.70	$\frac{\pi}{B}$ (1.23)
3	3	0.75	$\frac{\pi}{B}$ (1.25)
3	15	0.88	$\frac{\pi}{B}$ (1.29)
5	15	0.90	$\frac{\pi}{B}$ (1.18)

of Appendix B and ω_2 from Equation 22. Very high values of α are obtained as solutions of Equation B-13 so that the resultant value of ω_2 essentially depends on the width of the second loop (Equations 12 and 13) and therefore of the number of pulses, N, in the sequence. This arises because of the inverse variation in the noise energy with the square of the frequency (see Equation B-8) so that at the upper portion of the filter band width the increase in noise due to an extension of the upper corner frequency ω_2 is very much less than at the lower portion of the filter's frequency band.

4. CALCULATION OF OMNIDIRECTIONAL FILTER FOR OIL TANKS

The preceding theory of frequency domain filtering was applied to the design of an omnidirectional filter (Figure 18) that will pass the signal energy associated with oil tanks. The study of oil tanks indicated that oil refineries will almost certainly have tanks between 5 and 40 m in diameter and in groups that have duty cycles, a/a + b, between 0.3 and 0.5. A maximum one-half-period, A = 67 m, is associated with a 40-m tank sequence with a minimum duty cycle of 0.3; while the minimum one-half-period, B = 5 m, is obtained from a 5-m tank sequence with a duty cycle of 0.5. Approximate values for the ratios $\pi/\omega_2 A = 0.10$ and $\pi/\omega_1 B = 15$ and an assumed value of N = 3 result in the following values from Tables IV and V for ω_1 and ω_2:

$$\omega_1 = \frac{\pi}{67}(0.84)$$

$$= 0.039 \text{ radians per meter}$$

$$\omega_2 = \frac{\pi}{5}(1.29)$$

$$= 0.81 \text{ radians per meter .}$$

The conversion of these radial frequencies into the proper physical dimensions of a coherent channel omnidirectional filter is accomplished as follows. Since the coherent optical channel is fundamentally a Frauhafer

diffraction experiment, its frequency transform plane where the filter is located can be described by the following expression, given above as Equation 5:

$$\omega = \frac{2\pi \sin \theta}{\lambda} ,$$

where θ and λ are, respectively, the ray angle with respect to the central optical axis and the wave length of the coherent light source. The desired relationship between a given radial frequency ω_x and its corresponding locating point, L_x, at the filter transform plane, for a given focal length, L_f, is therefore

$$\omega_x = \frac{2\pi L_x}{L_f \lambda} , \qquad (23)$$

which assumes that $\sin \theta \cong L_x/L_f$ and that the origin at the frequency transform plane coincides with the optical axis of the coherent optical channel. For an assumed reduction of 1.11×10^{-5} in the scale of the input scene, a coherent source wave length of $\lambda = 5.44 \times 10^{-5}$ cm, and a coherent optical channel focal length of 60.9 cm, the physical lengths of the outer and inner radiuses, L_o (corresponding to ω_2) and L_i (corresponding to ω_1), for the transmission annulus of the filter, in accordance with Equation 23, are

$$L_o = 0.384 \text{ cm}$$

and

$$L_i = 0.0181 \text{ cm} .$$

SECTION III - ANALYTICAL STUDY OF PATTERN ATTRIBUTES

Subsection Four - Time Domain Filtering with Expanding-Spot Scanner

1. GENERAL

The expanding-spot scanner detects in the time domain those patterns that have nearly unity length-to-width ratios and that may or may not be rectangular. It can also detect the opposite boundaries of a pattern having a larger-than-unity value of length-to-width ratio.

The limitations of frequency domain filtering - namely, that the target pattern must be recurrent with restricted allowable ratios of target length to spacing and that the pattern intensity must be white with a black background - are overcome to a large degree with the expanding-spot scanner. With such a scanner, the pattern need not be recurrent, can have a much wider range of target-length-to-spacing ratios, and can be either white or black in intensity.

In an expanding-spot examination of a given point in a scene, the spot at the given point expands from a minimum to some maximum size. The overall light flux emitted by the expanding spot is constrained to remain constant throughout the variations in spot size. Both minimum and maximum sizes are dictated by the dimensions of the patterns that are to be recognized.

The time derivative of the expanding spot readout at a given point permits a spectral examination of the pattern existing at that point. For example, if it is assumed that at a given point the pattern is larger than the largest acceptable pattern size and therefore the largest spot size, as the spot expands at this point to its maximum size, the constant readout of this large pattern results in an essentially zero time derivative and the pattern is therefore rejected. On the other hand, an acceptable target pattern having

dimensions within the range of the two extreme expanding-spot sizes will exhibit time derivative peaks as the expanding spot intersects the target boundaries. Since the target is either brighter or darker than the surrounding background, the polarities of the edge gradients of a given target are alike and may be either positive or negative. Therefore, an acceptable pattern, all of whose edges are intersected by the expanding spot, may be recognized through the sum of the edge-contributed deviative peaks.

The filtering action has been described in terms of the intersection of the target edge by the expanding spot. Actually, the value of the derivative is a function of the change in the relative distribution of the boundary-divided high and low transmissivity areas as these areas are brought under the expanding spot. This dependence on the transmissivity of areas is an important difference since the determination of the dimensions of the target does not then depend on the prior detection of an edge, which is very difficult and in some cases introduces error.

2. FREQUENCY DOMAIN ANALYSIS OF TWO-SPOT SCANNER

The spectral filtering action of the expanding spot can be demonstrated through the frequency domain analysis of a two-spot scanner. The transfer function $F(\omega)$ of a circularly symmetrical spot of uniform intensity I and of radius R is given by

$$F(\omega) = (2\pi R^2)(I)\left[\frac{J_1(\omega R)}{\omega R}\right], \qquad (24)$$

where $J_1(\omega R)$ is the Bessel function of the first order.[6]

The spectral characteristics, $G(\omega)$, of the transfer function that originate in the difference between the readouts of two spots of radiuses R_1 and R_2 are

$$G(\omega) = I_1 2\pi R_1^2 \frac{J_1(\omega R_1)}{\omega R_1}$$

and

$$G(\omega) = I_2 2\pi R_2^2 \frac{J_1(\omega R_2)}{\omega R_2} .$$

If the total fluxes, C, of each of the two spots are equal,

$$2C = (2I_1)(\pi R_1^2)$$

$$= (2I_2)(\pi R_2^2) ,$$

an equivalent band pass filter is obtained whose transfer function becomes

$$G(\omega) = (2C)\left[\frac{J_1(\omega R_1)}{\omega R_1} - \frac{J_1(\omega R_2)}{\omega R_2}\right] . \qquad (25)$$

The band pass characteristics, $G(\omega)$, of such a two-spot time domain filter are plotted in Figure 20 for a pair of spots, of which the larger radius, R_2, is 10 times the smaller radius, R_1. The spectr- width, $\Delta\omega$, between the half-amplitude points of the two-spot transfer function is

$$\Delta\omega = \frac{21}{R_2} - \frac{2.3}{R_2}$$

$$= \frac{18.7}{R_2} \text{ radians per unit radius} . \qquad (26)$$

Since the band width of a two-spot transfer function is a function of the difference between the radiuses of the two spots, the derivative readout of an expanding spot, at a given value of R, should exhibit a very narrow band pass. Consequently, the derivative function over the entire expansion range of the spot should provide a picture of the spectral distribution of the examined pattern.

Since the filtering action of the expanding-spot scanner occurs in the time or space domain, it is more convenient to use a space rather than a frequency representation of the action. Such an analysis is presented in the next section for the normally encountered Gaussian spots.

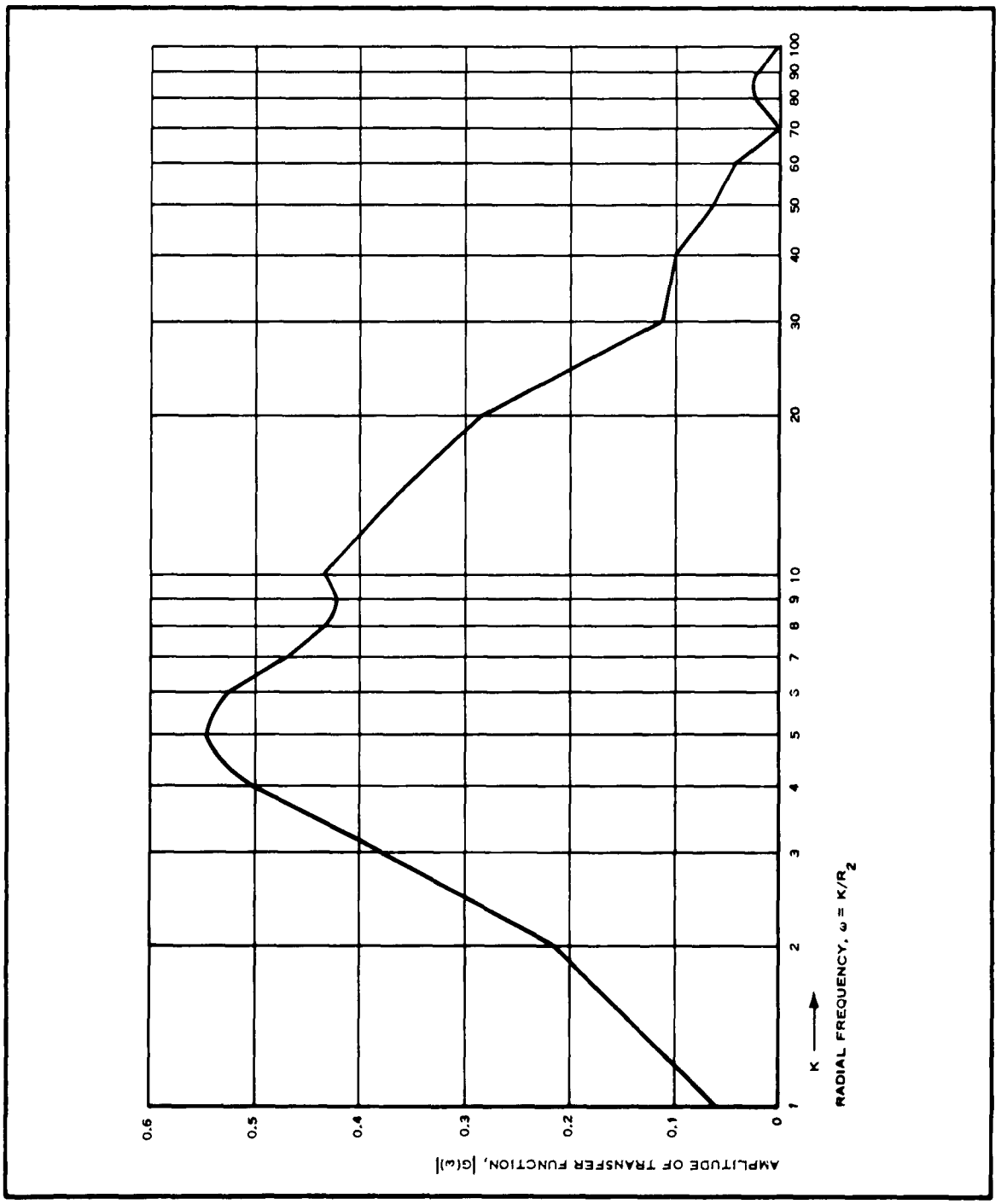

Figure 20 - Spectral Characteristic of Two-Spot Transfer Functions

3. TIME DOMAIN FILTERING OF TWO-BOUNDARY PATTERN

a. Preliminary Calculation of Single-Boundary Two-Level Pattern

The description of the filtering action of the expanding Gaussian spot is facilitated through solution of the light flux passed by a Gaussian spot through a two-level pattern area. The geometry of the problem is given in Figure 21. A two-level ($T_h = 1$, $T_L = 0$) target area is intersected by a spot that has a radius, R, of 3σ and whose azimuthally constant intensity, f(r), varies along its radiuses in accordance with the Gaussian distribution function

$$f(r) = e^{-4.5(r/R)^2} .$$

The boundary between the two target levels is separated along the x axis by a distance u from the center of the spot and is oriented at an angle α with respect to the vertical y axis. The portion of light flux, g, emitted by the spot and passed by the target, is transmitted through the shaded area of Figure 21, is defined by the target boundary and outer circumference of the spot, and has the value

$$g = \int_{\theta_L}^{\theta_h} \int_{R_h}^{R} e^{-4.5(r/R)^2} \, r \, dr \, d\theta \ , \qquad (27)$$

where R_h is the radial separation at a given angle θ between the center of the spot and the target boundary. The solution of the double integral (see Appendix C) is obtained through conversion of the exponential into a power series and yields

$$g(V) = I_o \frac{R^2}{4.5} \left[0.99 \cos^{-1} V + \sum_{n=1}^{\infty} \frac{(-4.5)^n}{n!} V^{2n} Z_{2n} \right] \qquad (28)$$

as a function of the dimensionless variable V, which is the normalized projected separation between the spot center and the target boundary, namely

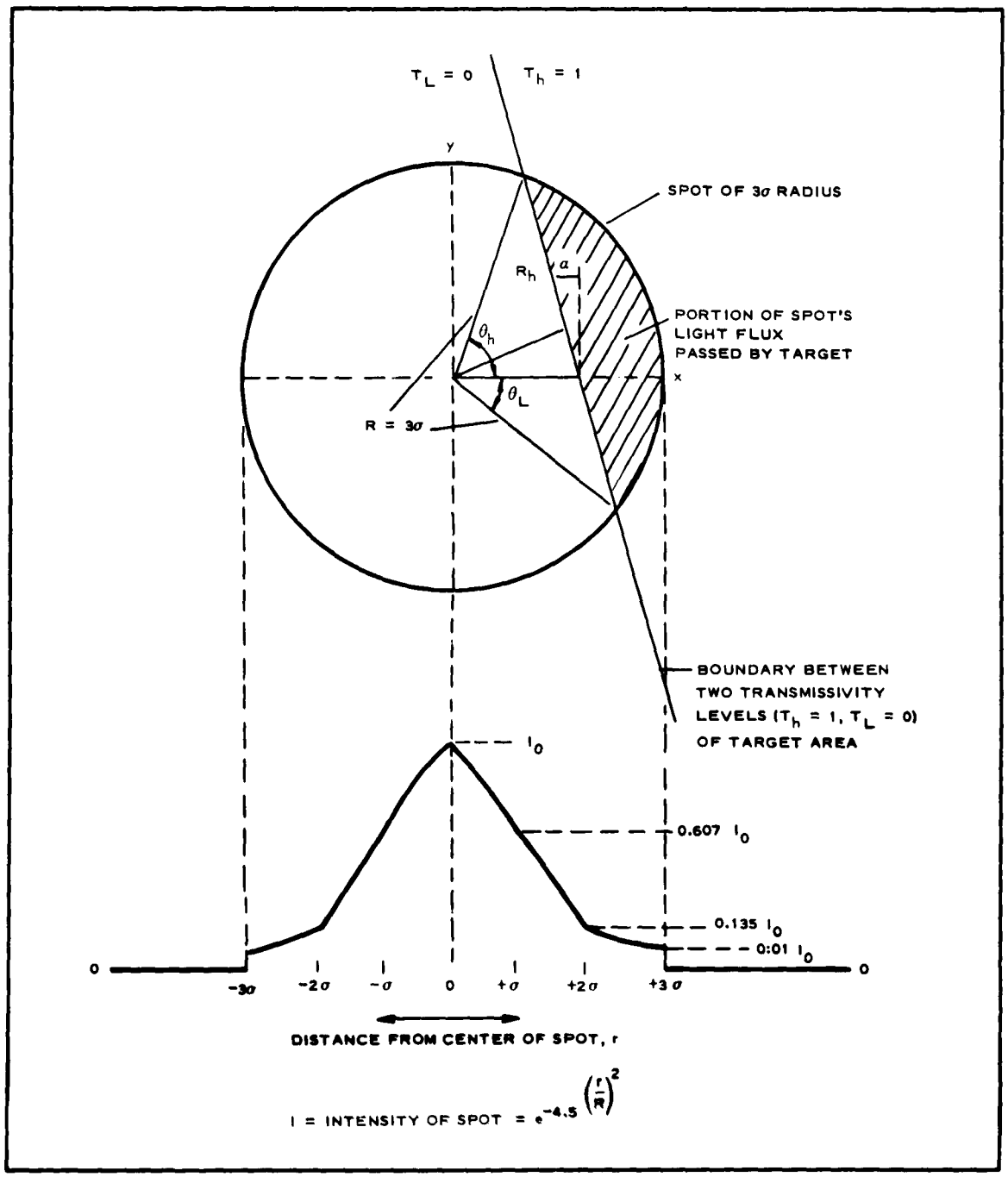

Figure 21 - Geometry of Intersection of Gaussian Spot with Two-Level Target Area

$$V = \frac{u}{R} \cos \alpha \quad . \tag{29}$$

The coefficients Z_{2n} are formed from a recursive series, also in terms of V, or

$$Z_{2n} = \frac{1}{2n - 1} \frac{\sin (\cos^{-1} V)}{(V)^{2n - 1}} + \left(\frac{2n - 2}{2n - 1}\right)(Z_{2n - 2}) \quad , \tag{30}$$

where

$$Z_2 = \tan(\cos^{-1} V) \quad .$$

The determination of the derivative output of an expanding Gaussian requires the derivative of the flux g(V) with respect to the separation variable V. The total flux, F, is obtained from Equation 28 at V = o, or

$$F = 2\Big[g(V)\Big] = \left(\frac{2I_o R^2}{4.5}\right)\left(\frac{\pi}{2}\right) \quad . \tag{31}$$

If, as the spot expands, the total spot flux, F, remains constant for all values of R (see item 2), the following equivalence exists:

$$\frac{I_o R^2}{4.5} = \frac{F}{\pi} \quad .$$

After this equivalence has been inserted into Equation 28 for the intersected flux, g(V), the derivative of the flux can be taken to yield

$$\frac{d\Big[g(V)\Big]}{dV} = \frac{F}{\pi}\left\{-\frac{1}{\sqrt{1 - V^2}} + \sum_{n=1}^{\infty} \frac{(-4.5)^n}{n!}\Big[(2n)(V)^{2n - 1}(Z_{2n}) + V^{2n} K_{2n}\Big]\right\} \quad . \tag{32}$$

The coefficients Z_{2n} are defined by Equations 30 and 31; the coefficients K_{2n} are the derivatives of the corresponding Z terms, or

$$K_{2n} = \frac{d(Z_{2n})}{dV}$$

$$= \left(\frac{-1}{V^{2n-2}}\right)\left[\frac{1}{(2n-1)(\sqrt{1-V^2})}\right] - \frac{\sin(\cos^{-1} V)}{V^{2n}} + \left(\frac{2n-2}{2n-1}\right)(K_{2n-2}) \quad , \tag{33}$$

where

$$K_2 = \frac{1}{V^2\sqrt{1-V^2}} \quad . \tag{34}$$

The values of g(V) and dg(V)/dV have been computed and are plotted in Figure 22. The second derivative, d^2g/dV^2, obtained approximately through successive differences of the first derivative function, is also plotted in Figure 22.

b. Readout of Target Patterns and First Two Derivatives

The readout, H, of a simple two-level (of transmissivities T_h and T_L) pattern whose boundary lies V_1 units from the center of the spot as in Figure 21 is in terms of the flux functions developed in Equations 28 through 31:

$$H = (T_h)\left[2g(o)\right] - (T_h - T_L)\left[g(V_1)\right] \quad . \tag{35}$$

The absolute value of the derivative of this flux with respect to R, the instantaneous radius of the spot, becomes

$$\left|\frac{dH}{dR}\right| = -\left|\Delta T\right|\left(\frac{\partial g}{\partial V}\right)\left(\frac{u_1 \cos\alpha}{R^2}\right) \quad , \tag{36}$$

since

$$\frac{\partial V}{\partial R} = -\frac{u_1 \cos\alpha}{R^2} \quad . \tag{37}$$

The required term $\left|\Delta T\right|$ represents the absolute difference between

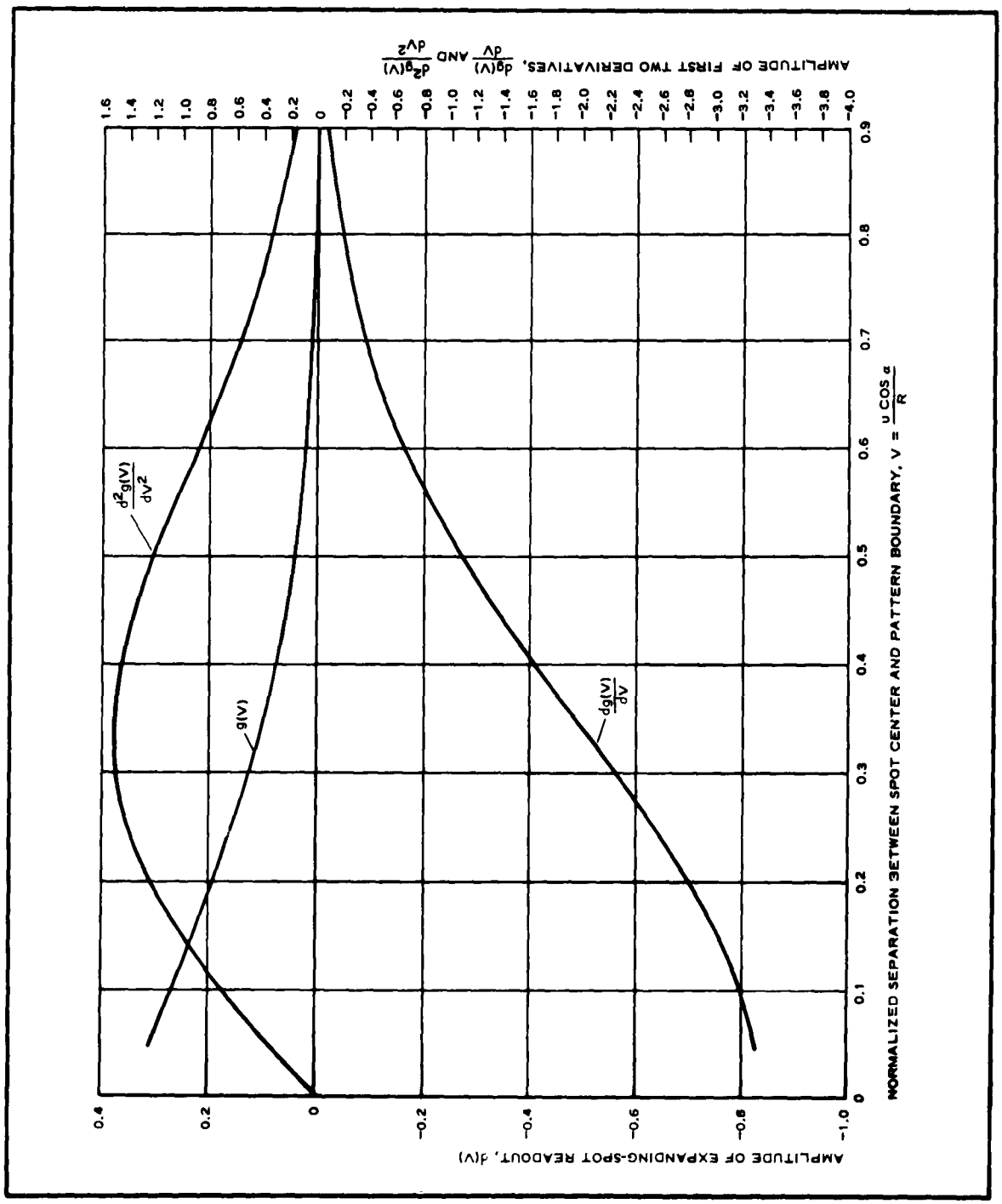

Figure 22 - Expanding-Spot Readout Functions

the transmissivities of the two pattern areas. Since it is desirable for the amplitude of the derivative to be independent of R, the derivative is modified through multiplication by R to become a function of V, or

$$R\left|\frac{dH}{dR}\right| = -\left|\Delta T\right|\left(\frac{dg}{dV}\right)(V) \quad . \tag{38}$$

This function, evaluated from the computed data of Figure 22 is plotted in Figure 23 for several separation distances ($u \cos \alpha / R_{min}$ = 1, = 3, and = 5) as a function of spot radius, R/R_{min}. The derivative peaks for the individual pattern boundaries have a constant amplitude and occur at a fixed value of V = 0.33, so that the value of the separation distance and consequently of the pattern widths is a known function of the spot's radius at which the derivative peak occurred. Thus, a peak of twice the plotted amplitude (approximately 0.35) will indicate the presence of a pattern that is defined by two boundaries that are placed symmetrically about the spot's center and are separated from one another by a distance of (2)(0.33)(R), where R is the spot's radius at which the peak occurred.

However, because the slow falloff from the derivative peak tends to blur the location of such a double peak, the design of a proper threshold-locating circuit would be very difficult. For this reason a modified second-derivative function is used, which is also multiplied by R to provide a V-dependent function; namely,

$$R\frac{d}{dR}\left|R\frac{dH}{dR}\right| = \left|\Delta T\right|\left[\left(\frac{d^2g}{dV^2}\right)(V^2) + \left(\frac{dg}{dV}\right)(V)\right] \quad , \tag{39}$$

which is obtained from Equations 37 and 38. The above second-derivative function is plotted in Figure 23 for the same separation distances used in computing the first-derivative data. The constant valued peaks of the second-derivative function occur at a fixed value of V = 0.625; because of the rapid falloff from the peak, their locations are much more sharply delineated.

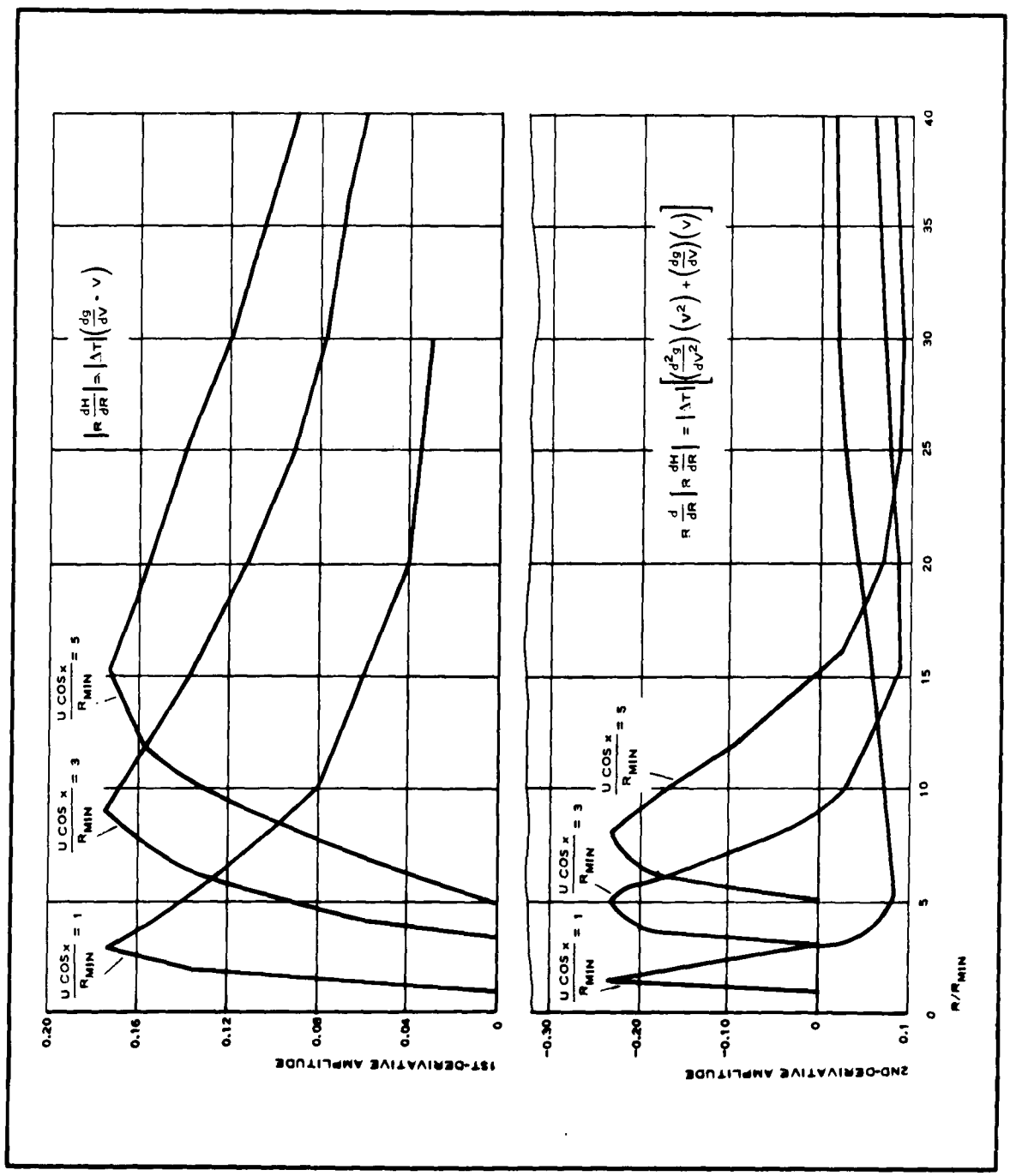

Figure 23 - First and Second Derivatives of Intersection of Expanding Spot with Single Boundary of Two-Boundary Pattern

c. Detection of Pattern Centroid

The location of a double-amplitude peak (approximately 0.45), which would mark the symmetrical location of the two boundaries of a pattern about the spot's center, is now much more sharply defined. Displacement of the pattern from the center of the spot is evidenced, for example, by the appearance of the first and second derivative curves (see Figure 23) for

$$\frac{u \cos \alpha}{R_{min}} = 1$$

and

$$\frac{u \cos \alpha}{R_{min}} = 3 \ .$$

Since the gradients of a given pattern will have the same polarity at each of the boundaries, these curves can be summed to give two peaks: the first, a single-amplitude second-derivative peak at

$$\frac{R}{R_{min}} = 1.5 \ ,$$

and the second, a very much reduced peak at

$$\frac{R}{R_{min}} = 5$$

because of the negative contributions of the first boundary. However, as the pattern is displaced toward the spot's center, a well-defined double-amplitude peak is generated.

d. Pattern Resolution and Duty Cycle Limitations

The use of the second-derivative function enhances the pattern resolution capability of the expanding spot. The spacing between two patterns is defined (see Figure 24) by the terminating boundary of the examined pattern and an oppositely polarized initial boundary of the next pattern. Since both these oppositely polarized boundaries occur on the same

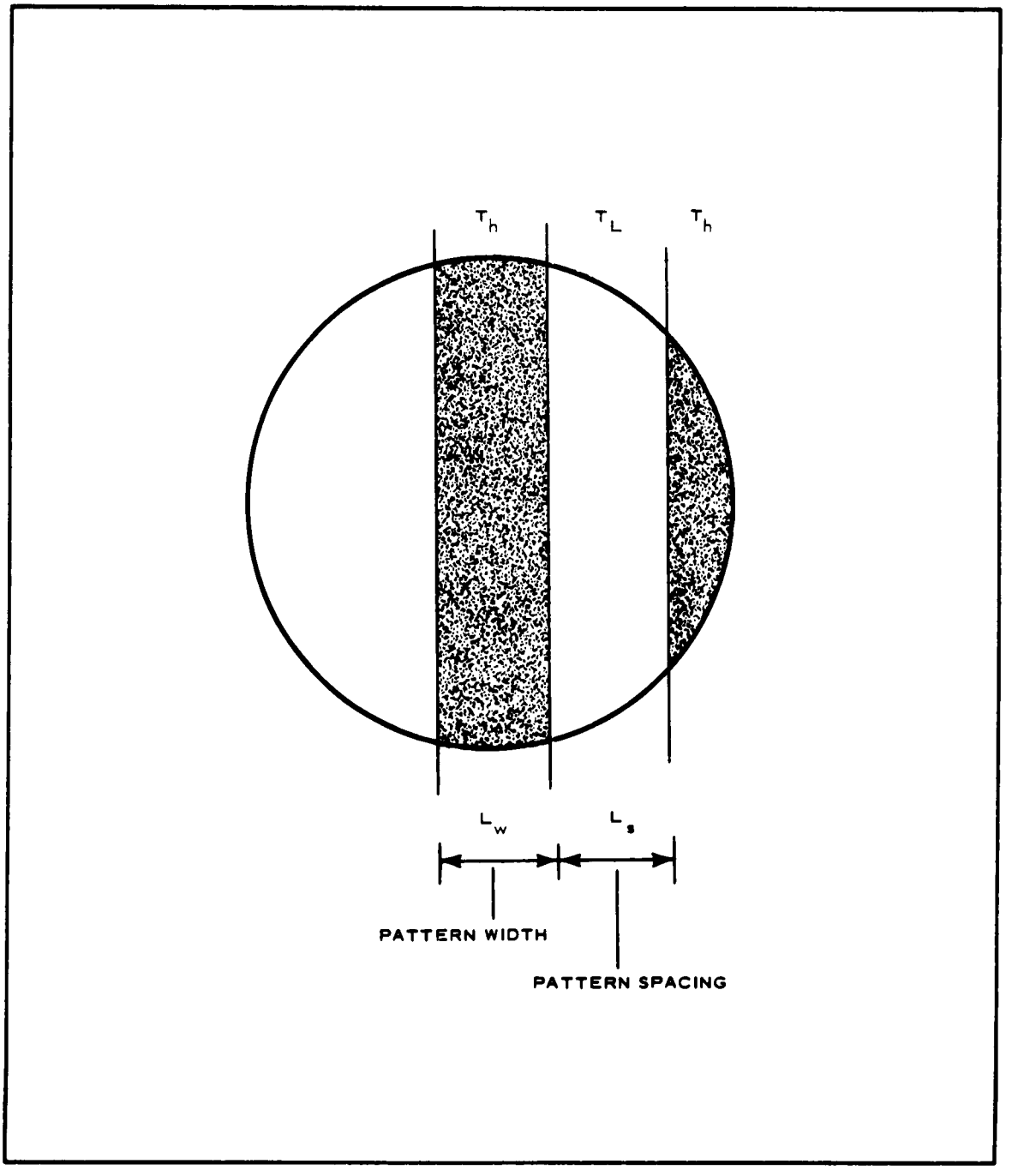

Figure 24 - Geometry of Pattern Spacing in Determining Minimum Detectable Pattern Resolution

side of the spot's center, their first-derivative contributions will subtract from one another. If the spacing between the two boundaries is not large enough, the required value for the second-derivative peak of the first boundary will not be reached and the pattern will not be detected.

The minimum resolvable spacing is determined from the value V = 0.625, which defines the location of the second-amplitude peak. The pattern width, L_w, (see Figure 24) associated with the double-amplitude second-derivative peak encountered at spot radius R, is

$$L_w = 2(0.625)R \quad .$$

With the minimum pattern spacing, L_s, required for the detection of this double-amplitude peak, at the above value of R the oppositely polarized terminal spacing boundary has not yet been intersected by the spot edge, or

$$\frac{L_w}{2} + L_s = R \quad .$$

The maximum duty cycle or the ratio of pattern width to period that can be handled by the expanding spot is therefore

$$\frac{L_w}{L_s + L_w} = \frac{1.25}{1.625}$$

$$= 0.77 \quad ,$$

which corresponds to a minimum spacing of approximately 3/8 of the pattern width. The maximum duty cycle of 0.77 is larger than that of the frequency domain filter (approximately 0.5). The signal energy obtained for duty cycles of less than 0.2 is very much reduced for the frequency domain filter, whereas in the expanding-spot filter all patterns having duty cycles of less than 0.77 can be readily detected. In fact, single isolated targets can be detected, whereas the frequency domain filter requires that the target pattern be a recurrent sequence of at least two targets.

4.. FILTERING OF FOUR-BOUNDARY PATTERN

a. General

The intersection of an expanding spot with the two boundaries of a pattern was discussed in item 3; presumably the other two boundaries fall outside the maximum dimensions of the spot. In some cases, where the patterns have lengths and widths of the same order of magnitude, all four boundaries will be intersected by the expanding spot. Such a situation is shown in Figure 25, where the y-oriented boundary is now assumed to include the two quadrature halves of the x-oriented boundaries. It is obvious that the contributions of two such boundary complexes will be somewhere between those obtained for two and for four single boundaries. The additional readout of such a pattern (compared with that obtained for a pair of single boundaries) is considered in the following p- agraphs.

The following problem simplifications have been made:

1. Quadrature-oriented boundaries are assumed. The resulting contribution is intermediate to that when the angle between the adjoining boundaries is either less than or greater than 90 deg.
2. The center of the spot is placed symmetrically between the two x-oriented boundaries. The solution obtained will thus represent the maximum contribution of the two additional boundaries.
3. Circular symmetry of the spot permits orientation of the boundaries so that they are parallel to the quadrature x and y coordinate axes.

b. Expanding-Spot Readout of Quadrature Boundary Complex

The single-boundary solution for g(V) considers the flux that intersects the pattern areas labeled A and B in Figure 25. A representation, h(V),

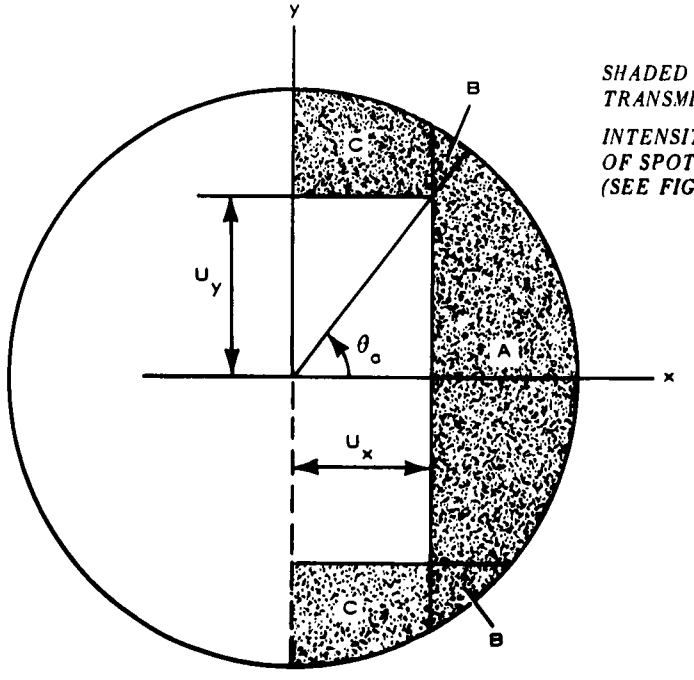

SHADED AREA HAS UNITY TRANSMISSIVITY

INTENSITY DISTRIBUTION OF SPOT IS GAUSSIAN (SEE FIGURE 21)

Figure 25 - Geometry of Four-Sided Pattern

for the desired four-boundary solution in terms of the expression for a single boundary, g(V), is then, from Figure 25,

$$h(V) = g(V) - 2B(V_x) + 2C(V_y) \quad . \tag{40}$$

The last two contributions from the areas labeled B and C in Figure 25 can be calculated in much the same manner as was used for g(V). (See Appendix C.) The expression for the B areas is

$$2B(V) = 2I_0 \int_{\theta_a}^{\theta_h} \int_{R_h}^{R} e^{-4.5(r/R)^2} \, r \, dr \, d\theta \quad , \tag{41}$$

in which the terms R_h and θ_h as for g(V), indicate respectively the radial separation distance to the y-oriented boundary and the maximum azimuthal angle associated with the y boundary. The azimuthal angle θ_a defines the point of intersection of the x- and y-oriented boundaries (see Figure 25). The representations of these terms are:

$$\left.\begin{aligned} \theta_h &= \cos^{-1}\left(\frac{U_x}{R}\right) \\ &= \cos^{-1}(V_x) \quad ; \\ \theta_a &= \tan^{-1}\left(\frac{U_y}{U_x}\right) \quad ; \end{aligned}\right\} \tag{42}$$

and

$$\left.\frac{R_h}{R} = \frac{V}{\cos\theta} \quad .\right\}$$

The solution of the double integral of Equation 41 permits

$$2B(V) = \frac{I_0 R^2}{4.5}\left\{(0.99)\left[\cos^{-1}(V) - \tan^{-1}\frac{U_y}{U_x}\right] + \sum_{n=1}^{n=\infty} \frac{(-4.5)^n}{n!} V^{2n} Z_{2n}^{B}\right\} . \tag{43}$$

The coefficients Z_{2n}^{B} are obtained from the recursive series

$$Z_{2n}{}^{B} = \left(\frac{1}{2n-1}\right)\left[\frac{\sin(\cos^{-1} V)}{V^{2n-1}} - \frac{\frac{U_y}{U_x}}{\cos^{2n-2}\tan^{-1}\frac{U_y}{U_x}}\right] + \left(\frac{2n-2}{2n-1}\right)\left(Z_{2n-2}{}^{B}\right), \tag{44}$$

where

$$Z_2{}^{B} = \tan(\cos^{-1} V) - \frac{U_y}{U_x} .$$

Similarly, the flux C(V) intersecting the area C is

$$2C(V_y) = 2I_0 \int_0^{\frac{\pi}{2} - \theta_a} \int_{R_h}^{R} e^{-4.5(r/R)^2} \, r \, dr \, d\theta , \tag{45}$$

where

$$V_y = \frac{U_y}{R}$$

and the other terms are as defined in Equation 42. The solution of the integral, as before, permits

$$C(V_y) = \frac{I_0 R^2}{4.5}\left\{(0.99)\left[\frac{\pi}{2} - \tan^{-1}\left(\frac{U_y}{U_x}\right)\right] + \sum_{n=1}^{n=\infty} \frac{(4.5)^n}{n!}(V_y)^{2n} Z_{2n}{}^{C}\right\} . \tag{46}$$

The coefficients $Z_{2n}{}^{C}$ are defined by

$$Z_{2n}{}^{C} = \left(\frac{1}{2n-1}\right)\left[\frac{\frac{U_x}{U_y}}{\sin^{2n-2}\left(\tan^{-1}\frac{U_y}{U_x}\right)}\right] + \left(\frac{2n-2}{2n-1}\right)\left(Z_{2n-2}{}^{C}\right), \tag{47}$$

where

$$Z_2{}^C = \frac{U_x}{U_y} \quad . \tag{48}$$

The combined contributions of the two additional terms (Equations 46 and 43) are

$$2C(V_y) - 2B(V_x) = \frac{I_0 R^2}{4.5}\left\{(0.99)\left[\frac{\pi}{2} - \cos^{-1}(V_x)\right] + \sum_{n=1}^{n=\infty}\left[\frac{(-4.5)^n}{n!}V_x{}^{2n}\right]\left[\left(\frac{U_y}{U_x}\right)^{2n}\left(Z_{2n}{}^C\right) - Z_{2n}{}^B\right]\right\} . \tag{49}$$

The rate of change of the flux (Equation 49) with respect to the separation variable V_x, when the ratio U_y/U_x and the spot's flux F of Equation 31 remain constant, is

$$\frac{d\left[2C(V_y) - 2B(V_x)\right]}{dV_x} = \frac{F}{\pi}\left(0.99\frac{1}{\sqrt{1 - V_x{}^2}} + \sum_{n=1}^{n=\infty}\frac{(-4.5)^n}{n!}\left\{2nV_x{}^{2n-1}\left[\left(\frac{U_x}{U_y}\right)^{2n}\left(Z_{2n}{}^C\right) - Z_{2n}{}^B\right] + \left(V_x{}^{2n}\right)\left[\left(\frac{U_y}{U_x}\right)^{2n}\left(K_{2n}{}^C\right) - K_{2n}{}^B\right]\right\}\right) , \tag{50}$$

where

$$\left.\begin{aligned} K_{2n}{}^C &= \frac{d}{dV_x}\left(Z_{2n}{}^C\right) , \\ K_{2n}{}^B &= \frac{d}{dV_x}\left(Z_{2n}{}^B\right) , \\ K_2{}^C &= 0 , \end{aligned}\right\} \tag{51}$$

and

$$K_2{}^B = -\frac{1}{V_x{}^2\sqrt{1 - V_x{}^2}} . \qquad (51)$$

Equations 49 and 50 were computed for values of U_y/U_x = 1, 1.5, 2, and 4. Numerical solutions of the second derivative were obtained by taking successive differences of the first-derivative values. The combined sums of the computed quantities and the corresponding values of h(V), dh(V)/dV, and $d^2h(V)/dV^2$ are plotted, respectively, in Figures 26, 27, and 28.

Finally, expanding-spot second-derivative readout signals of the double-quandrature boundaries are plotted in Figure 29 for a separation distance, U_x/R_{min} = 5, and above separation distance ratios U_y/U_x = 1, 1.5, 2, and 4. As in the case of the single boundary, the second derivative signal is

$$R\frac{d}{dR}\left|R\frac{dH'}{dR}\right| = |\Delta T|\left[\left(\frac{d^2H}{dV^2}\right)(V^2) + \left(\frac{dg}{dV}\right)(V)\right] . \qquad (52)$$

The curves for h(V) and its derivatives (Figure 26, 27, and 28) show that as the separation distances ratio U_y/U_x increases, the effects of the additional x-oriented boundaries, since their separation distance U_y is so much larger than U_x, are not felt until the spot becomes larger or the value of $V = U_x/R$ decreases. For example, when U_y/U_x = 2, the additional x-oriented boundary does not influence the readout until a spot size equal to V = 0.625 is attained; and for U_y/U_x = 4, a value of V = 0.25 is necessary.

This situation is reflected in the expanding-spot readout signal of Figure 29. Since the second derivative peak occurs at V = 0.6 and the entire positive loop returns to zero at V = 0.33, the first case, U_y/U_x = 2, attains the same valued peak, 0.225, as did the single boundary (see Figure 23) but did change the remainder of the positive loop, while the second case, U_y/U_x = 4, has no effect whatsoever upon the

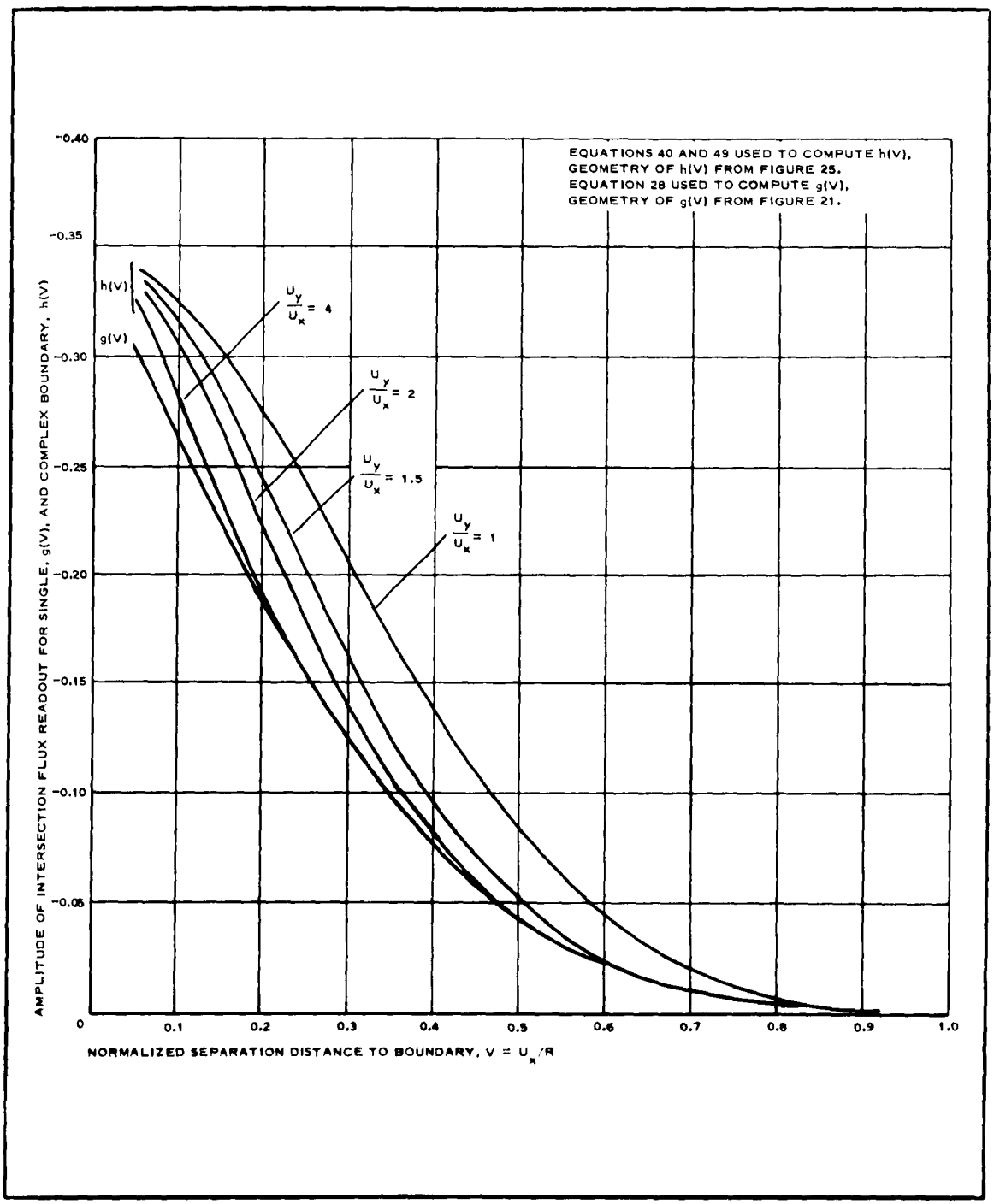

Figure 26 - Comparison of Readout of Single and Quadrature Boundaries

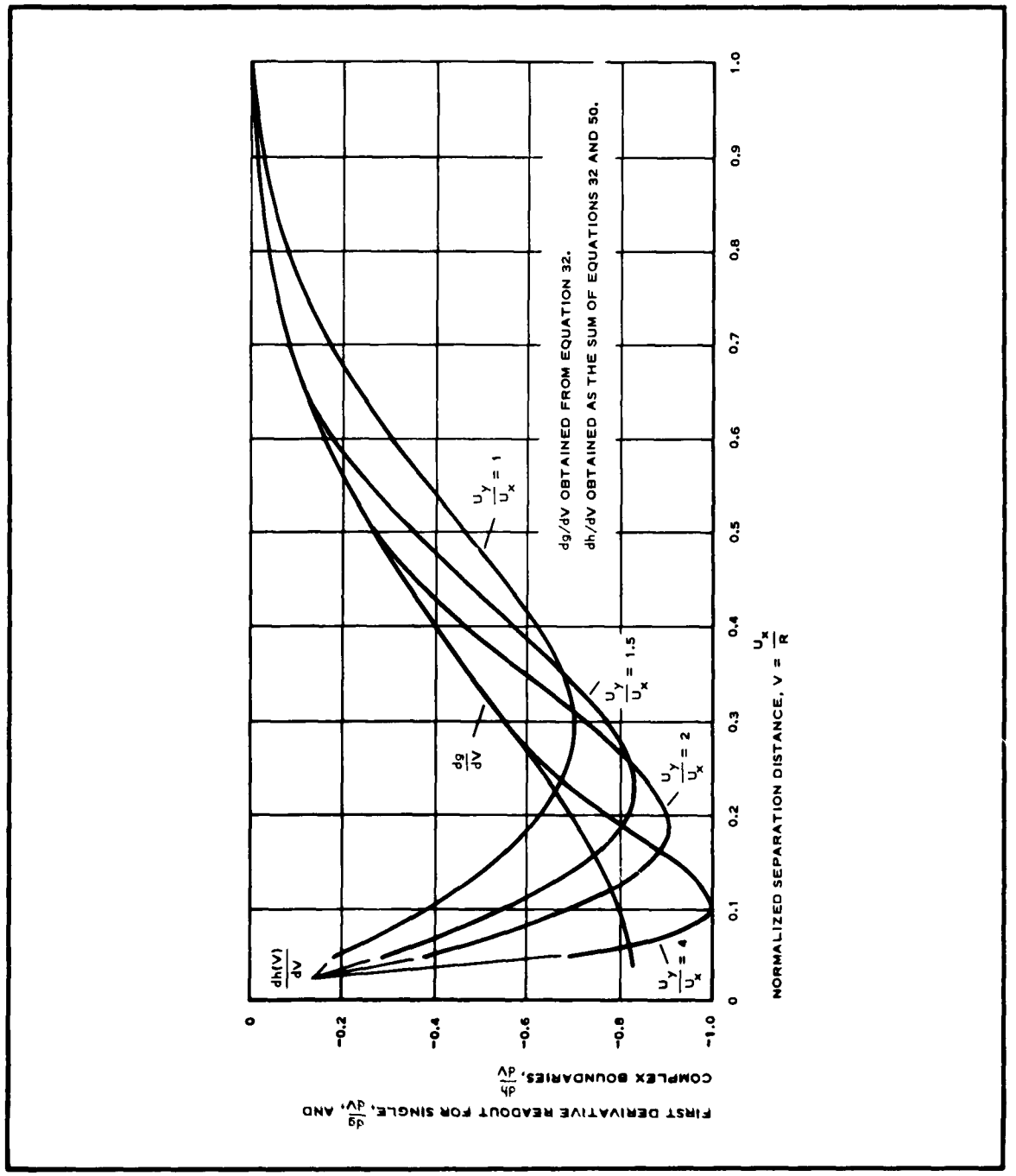

Figure 27 - Comparison of First-Derivative Readout of Single- and Double-Quadrature Boundaries

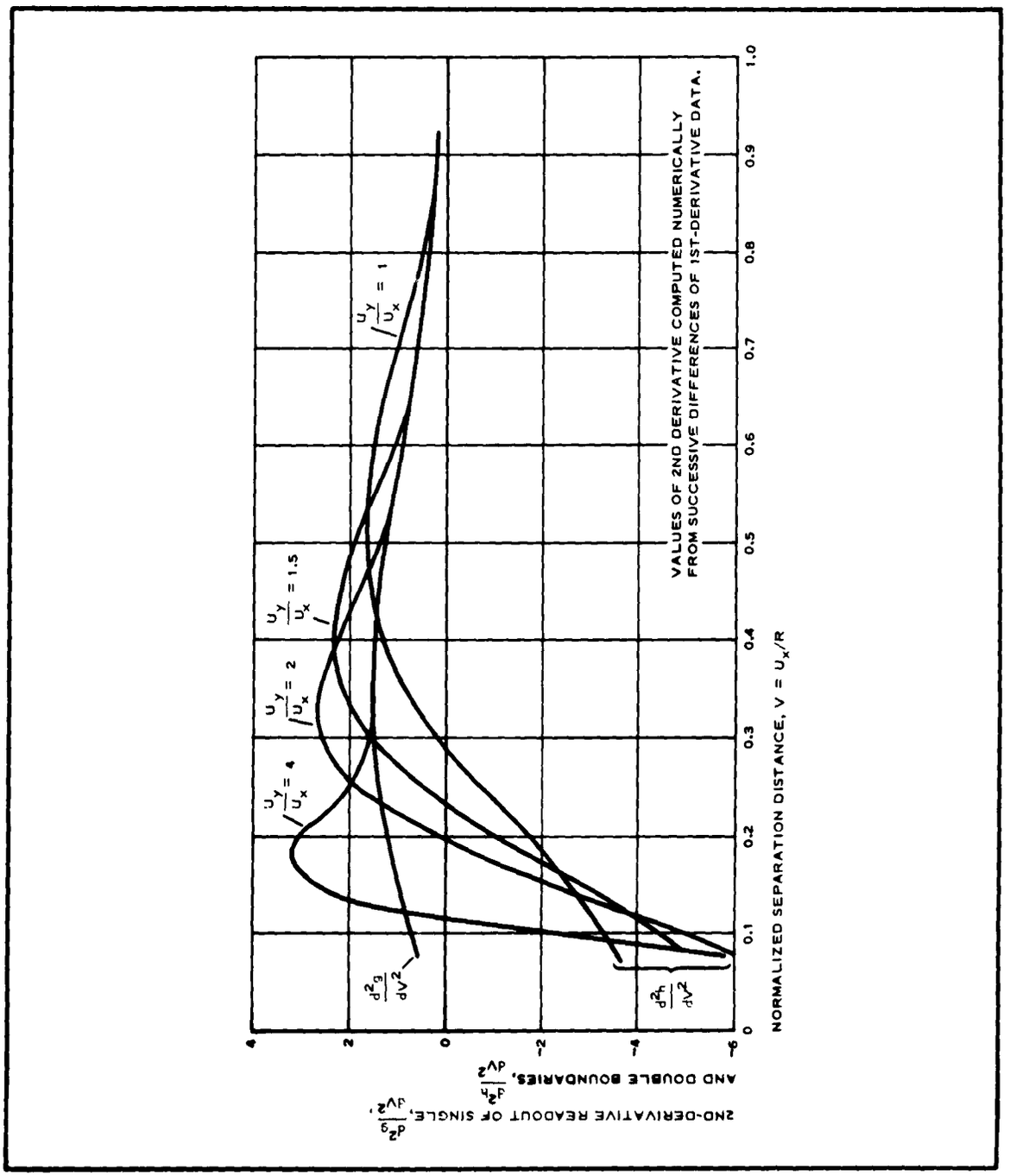

Figure 28 - Comparison of Second-Derivative Readout of Single- and Double-Quadrature Boundaries

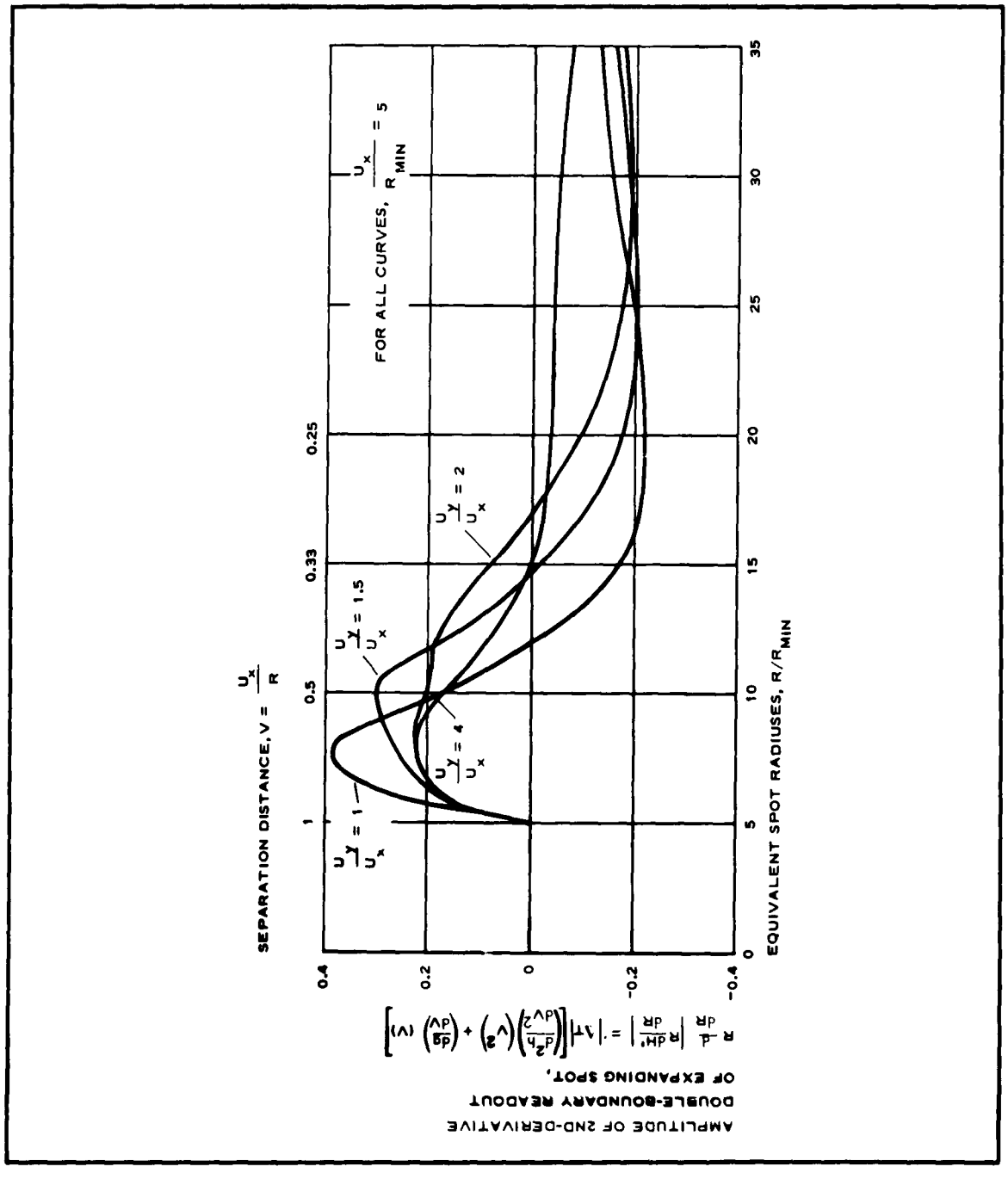

Figure 29 - Expanding-Spot Readout Signal of Double-Quadrature Boundaries

loop. As might be expected, the peak for the quadrature boundaries defined by $U_y/U_x = 1$ is almost twice as large as that for the single boundary; and for $U_y/U_x = 1.5$ the peak is reduced to almost 1.5 times that of the single boundary.

c. Detection of Four-Boundary Pattern

The readout signal for an entire rectangular pattern whose four boundaries correspond to two-quadrature boundary pairs of Figure 25, is therefore twice the corresponding quadrature signal, examples of which appear in Figure 29. If both the second-derivative peak and the integral of the positive second-derivative loops are examined, reliable identification of four-boundary patterns can be achieved for cases in which the pattern length-to-width ratio does not exceed 1.5 or perhaps 2.

It should be noted that although the preceding analyses of the two- and four-boundary output signals were based on straight boundaries, detection is possible for irregularly shaped patterns or blobs - as long as they possess the proper aspect ratio - as well as for straight-sided patterns. This arises because of the circular symmetry of the spot and the fact that the signal is a function of the pattern area as well as of the boundary.

5. NORMALIZATION OF PATTERN TRANSMISSIVITIES

The output signals (Equations 39 and 52) for both two- and four-boundary patterns are functions of the transmissivity difference as well as of the boundary geometry. The removal of the pattern-to-pattern variations in transmissivity difference is required so that the output signal will reflect only differences in boundary geometry. The required transmissivity normalization at each point can be achieved through utilization of readout information of the expanding spot for a finite distance prior to the given point; or, if a combined flying-spot and expanding-spot scan is used, the

pattern transmissivity difference information will be available from the prior flying-spot scan.

6. FILTER PROCESSING TIME

A very rapid rate of spot expansion is desirable to minimize processing time; however, the rate must be sufficiently slow to permit the second-derivative output signal (Figure 23) to meet the band width limitations of the amplifier. In addition, a constant rate of spot expansion, adjusted to accommodate the smallest expected target size, is required so that the time derivative that is actually obtained is equivalent to the desired derivative, which is to be taken with respect to the spot's radius.

Under these conditions, the detection at a given point of a 10-to-1 range of possible target sizes will, for a 1-mc band width, require approximately 45 μsec. The time required for a complete point-by-point examination of a given frame will not permit real-time processing of the data.

A hybrid scan, utilizing a conventional flying-spot scan in addition to the expanding-spot scan, is therefore suggested to obtain faster processing.

The conventional flying-spot scan would locate on a one-dimensional basis those patterns whose widths fall within the allowable range, as well as the centroids of these patterns. The expanding-spot scan would then examine at the centroidal point the acceptability of the pattern on a two-dimensional basis. This eliminates the time-consuming examination by the expanding-spot scan at all those points that neither belong to an accepted pattern nor, if they do belong, are the proper centroidal point. An additional time saving is realized if the range of the spot's expansion is restricted to match the pattern width, as measured by the prior flying-spot scan.

7. CONCLUSIONS

An expanding-spot scanner was investigated that utilizes the second derivative of the readout of an expanding cathode ray tube spot to detect the presence of two boundaries, whenever their separating distance lies within a

given range and the pattern defined by the boundaries has an aspect ratio greater than two. In addition, the expanding-spot scanner can detect four-boundary patterns if their aspect ratios are less than two and their dimensions lie within the allowable range. Equations have been developed and computed that describe the action of the expanding spot and predict the results obtained with two- and four-boundary patterns.

Some advantages and characteristics of the expanding-spot scanner in the enhancement and recognition of two- and four-boundary patterns are:

1. Because of the spot's circular symmetry, knowledge of the pattern's orientation is not necessary.
2. The centroid point and the separating distance between boundaries of a given pattern are obtained from the expanding-spot scan, so that the pattern can be reproduced at a monitor or storage tube for further processing.
3. The detection of acceptable patterns is based on the examination of the entire pattern area as well as of the gradient at its edges.
4. Since the recognition and detection decision depends in part upon an absolute-valued derivative of the expanding spot, the target-to-background transmissivity difference can be of either polarity.
5. Pattern detection by an expanding-spot scan requires no definite shape characteristics except that their approximate dimensions and aspect ratios be within an acceptable range, which is of great advantage in low-resolution sensors that have no definite pattern shape available.

A hybrid scan, in which a conventional flying-spot scan precedes the expanding-spot scan, is introduced to decrease the time of the filtering process.

SECTION III - ANALYTICAL STUDY OF PATTERN ATTRIBUTES

Subsection Five - Summary and Conclusions

A study has been made in the frequency and time domains to uncover new pattern-describing attributes that can be applied to pattern recognition.

The frequency domain study was oriented toward providing a unique spectral energy attribute that would describe the multiple patterns of, for example, an industrial complex or urban area. Results of the study indicated that the most useful spectral density attributes were associated with a repetitive sequence of patterns that have a duty cycle of 0.3 to 0.5 (i.e., the pattern-to-spacing ratio varies from slightly less than unity to unity) and that have a positive polarity (white on black background).

The distribution of oil tanks in a petroleum refinery has been shown to possess such characteristics and therefore is amenable to a filtering process that would take advantage of the unique spectral energy content of oil tanks. Accordingly, an omnidirectional filter, to be used with a coherent optical channel, was designed to accommodate the oil tank distribution data.

The time domain study was initiated to overcome some of the geometrical restrictions of frequency domain filtering. An expanding-spot scanner was introduced that utilizes a modified second-derivative readout of an expanding crt spot to detect those four-boundary patterns that have a unity or slightly larger length-to-width ratio and the two opposing boundaries of those patterns that have a much-larger-than-unity length-to-width ratio. With this scanner, the pattern sequence need not be recurrent and can have a maximum pattern-to-spacing ratio of almost 3 to 1, and the individual patterns can be either black or white in intensity. Equations have been developed and computed that describe the action of the expanding spot and that predict the results obtained with two- and four-boundary patterns. These calculations permit evaluation of the minimum

and maximum spot sizes of the expanding-spot scan. Finally, a two-stage hybrid scan, consisting of a flying-spot scan followed by an expanding-spot scan, is introduced to decrease the processing time required when only the expanding-spot scan is used.

SECTION IV - EXPERIMENTAL EVALUATION OF CORRELATION TECHNIQUES

Subsection One - General

Three experimental laboratory studies were made of correlation techniques. The first was a general study of the correlation function of aircraft runways and various templates.

The second was directly related and was a natural follow-on to the first. A precision crosscorrelator generated the correlation functions of many targets and a rectangular slit. The second derivative of the correlation function was obtained by an analog computer and is shown to be an index or attribute by which straight-line patterns can be detected.

During the third study, instrumentation was developed that extracts straight-line patterns from aerial photographs by measuring edge gradient and pattern width attributes.

SECTION IV - EXPERIMENTAL EVALUATION OF CORRELATION TECHNIQUES

Subsection Two - Study of Correlation Functions with Correlograph

1. GENERAL

The correlograph is an optical device that produces an image of a two-dimensional correlation function on a photographic plate. It is an excellent means of examining the correlation function of two images since the entire function is visible and one-dimensional slices can be obtained with a microdensitometer.

The successful application of correlation techniques to target recognition requires the selection of appropriate templates and the measurement of pertinent characteristics of the correlation function. This section describes the study of these two factors in the recognition of airport runways.

To meet the objectives indicated above, the study was carried out as follows.

1. Nine aerial photographs were selected for analysis by the correlograph; four contained airfields and five did not.
2. Five templates were prepared to be used as references; these were templates of the airfields (runways, adjacent taxi strips, and parking areas) of each scene and a template of an average runway.
3. With the correlograph, two-dimensional correlation

functions (correlograms) of runway scenes and non-runway scenes with the templates were obtained.

4. For evaluation a trace was obtained by scanning the correlograms with a Leeds and Northrup micro-densitometer.

2. THEORY OF LENSLESS CORRELOGRAPH

A simplified diagram of the lensless correlograph is shown in Figure 30. Plane A is a transparency of the scene to be analyzed. In this experiment the scene is an aerial photograph that either does or does not contain an airfield complex. Plane B, located at a distance a from Plane A, contains the reference scene. The reference can be a duplicate of the scene, if the autocorrelation surface is desired, or any pattern to be correlated with the scene. In the experiment, two reference scenes were used: (1) a template containing the runway configuration, taxi strips, administration building, etc., and (2) a template containing a rectangle that represents the most frequently occurring runway size.

Plane C, located at a distance b from Plane B, is either a photographic plate or a ground glass screen for viewing the correlogram. Planes A, B, and C are parallel to each other and the scene (Plane A) is back-lighted by a diffused light source.

The scale factor between the scene (Plane A) and the reference (Plane B) is given by

$$k = \frac{b}{a + b} .$$

For this experiment, a = b = 15 in. Therefore, k = 1/2 and the scale of the reference is 1/2 times the scale of the scene.

The relationship between the coordinates x, y and x', y' can be written as

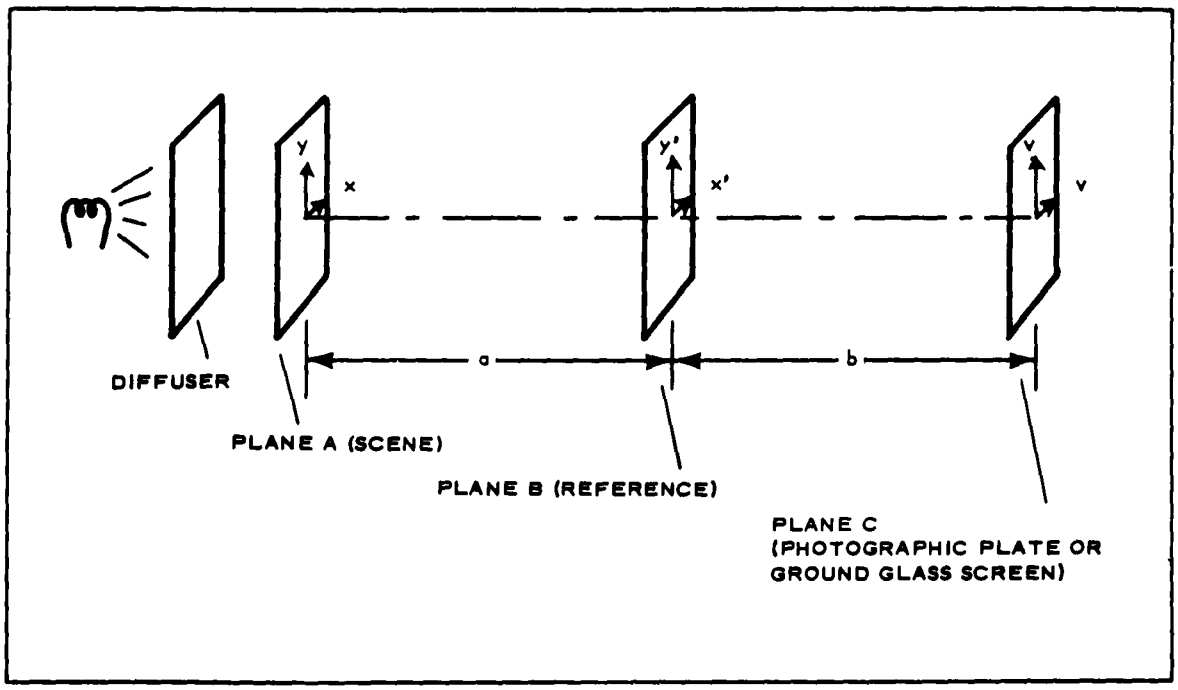

Figure 30 - Lensless Correlograph Arrangement

$$x' = kx$$

and

$$y' = ky \ .$$

If the function of the scene is $T_1(x, y)$ and the function of the reference is $T_2(x', y')$ where $0 \leq T \leq 1$, then the light value of the screen, $\phi(u, v)$, is

$$\phi(u, v) = \int\int T_1(x, y) T_2\left(x + \frac{a}{b} u,\ y + \frac{a}{b} v\right) dx\, dy \ .$$

In this case, since a = b,

$$\phi(u, v) = \int\int T_1(x, y) T_2(x + u,\ y + v)\, dx\, dy \ ,$$

which is the correlation surface obtained by correlating the scene with

the reference. The correlograph provides the total correlation surface, which then can be traced in any desired direction.

3. DESCRIPTION OF STUDY

Nine near-vertical aerial photographs covering various areas of the United States were selected for this study. Four of these photographs contain airfields, five do not. These photographs, their correlograms, and microdensitometer traces are shown in Figures 31 through 52.

Table VI identifies the photographs.

TABLE VI - AERIAL PHOTOGRAPH IDENTIFICATION FOR EXPERIMENTAL EVALUATION

Scene	Code no.	Figure no.
Vandenberg AFB	T-1	31
Dallas NAS	T-3	34
Luke AFB	T-4	37
Carswell AFB	T-2	40
Ft. Worth, Dallas area	T-12	43
Ft. Worth, Dallas area	T-15	45
Florida coastal area	T-11	47
Ft. Worth, Dallas area	T-21	49
Phoenix area	T-10	51

Each of these scenes was photographed on 3-1/4- by 4-1/4-in., continuous-tone, K-33 glass plates. A scale of 1 to 60,000 was used for all scenes. The runway scenes were selected so that they contained a variety of backgrounds and two or more runways oriented in different directions. Four of the five nonrunway scenes are of areas that do not include runways; however, they contain runway-like patterns such as highways, streets, and rivers. Only Scene T-21 (Figure 49) does not contain targets of the

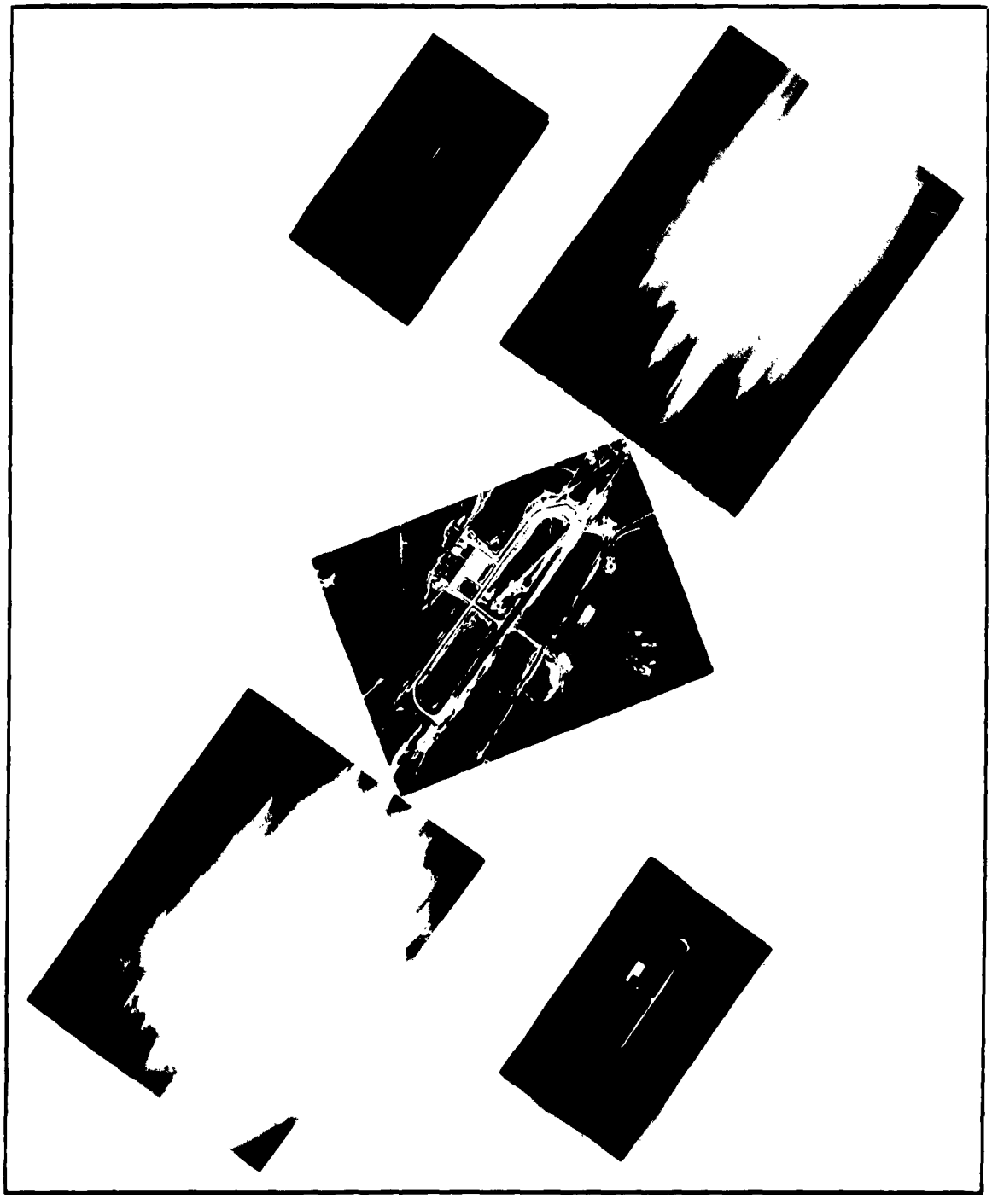

Figure 31 - Runway Scene T-1

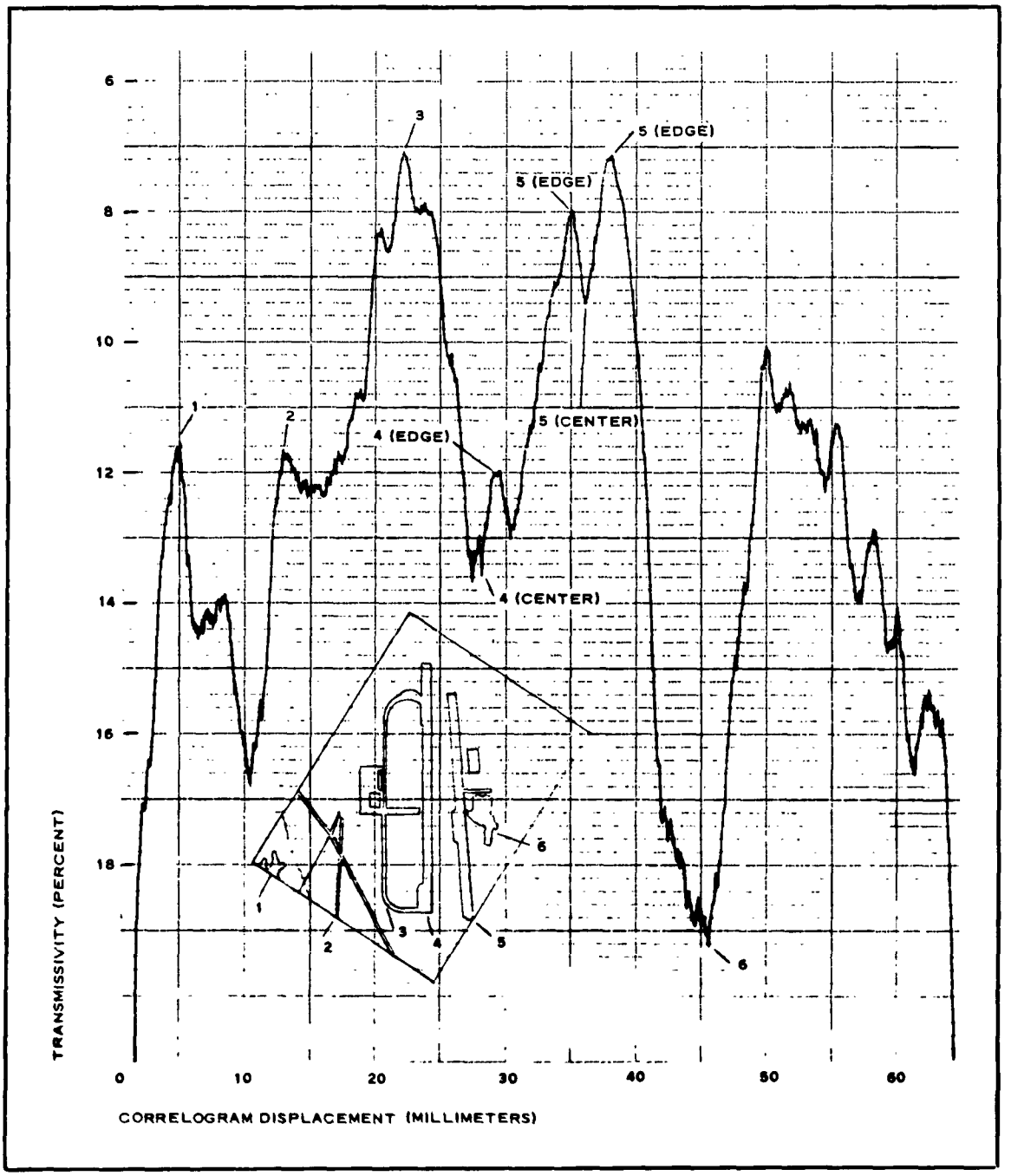

Figure 32 - Microdensitometer Trace of Scene T-1 and Template No. 5 Correlogram

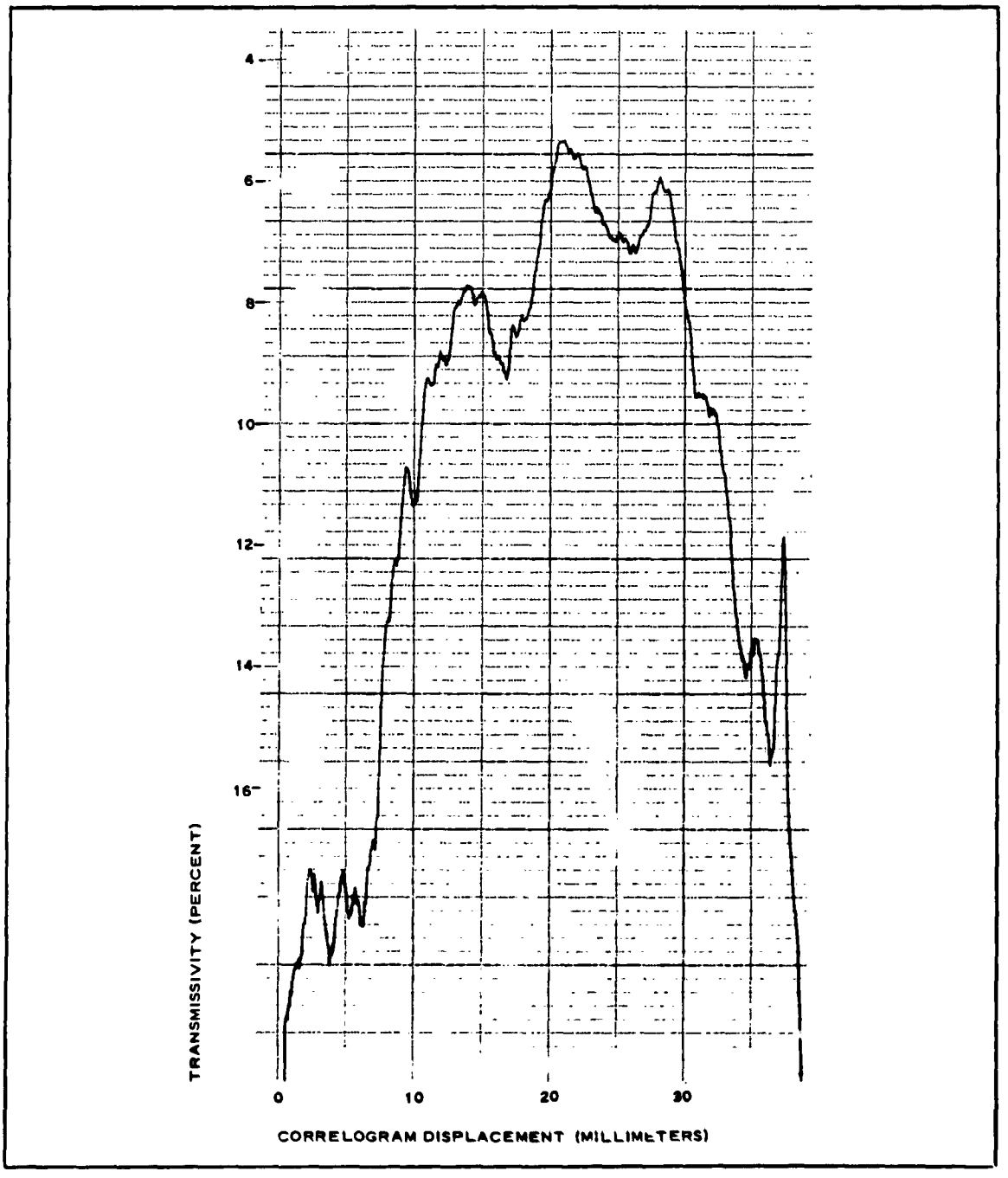

Figure 33 - Microdensitomenter Trace of Scene T-1 and Template No. 1 Correlogram

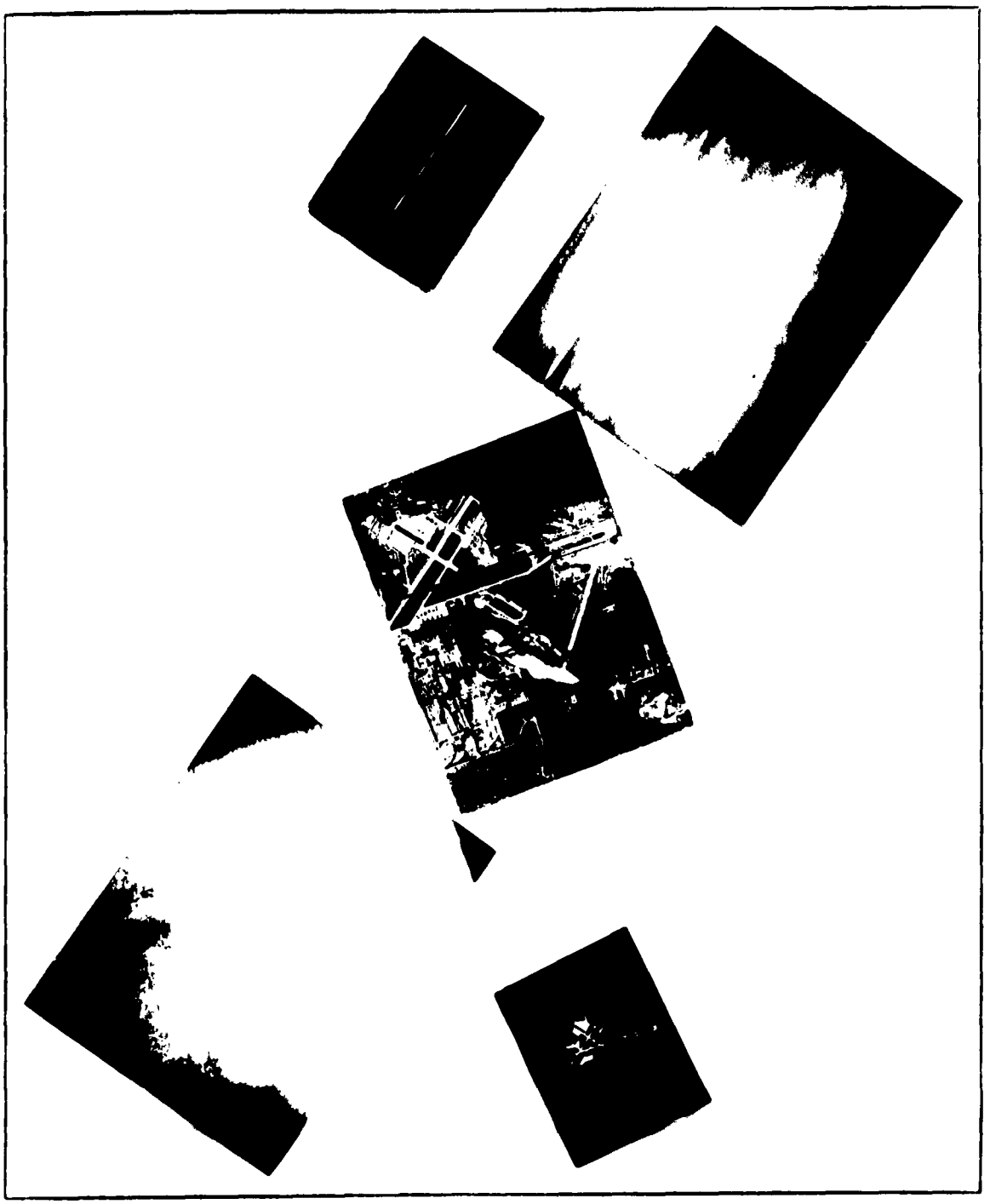

Figure 34 - Runway Scene T-3

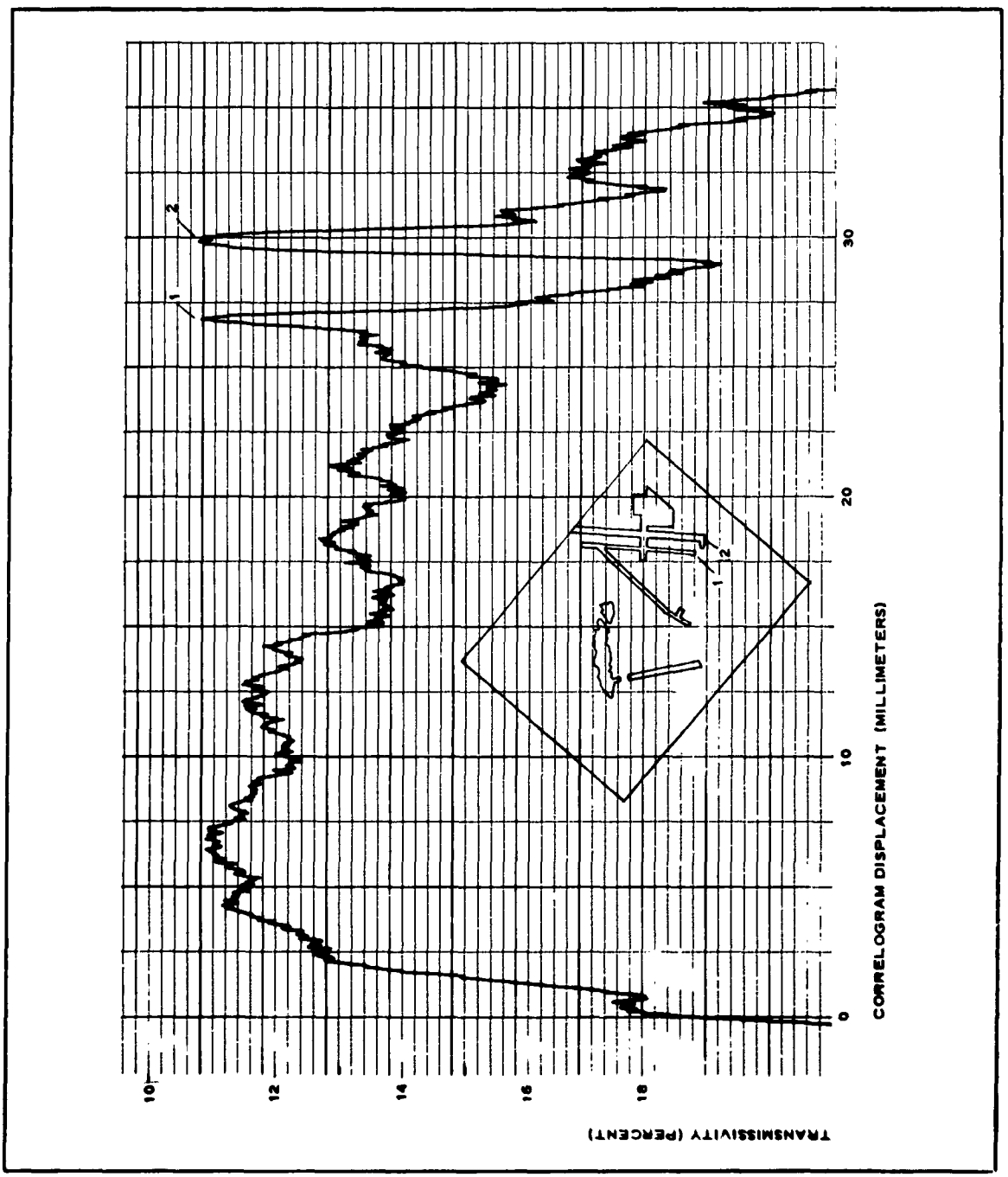

Figure 35 - Microdensitometer Trace of Scene T-3 and Template No. 5 Correlogram

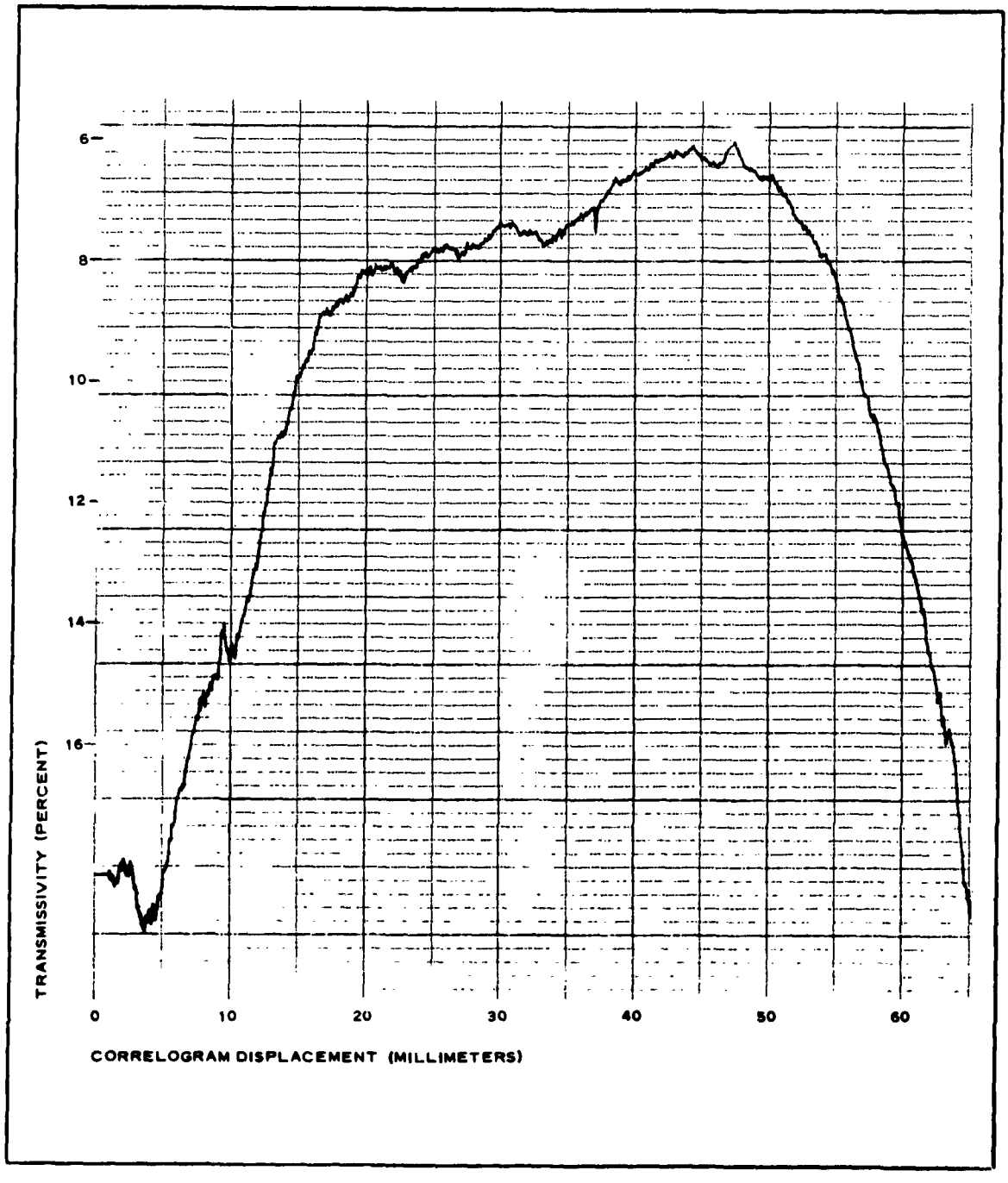

Figure 36 - Microdensitometer Trace of Scene T-3 and Template No. 2 Correlogram

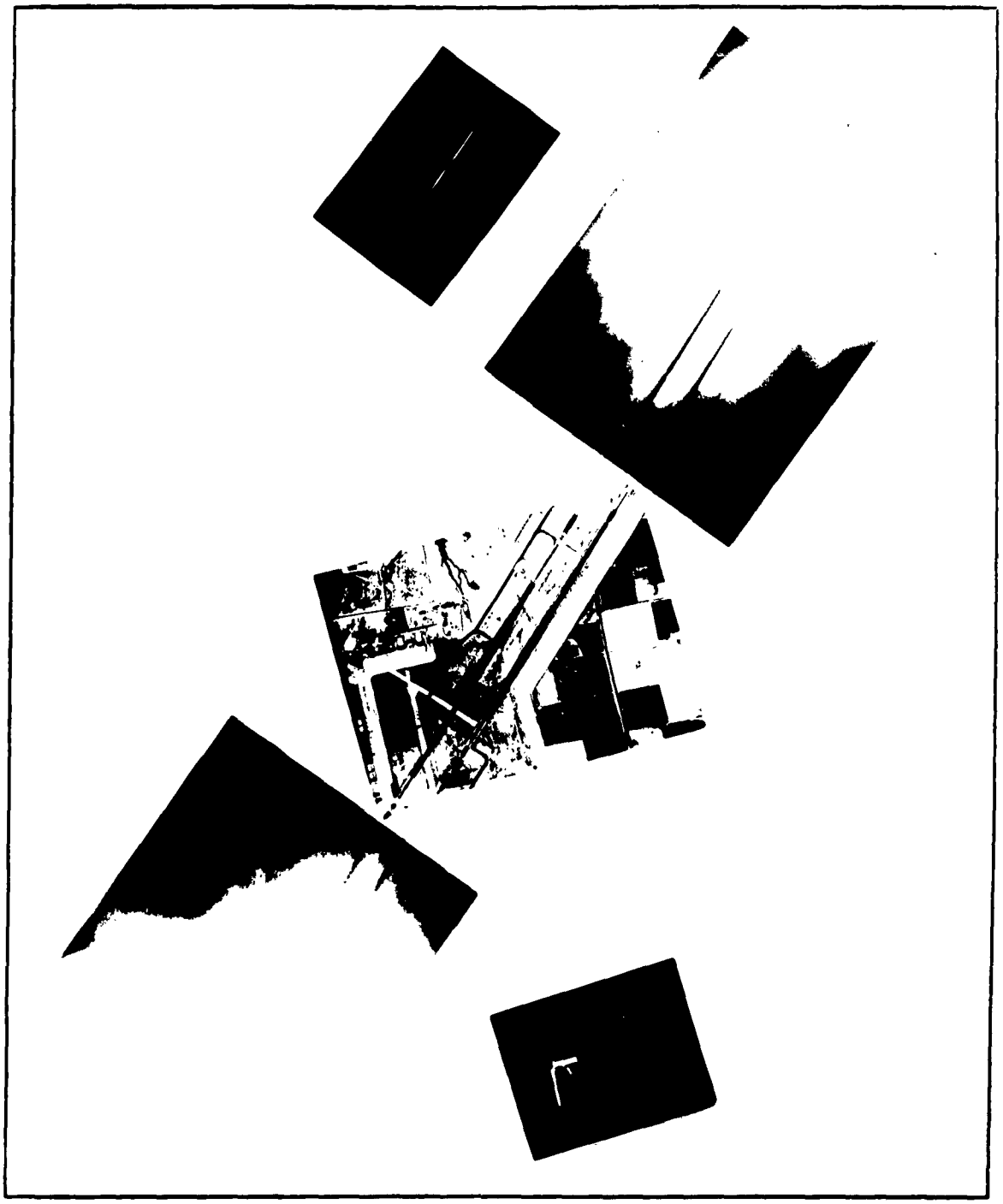

Figure 37 - Runway Scene T-4

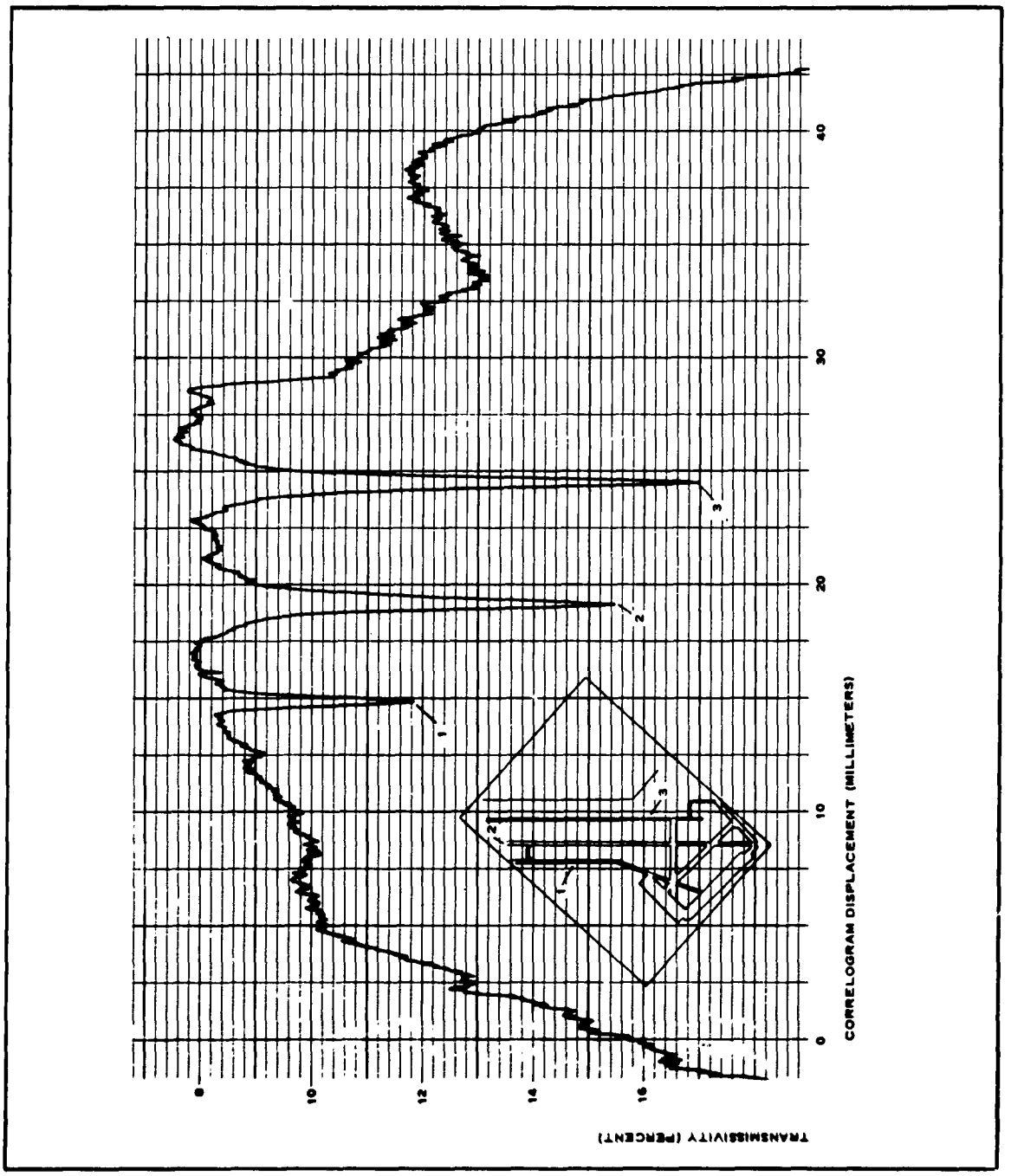

Figure 38 - Microdensitometer Trace of Scene T-4 and Template No. 5 Correlogram

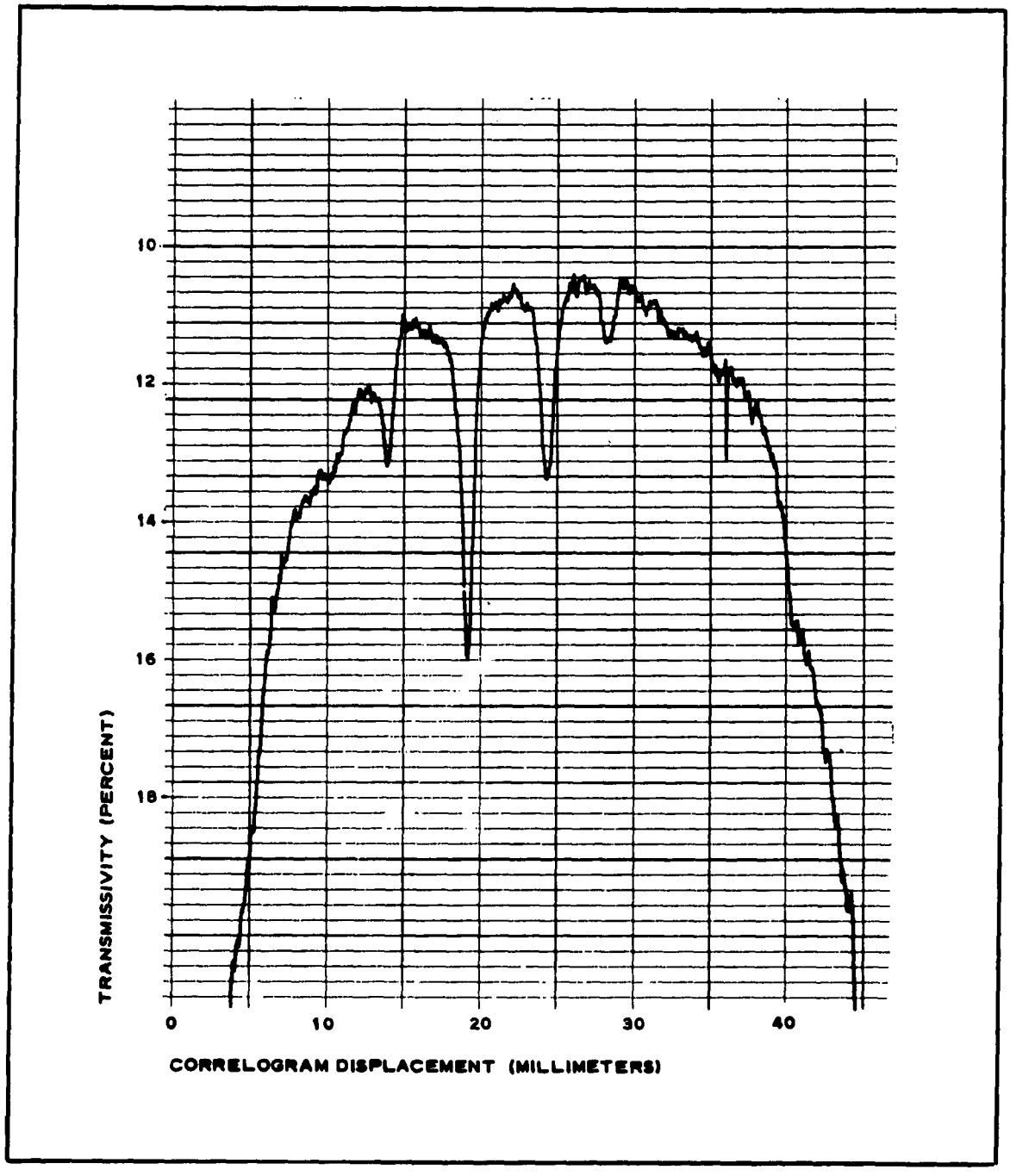

Figure 39 - Microdensitometer Trace of Scene T-4 and Template No. 3 Correlogram

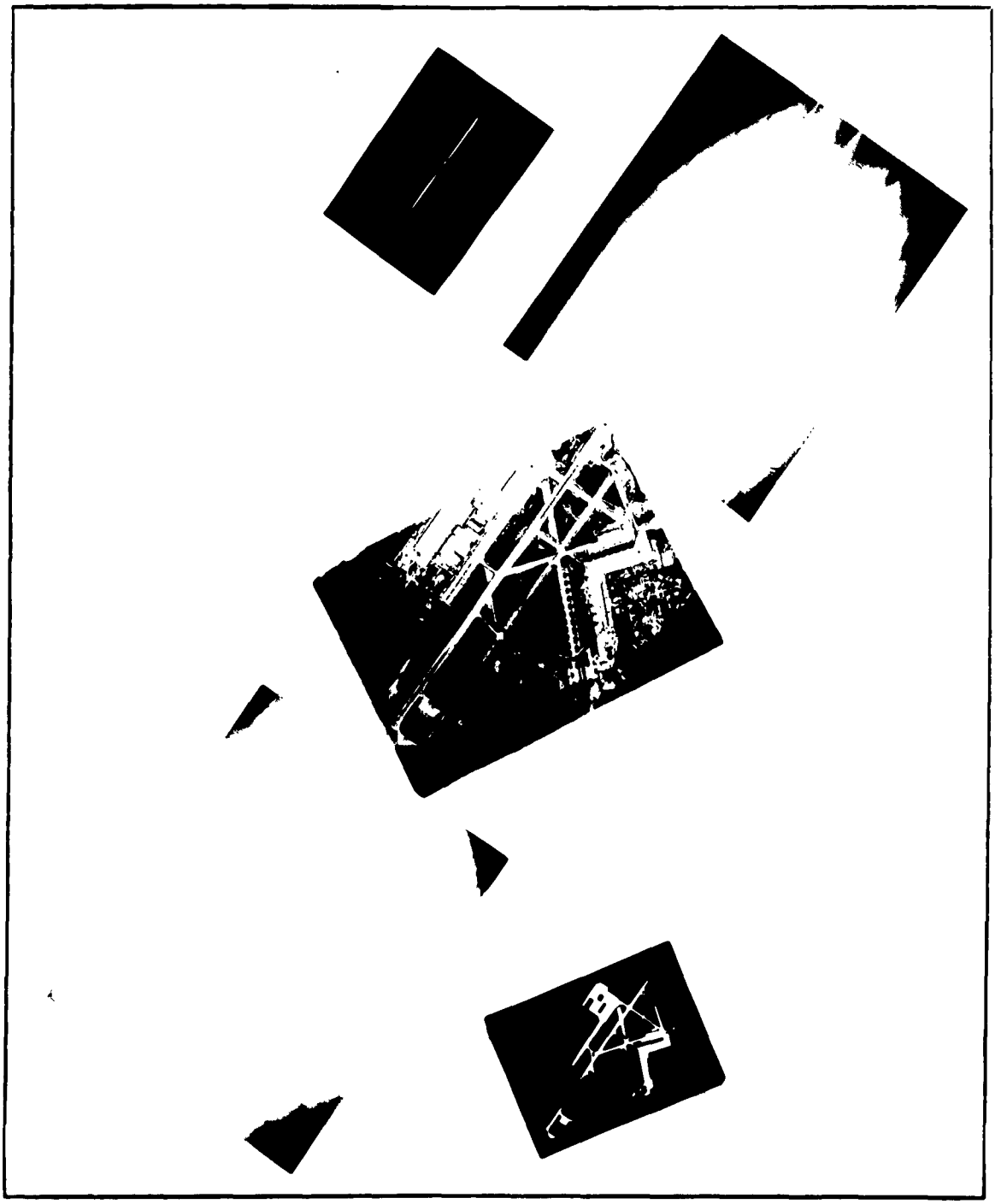

Figure 40 - Runway Scene T-2

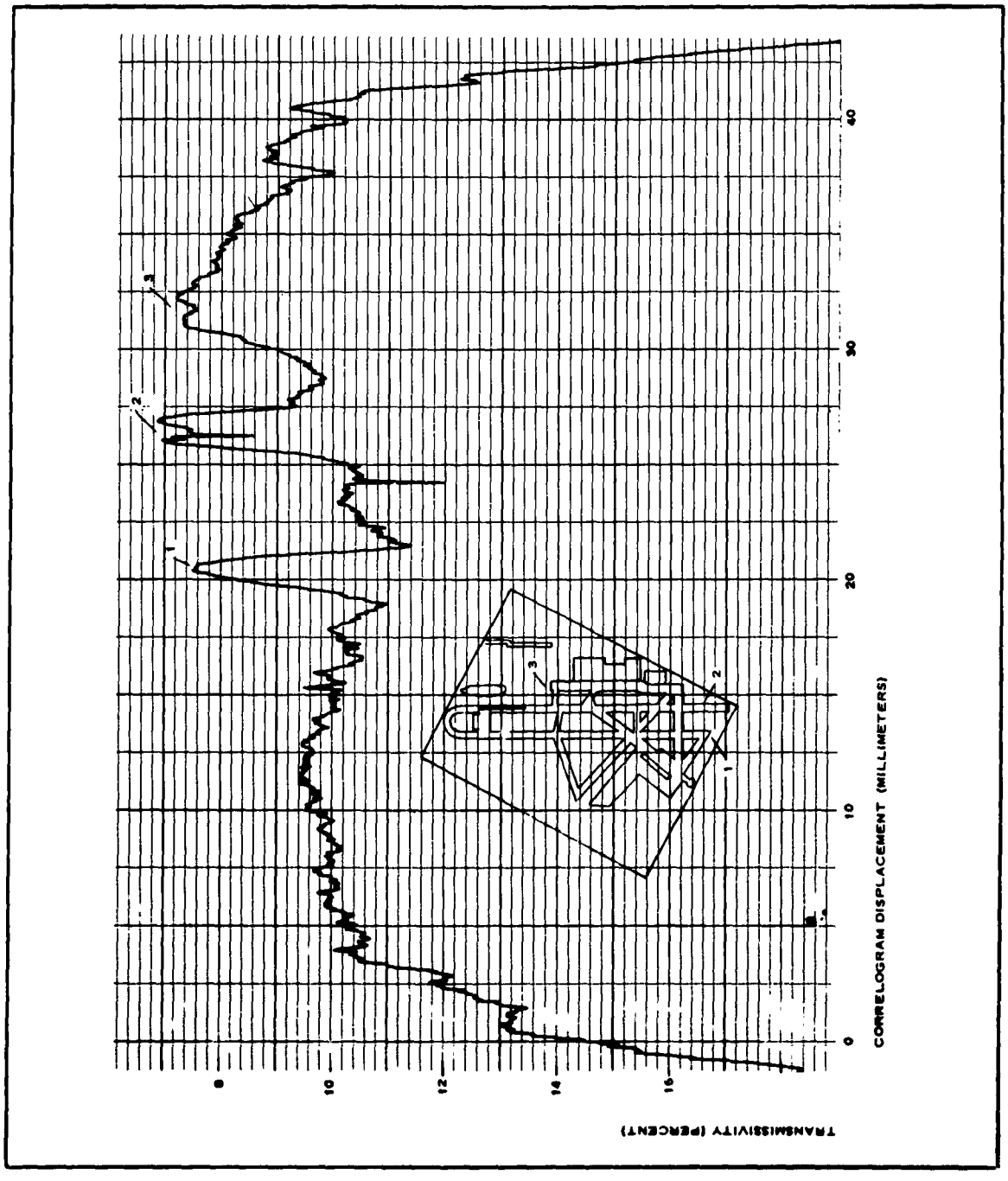

Figure 41 - Microdensitometer Trace of Scene T-2 and Template No. 5 Correlogram

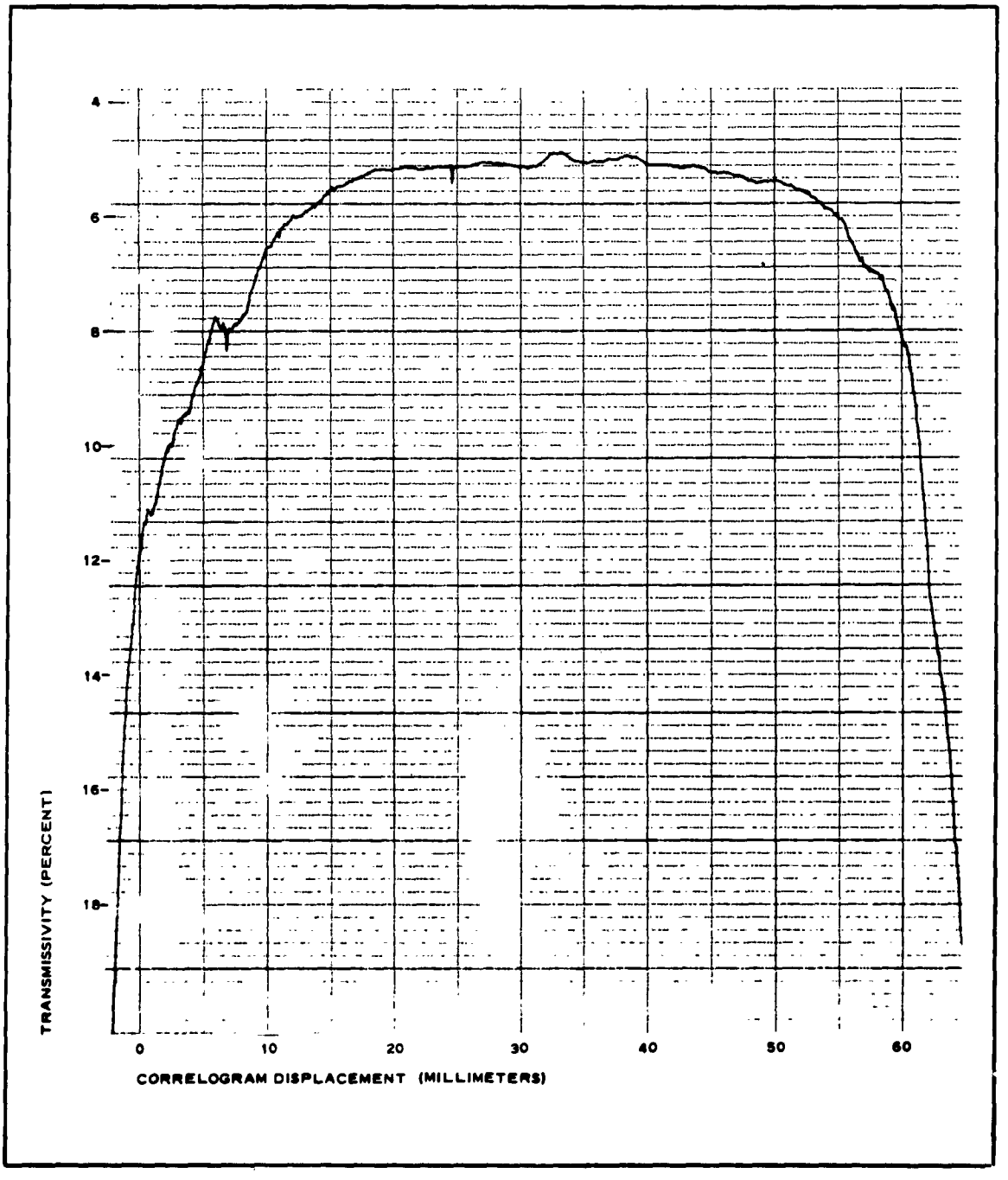

Figure 42 - Microdensitometer Trace of Scene T-2 and Template No. 4 Correlogram

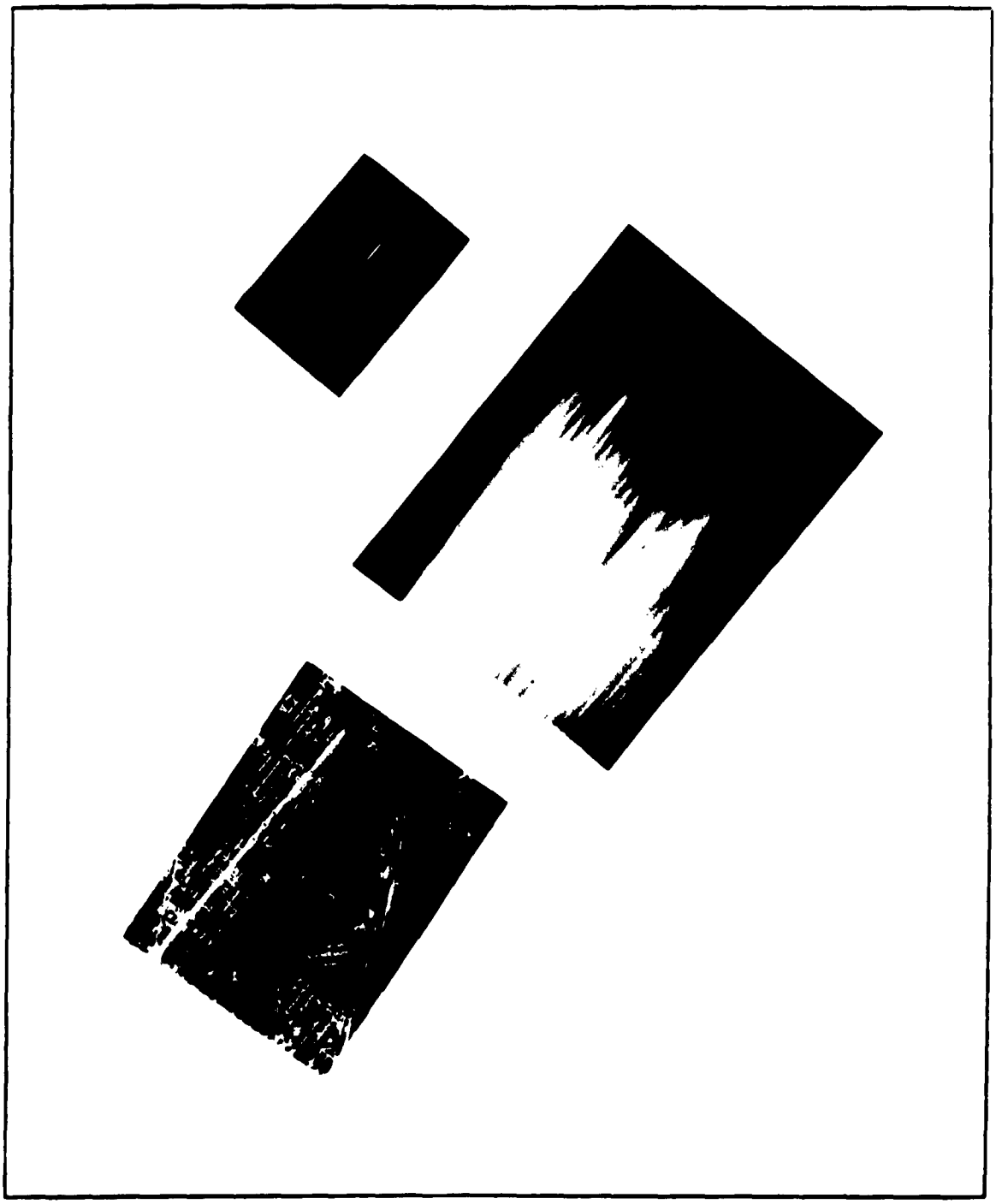

Figure 43 - Scene T-12

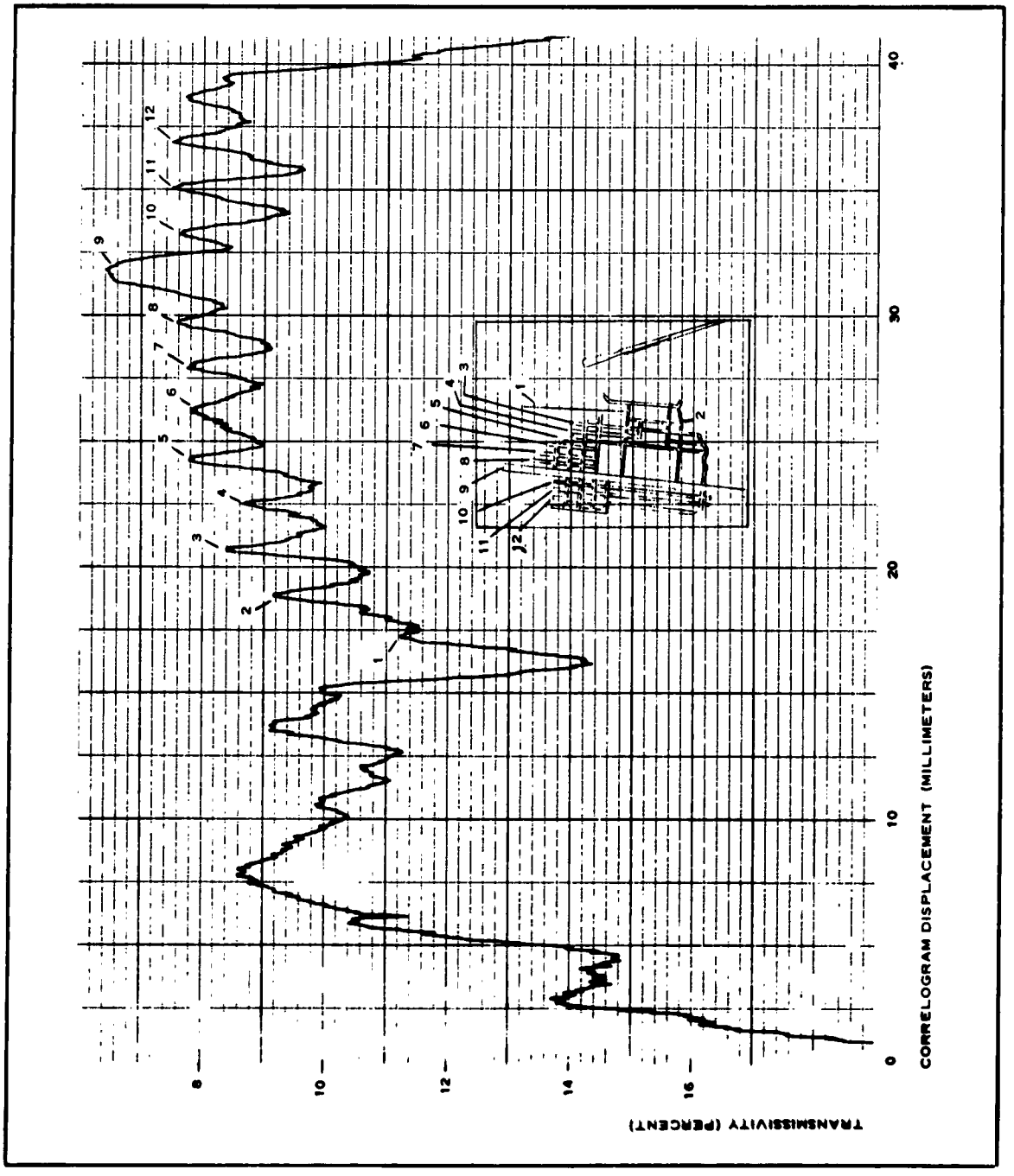

Figure 44 - Microdensitometer Trace of Scene T-12 and Template No. 5 Correlogram

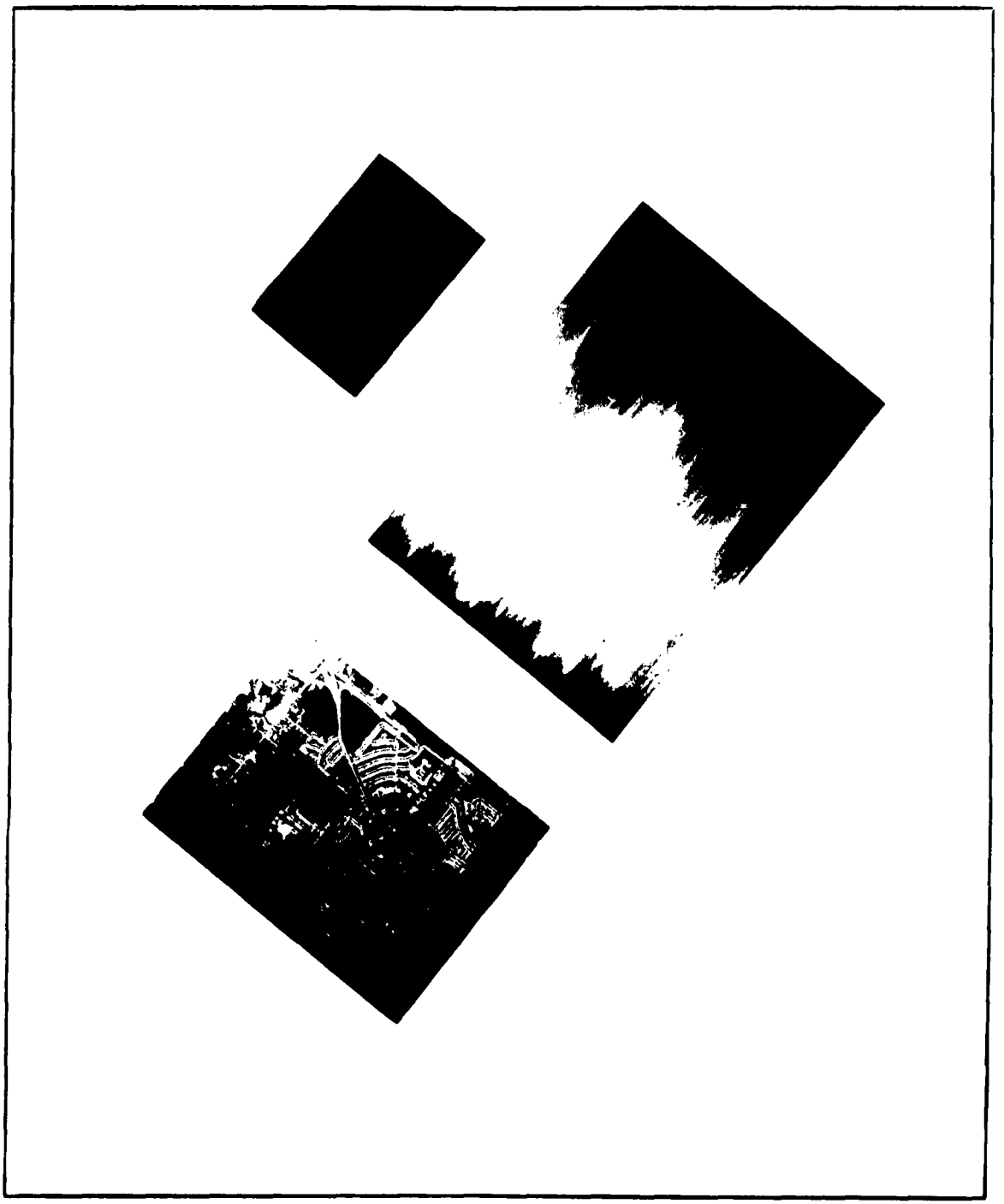

Figure 45 - Scene T-15

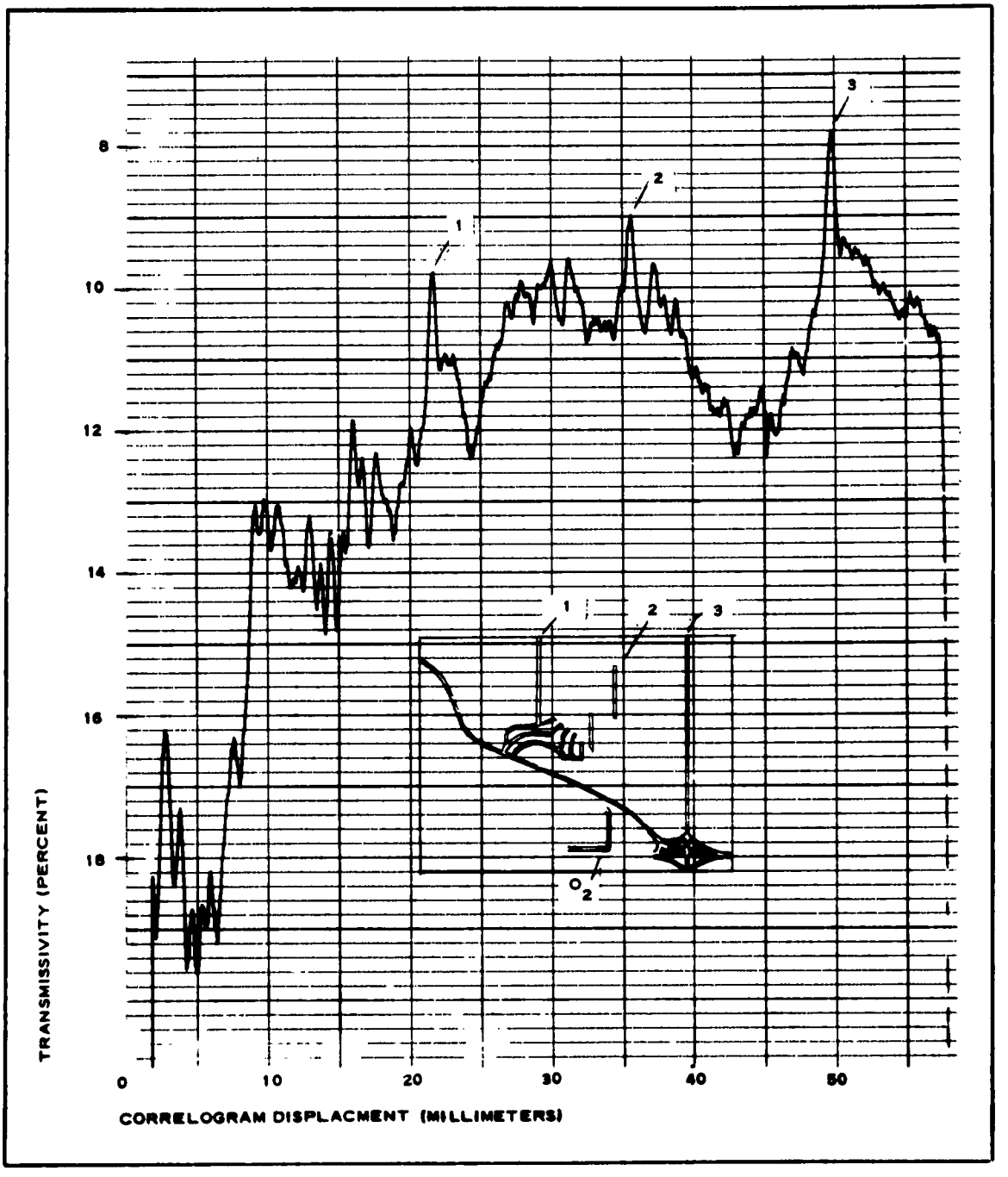

Figure 46 - Microdensitometer Trace of Scene T-15 and Template No. 5 Correlogram

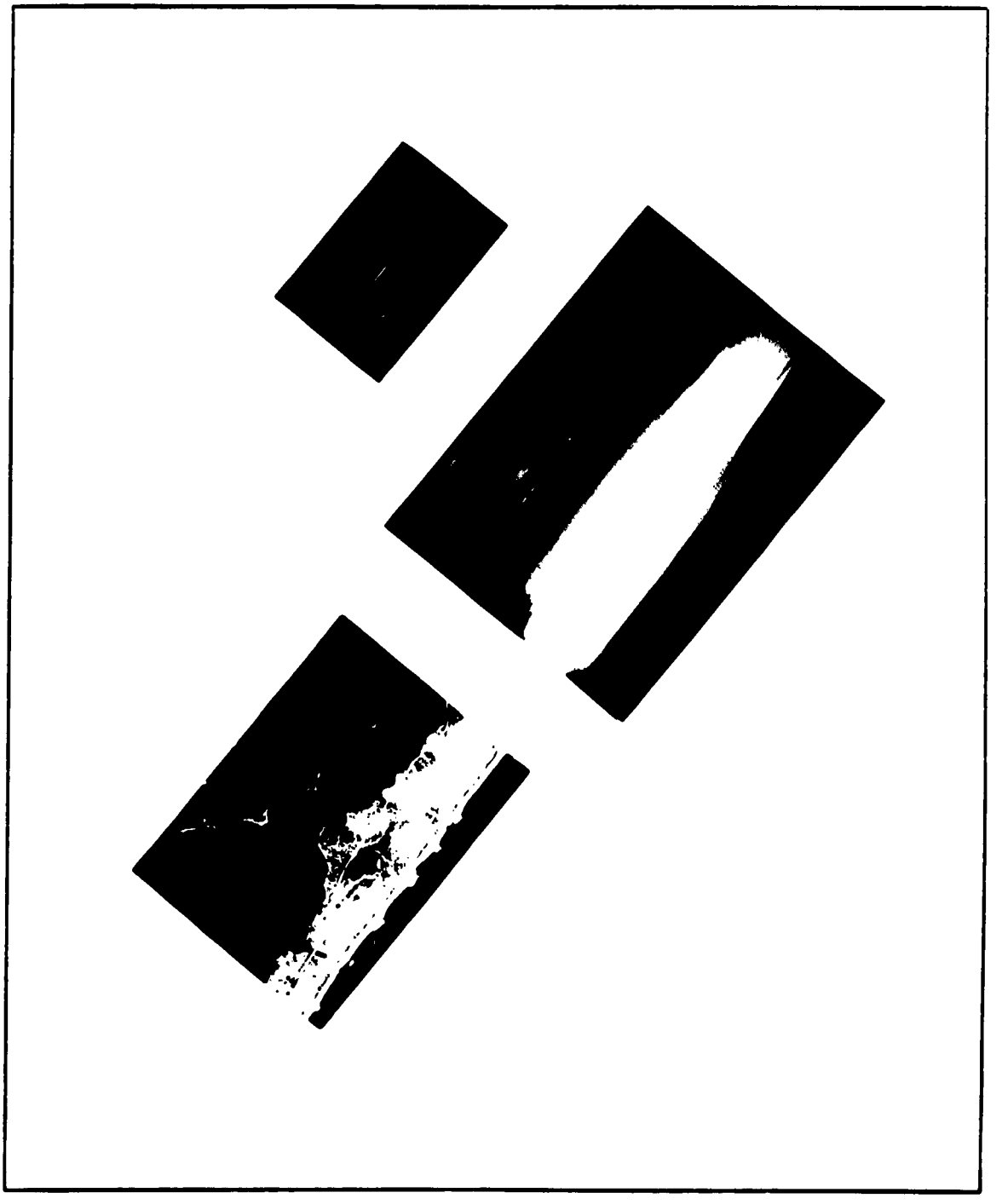

Figure 47 - Scene T-11

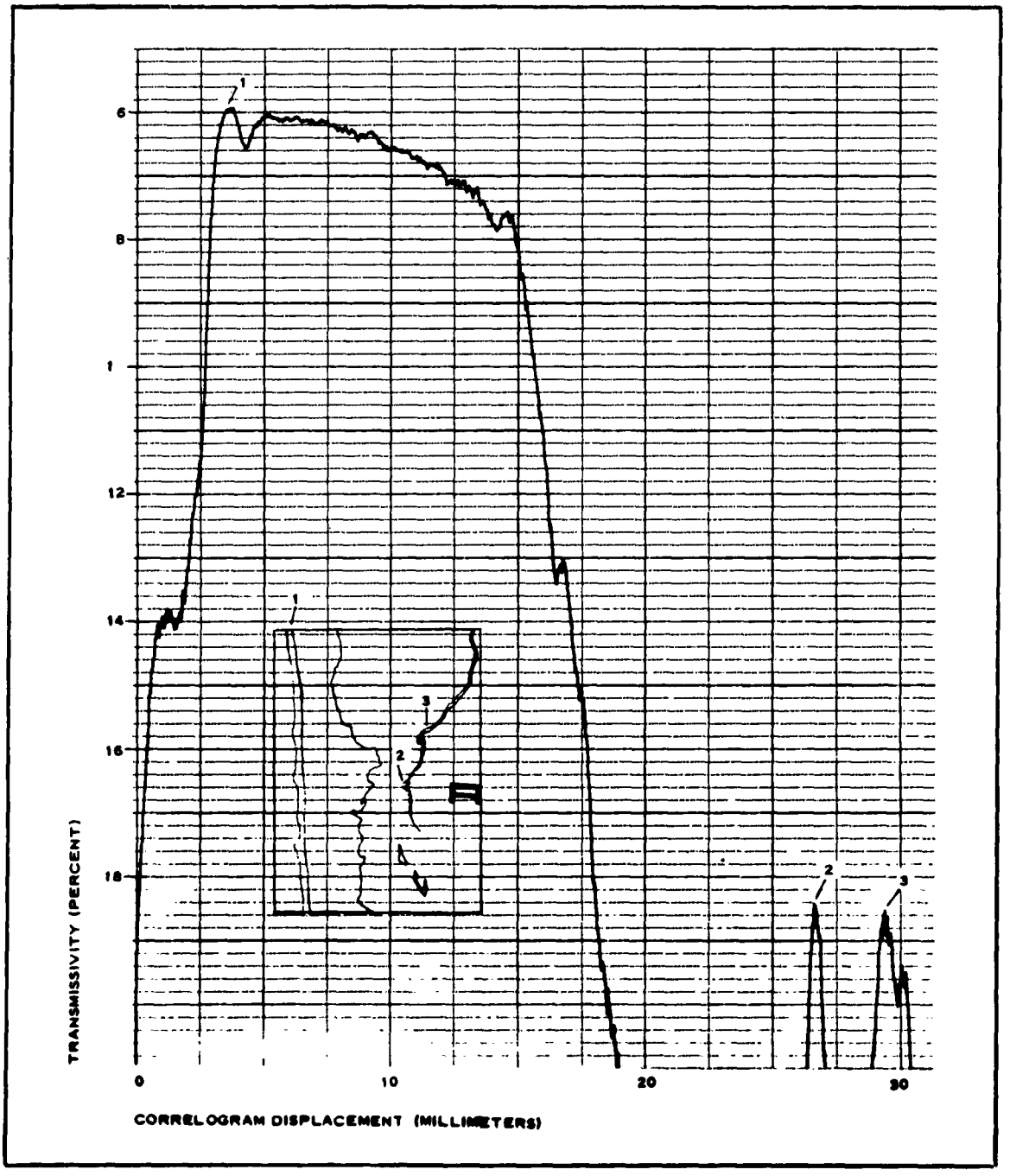

Figure 48 - Microdensitometer Trace of Scene T-11 and Template No. 5 Correlogram

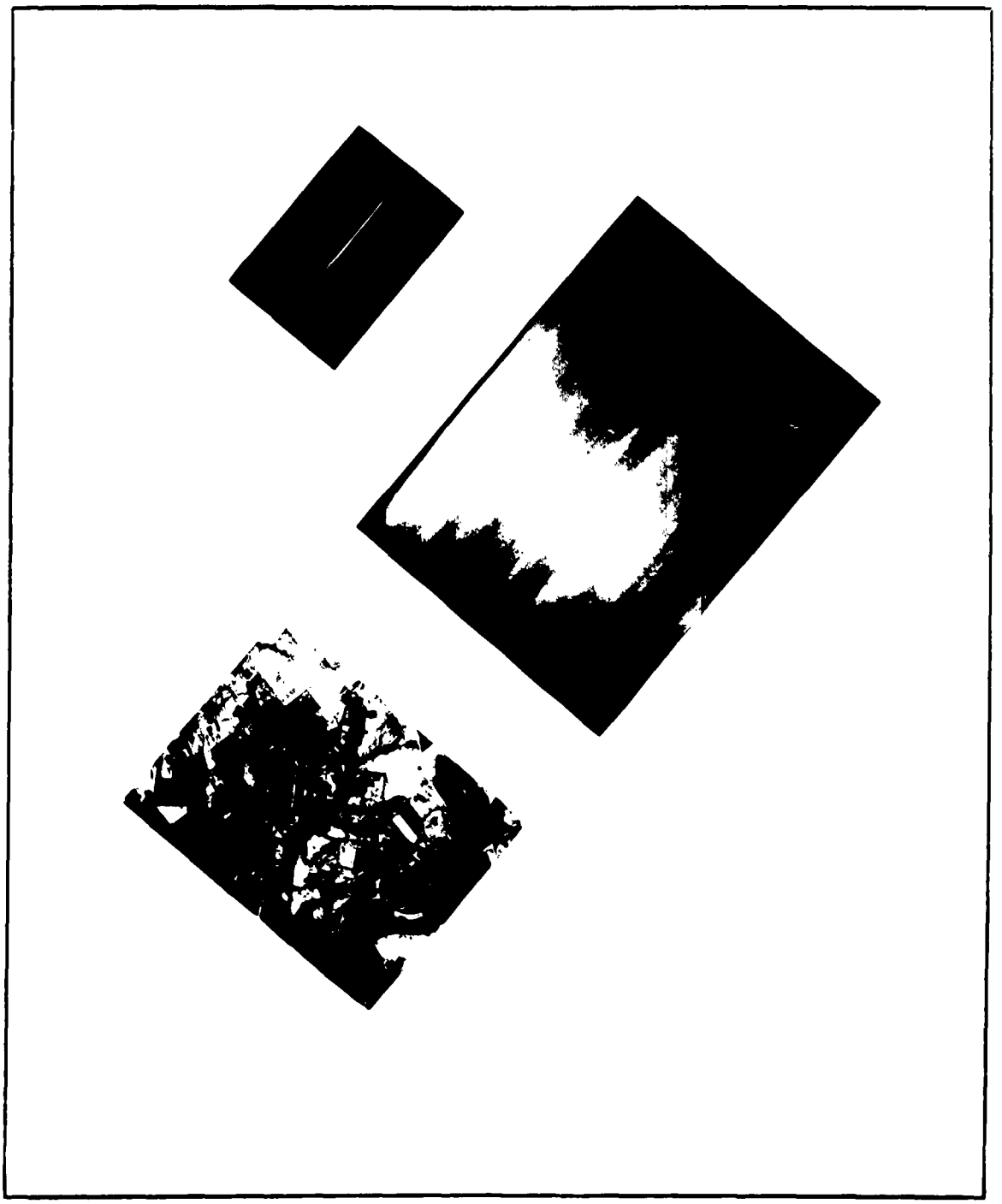

Figure 49 - Scene T-21

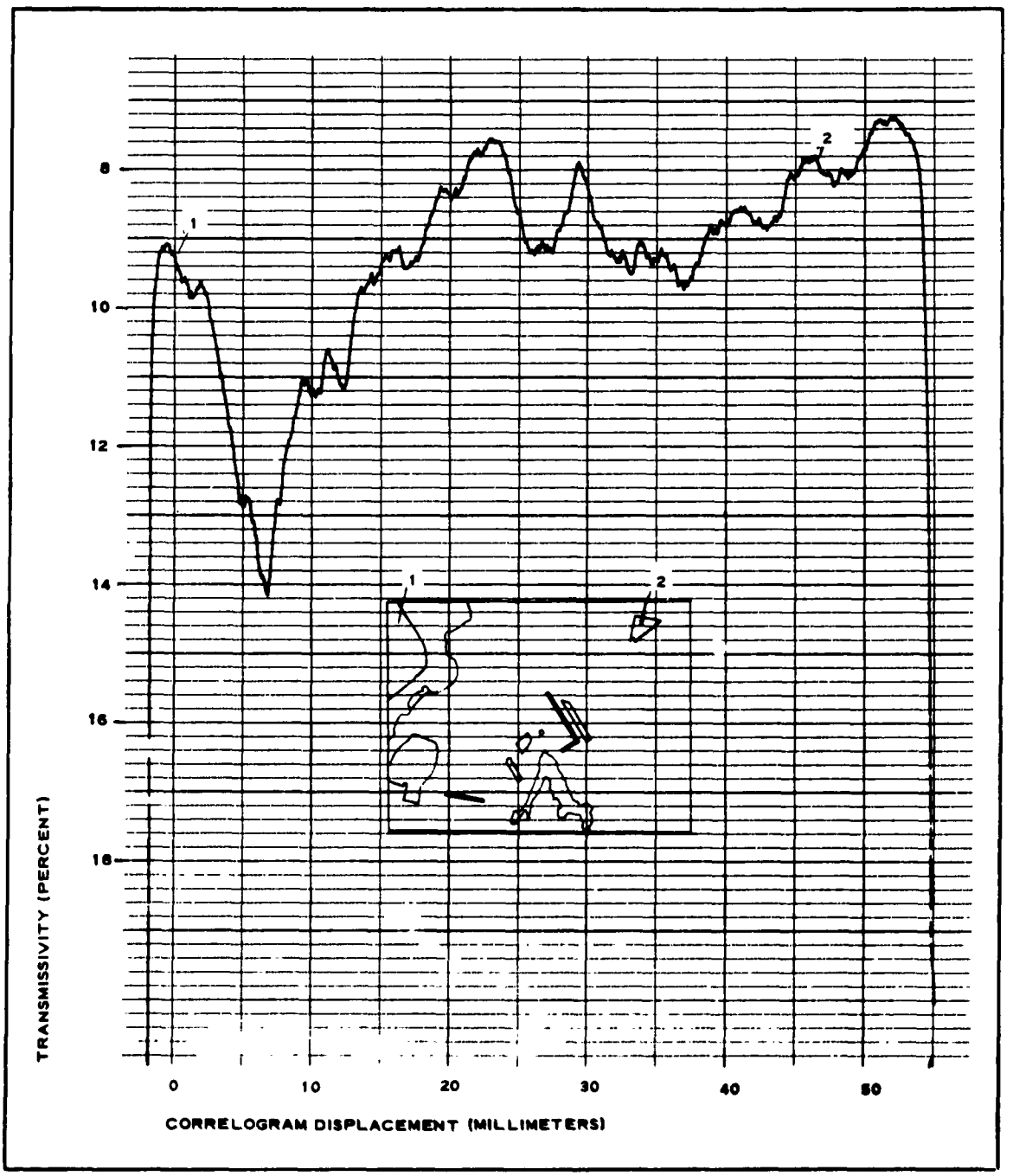

Figure 50 - Microdensitometer Trace of Scene T-21 and Template No. 5 Correlogram

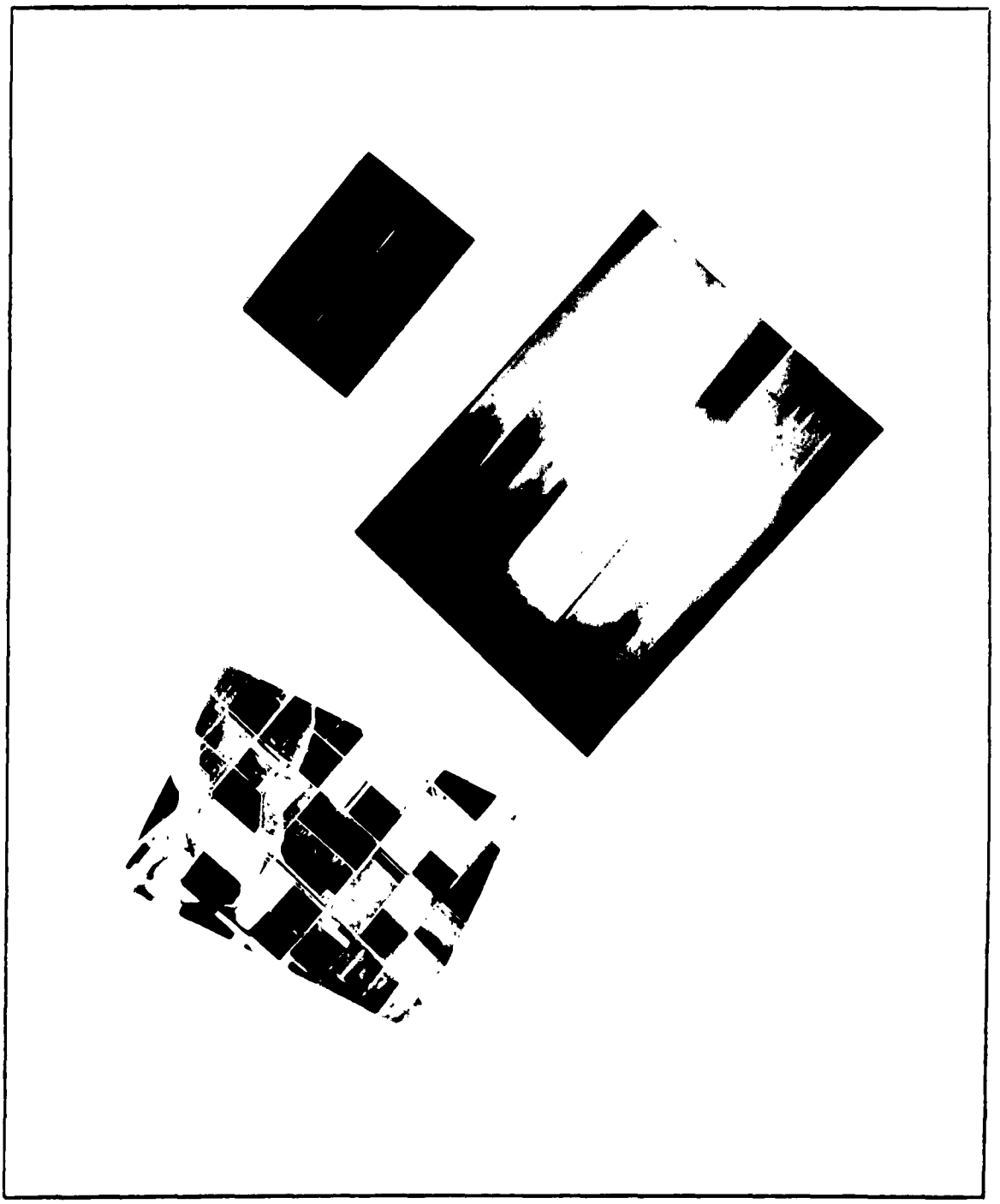

Figure 51 - Scene T-10

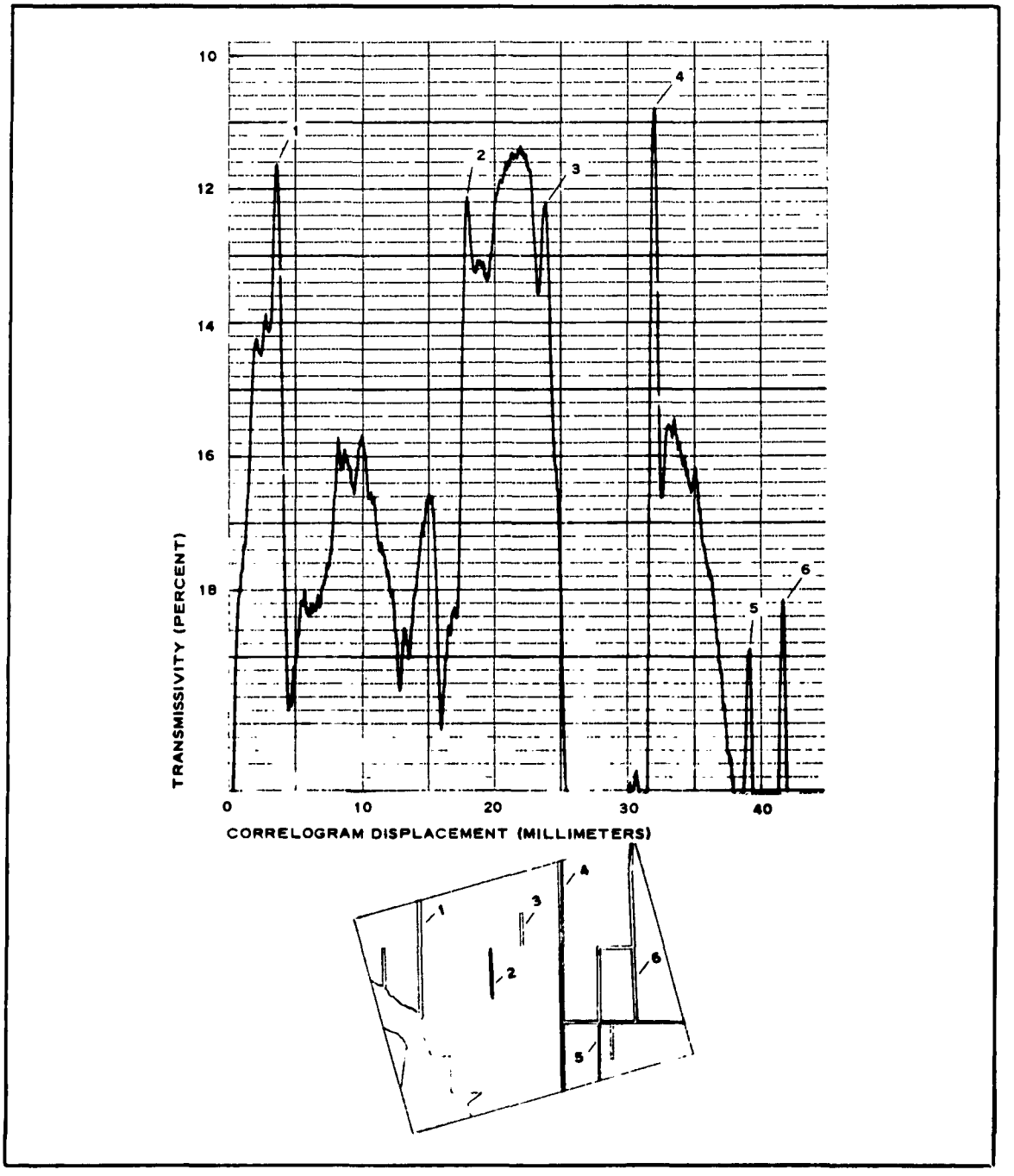

Figure 52 - Microdensitometer Trace of Scene T-10 and Template No. 5 Correlogram

class (runways) considered. The reason for this choice of scenes is to obtain a comparison among (1) photographs that contain runways, (2) photographs that contain runway-like patterns, and (3) photographs that contain no patterns of the runway class.

For each reference scene a template was made of the exact runways and surrounding area. Four of these reference templates were made for the four runway scenes. The templates were constructed by placing transparent paper over the aerial photograph, then tracing all the runways and targets associated with the airfield (buildings, terminal, parking lots, etc.). This trace then was reduced to a scale of 1 to 120,000 and photographed on 3-1/4- by 4-1/4-in., high-contrast, Kodalith glass plates. Because of the method of generation, the templates do not reveal any information concerning the density distribution of the runways and other targets. The only common characteristic between the templates and the airfields is shape.

A study was made to determine the runway lengths and widths that occur most frequently in the northeastern U.S. The results indicate that 150 ft is the width that occurs most frequently and 5250, 8500, and 10,500 ft are the most frequent lengths. A template of a 150- by 10,500-ft runway was drawn, reduced to a scale of 1 to 120,000, and photographed on 3-1/4- by 4-1/4-in., high-contrast, Kodalith glass plates.

The scale of all the templates is half the scale of the scenes because of the correlograph geometry. The template-scene correspondence is as follows:

Template	Scene
1	T-1 (Figure 31)
2	T-3 (Figure 34)
3	T-4 (Figure 37)
4	T-2 (Figure 40)
5	Average runway (Figure 31)

4. RESULTS AND CONCLUSIONS

a. General

The data obtained are in the form of photographic correlograms and microdensitometer traces of the correlograms.

The format of the photographs in Figures 31 through 52 allows the correlograms, obtained by correlating the scene and the depicted reference template, to be related to the scene by projecting along a straight edge parallel to the lines on the correlogram. The microdensitometer traces for each of the correlograms immediately follow the illustrations.

b. Correlograms

Correlograms of the runway scenes convolved with their corresponding templates (nos. 1 through 4) and the average runway template (5), are given in Figures 31, 34, 37, and 40.

Correlograms of the nonrunway scenes correlated with template 1 are given in Figures 43, 45, 47, 49, and 51.

Each correlogram was photographed on 3-1/4- by 4-1/4-in., continuous-tone, K-33 glass plates, which were developed to unity gamma.

c. Microdensitometer Traces

A microdensitometer trace was obtained of each correlogram. This trace represents one slice through the center of the correlation surface. The traces of correlograms obtained by correlating the runway scenes with their corresponding templates are shown in Figures 33, 36, 39, and 42. Microdensitometer traces obtained by correlating the runway scenes with template 5 (average runway) are shown in Figures 32, 35, 38, and 41. Microdensitometer traces of correlograms obtained by correlating nonrunway scenes with template 5 are shown in Figures 44, 46, 48, 50, and 52.

A sketch of the scene appears beneath the microdensitometer traces

of the runway and nonrunway scenes correlated with template 5 (average runway). Individual objects are identified on the correlogram traces to enable the object attributes and curve characteristics to be related.

5. EVALUATION OF RESULTS

Each correlogram was examined and a single microdensitometer trace was generated perpendicular to the long dimension of the line pattern. Contrary to what was expected, the correlograms obtained from the detailed templates do not exhibit much potential and no strong characteristics appear that could be used for recognition.

The correlograms generated with the rectangular slit contain lines corresponding to those lines in the photograph parallel to the slit. Since the photograph and the correlogram are in the same scale, this correspondence can be observed by extending each line in the correlogram to a line in the photograph. The microdensitometer traces of these correlograms were examined for amplitude, periodicity, and sharpness of these lines.

The amplitude of the correlation function does not appear favorable as a characteristic for runway recognition. Runways can generate either peaks or valleys in the correlation function, depending on the surfacing material and the polarity of its contrast with the background. Furthermore, these peaks are not necessarily the maximum amplitude of the correlation function.

Periodic line patterns in an aerial photograph also produce either periodic peaks or valleys in the correlation function: e.g., the periodicity of the correlation function of Scene T-12 (Figures 43 and 44) even though the slit was considerably wider than any of the streets except the expressway.

Runways and all other line patterns generate either peaks or valleys that are much sharper (i.e., more peaked) than almost all other objects in the photographs. It was anticipated that this characteristic could be used as

an index for runway recognition. Since these sharp peaks or valleys indicate a high rate of change of the slope of the correlation function, it was concluded that the second derivative of the correlation function (examined in Subsection Three, below) might be an adequate index for recognition.

SECTION IV - EXPERIMENTAL EVALUATION OF CORRELATION TECHNIQUES

Subsection Three - Detection of Straight Lines by Slit Correlation

1. GENERAL

It was concluded in Subsection Two that the second derivative of the correlation function should be examined in more detail. During the study of straight-line detection by slit correlation an analytical expression was developed for the amplitude of the second derivative as a function of edge gradient, contrast, and edge length.

The correlation functions of a rectangular slit and many line patterns were obtained with a precision crosscorrelator. The second derivatives were generated with an analog computer and were measured, tabulated, and related to the line patterns in the aerial photographs.

2. THEORY

a. Crosscorrelation Function of Rectangular Patterns

The problem of deteriming the second derivative of the correlation function of the two rectangular patterns in Figure 53 is considered in the following paragraphs. Both scenes are photographic transparancies. Figures 53a and 53b show the variation of transmissivity as a function of x for the two scenes.

It is clear that the gradient is zero everywhere except in the interval $b' \leq |x| \leq a'$ for the reference scene and $b \leq |x| \leq a$ for the test scene. The gradients in these intervals can be expressed as follows:

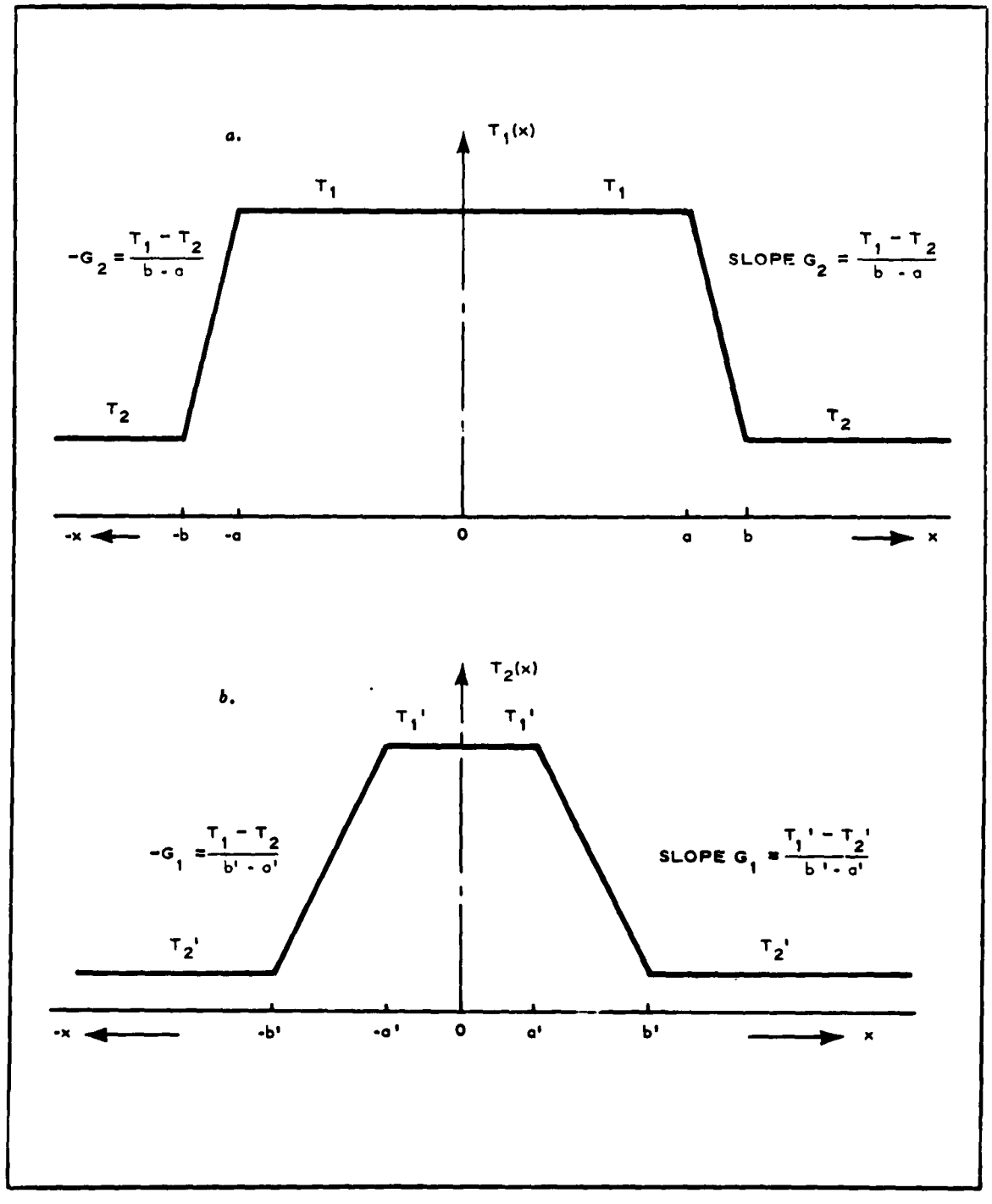

Figure 53 - Transmissivity Variation as Function of x for Two Scenes

for $b' \leq |x| \leq a'$,

$$\frac{\partial}{\partial x} T_1(x) = G_1$$

$$= \frac{T_1' - T_2'}{b' - a'} \quad ; \tag{53}$$

and for $b \leq |x| \leq a$,

$$\frac{\partial}{\partial x} T_2(x) = G_2$$

$$= \frac{T_1 - T_2}{b - a} \quad . \tag{54}$$

To simplify the problem, it is assumed that there is no variation in transmissivity in the y direction.

If the reference scene is moved with respect to the test scene so that the vertical axes of both patterns are always parallel, the correlation function can be written

$$H(u, v) = \int_{-\infty}^{\infty} T_1(x, y) T_2(x + u, y + v)\, dxdy \quad . \tag{55}$$

If now $v = 0$ and there is no variation of T_1 or T_2 is the y direction,

$$H(u) = \int_{-e}^{e} \left[\int_{-(b + b')}^{(b + b')} T_1(x) T_2(x + u)\, dx\, dy \right] \tag{56}$$

or

$$= 2e \int_{-(b + b')}^{(b + b')} T_1(x) T_2(x + u)\, dx \quad . \tag{57}$$

Differentiating both sides of Equation 57 gives

$$\frac{\partial}{\partial u}H(u) = 2e\frac{\partial}{\partial u}\int_{-(b+b')}^{(b+b')} T_1(x)T_2(x+u)\,dx \tag{58}$$

or

$$= 2e\int_{-(b+b')}^{(b+b')} T_1(x)\frac{\partial}{\partial u}T_2(x+u)\,dx \quad . \tag{59}$$

If the transformation $z = x + u$ is made and since

$$\frac{\partial}{\partial u}T_2(x+u) = \frac{\partial}{\partial x}T_2(x+u)$$

$$= \frac{\partial}{\partial z}T_2(z) \quad ,$$

Equation 59 then becomes

$$\frac{\partial}{\partial u}H(u) = 2e\int_{-(b+b')}^{(b+b')} T_1(z-u)\frac{\partial}{\partial z}T_2(z)\,dz \quad . \tag{60}$$

Differentiating Equation 60 gives

$$\frac{\partial^2}{\partial u^2}H(u) = 2e\int_{-(b+b')}^{(b+b')} -\frac{\partial}{\partial u}T_1(z-u)\frac{\partial}{\partial z}T_2(z)\,dz$$

or

$$= -2e\int_{-(b+b')}^{(b+b')} \frac{\partial}{\partial z}T_1(z-u)\frac{\partial}{\partial z}T_2(z)\,dz \quad . \tag{61}$$

If the same transformation, $z = x + u$, is made as before, then the following general equation results:

$$\frac{\partial^2}{\partial u^2}H(u) = S(u)$$

$$\frac{\partial^2}{\partial u^2} H(u) = -2e \int_{-(b+b')}^{(b+b')} \frac{\partial}{\partial x} T_1(x) \frac{\partial}{\partial x} T(x+u)\, dx \quad . \tag{62}$$

Therefore the second derivative of the correlation function is equal to the correlation function of the first derivatives of two functions. The integral of Equation 60 can be evaluated using Equations 53 and 54.

Therefore, if integration is made in the interval $-b \leqq x \leqq -a$, the second derivative S(u) will be obtained, which will reach its maximum value in the interval $(b - b') \leqq (-u) \leqq (a - a')$ from Figure 53:

$$S(u) = -2e \int_{-b}^{-a} G_1 G_2\, dx$$

$$= -2e\, G_1 G_2 (b - a). \quad \left[(b - b') \leqq (-u) \leqq (a - a')\right] \tag{63}$$

And if integration is made in the interval $a \leqq x \leqq b$, the second derivative S(u) will be obtained, which will reach its maximum value in the interval $(a - a') \leqq u \leqq (b - b')$ from Figure 53:

$$S(u) = -2e \int_{a}^{b} G_1 G_2\, dx$$

$$= -2e\, G_1 G_2\, (b - a)\,. \quad \left[(a - a') \leqq u \leqq (b - b')\right] \tag{64}$$

Substituting Equation 54 into Equation 63 or 64 gives

$$S(u) = e_y G_1 \frac{T_1 - T_2}{b - a} (b - a)\,,$$

where e_y is the projected edge of the target. Therefore, for $(a - a') \leqq |u| \leqq (b - b')$,

$$S(u) = -e_y G_1 (T_1 - T_2) \quad . \tag{65}$$

b. Autocorrelation Function of Rectangular Patterns

The problem of autocorrelation of rectangular patterns can be examined by assuming two identical rectangles, such as in Figure 53(b). In this case the second derivative of the autocorrelation function can be written as

$$S(u) = \frac{\partial^2}{\partial u^2} H(u)$$

$$= -2e \int_{-\partial b}^{\partial b} \frac{\partial}{\partial x} T(x) \frac{\partial}{\partial x} T(x + u)\, dx \quad . \tag{66}$$

In the autocorrelation case, when u = 0 both edges of one rectangle will coincide simultaneously with the corresponding edges of the other, and S(u) will reach its maximum when u = 0; therefore,

$$S(0) = \frac{\partial^2}{\partial u^2} H(0)$$

$$= -2e \int_{-b}^{b} \left[\frac{\partial}{\partial x} T(x)\right]^2 dx \quad . \tag{67}$$

Here again

$$\frac{\partial}{\partial x} T(x) = G$$

for $-b \leq |x| \leq -a$ and $a \leq |x| \leq b$; it is zero in any other interval. Therefore,

$$S(0) = -2e \int_{-b}^{-a} G^2 dx - 2e \int_{a}^{b} G^2 dx$$

$$= -2eG^2(b - a) - 2eG^2(b - a)$$

$$= -2(2e)G^2(b - a) \quad . \tag{68}$$

Substituting Equation 54 into Equation 68 gives

$$S(0) = -2e_y G \frac{T_1 - T_2}{b - a}(b - a)$$

$$= -2e_y G(T_1 - T_2) \quad . \tag{69}$$

From Equations 63 and 66 it can be concluded that the amplitude of the second derivative of the correlation function of two rectangular patterns is:

1. Directly proportional to the edge length common to both patterns
2. Directly proportional to the difference in transmissivity between the background and the test pattern
3. Directly proportional to the gradient of the reference rectangle

The amplitude of S(u) is maximum when the width of the reference rectangle is equal to the width of the test rectangle (autocorrelation case). If the widths differ by any amount, the amplitude of S(u) is half of that of the autocorrelation case, all the other parameters remaining constant.

c. Effect of Width

The amplitude of the second derivative of the correlation function is greatest when the widths of both the reference and the test rectangles are identical, which is the case for autocorrelation. If the widths differ by any amount, the amplitude of the second derivative of the correlation function will be half of the amplitude of the autocorrelation case.

If the length of the rectangles is L and the light flux through them remains constant, and if the width of the reference rectangle is changed, the area of the rectangle changes proportionally as does the light flux

therefore; but the slope of the correlation function remains constant and therefore the amplitude of the second derivative remains unchanged. Figure 54 shows the amplitude of S(u) as a function of width.

3. DESCRIPTION OF EXPERIMENTAL EQUIPMENT

a. Precision Crosscorrelator

The precision crosscorrelator, a sensitive and accurate instrument, is used to determine the correlation function between two transparancies. It consists of a light source that directs light through the two transparancies onto the cathode of a photomulitplier tube. The 3-1/4- by 4-1/4-in. photographic glass plates are mounted in two frames between the light source and the photomultiplier tube, as shown in Figure 55. Frame 1 is movable and is driven in the longitudinal and lateral directions at constant speeds of 0.0045 in. per second by synchronous motors. The spacing between the photographic plates is exaggerated in Figure 55; actually, the plates are brought as close together as possible without the emulsions scraping each other when one plate is moved. The box containing the photomultiplier tube is hinged to allow a visual examination of the photographic plates.

b. Analog Computer

The output of the photomultiplier tube is applied to an analog computer circuit from which the correlation function and its first and second derivatives are obtained. Two recorders are available: a dual-channel recorder that graphs the correlation function and its second derivative, and a single-channel recorder that graphs the first derivative of the correlation function. The circuit diagram of the analog computer is shown in Figure 56. Three Philbrick operational amplifiers were used.

At point A the correlation function of the scene and the slit template is obtained. At point B the first derivative of the correlation function

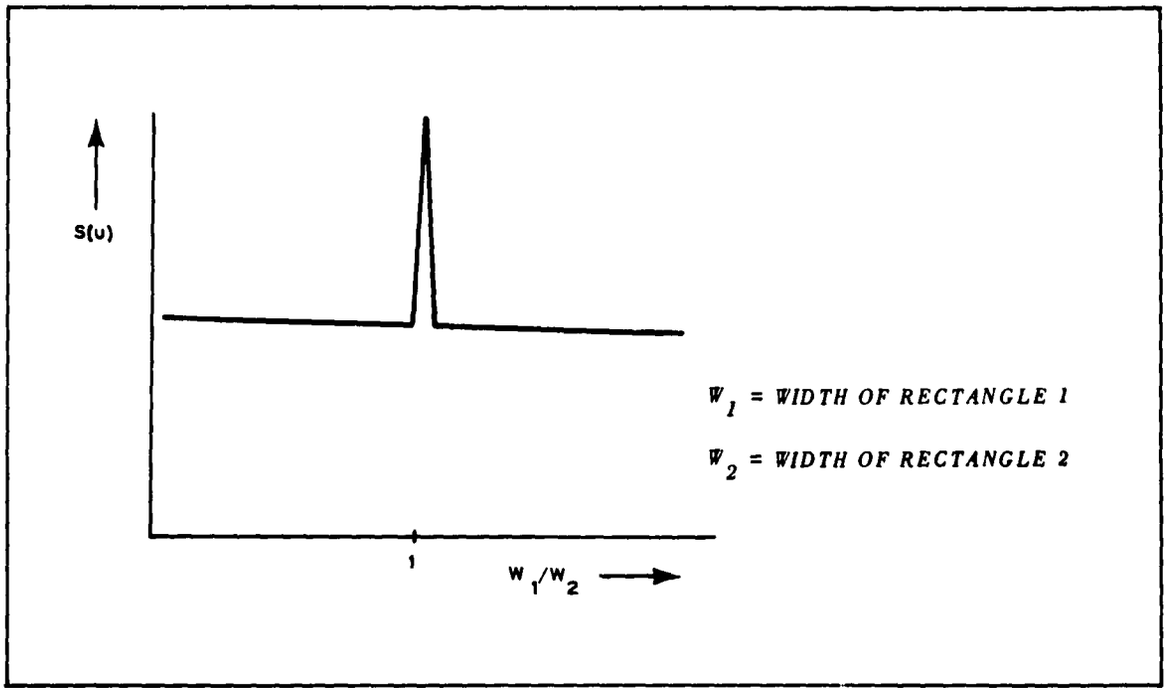

Figure 54 - Amplitude of S(u) as Function of Width

is obtained. And at point C the second derivative of the correlation function is determined.

In amplifiers 2 and 3 is was necessary to provide filtering to reduce system noise. The value of 0.20 μf for the feedback capacitors was experimentally determined by correlating two slit templates of identical dimensions, 1 by 0.020 in. With the feedback capacitors disconnected, the peak signal of the second derivative of the correlation is 22 units and the peak noise, 10 units. Therefore, the signal-to-noise ratio (S/N) is 2 to 1. When the capacitors are introduced in the feedback loop the peak signal is reduced to 13 units but the peak noise is reduced to 1 unit; therefore, the signal-to-noise ratio becomes 13 to 1, which is approximately 6 times greater than the unfiltered case.

The transfer function of the differentiating circuits is

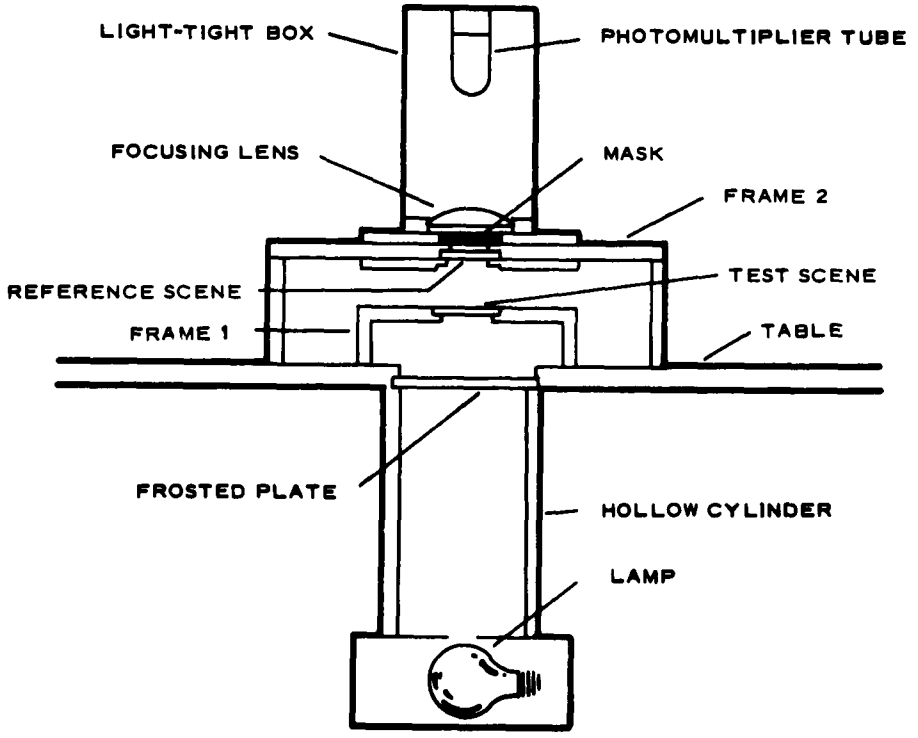

Figure 55 - Precision Crosscorrelator Arrangement

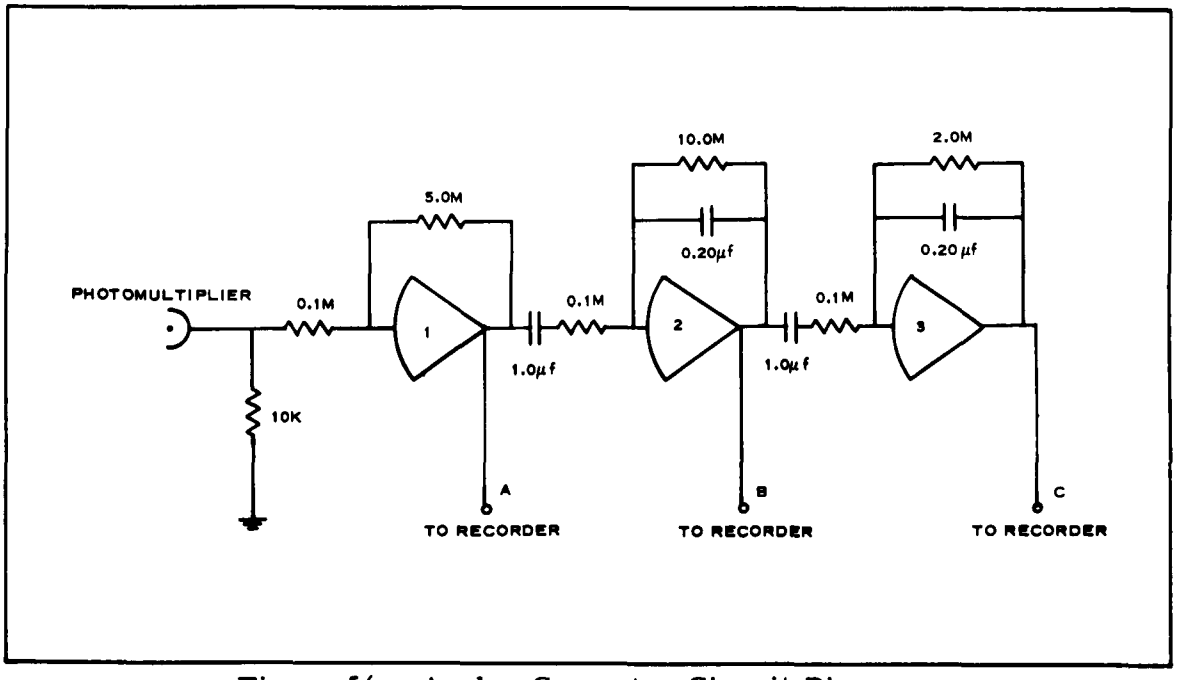

Figure 56 - Analog Computer Circuit Diagram

$$\frac{e_o}{e_i} = -\frac{z_f}{z_i}$$

$$= -\frac{R_2\left[\left(\frac{\frac{1}{C_2S}}{R_2}\right)\right] + \frac{1}{C_2S}}{R_1 + \frac{1}{C_1S}}$$

$$= -\frac{\left(\frac{R_2}{R_2C_2S + 1}\right)}{\left(\frac{R_1C_1S + 1}{C_1S}\right)}$$

$$= -\frac{R_2C_1S}{(R_1C_1S + 1)(R_2C_2S + 1)} , \qquad (70)$$

where

$$z_f = \text{feedback impedence}$$

$$= \frac{R_2 \frac{1}{C_2 S}}{R_2 + \frac{1}{C_2 S}}$$

and

$$z_i = \text{input impedence}$$

$$= R_1 + \frac{1}{C_1 S}$$

$$= \frac{R_1 C_1 S + 1}{C_1 S} \quad .$$

For amplifier 2, the transfer function is

$$\frac{e_o}{e_i} = - \frac{10S}{(0.1S + 1)(2S + 1)} \quad .$$

For amplifier 3, the transfer function is

$$\frac{e_o}{e_i} = - \frac{2S}{(0.1S + 1)(0.4S + 1)} \quad .$$

Graphs of these transfer functions are given in Figure 57.

4. DESCRIPTION OF EXPERIMENT

a. Procedure

To evaluate the uniqueness of the second-derivative attribute of runways or runway-like objects, the following experiment was performed.

The precision crosscorrelator described in item 3 was used. The test scenes were aerial photographs and the reference scene, a

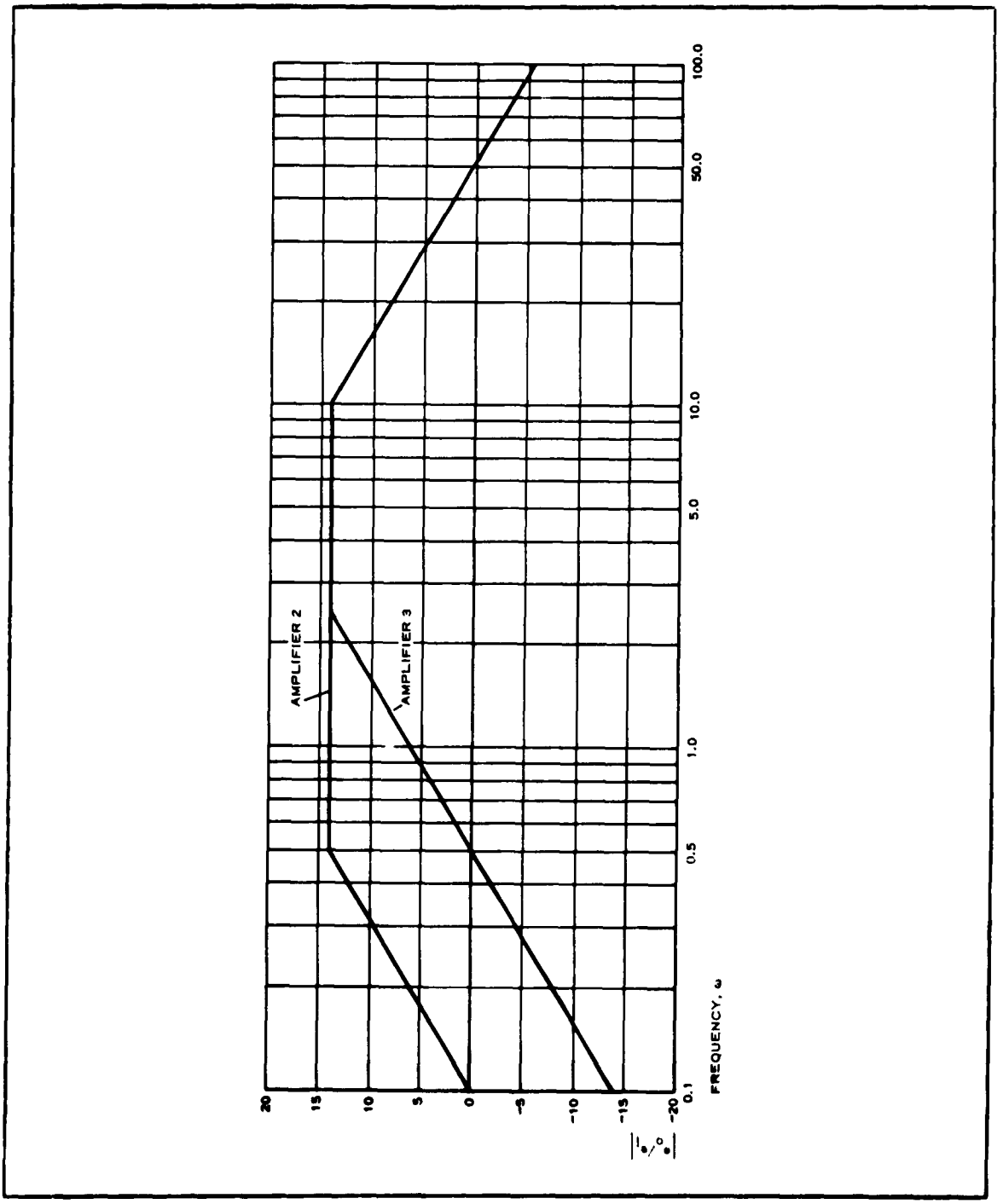

Figure 57 - Transfer Functions for Amplifiers 2 and 3

1.0- by 0.020-in. rectangle. The transmissivity inside the rectangle was 1 and outside the rectangle, zero. The test scene was scanned with the rectangle in a direction perpendicular to its long dimension. The output of the precision crosscorrelator was the correlation function of the rectangle and the test scene (aerial photograph). The first and second derivatives of the correlation function were obtained with the analog computer.

The precision crosscorrelator was calibrated frequently to compensate for changes in light flux and photomulitplier gain. A standard circular aperture was inserted into the light path; the variac controlling the light source voltage was adjusted so that the output of the first operational amplifier remained constant.

The maximum amplitude of the second derivative is obtained when the rectangular patterns in the aerial photograph are scanned with the reference slit so that the v tical axes of the scene and the reference are parallel and the direction of scan is perpendicular to the length of the rectangles.

To fulfill this condition the precision crosscorrelator was set up as follows.

1. The reference slit was oriented so that its length was perpendicular to the direction of translation.
2. For target scenes, each runway was scanned separately by orienting the scene so that the vertical axis of the runway was parallel to the vertical axis of the reference slit.
3. For nontarget scenes containing runway-like objects, each object was oriented so that its vertical axis was parallel to the vertical axis of the reference rectangle.
4. The nontarget scenes that do not contain any straight-line objects were scanned at several random orientations.

b. Test Scenes

A sample of 19 near-vertical aerial photographs was selected. Of these, 9 contain one or more runways; the other 10 do not contain runways but do contain runway-like objects such as highways, roads, railroads, and streets. These photographs are identified in Table VII. Photographic glass plates 3-1/4 by 4-1/4 in. were obtained of each aerial photograph at $\gamma = 1$. The scale of every photograph is 1 to 100,000. According to this scale the dimensions of the reference rectangle on the ground correspond approximately to 170 by 8400-ft, which is a representative runway size.

c. Effect of Edge Length and Orientation

An experiment was performed to determine the effect of the edge length of a slit on the second derivative of the correlation function. The test scene was a rectangle of 1.50 by 0.0054 in., and the reference scene was a rectangle of L by 0.020 in. The length of the rectangle, L, was varied from 0 to 1.20 in. in steps of 0.10 in. The two scenes were aligned so that when frame 1 was translated it moved in a direction perpendicular to the long dimension of the reference rectangle. The light flux was kept constant. The amplitude of the second derivative for each length of the reference scene was recorded and the results are plotted in Figure 58. This experiment indicates that the amplitude of the second derivative of the correlation function of two rectangles is directly proportional to the edge length of the rectangles.

A second experiment was performed to study the effect of the orientation of two identical rectangles on the second derivative of the correlation function when the dimensions of the rectangles and the light flux remain constant. The two rectangles were aligned so that the angle between them was 0 deg. Then one of the rectangles was rotated with respect to the other from 0 to 4 deg in 0.5-deg increments.

TABLE VII - AERIAL PHOTOGRAPHS OF RUNWAY AND NONRUNWAY SCENES

Photograph	Code no.
Runway scenes	
Vandenberg AFB	T-1
Carswell AFB	T-2
Dallas NAS	T-3
Luke AFB	T-4
Eglin AFB	T-5
Saufley NAS	T-6
Keesler AFB	T-7
Eglin AFB No. 8	T-8
Eglin AFB No. 2	T-9
Nonrunway scenes	
Phoenix area	T-10
Florida coastal area	T-11
Dallas area	T-12
Dallas area	T-13
Florida swamp	T-14
Ft. Worth area	T-15
Ft. Worth area	T-16
Toledo area	T-17
Toledo area	T-18
Toledo area	T-19

The amplitude of the correlation function and the amplitude of its second derivative were recorded for each angle and the results are plotted in Figure 59. As before, the direction of scan was perpendicular to the long dimension of the reference rectangle. The size of the rectangle was 1.0 by 0.020 in.

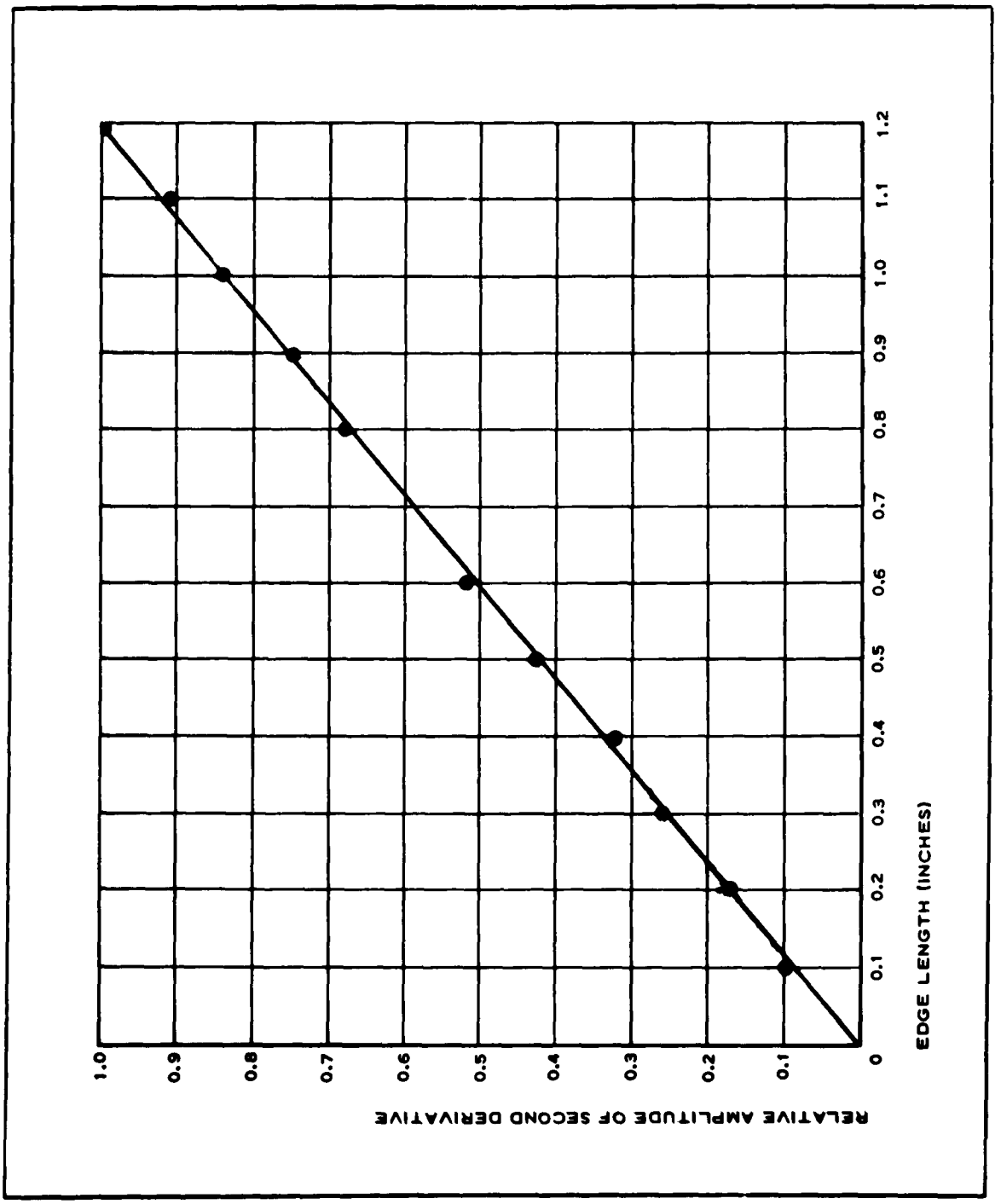

Figure 58 - Amplitude of Second Derivative vs Edge Length of Reference Slit

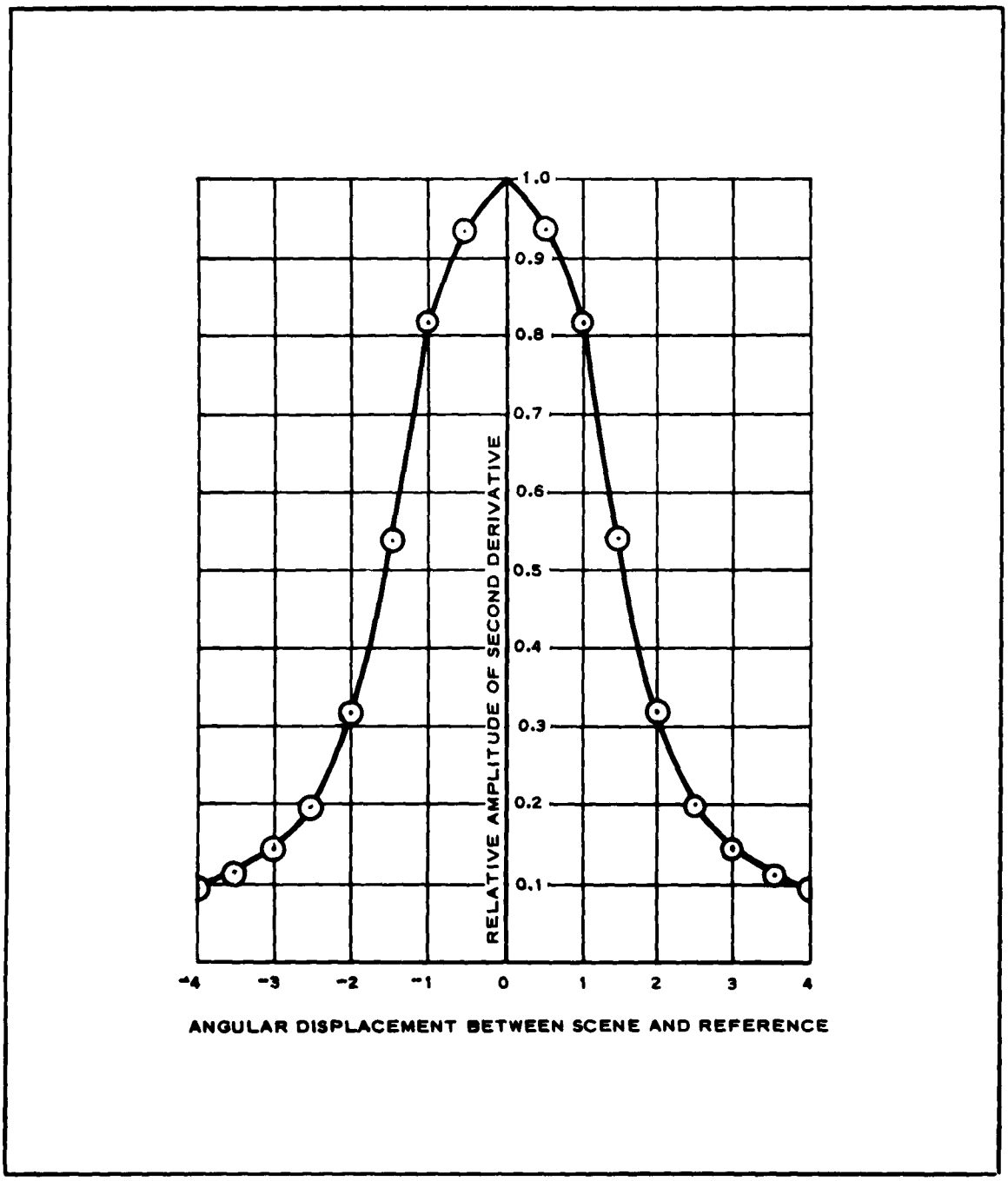

Figure 59 - Amplitude of Second Derivative vs Angular Displacement between Scene and Reference

5. EXPERIMENTAL RESULTS

The crosscorrelation function and its second derivative for scenes with runways, urban street patterns, rural road and field patterns, bridges, ships, isolated noninhabitable areas, and land-water boundaries was obtained with the precision crosscorrelator and recorded. The amplitude of the second derivative for various patterns of interest as well as the largest-amplitude second derivative for the background are tabulated in Tables VIII and IX. Several scenes with their corresponding dual-channel recordings are shown in Figures 60 through 68. Scenes T-1 and T-4 are shown in Figure 60 with the reference slit; the respective dual-channel recordings are shown in Figures 61 and 62. Scenes T-10 and T-12 are shown in Figure 63, with the respective recordings shown in Figures 64 and 65. Scenes T-14 and T-16 are shown in Figure 66, with the respective recordings shown in Figures 67 and 68.

6. EVALUATION OF RESULTS

The data of Tables VIII and IX can be analyzed by several methods, depending on the definitions of "target" and "nontarget." One method of analysis is based on the following definition:

Definition 1: Target (T_1) is any straight-line pattern in an aerial photograph.

Nontarget (N_1) is any pattern in an aerial photograph that does not consist of straight lines.

Based on this definition, the frequency distributions of the second-derivative amplitudes for all straight-line patterns are plotted in Figure 69. The vertical ordinate of the second derivative S = 7.3 is the maximum second derivative of the background (or nontarget) for any of the scenes.

A second method of evaluating the data to determine the probability that runways can be distinguished from other straight-line patterns is based on the following definitions, which apply only to Table X and XI:

(Text continued on p. 136.)

TABLE VIII - SECOND-DERIVATIVE AMPLITUDE AND BACKGROUND SIGNAL FOR RUNWAY SCENES

Aerial photograph	Object	2nd-derivative amplitude	Maximum background signal
T-1	Runway	36.7	7.3
	Taxi strip	58.8	
	Road	54.4	
T-2	Runway	35.3	7.3
	Taxi strip	30.9	
	Building edge	20.6	
T-3	Runway	14.7	4.4
	Runway	33.8	
	Runway	54.4	
	Taxi strip	30.9	
	Highway	22.1	
	Canal	51.4	
T-4	Runway	94.1	4.4
	Runway	97.0	
	Taxi strip	91.1	
	Field edge	64.7	
T-5	Runway	36.7	4.4
	Runway	38.2	
	Runway	39.7	
	Road	39.7	
T-6	Runway	8.8	4.4
	Runway	16.2	
	Runway	10.3	
	Runway	25.0	
	Road	22.0	
	Road	22.0	
	Road	25.0	

TABLE VIII - SECOND-DERIVATIVE AMPLITUDE AND BACKGROUND SIGNAL FOR RUNWAY SCENES (Continued)

Aerial photograph	Object	2nd-derivative amplitude	Maximum background signal
T-7	Runway	19.1	1.5
	Streets	10.3	
	Beach	63.2	
T-8	Runway	14.7	1.5
	Road	45.5	
T-9	Runway	14.7	1.5
	Runway	33.8	
	Road	11.7	
	Road	45.5	

TABLE IX - SECOND-DERIVATIVE AMPLITUDE FOR NONRUNWAY SCENES

Aerial photograph	Object	2nd-derivative amplitude
T-10	Road	32.3
	Road	41.1
	Road	41.1
	Road	44.1
	Road	100.0
T-11	Beach	57.3
	Beach	64.7
T-12	Highway	42.6
	Railroad	44.1
	Railroad	48.5
	Streets	19.1 to 27.9

TABLE IX - SECOND-DERIVATIVE AMPLITUDE FOR NONRUNWAY SCENES (Continued)

Aerial photograph	Object	2nd-derivative amplitude
T-13	Road	11.7
	Background	4.4
T-14	Background	1.5
T-15	Highway	16.2
	Streets	10.3
T-16	Road	39.7
	Background	7.3
T-17	Highway and bridge	85.3
	Road	22.0
	Railroad	11.7
	Background	7.3
T-18	River	13.2
	Highway and bridge	11.7
	Streets	13.2
T-19	Railroad and bridge	29.4
	Streets	13.2
	River edge	25.0
	Background	4.4

Definition 2: Target (T_2) is an aerial photograph (of an area of approximately six square miles) that contains one or more runways. The amplitude of the target is defined as the amplitude of the runways within the aerial photograph.

Nontarget (N_2) is an aerial photograph that does not contain runways. The amplitude of the nontarget is that of the straight-line patterns other

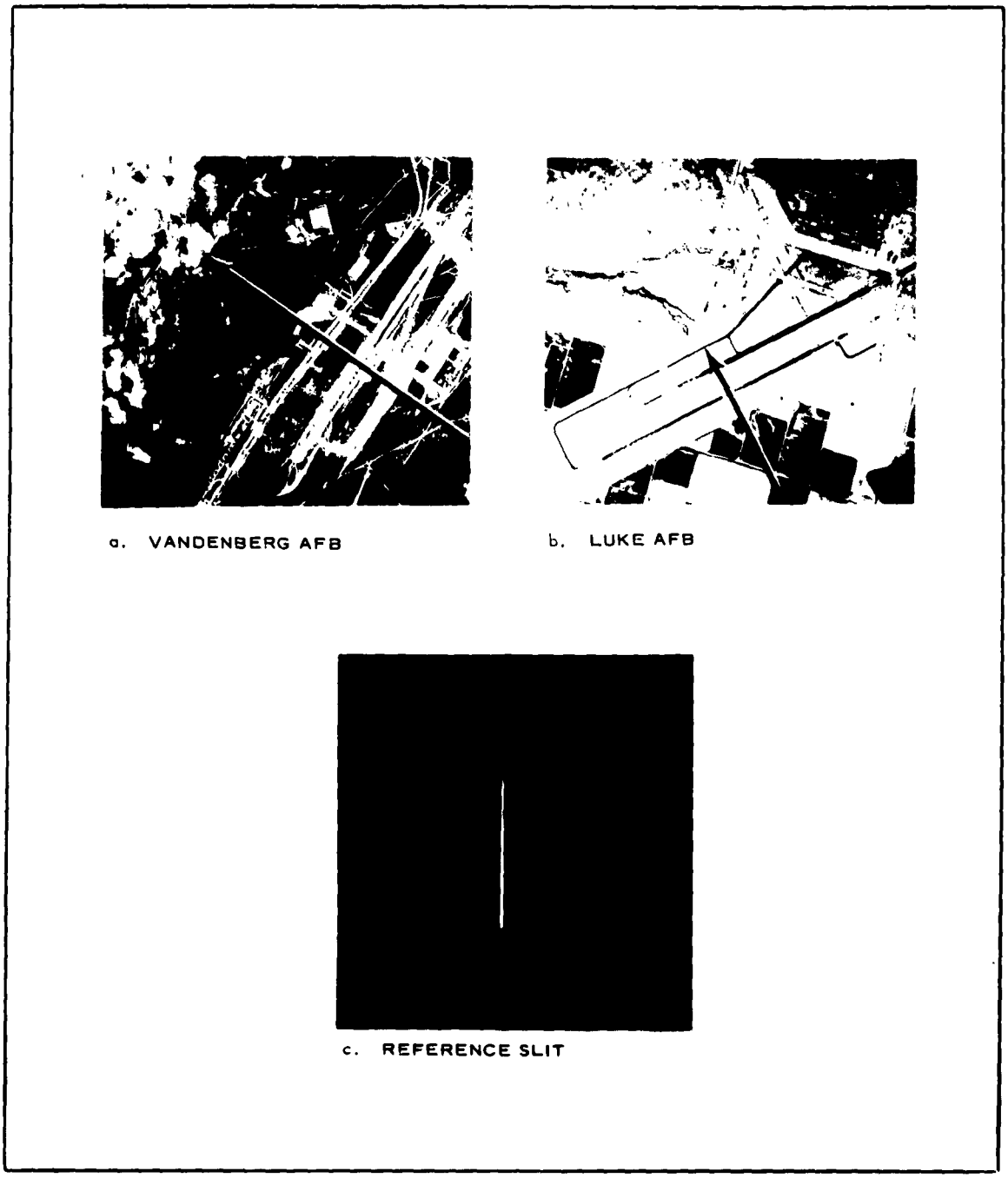

Figure 60 - Aerial Photographs of (a) Vandenberg AFB and (b) Luke AFB with Reference Slit (c)

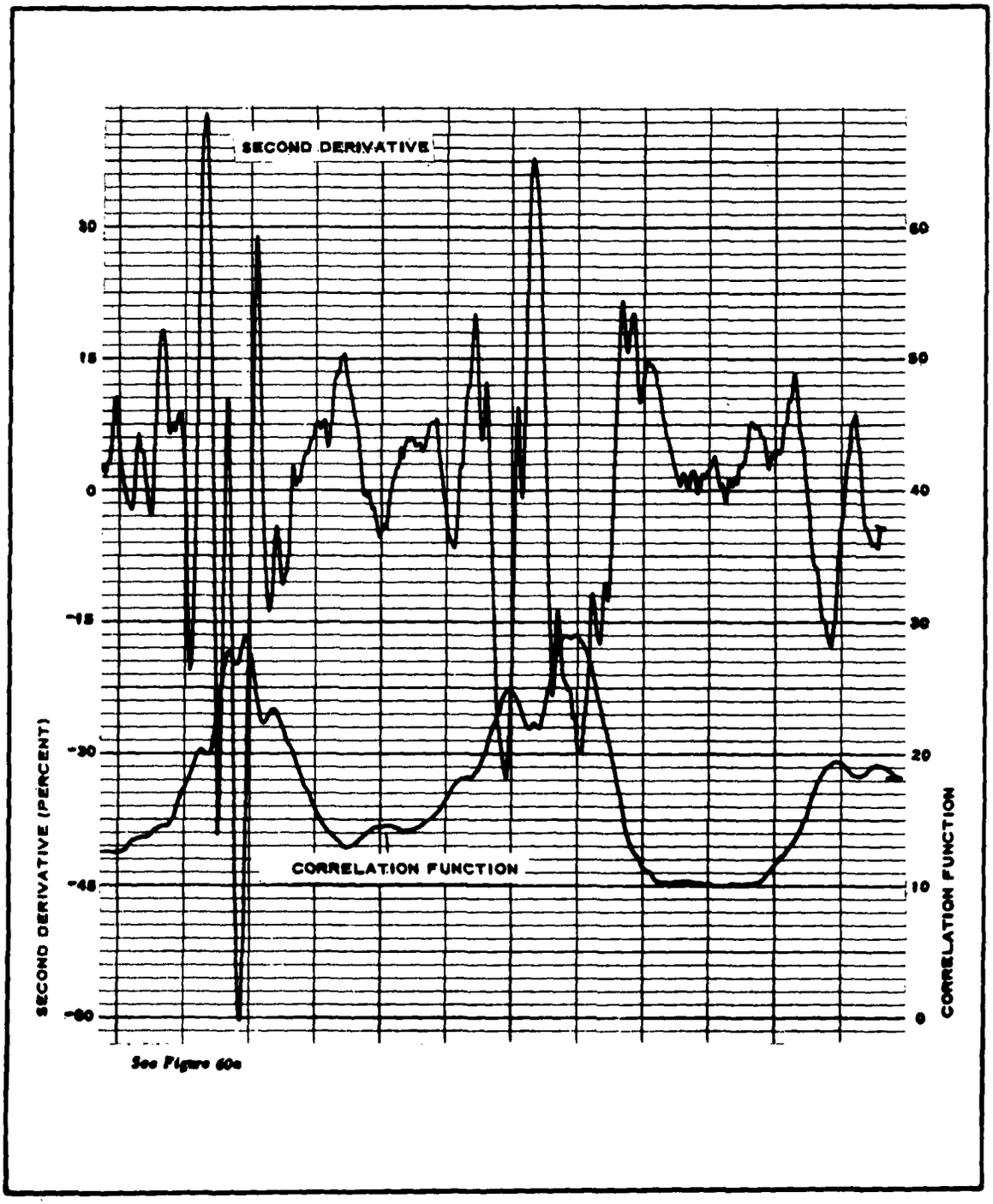

Figure 61 - Dual Channel Recording for Vandenberg AFB Aerial Photograph

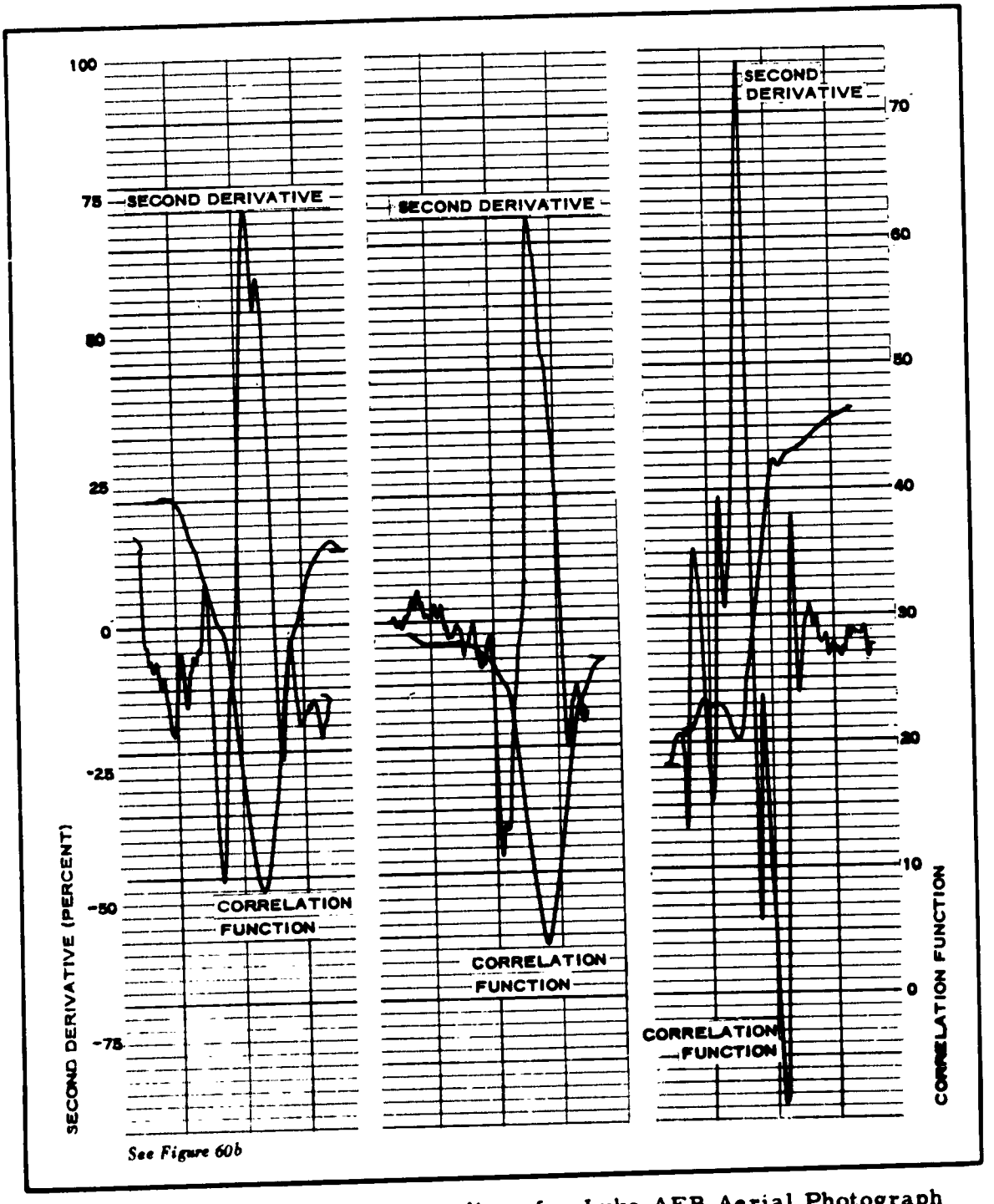

Figure 62 - Dual Channel Recordings for Luke AFB Aerial Photograph

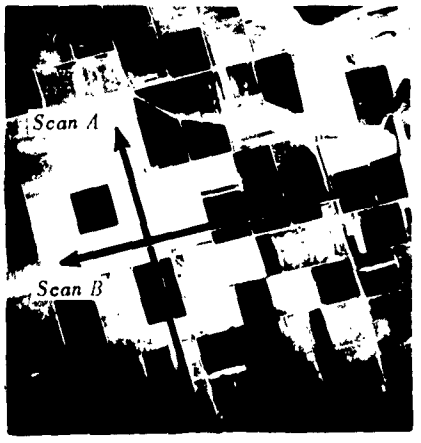

a. PHOENIX AREA

b. DALLAS AREA

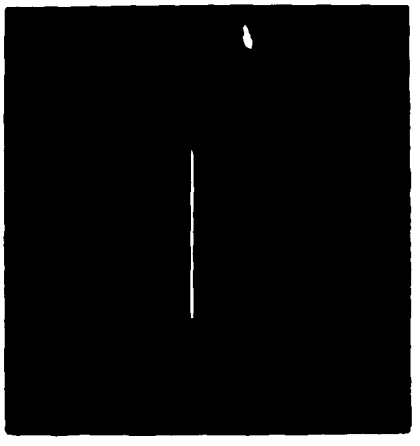

c. REFERENCE SLIT

Figure 63 - Aerial Photographs of (a) Phoenix Area and (b) Dallas Area with Reference Slit (c)

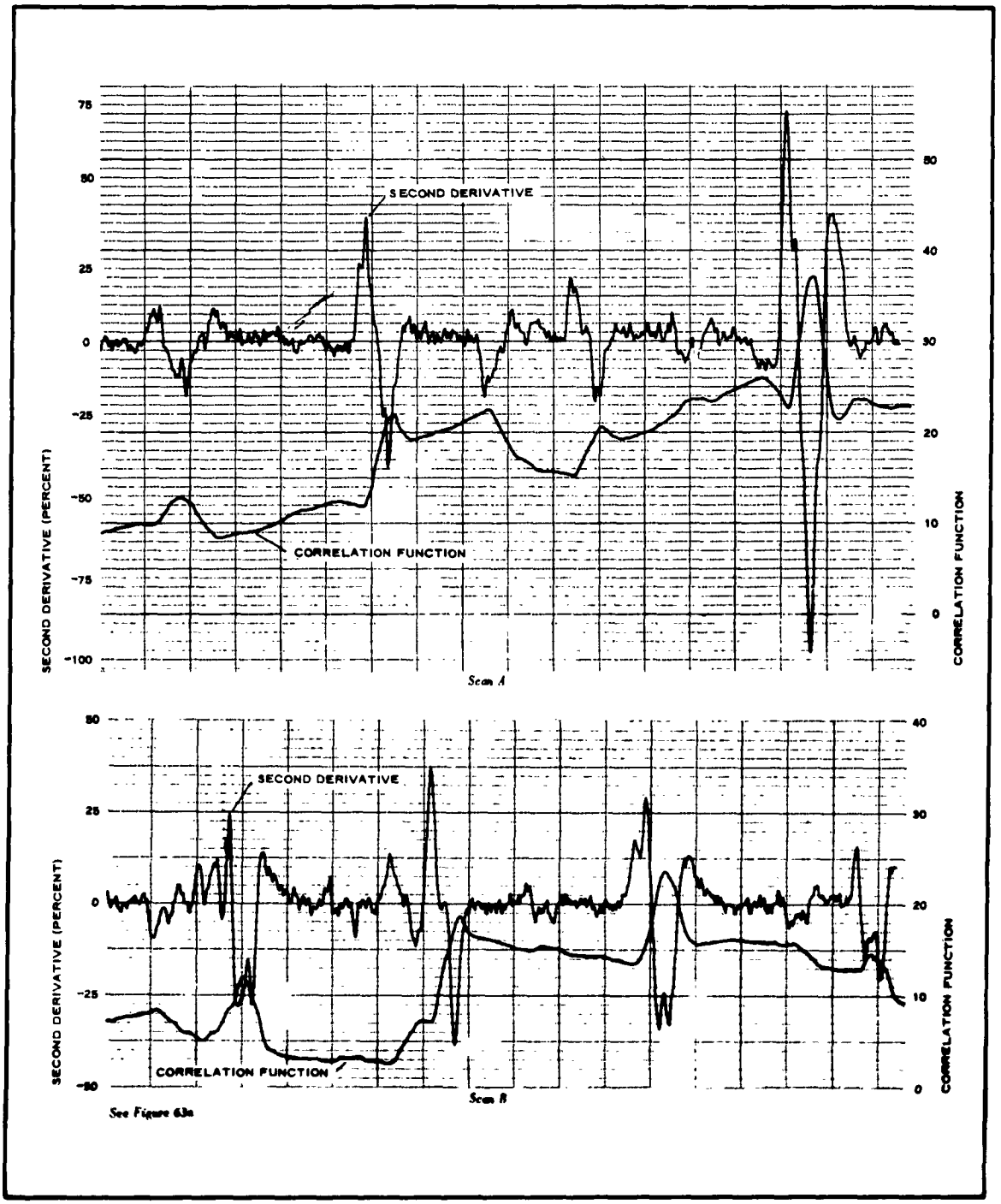

Figure 64 - Dual Channel Recordings for Phoenix Area Aerial Photograph

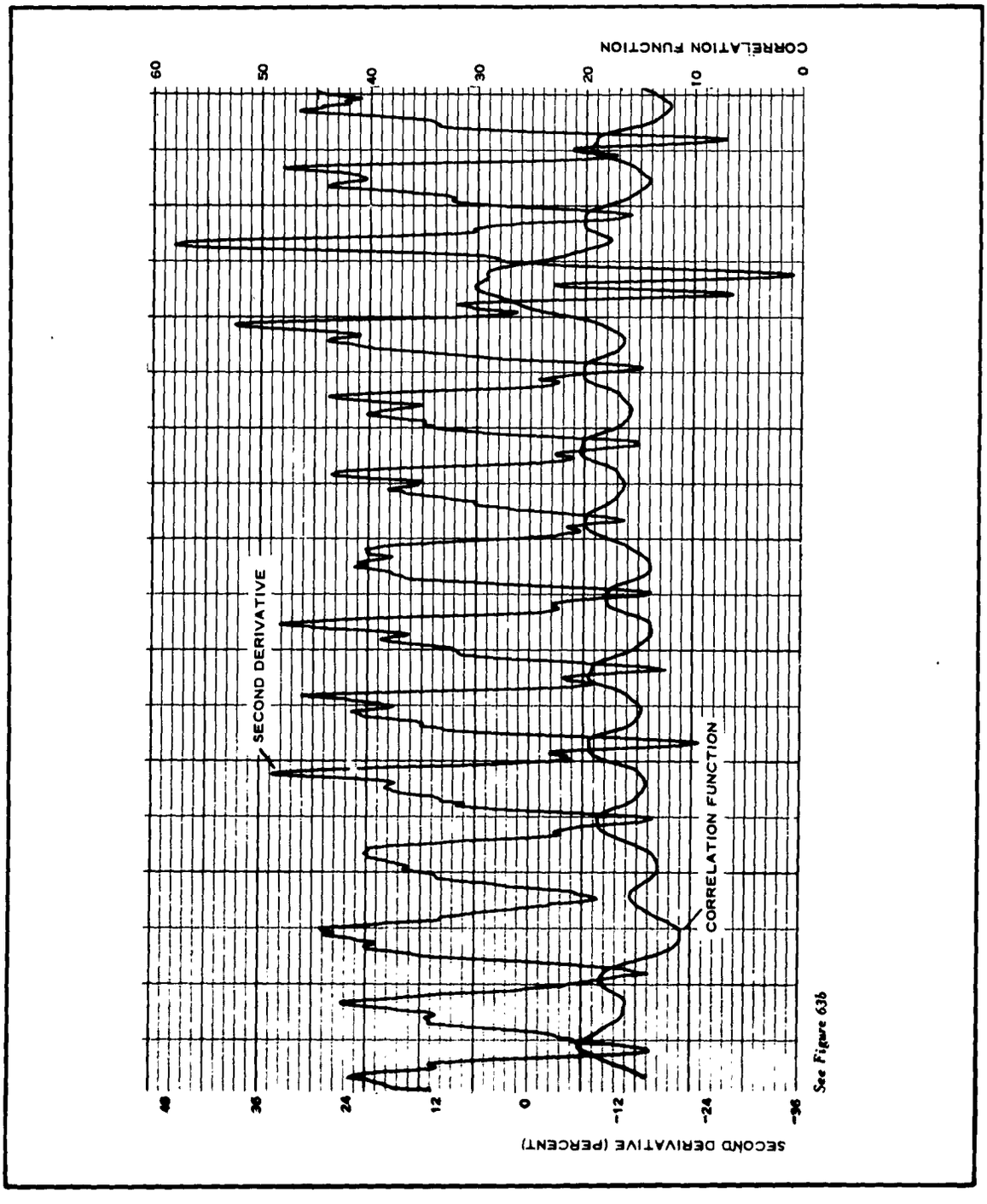

Figure 65 - Dual Channel Recording for Dallas Area Aerial Photograph

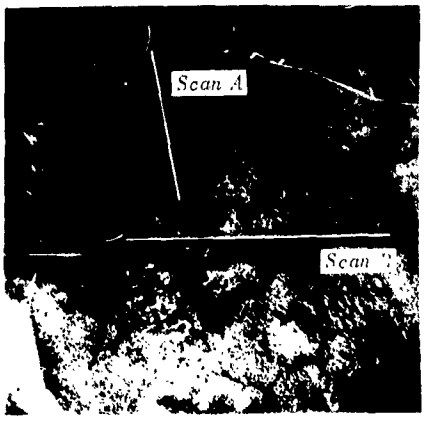

a. FLORIDA SWAMP

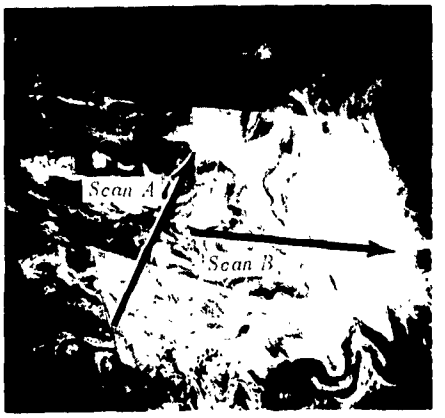

b. FT. WORTH AREA

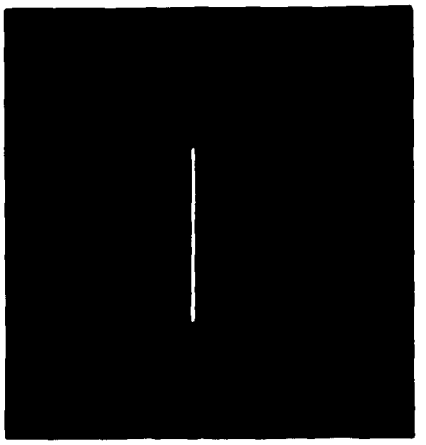

c. REFERENCE SLIT

Figure 66 - Aerial Photographs of (a) Florida Swamp and (b) Ft. Worth Area with Reference Slit (c)

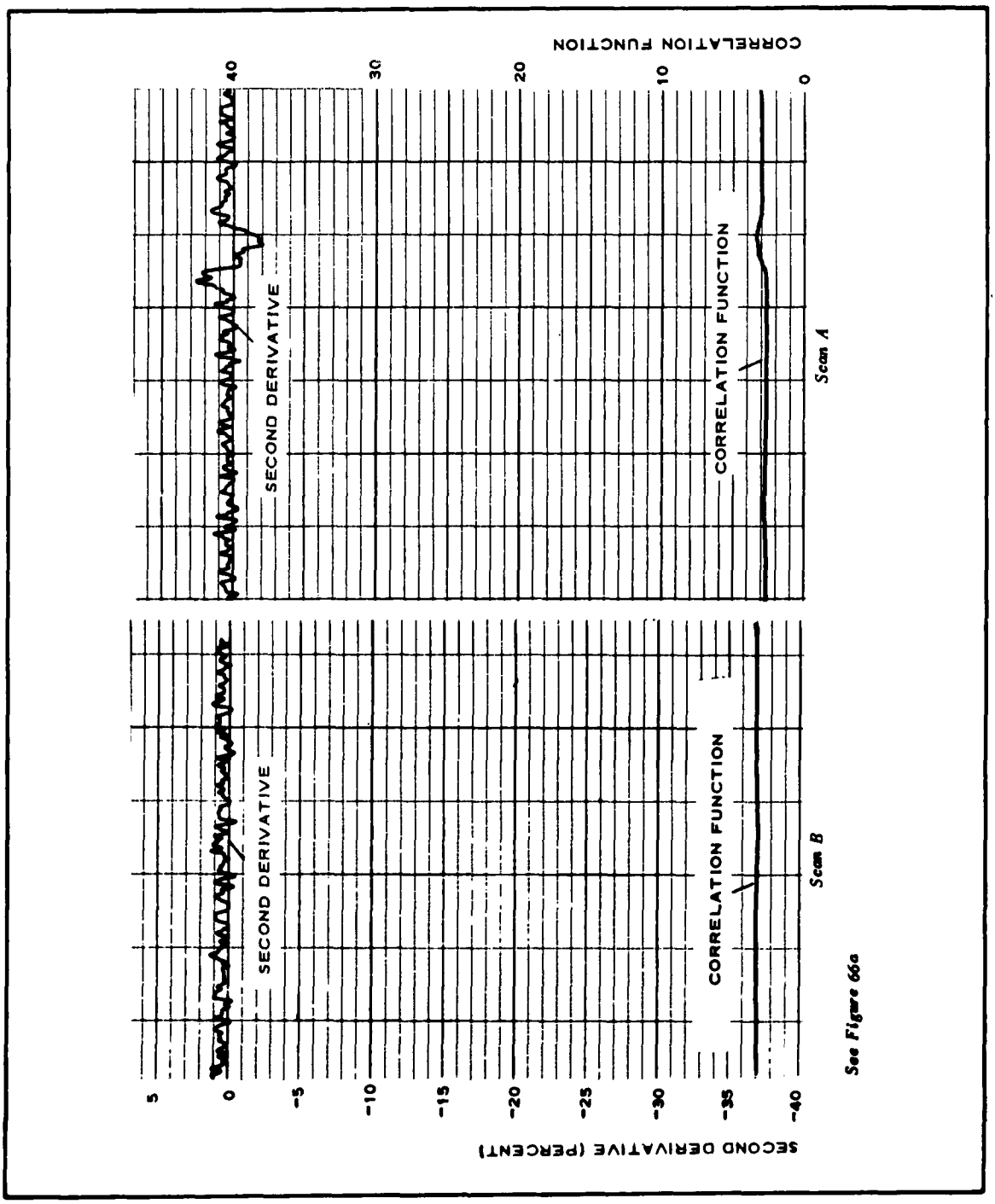

Figure 67 - Dual Channel Recordings for Florida Swamp Aerial Photograph

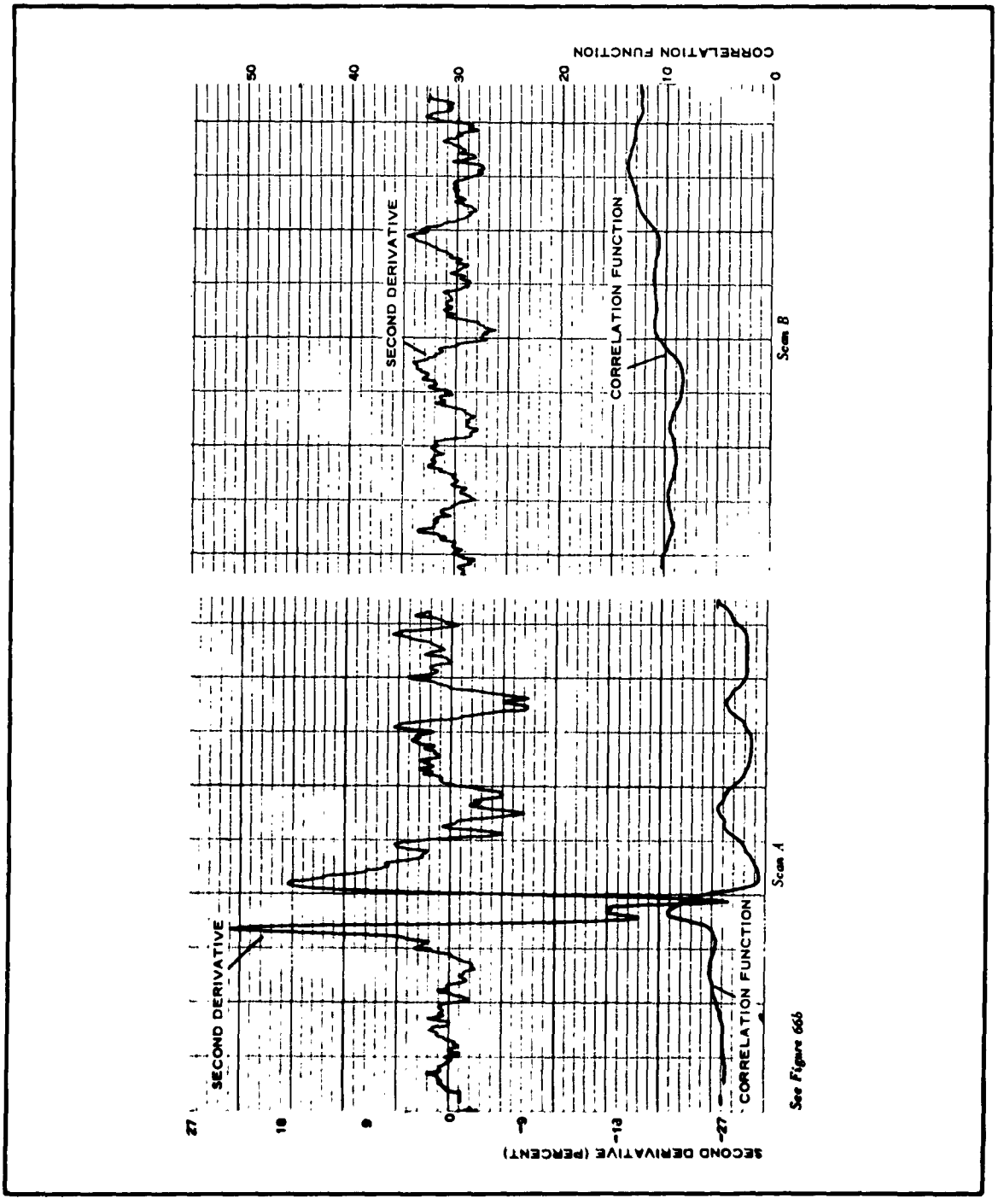

Figure 68 - Dual Channel Recordings for Ft. Worth Area Aerial Photograph

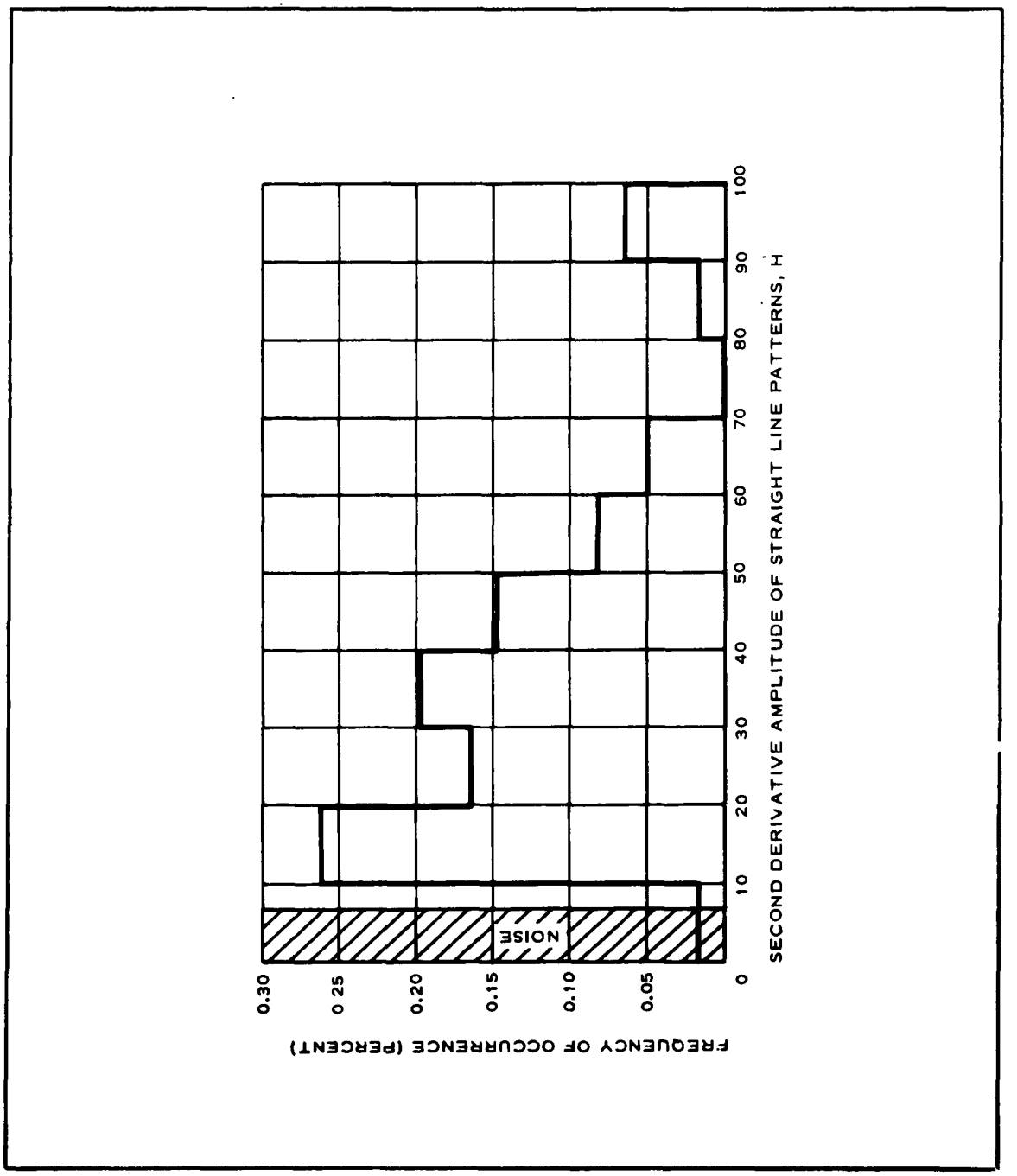

Figure 69 - Frequency of Occurrence vs Second Derivative Amplitude of Straight-Line Patterns

than runways that are contained in the aerial photograph.

Definition 3: Target (T_3) is a runway in an aerial photograph.

Nontarget (N_3) is an aerial photograph that does not contain runways.

Based on these two definitions, the data can best be evaluated in terms of conditional probability and the likelihood ratio, r, which is defined as

$$r = \frac{P(X/T)}{P(X/N)} ,$$

where

X = threshold amplitude of the second derivative,
P(X/T) = probability that X exists given T, and
P(X/N) = the probability that X exists given N.

Table X and XI show the calculated values of P(X/T), P(X/N), and r corresponding to Definitions 2 and 3 for different threshold amplitudes, X.

Table X shows that for a threshold amplitude of X = 15, for example, the probability that a target T_2 (Definition 2) will be detected is unity. Therefore, all target scenes will be detected; but, in addition, 70 percent of the nontarget scenes will be detected.

Table XI indicates that for a threshold amplitude of X = 15, for example, the probability that a target T_3 (Definition 3) will be detected is 20/22. Therefore, 20 out of 22 targets will be detected; but, in addition, 70 percent of the nontarget scenes will be detected.

The number of aerial photographic scenes is relatively small and was selected as being representative of certain target types. Consequently, the calculated probabilities should be understood to represent the best estimate of target recognition based on the limited sample of aerial photographs.

Although the data sample is small, several conclusions are in order.

First, the detection of straight-line patterns appears feasible since the second-derivative amplitude for the great majority of straight-line patterns is above the maximum for the background (see Figure 69).

TABLE X - CONDITIONAL PROBABILITY AND LIKELIHOOD RATIO FOR DEFINITION 2

Threshold amplitude, X	$P(X/T_2)$	$P(X/N_2)$	$\frac{P(X/T_2)}{P(X/N_2)}$
10	9/9	9/10	1.111
15	9/9	7/10	1.428
20	7/9	6/10	1.296
25	7/9	6/10	1.296
30	6/9	5/10	1.333
35	5/9	5/10	1.111
40	5/9	5/10	1.111

TABLE XI - CONDITIONAL PROBABILITY AND LIKELIHOOD RATIO FOR DEFINITION 3

Threshold amplitude, X	$P(X/T_3)$	$P(X/N_3)$	$\frac{P(X/T_3)}{P(X/N_2)}$
10	21/22	9/10	1.060
15	20/22	7/10	1.379
20	15/22	6/10	1.136
25	15/22	6/10	1.136
30	14/22	5/10	1.272
35	10/22	5/10	0.9090
40	5/22	5/10	0.454

Second, recognition of straight-line patterns by the amplitude of the second derivative of the correlation function alone does not appear feasible; i.e., runways cannot be separated from roads, bridges cannot be separated from runways, etc.

Third, it appears feasible to measure the width of the strip from the second-derivative signals. Theoretically, when a strip is correlated to a strip that is wider than the slit, two second-derivative pulses of opposite polarity are generated at each edge of the strip. If the signal is rectified, four pulses are obtained for each strip. It is hoped that this principle can be used to measure the width of the strip by measuring the distance between the pulses. However, in some of the cases observed in the laboratory the pulses are not always of equal amplitude nor does the signal between them necessarily return to a zero level. Consequently, a satisfactory threshold level might be difficult to establish.

7. DETECTION OF SHIPS BY SLIT TEMPLATE CORRELATION

The correlation of various line patterns with a rectangular slit offered the possibility that ships might be detected by the same method. Accordingly, an aerial photograph, with a scale of 1 to 10,000, of three ships in the Mississippi River was prepared (Figure 70). The middle ship was correlated with a rectangular slit of 0.020 by 1.00 in. The correlation function and the second derivative of the correlation function are shown in Figure 70. Reflected sunlight from one side of the ship and the shadow on the other side resulted in a correlation function with positive and negative peaks.

These ships could be detected by any reasonable threshold level since the maximum signal-to-noise ratio is 19 to 1. An increase in the roughness of the water would be accompanied by a reduction in the maximum signal-to-noise ratio.

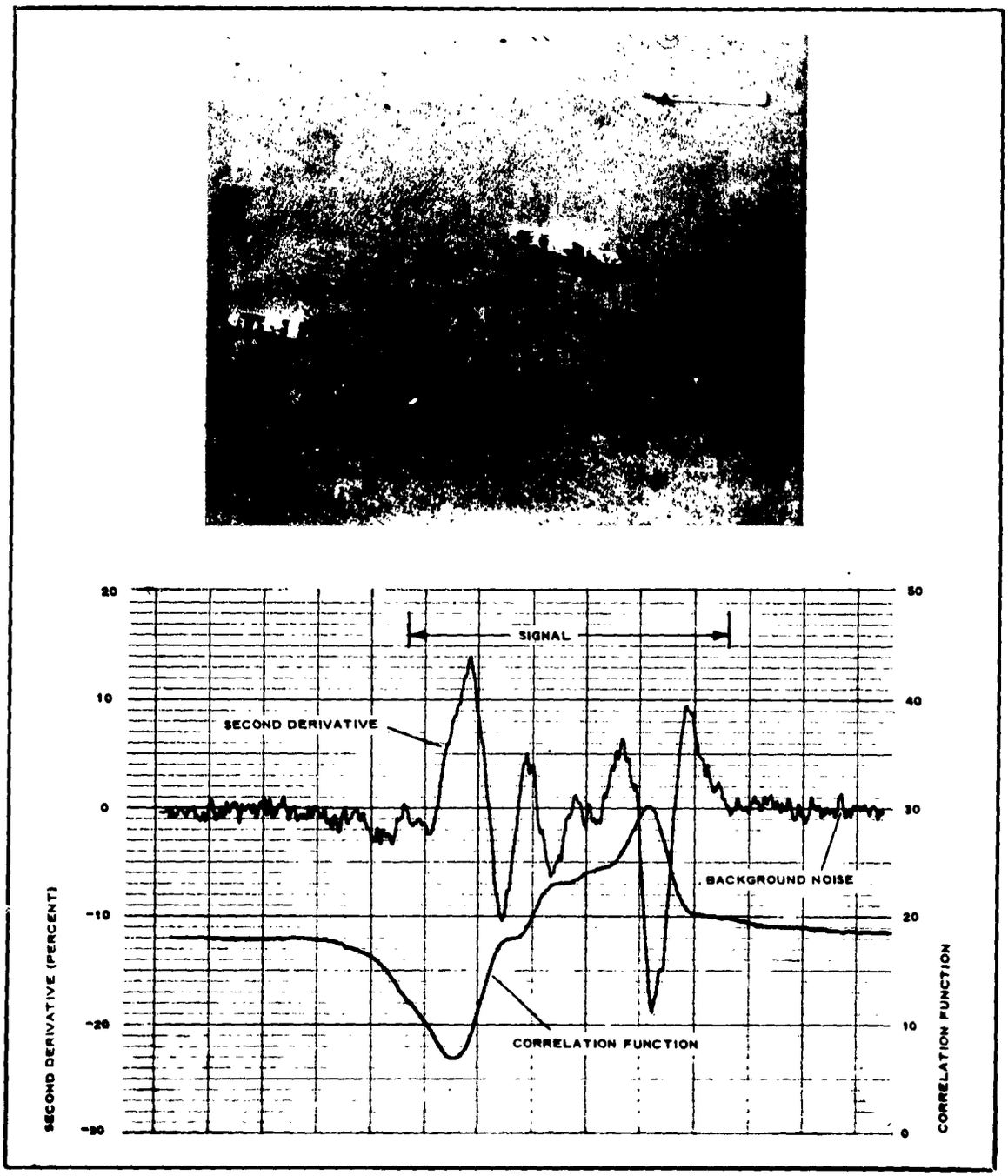

Figure 70 - Correlation Function and Second Derivative of Slit Template and Ship

SECTION IV - EXPERIMENTAL EVALUATION OF CORRELATION TECHNIQUES

Subsection Four - Runway Detection by Width Gating

1. GENERAL

Width gating or sifting was studied as part of a process for recognizing airport runways. It is based on correlation of a spot with the scene and the attributes of edge gradient and width. The amplitude of the first derivative of the correlation function is proportional to scene gradients. An amplitude threshold filters out the low gradients and logic circuitry analyzes gradient separation. Two gradients separated by an interval greater than some arbitrary minimum and less than some arbitrary maximum causes an output pulse to be generated. If the spot is scanned in a rectangular raster and the output pulses displayed, lines in the scene of the proper width are mapped onto the output display as a line. The great majority of the background is filtered out. In the following experimental study, instrumentation, hereafter called the "width-sifter," was developed to perform these operations.

The width-sifter consists of an fss, a processor, and an output monitor. A simplified system block diagram is given in Figure 71; Figure 72 is a photograph of the system.

A number of aerial photographs were processed by the width-sifter to evaluate the device. Measurement of the length of displayed lines provides a basis for recognition of runway patterns. However, no provision was made for measurement of line lengths in this study. Suggested implementations for this purpose are described in Section V.

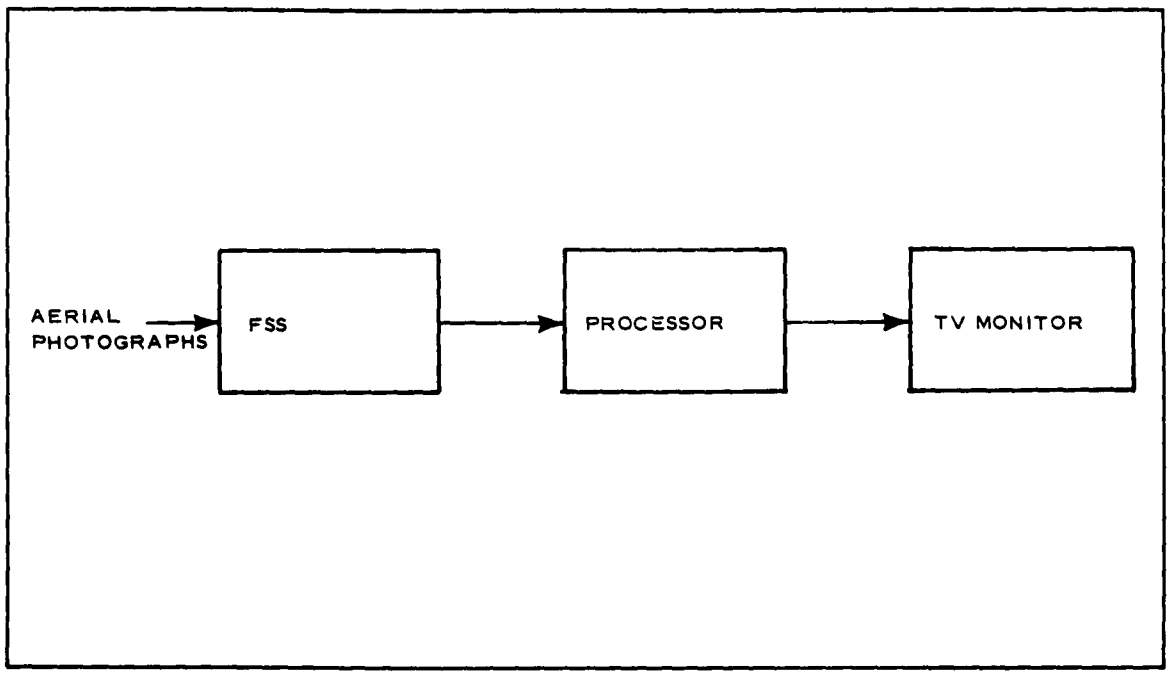

Figure 71 - Width-Sifter Block Diagram

2. DESCRIPTION OF WIDTH-SIFTER

a. Flying-Spot Scanner

The purpose of the fss is to convert the photographic data into electrical signals that can be processed through the logic circuitry part of the system. The inputs to the fss are aerial photographs in the form of transparencies.

For this experiment, a B and K television analyst (Model 1076) was used. An approximate measurement indicated that the spot size of the fss is 0.025 in. If a black strip is placed on the face of the crt of the fss, the video pulse output has a rise time of 0.5 μsec (see Figure 73a).

Figure 73b shows the dimensions of the aerial photograph placed on the face of the crt. The time required for the spot to travel the

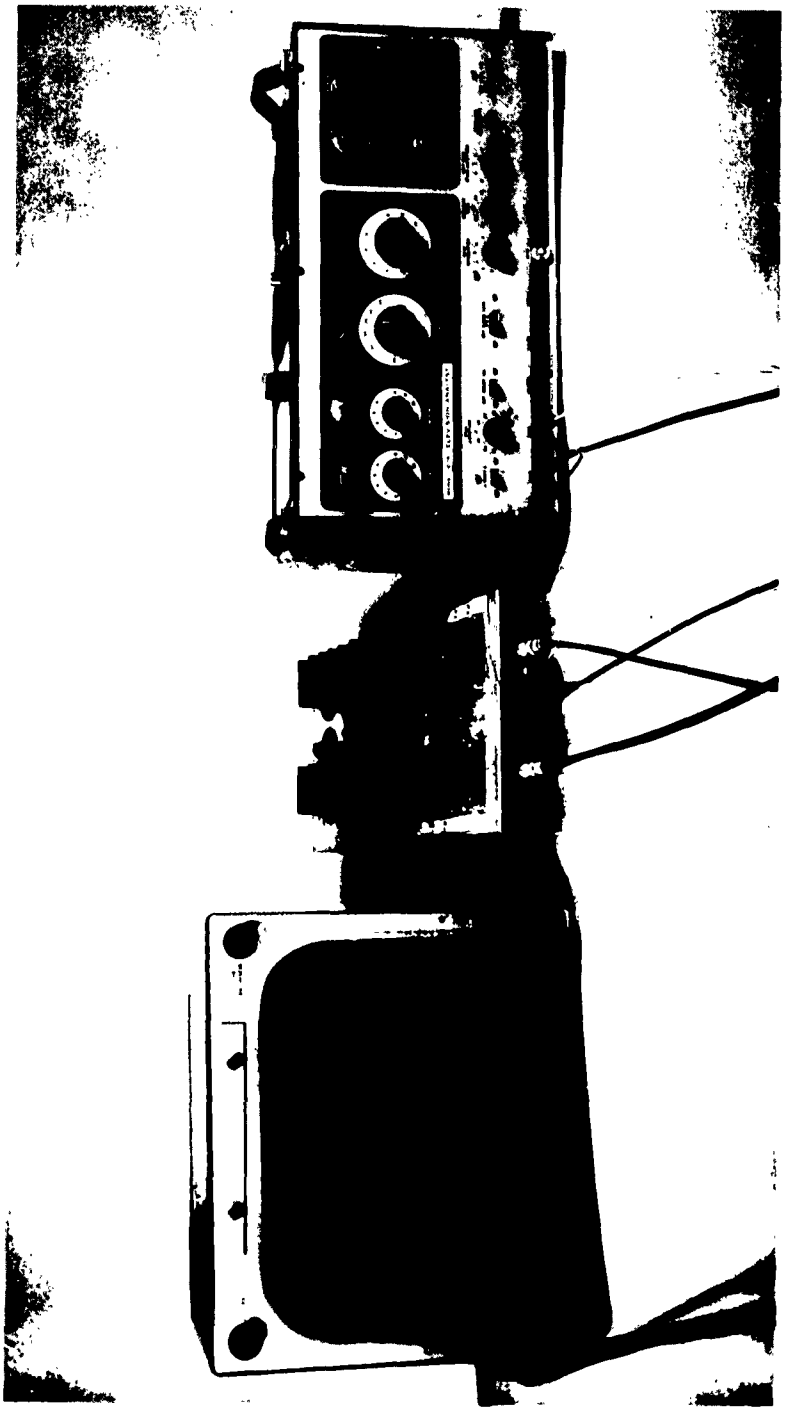

Figure 72 - Width-Sifter Arrangement

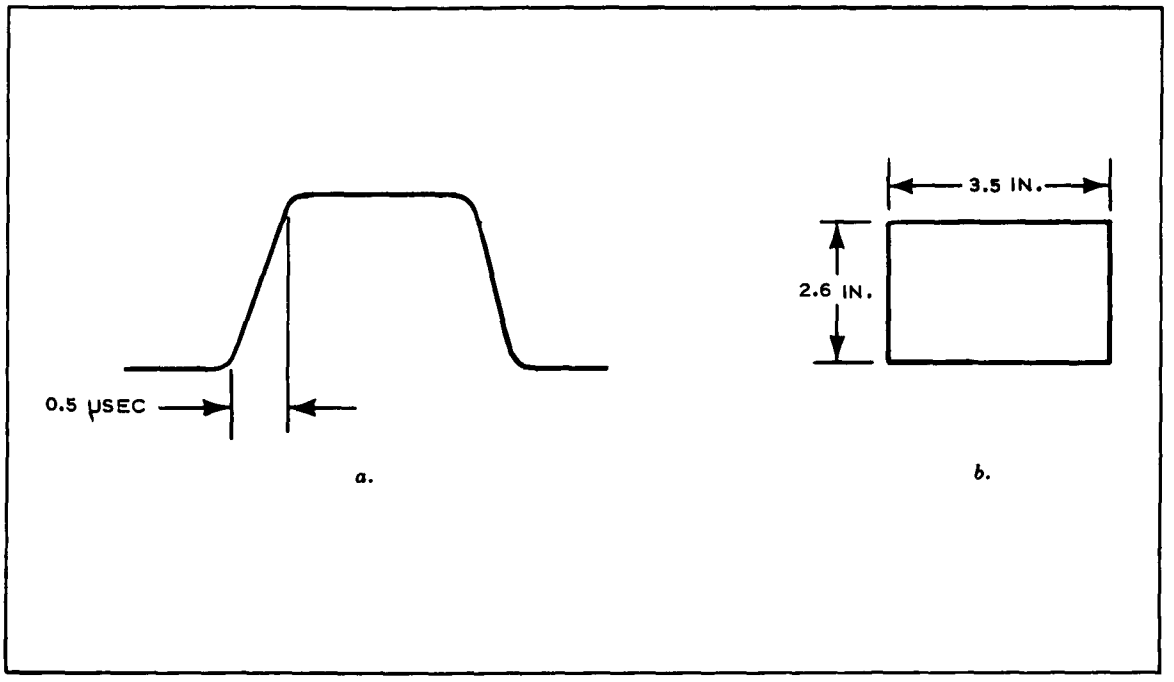

Figure 73 - Video Pulse Output and Aerial Photograph Dimensions

3.5 in. across the face of the crt is 53.7 μsec. There is also a considerable degree of shading in the fss.

The B and K television analyst is not the optimum fss, but it is adequate for the evaluation of the processor. It was chosen because it was readily available.

b. Processor

(1) General

The processor consists basically of a gradient detector, a minimum-width circuit, and a maximum-width circuit. (See Figure 74.) The gradient detector differentiates the input video and selects those pulses that have an amplitude exceeding a certain minimum; only those gradients above the minimum are permitted through the rest of the processing.

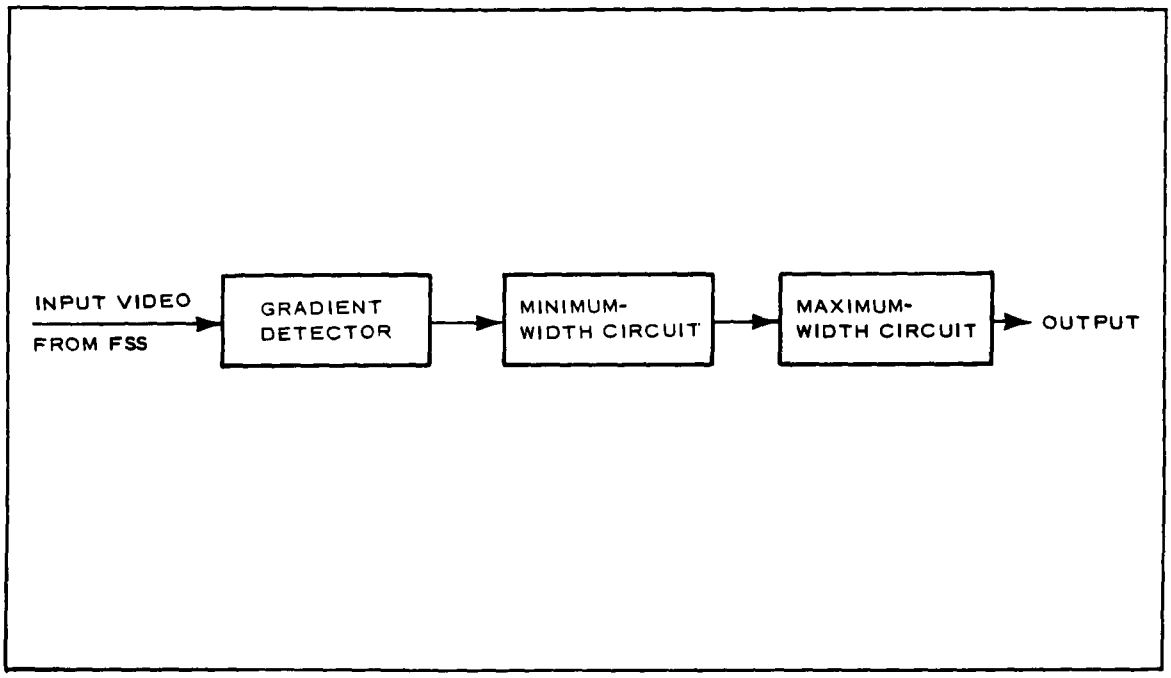

Figure 74 - Processor Simplified Block Diagram

The minimum-width circuit actually checks the width of every input pulse and accepts only pulses whose width exceeds a minimum. The minimum acceptable width can be varied by programming the minimum-width circuit.

The maximum-width circuit accepts all pulses that are shorter than a given maximum width. This circuit can also be programmed for any desired width.

The output of the processor is a series of pulses that occur at the trailing edge of every pulse and that meet the gradient and width requirements.

A functional block diagram of the processor is shown in Figure 75. The input video is first fed into a video amplifier (B-1). This experiment was carried out with the first amplifier bypassed, since the output of the fss was sufficient to drive the rest of the circuits.

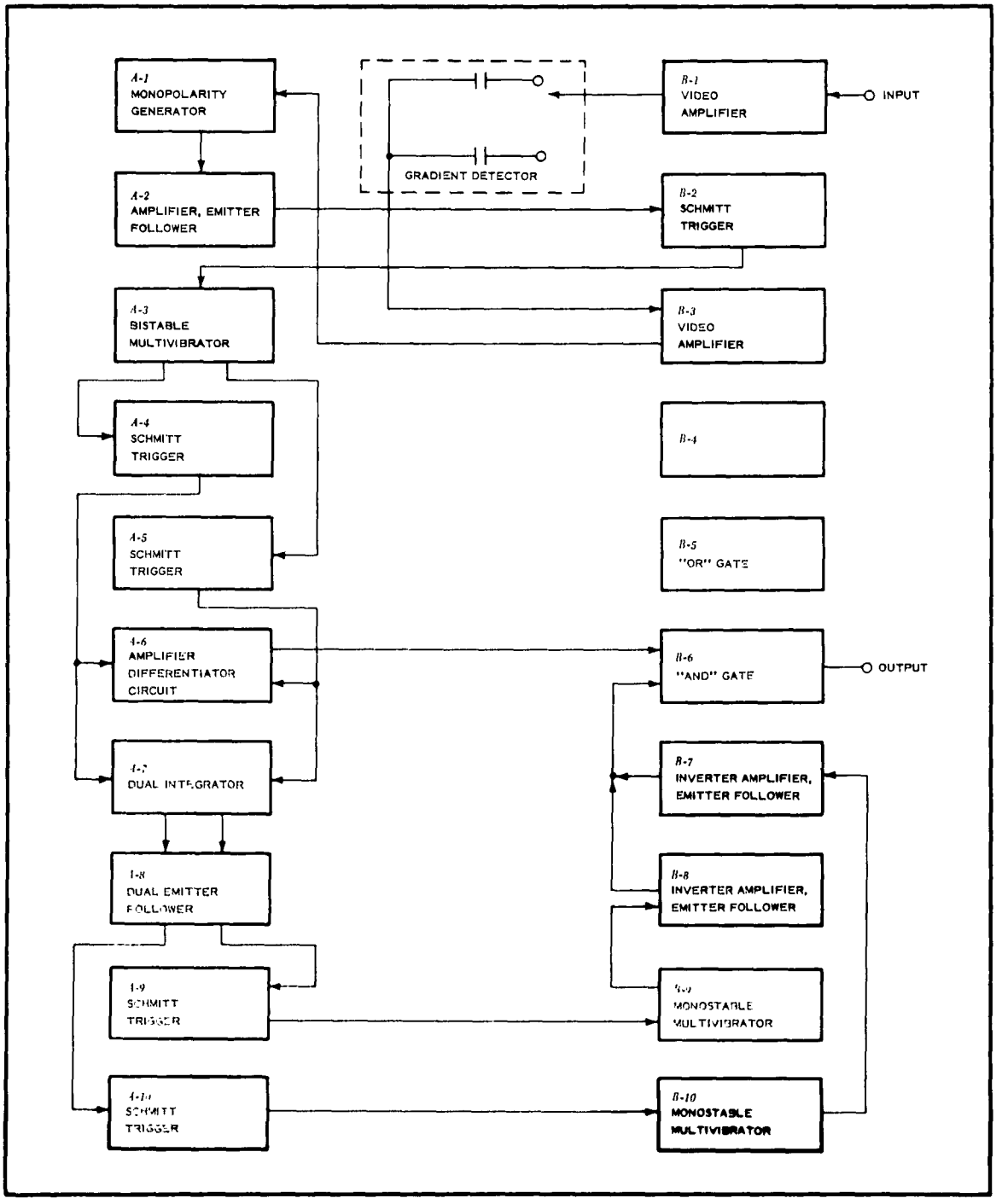

Figure 75 - Processor Functional Block Diagram

(2) Gradient Detector

The gradient detector consists of an r-c-type differentiating circuit, a monopolarity generator (A-1, Figure 75), an amplifier and emitter follower (A-2), and a Schmitt trigger (B-2). After the input video is differentiated, all the negative pulses are inverted through the monopolarity generator and amplified. The emitter follower is used for impedance matching. To this point, the video is converted into a series of negative pulses corresponding to the leading and trailing edges of each video pulse.

The Schmitt trigger (B-2) has an adjustable trigger level that can be set to a desirable value. Since the amplitude of the pulses is proportional to the gradient, the gradient can be detected by selecting a particular trigger level.

Following the Schmitt trigger is a bistable multivibrator (A-3), the output of which is the reconstruction of the input video pulses, except for those that do not meet the gradient criterion. Since the targets under consideration (runways) can be either black or white (positive or negative), both outputs of the bistable multivibrator are processed separately. There are two Schmitt triggers (A-4 and A-5) following each of the outputs of the bistable multivibrator. The purpose of the Schmitt trigger circuits is to improve the rise time of the pulse. The leading edge of each pulse becomes the basis for the time- or width-measuring circuits that follow.

(3) Minimum-Width Gate

The minimum-width measuring part of the processor consists of a dual integrator (A-7), a dual emitter follower card (A-8), and a Schmitt trigger for each channel (A-9 and A-10).

The output of the bistable multivibrator is clamped to the level

shown in Figure 76, wave forms 4 and 5. Both channels are integrated individually to a desired degree and each channel is fed into a Schmitt trigger circuit having a trigger level that can be adjusted to the desired value.

By selecting the r-c time constant of the integrator and setting the trigger level of the Schmitt trigger, the desired time delay can be obtained between the leading edges of the bistable multivibrator output pulses and the leading edges of the Schmitt trigger output pulses. This time delay corresponds to the minimum target width. If the duration of the pulse (target width) is less than the time delay, the pulse (target) will be rejected. If the pulse exceeds this minimum width, it will be accepted and fed into the following stage, which employs the maximum-width criterion.

(4) Maximum-Width Gate

The maximum-width measuring part of the processor consists of two monostable multivibrators (B-9 and B-10) followed by two amplifiers and emitter follower cards (B-7 and B-8), one for each channel. The monostable multivibrators are triggered by the leading edge of each of the Schmitt trigger outputs. By adjusting the r-c time constant in the monostables, the duration of the pulses from the monostables can be adjusted to a desired value.

The outputs of both monostable multivibrators are added and they become the input to the "and" circuit (B-6), which is the final stage of the video processing.

The other input to the "and" circuit is a series of pulses that correspond to the differentiated bistable multivibrator output (A-6). If any of the pulses occur during the time the monostable multivibrator is on, then there is an output from the "and"

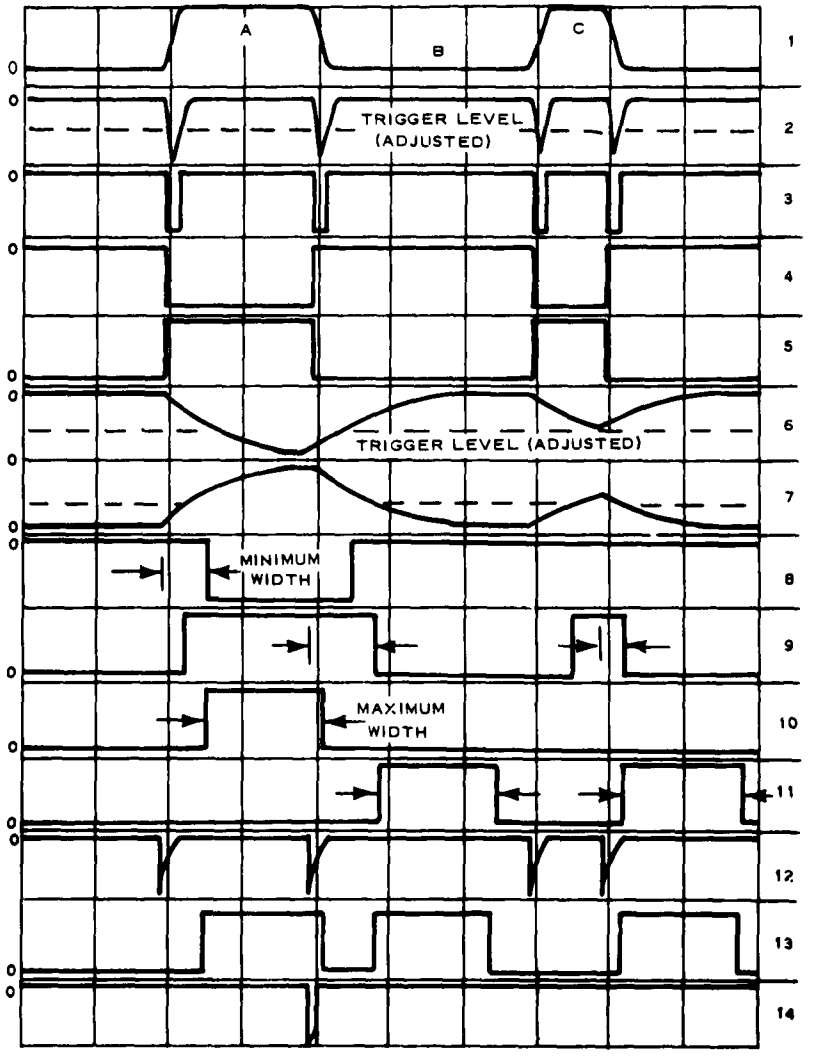

1. INPUT VIDEO
2. DIFFERENTIATED VIDEO AND RECTIFIER
3. SCHMITT TRIGGER OUTPUT
4. BISTABLE MULTIVIBRATOR, CHANNEL A
5. BISTABLE MULTIVIBRATOR, CHANNEL B
6. INTEGRATOR OUTPUT, CHANNEL A
7. INTEGRATOR OUTPUT, CHANNEL B
8. MINIMUM-WIDTH GATE, CHANNEL A
9. MINIMUM-WIDTH GATE, CHANNEL B
10. MAXIMUM-WIDTH GATE, CHANNEL A
11. MAXIMUM-WIDTH GATE, CHANNEL B
12. DIFFERENTIATED BISTABLE MULTIVIBRATOR OUTPUTS
13. MONOSTABLE MULTIVIBRATOR OUTPUTS ADDED
14. "AND" CIRCUIT OUTPUT

Figure 76 - Theoretical Wave Forms

circuit that corresponds to the trailing edge of the target. This output is then fed into the TV monitor for viewing or photographing.

(5) Wave Forms

To describe the basic concept of the system more effectively, a set of theoretical wave forms is shown in Figure 76. The input video as shown consists of three targets: A, B, and C. The gradient level has been selected so that all differentiated pulses are accepted. The time delays for the minimum and maximum width criteria have been selected so that only target A meets the requirements; target C is too small and target B, too large.

In addition to the theoretical wave forms (Figure 76), a complete set of actual wave forms is shown in Figure 77. These were obtained by using a pulse generator as the input to the processor.

The last three pairs of wave forms shown in Figure 77 demonstrate the principle of operation of the processor. In Figures 77k and 77m, the width of the input pulse falls outside the limits of acceptable width and therefore there is no output. In Figure 77l, the width of the input pulse falls within the minimum and maximum width limits for which the processor was programmed, and therefore there is an output pulse corresponding to the trailing edge of the input pulse (target).

In Figure 77k, l, and m, some time delay exists between the trailing edge of the input target and the output pulse. This delay is caused by the preceeding stages and is of no consequence.

3. EVALUATION OF WIDTH-SIFTER

Nine near-vertical aerial photographs were selected to be used as the input to the width-sifter (Figures 78 through 86). Four of these photographs

1

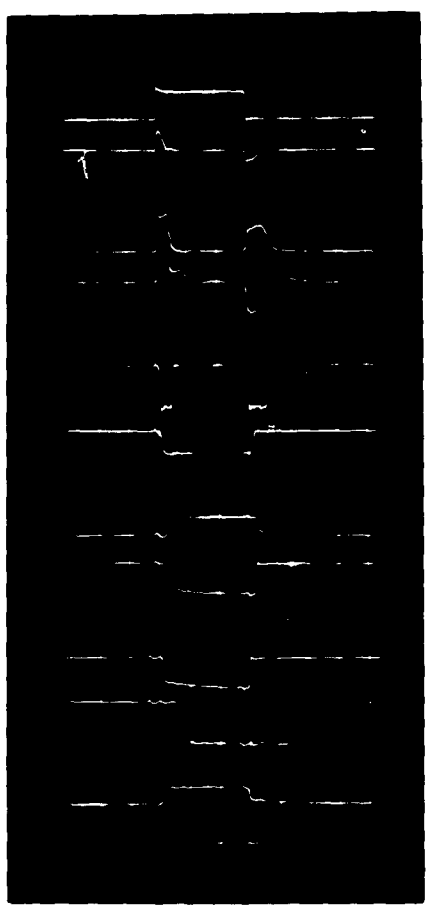

a. INPUT VIDEO
DIFFERENTIATED VIDEO

b. DIFFERENTIATED VIDEO RECTIFIED
DIFFERENTIATED VIDEO INVERTED

c. SCHMITT TRIGGER OUTPUT
BISTABLE MULTIVIBRATOR

d. BISTABLE MULTIVIBRATOR OUTPUTS (2 CHANNELS)

e. TIME DELAY FOR CHANNEL 1
MINIMUM WIDTH

f. TIME DELAY FOR CHANNEL 2
MINIMUM WIDTH

g. MAXIMU

h. MAXIMI

i. AMPLI

j. INPUT

k. INPUT
OUTP

l. INPUT
OUTPI

m. INPU
OUTP

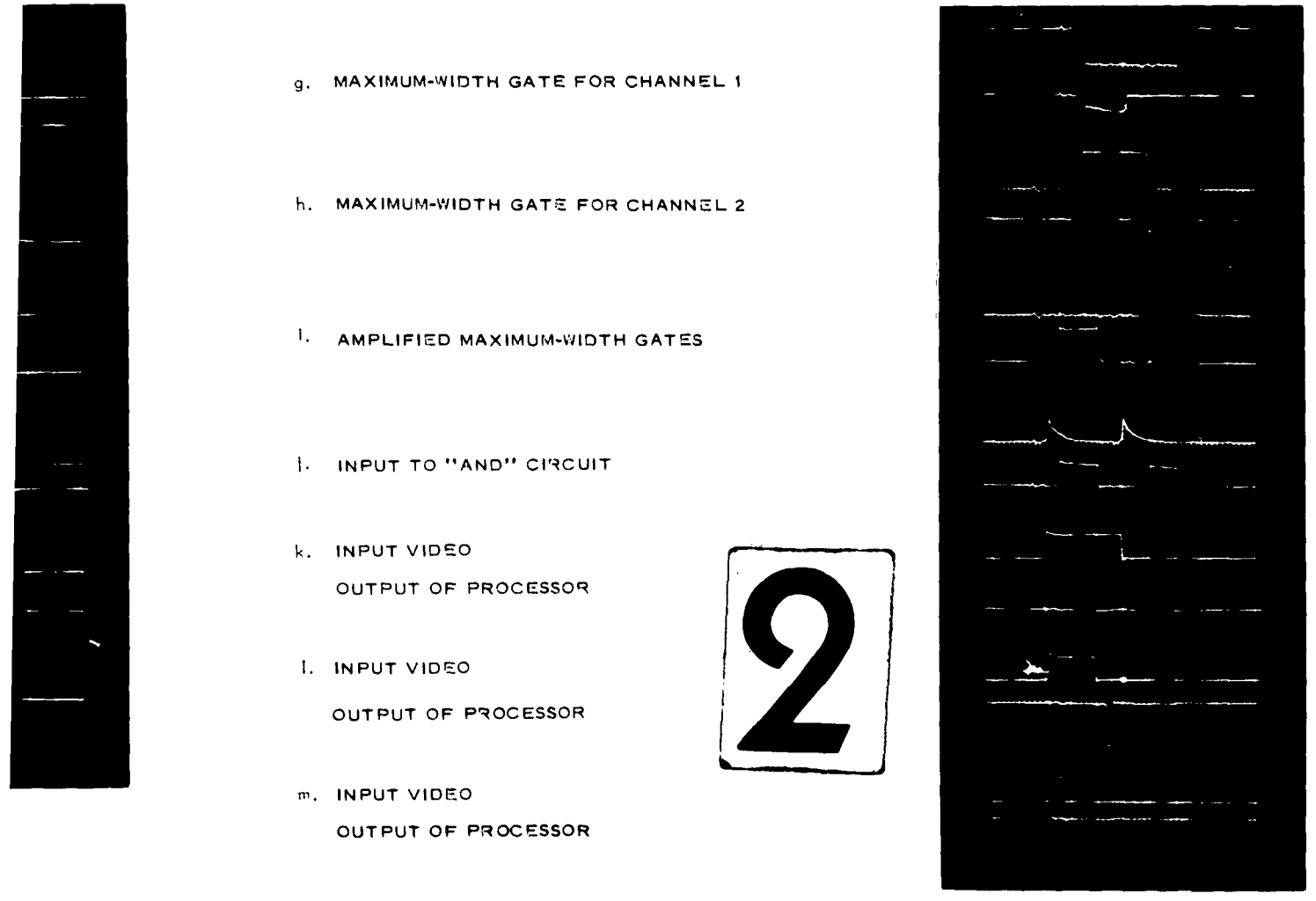

Figure 77 - Processor Wave Forms with Square Pulse Input

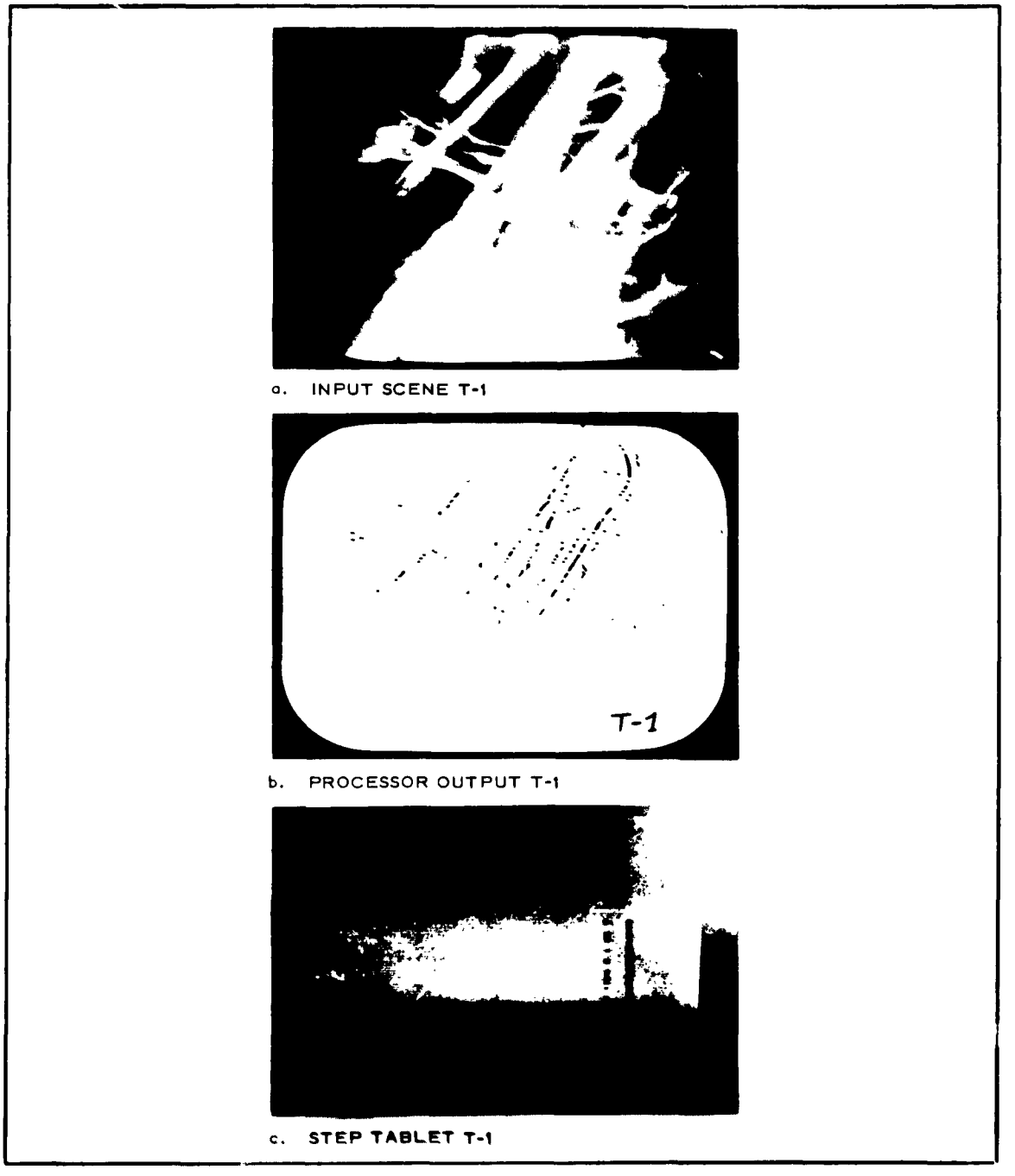

Figure 78 - Input Photograph of Vandenberg AFB (a) with Processor Output (b) and Step Tablet (c)

a. INPUT SCENE T-2

b. PROCESSOR OUTPUT T-2

c. STEP TABLET T-2

Figure 79 - Input Photograph of Carswell AFB (a) with Processor Output (b) and Step Tablet (c)

a. INPUT SCENE T-3

b. PROCESSOR OUTPUT T-3

c. STEP TABLET T-3

Figure 80 - Input Photograph of Dallas NAS (a) with Processor Output (b) and Step Tablet (c)

a. INPUT SCENE T-4

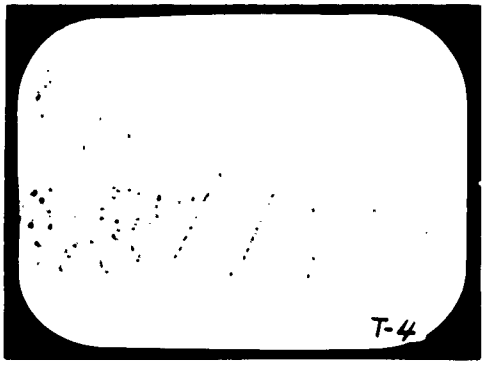

b. PROCESSOR OUTPUT T-4

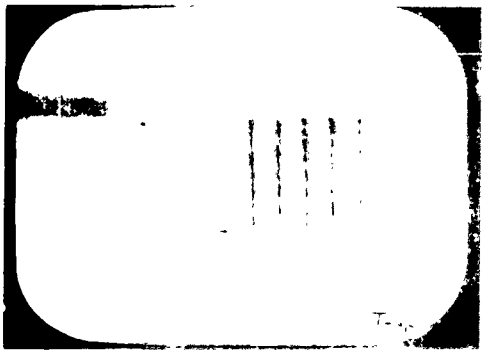

c. STEP TABLET T-4

Figure 81 - Input Photograph of Luke AFB (a) with Processor Output (b) and Step Tablet (c)

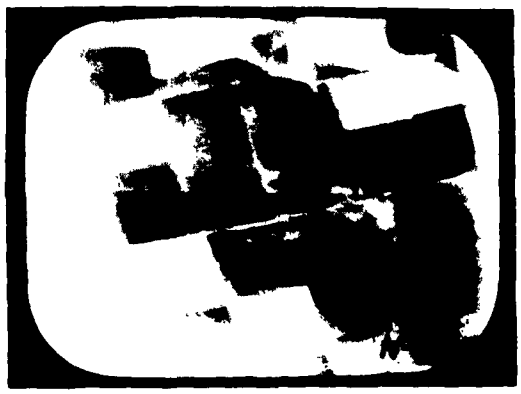

a. INPUT NONRUNWAY SCENE T-10

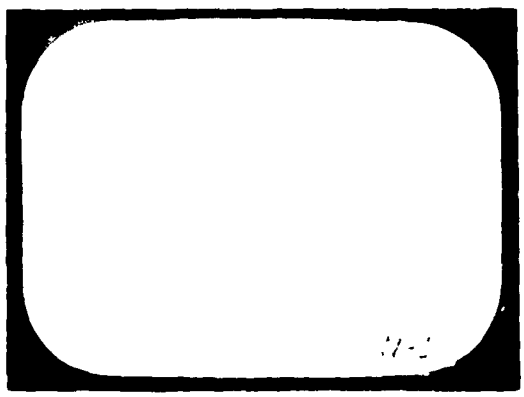

b. PROCESSOR OUTPUT T-10

Figure 82 - Input Photograph of Phoenix Area (a) with Processor Output (b)

a. INPUT NONRUNWAY SCENE T-12

b. PROCESSOR OUTPUT T-12

Figure 83 - Input Photograph of Ft. Worth-Dallas Area T-12 (a) with Processor Output (b)

a. INPUT NONRUNWAY SCENE T-21

b. PROCESSOR OUTPUT T-21

Figure 84 - Input Photograph of Ft. Worth-Dallas Area T-21 (a) with Processor Output (b)

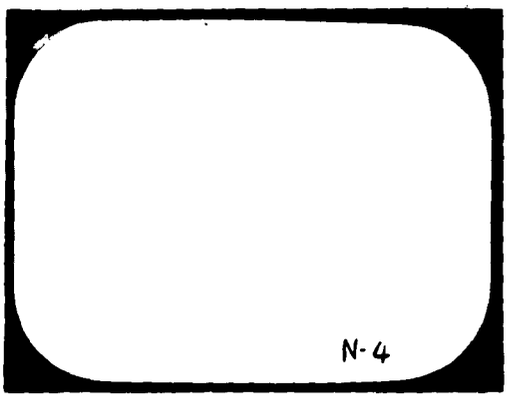

a. INPUT NONRUNWAY SCENE T-15

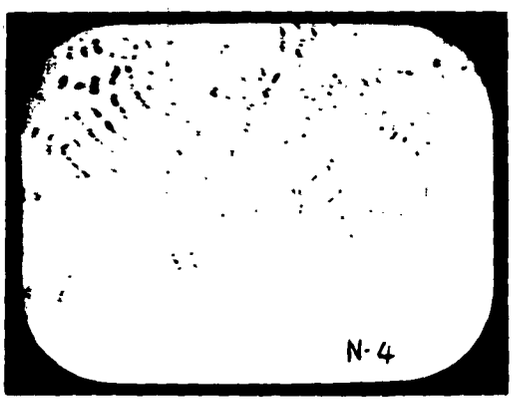

b. PROCESSOR OUTPUT T-15

Figure 85 - Input Photograph of Ft. Worth-Dallas Area T-15 (a) with Processor Output (b)

a. INPUT NONRUNWAY SCENE T-11

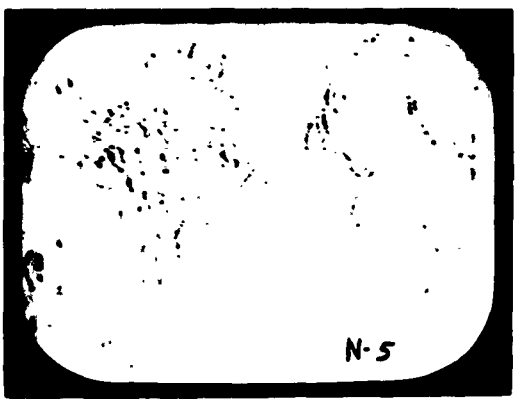

b. PROCESSOR OUTPUT T-11

Figure 86 - Input Photograph of Florida Coastal Area (a) with Processor Output (b)

contain runways and five do not. Some of the nonrunway scenes, however, contain roads or other runway-like patterns. The aerial photographs given in Table XII were used in this experimental study.

TABLE XII - AERIAL PHOTOGRAPHS FOR WIDTH-SIFTER EVALUATION

Aerial photograph	Code no.	Figure no.
Runway scenes		
Vandenberg AFB	T-1	78
Luke AFB	T-4	79
Dallas NAS	T-3	80
Carswell AFB	T-2	81
Nonrunway scenes		
Phoenix area	T-10	82
Ft. Worth, Dallas area	T-12	83
Ft. Worth, Dallas area	T-21	84
Ft. Worth, Dallas area	T-15	85
Florida coastal area	T-11	86

Each scene was photographed on continuous-tone film. Another set of photographs was made using high-contrast film. When processed, these photographs did not reveal significant differences.

A scale of 1 to 30,000 was selected for each aerial photograph used in this experiment. The basic factor for this selection of scale was the large spot size of the fss. The maximum distance that can be scanned across the face of the crt of the fss is 3.5 in.; at the scale of 1 to 30,000, this corresponds to 8750 ft on the ground.

The following relationship exists between time and distance on the face of the crt of the fss (see item 2, a, above):

$$\text{in. per } \mu\text{sec} = \frac{3.5}{53.7}$$

$$= 0.065 \text{ in. per } \mu\text{sec;}$$

$$\mu\text{sec per in.} = \frac{53.7}{3.5}$$

$$= 15.34 \ \mu\text{sec per in.}$$

This information then leads to the data in Table XIII.

TABLE XIII - ACTUAL AND EXPERIMENTAL RUNWAY WIDTH INFORMATION

Actual runway width (ft)	Reduced runway width (in.)	Runway width (μsec)
100	0.04	0.616
200	0.08	1.232
300	0.12	1.848
400	0.16	2.464
500	0.20	3.080

A statistical study of runway widths indicates that the lower limit of runway widths is 150 ft and the upper limit, 400 ft. Utilizing the results of the statistical study and the information in Table XIII, the width-measuring circuits can be programmed to the desired limits.

Before the processing of the photographs, the processor was calibrated using a pulse generator input (from a Hewlett-Packard, Model 212A, pulse generator). The time delay circuits were programmed to the limits of 0.9 and 2.5 μsec, which correspond to 150 and 400 ft, respectively.

After the processor was calibrated, each runway and nonrunway photograph was processed. The resulting outputs were photographed and are shown below their corresponding scenes in Figures 78 through 86.

To select the gradient detector level, the difference of transmissivity between background and runways must be determined statistically. Since such information is not available, the experiment was performed by adjusting the gradient detector for best results. A different setting was used for each target scene. A step tablet with steps of known transmissivity was used as the input scene, and the output of the gradient detector examined to determine the minimum difference in transmissivity required to trigger the gradient detector circuit. This step tablet has varying degrees of transmissivity with the transmissivity difference decreasing with each succeeding step. Following the processing of each target scene a step tablet was placed in the fss and the output of the gradient detector was photographed. A sketch of the step tablet and the transmissivity of each step are shown in Figure 87.

The photographs of the output of the gradient detector, with the step tablet

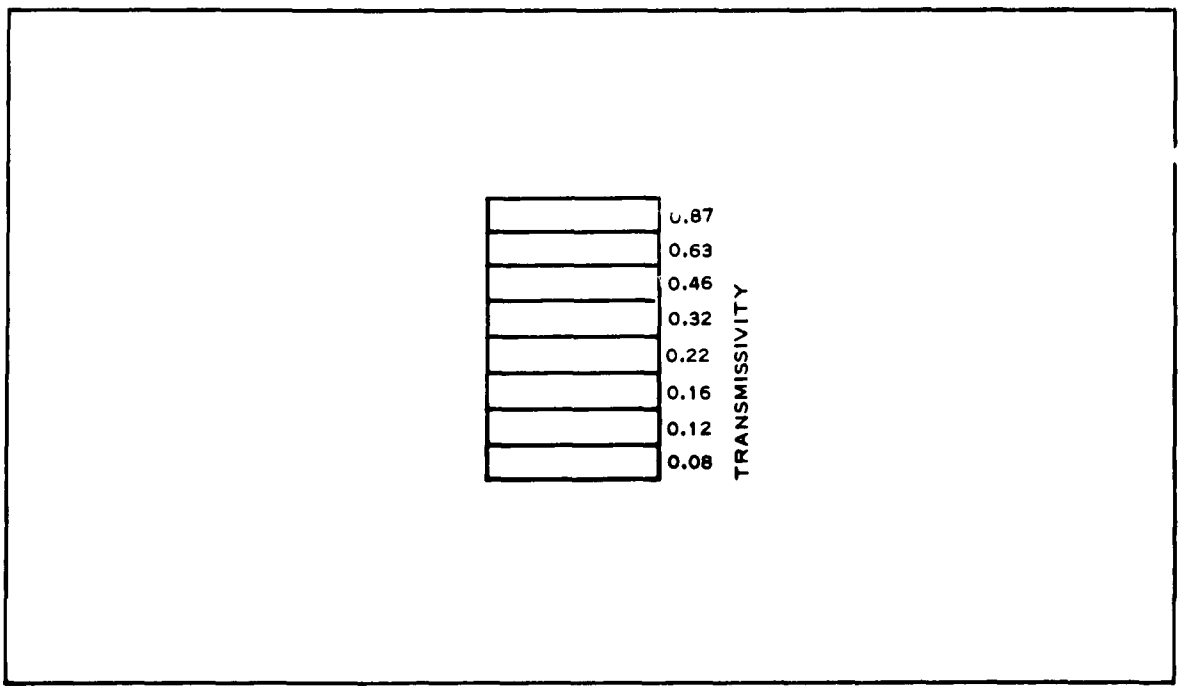

Figure 87 - Step Tablet

as the input scene, are shown below the corresponding targets in Figures 78 through 81. Table XIV indicates the minimum difference in transmissivity for which the gradient detector was set to trigger for scenes T-1 through T-4. For the other scenes only one setting of the gradient detector was made. The output of the processed step tablet is shown in Figure 88.

TABLE XIV - MINIMUM TRANSMISSIVITY DIFFERENCES

Target scene	Transmissivity difference
T-1	0.17
T-2	0.10
T-3	0.14
T-4	0.06

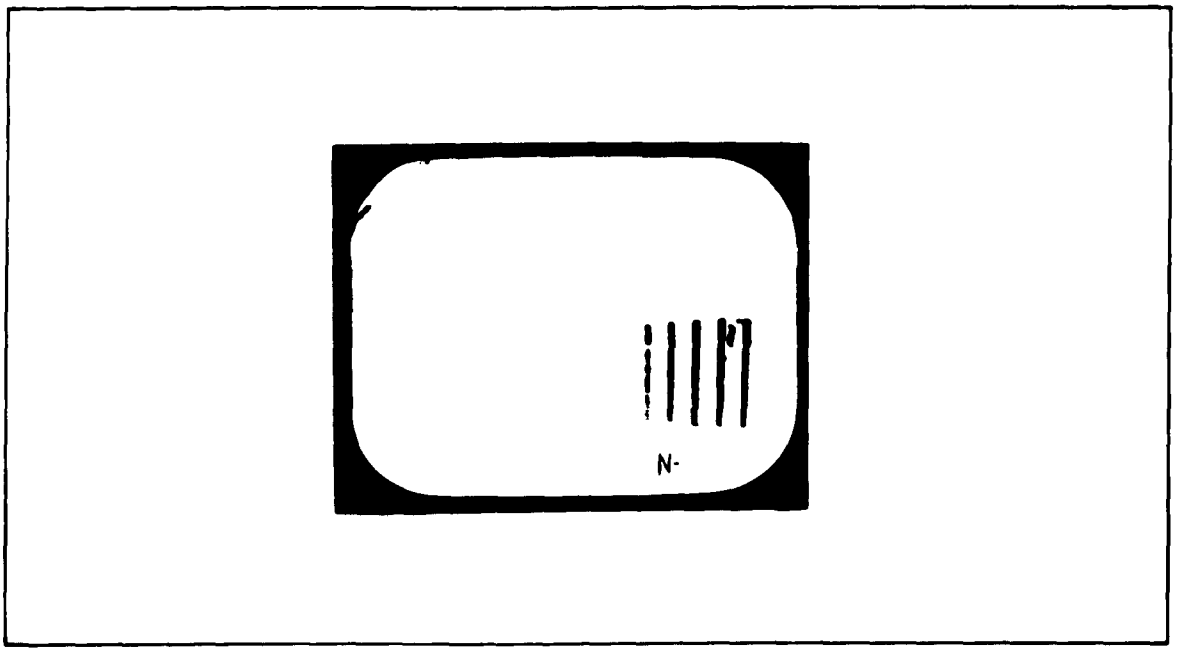

Figure 88 - Processed Step Tablet

The difference in transmissivity at which the gradient detector triggered was 0.05 for the nonrunway scenes.

4. LENGTH MEASUREMENT OF WIDTH-GATED PATTERNS

The concept of slit correlation described in Subsection Three can be used to measure the length of the width-gated line patterns. Since the lines shown in Figure 89 are made up of pulses of equal amplitude and width, the length could be measured by measuring the number of pulses. By correlating a slit with the pattern, the maximum amplitude of the correlation function will be proportional to the number of pulses in the line and also to the length of the line. The correlation function is also shown in Figure 89.

5. CONCLUSIONS

The width-sifter shows promise as a method for screening line-type patterns with widths between two preselected intervals. The major problem with this device is the selection of threshold levels. Since target gradients are affected by variations in exposure and photographic processing, some method of normalizing the image with respect to these variables may be necessary.

The length of lines in the width-gated display can be measured by correlation of the display and a rectangular slit.

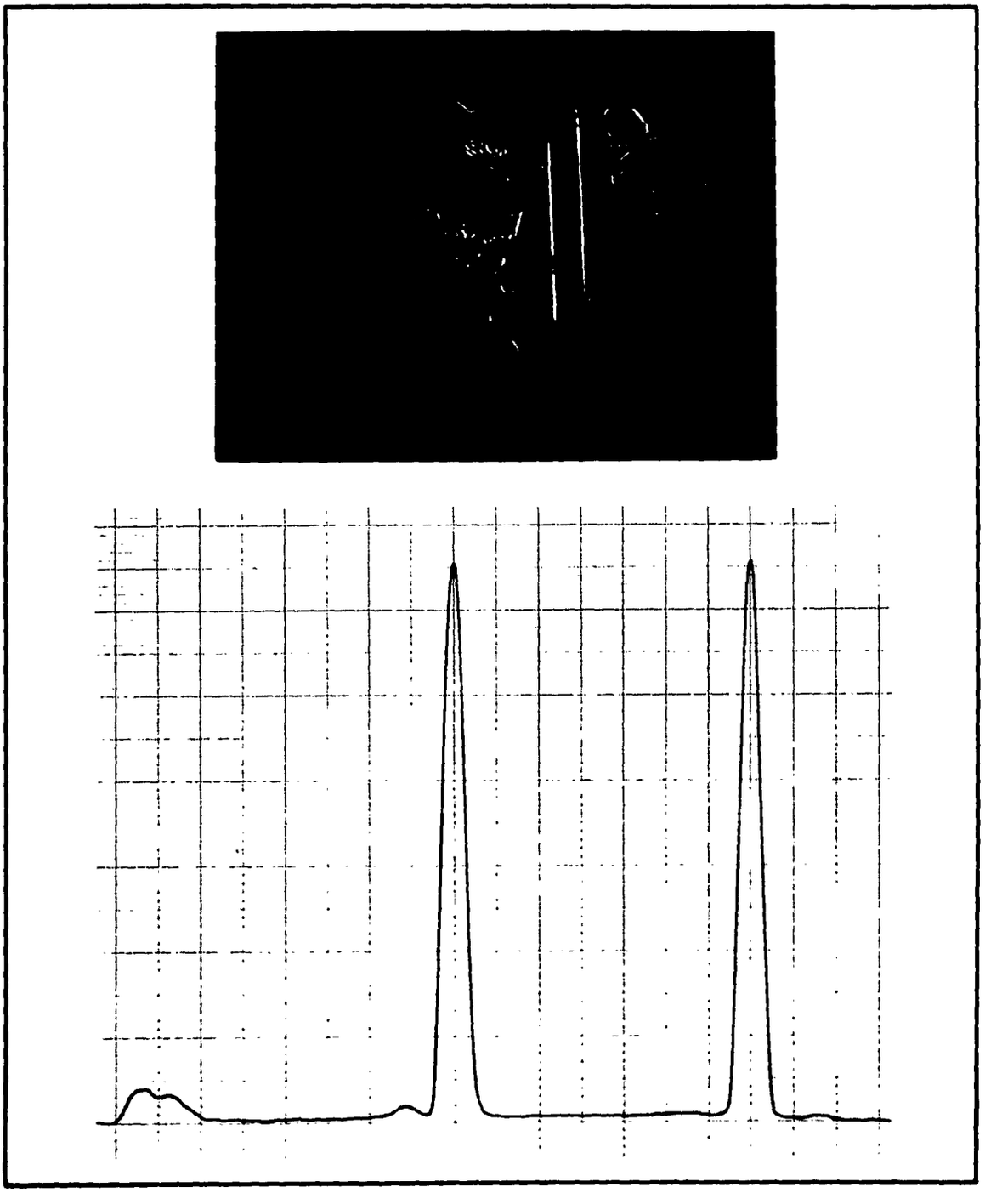

Figure 89 - Width-Gated Line Pattern with Correlation Function

SECTION V - DETECTION AND RECOGNITION SYSTEMS

1. GENERAL

Sections III and IV describe analytical and experimental studies of various correlation techniques and concepts for recognizing and detecting target patterns. These techniques are developed further in this section and are presented as suggested systems for recognition and detection of target patterns on aerial photographs. It should be recognized that some of the techniques that have been partially instrumented and experimentally tested with aerial photographs are more firmly grounded than the concepts developed from the analytical effort, although in principle the analytical concepts may be equally sound.

Three systems are grouped as straight-line pattern analyzers. The first two, Mod I and Mod II, are similar in function; both employ the width-sifter but differ in the approach to the measurement of line-pattern length. The third system, Mod III, is based on the principle of slit correlation.

The straight-line pattern analyzers detect attributes connected with the pattern edge. A fourth system, a pattern area detector, is designed to detect regular or irregular patterns that have acceptable dimensions and length-to-width ratios.

2. MOD I STRAIGHT-LINE PATTERN ANALYZER

a. General

The Mod I straight-line pattern analyzer utilizes the width-sifter and a position-gated counter developed by GAC under Air Force contracts. This analyzer will detect patterns in photographic transparencies that meet certain criteria for edge gradients, widths, and lengths. Such

an analyzer is ideally suited to the detection of objects with rather large aspect (length-to-width) ratios.

b. Width-Sifter

The straight-line pattern analyzer is shown in Figure 90. A scene in the form of a photographic transparency is scanned with a flying spot, thus converting the photographic information to a video signal. In this case, the raster is rectangular, similar to a TV raster. The output of the photomultiplier is differentiated and monitored by the gradient threshold detector. When a differentiated video signal exceeds a certain threshold to indicate the leading edge of a target, a trigger is generated that initiates the width-sifting circuitry. This circuitry consists of electronic timers that measure the time between two successive triggers generated by the gradient detector. The timing circuitry essentially measures the distance between the leading and trailing edges of targets and applies minimum- and maximum-width criteria to the target. When the width of a target exceeds the minimum width and is less than the maximum width, a pulse is generated at the trailing edge of the target. The gradient threshold, minimum-width, and maximum-width criteria are adjustable independently. A more detailed description and laboratory evaluation of this circuitry is given in Section IV, Subsection Four, items 2 and 3.

In the straight-line pattern analyzer, a photograph must be scanned at various azimuth orientations. This is done by either rotating the scene, rotating the yoke on the crt, or effectively rotating the sweep voltages through the use of resolvers. It appears that rotating the scene is least desirable, particularly if the scenes are located on a film strip. However, for simplicity of discussion, it is assumed that the scene is rotated.

c. Position-Gated Counter

The position-gated counter is a bank of capacitors with high-speed

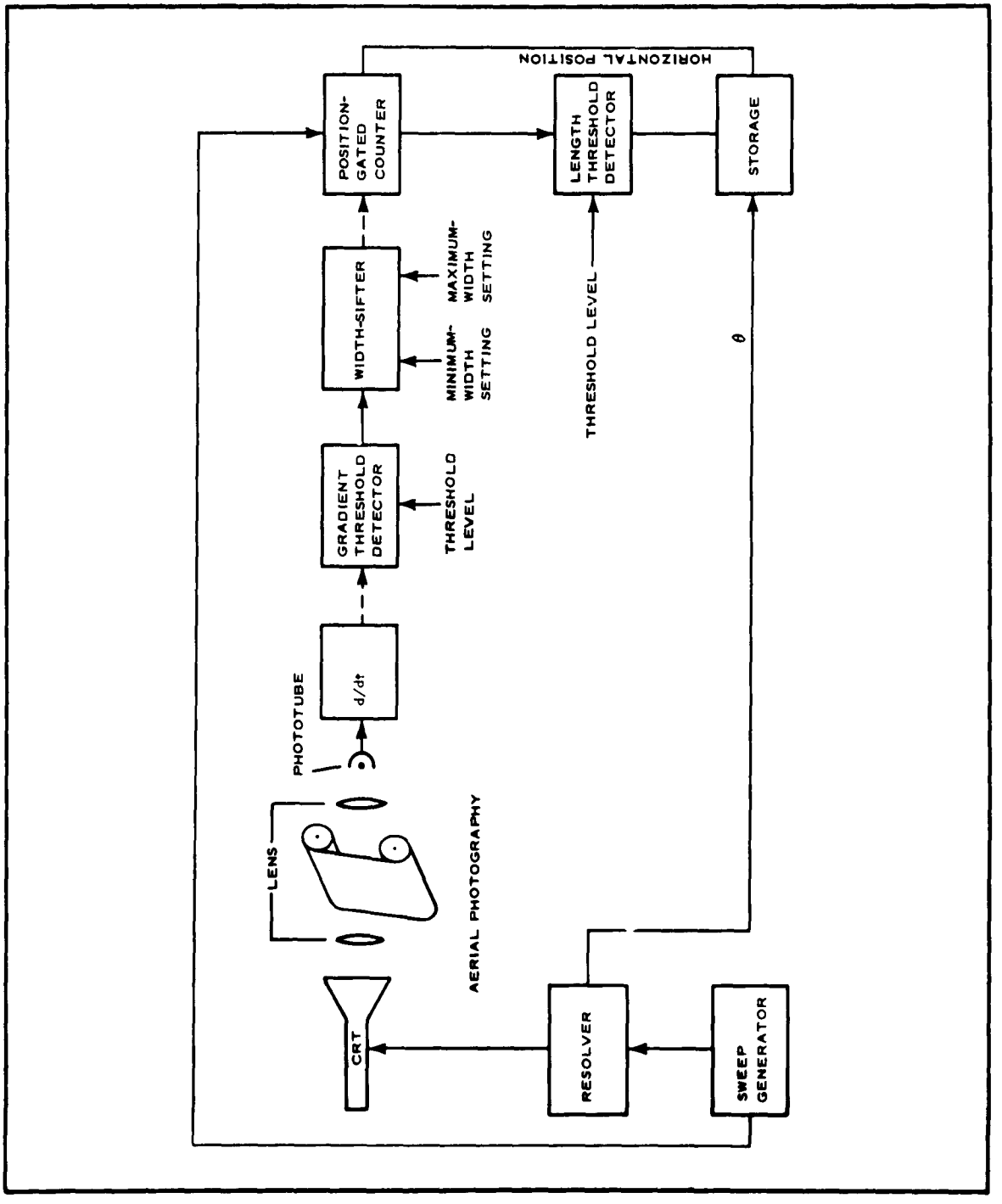

Figure 90 - Straight-Line Pattern Analyzer Block Diagram

switching circuitry to switch the output of the width-sifter to different capacitors as a function of the position of the flying spot on the crt. Figure 91 is a simplified diagram of the position-gated counter, which consists of a series of gates and capacitors. The input signal is sampled by the fast gates that operate in repeating sequence. Each fast gate is connected to a number of slow gates and capacitors. The output gates read out the capacitor voltage in real time and relay the output pulses into the line threshold detector. If the fss operates with a TV-type raster with a high-speed horizontal sweep and a slower vertical sweep, an r-c filter element is required for each horizontal resolution element. If a photograph with 25,000-ft ground coverage is assumed and if a 100-ft resolution is desired in the positioning of the pulse generated by the width-sifter, 250 filter elements are needed. The unit developed by GAC for the Air Force had considerably more elements than this.

In operation, the output of the width-sifter for a single azimuth orientation would be integrated on the various capacitors, each one corresponding to a given horizontal position. The switching circuitry would be controlled by the position of the crt and would switch the width-sifter output to the appropriate capacitor. After a complete frame has been scanned, the voltage stored on each capacitor corresponds to the number of pulses generated at that particular horizontal position. These voltages are then proportional to the total length of trailing edges of targets that meet the minimum and maximum width criteria of the width sifter. These voltages are monitored by a length-threshold detector to determine if the target length criterion is met. This criterion could consist of both a maximum and minimum length. The threshold is adjustable and can accept or reject targets of any predetermined length. If the voltage on each element is measured only after a complete frame, it is not possible to determine whether or not the total edge length measured constitutes a continuous line.

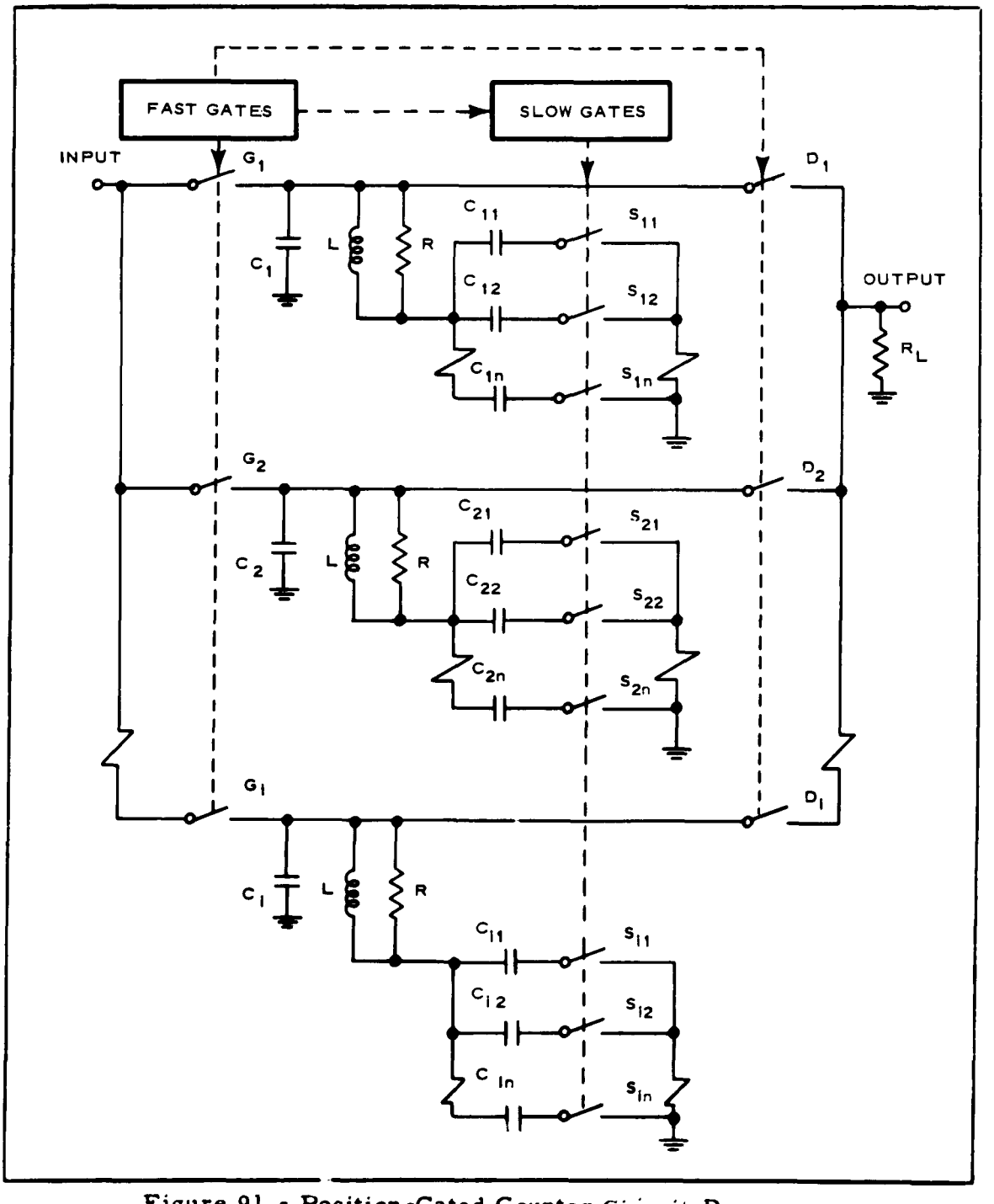

Figure 91 - Position-Gated Counter Circuit Diagram

Additional monitoring at various vertical positions will give an indication of line continuity.

In reading out the voltages stored on each element sequentially through the threshold detector, the horizontal spacing of targets can be determined, thus enabling the differentiation between street patterns and other targets that are more widely spaced such as a runways and dams.

After a single azimuth orientation is completed, the capacitors must be discharged preparatory for operation at the next azimuth setting.

d. Output

The output of the electronic scene analyzer will indicate the existence of targets that have (1) leading and trailing edge gradients that exceed a predetermined level, (2) the distance between edges greater than a certain minimum and less than a certain maximum value, and a length that meets both minimum and maximum criteria, and (3) relative spacing of targets and target orientation.

3. MOD II STRAIGHT-LINE PATTERN ANALYZER

a. Function

The primary function of the Mod II analyzer is the detection of straight-line patterns and the recognition of airport runways. It will detect patterns in photographic transparencies that meet certain edge gradients and width and length criteria.

b. Description

(1) General

The recognition of runways and other rectangular patterns requires (1) the generation of a set of target and nontarget lines from acceptable pattern edge gradients and pattern widths and (2) the detection of the desirable straight and sufficiently long

lines among the undesirable curves, shorter lines, and isolated points.

A width-sifter for generating the target and nontarget lines has been built. The following paragraphs describe an all-electronic method for detecting the straight and sufficiently long lines.

(2) Preliminary Gross Detection of Target Lines

The set of target and nontarget lines obtained from the width-sifter is inserted as a two-level representation of the line set into an electrical storage tube. A two-stage processing of the storage tube readout to separate the target and nontarget lines is then accomplished.

The preliminary search for the target lines is made at any given point by means of a ppi-type search configuration (see Figure 92), which extends over an azimuthal range of -45 deg from the vertical. A useable ppi sweep configuration includes 65 sweeps that are spaced azimuthally by slightly less than 1.5 deg. If the vertical projected lengths of the azimuthal sweeps are made equal to the vertical length of the photographic frame, a single horizontal line of 256 ppi configurations (assuming a usable 1.5-in. storage tube diameter and 10-mil spot size) is sufficient to read out any target or nontarget line present in the frame.

Since all line representations have a single level, the integrated readout of each azimuthal sweep provides an indication of the line length read by the given azimuthal sweep.

If the integrated readout of a given azimuthal sweep exceeds that obtained for a minimum target line length, the normal ppi pattern is stopped and the individual azimuthal sweep is repeated, but at a slower rate to determine that the azimuthal readout is, in fact, that of a target line.

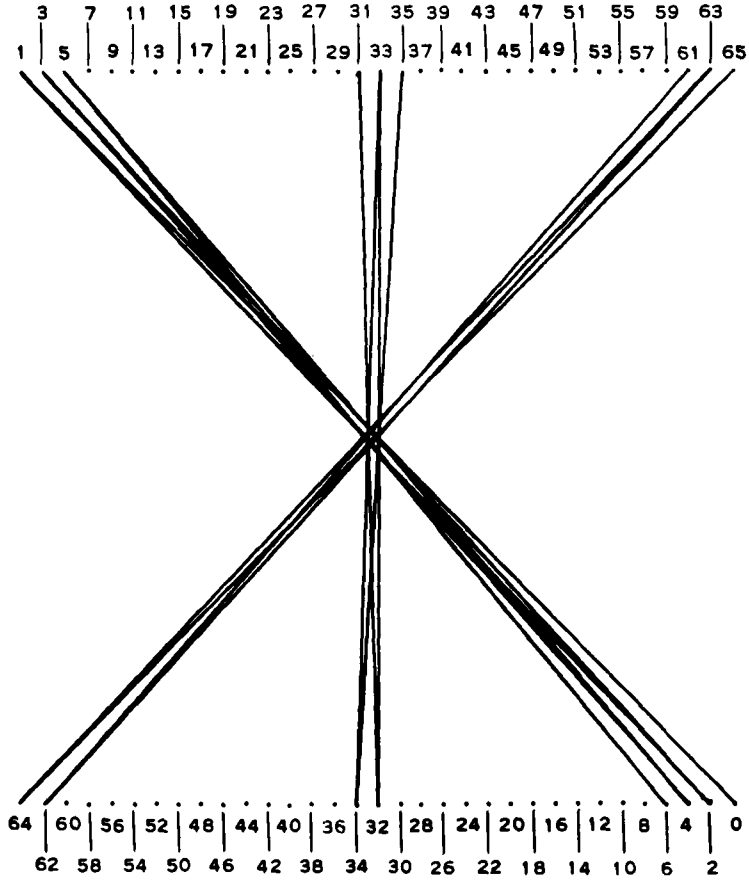

PATTERN GENERATION: SPOT PROCEEDS IN STRAIGHT LINES FROM 0 TO 1, 1 TO 2, 2 TO 3, ETC., TO 65 TO GENERATE 65 AZIMUTHAL LINES SPACED LESS THAN 1.5 DEG APART AND EACH OF 2 USEC DURATION; AZIMUTHAL RANGE, -45 TO +45 DEG.

Figure 92 - PPI Azimuthal Search Pattern

(3) Detection of Continuous Target Lines

The sweep speed is reduced to permit adequate readout resolution of isolated short lines and their intervening spacings. The now-separated line and space readouts are assigned positive and negative voltages, which permits the positive contributions of short isolated lines to be cancelled at the integrator by the negative contributions of the intervening spacings.

On the other hand, the presence of a continuous target-length straight line will readily permit the integrator to build up to the required voltage of a target line. The target integrator time constant must be modified to accommodate the slower azimuthal sweep. To prevent a long prior spacing from masking a target-length line, the integrator is never allowed to become negative.

The target output of the integrator, while the target threshold is exceeded, may be recorded for viewing and for comparing with the original target by the photo-interpreter or for further processing to obtain a more effective target isolation. Since a scan parallel to the ppi search scan of the storage tube readout is maintained at the viewing or recording monitor, the recorded position of the target line corresponds to the true location of the target in the original photograph.

Alternately, if the detection problem warrants, the position, the orientation, and the length of the straight line can be recorded. These attributes can then be combined with others to provide the required target decision.

The two quadrature scans, which are required to process each photographic frame, are processed sequentially in the line detector.

A block diagram of the rectangle-detection equipment is given in Figure 93.

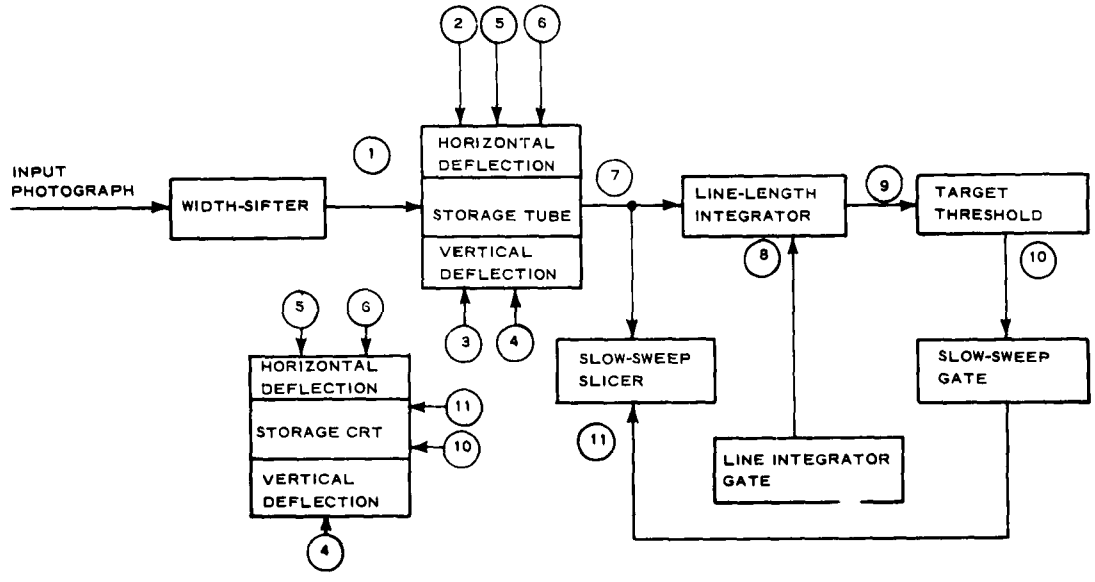

SIGNAL IDENTIFICATION:

1. WIDTH-SIFTER OUTPUT; TWO QUADRATURE SCANS REQUIRED FOR EACH PHOTOGRAPHIC FRAME
2,3. STORAGE TUBE READIN SCAN
4. VERTICAL TRIANGULAR WAVE SEQUENCE OF PPI SEARCH PATTERN; ALL WAVES OF SEQUENCE HAVE EQUAL AMPLITUDES
5. HORIZONTAL TRIANGULAR WAVE SEQUENCE OF PPI SEARCH PATTERN; AMPLITUDES MODIFIED TO PROVIDE AZIMUTHAL ORIENTATIONS REQUIRED OF PATTERN
6. SINGLE HORIZONTAL RASTER RAMP; YIELDS SINGLE RASTER LINE FOR 256 PPI SEARCH POINTS
7. VIDEO READOUT; FROM PPI SEARCH OF STORED WIDTH-SIFTER OUTPUT
8. LINE INTEGRATOR GATE; CONTROLS CHARGE AND DISCHARGE TIME OF LINE LENGTH INTEGRATOR TO DISCHARGE INTEGRATED VIDEO OF EACH PPI AZIMUTHAL LINE BEFORE NEXT LINE OCCURS
9. INTEGRATED VIDEO
10. TARGET SIGNAL; APPEARS WHEN 9 EXCEEDS THRESHOLD VOLTAGE
11. SLOW-SWEEP GATE; INITIATED BY 10, CONTROLS GENERATION OF REPEATED SLOW TRIANGULAR SWEEPS AT 4 AND 5 ACTIVATES POSITIVE-NEGATIVE SLICING OF 7, CONTROLS LINE LENGTH INTEGRATOR TIME CONSTANT AND BIASES STORAGE CRT SO THAT 10, OBTAINED DURING SLOW SWEEP, IS RECORDED

Figure 93 - Rectangle-Detection Equipment Block Diagram

c. Line Detector Performance

Since the integrated readout of each ppi azimuthal line is desired, the minimum time necessary to complete each azimuthal line is limited by the storage tube deflection circuitry and is on the order of 10 μsec. A single ppi pattern of 65 azimuthal lines will require about 650 μsec. The entire line search of 256 ppi search points will require 167 msec; 30 μsec must be added for each of the slow repeated azimuthal lines that further investigate the possibility that a target exists. The existence of 10 or 20 such possibilities will only add 0.3 to 0.6 msec, so that a search time of less than 0.175 sec per scan, or 0.35 sec for the two quadrature scans of a given frame, becomes very probable. This processing time compares very favorably with the real time of 0.65 sec required for transmission of the frame from an airborne vehicle. (This assumes a 20-mc transmission channel band width and 77×10^6 bits per frame.)

Since the width-sifter signal input to the storage tube is recorded in only two levels (on or off), the processing of the storage tube readout video is not very critical. Slicing of the two levels of video to accurately known voltages permits use of a length-threshold criterion that can truly reflect the minimum length of an acceptable target pattern.

4. MOD III STRAIGHT-LINE PATTERN ANALYZER

a. Function

The design goal of the Mod III line analyzer is the detection of straight line patterns and their position and orientation. Secondary design goals are the measurement of the width of straight line targets.

b. Description

The Mod III line analyzer combines the slit correlator and the width-sifter. A slit aperture is translated perpendicular to its major dimension across an aerial photograph to obtain the correlation function.

When the slit crosses a line parallel to it, the correlation function peaks sharply. If the correlation function is differentiated twice, a large improvement in the signal-to-noise ratio results. Since the noise is generated by the correlation of the slit aperture and general picture background, a physical basis exists for separation of lines from the picture background. An amplitude threshold rejects the noise and passes the desired second-derivative signals. The amplitude of the second derivative of the correlation is proportional to the product of target edge gradient and length. The results of the experiments described in Section IV show that straight-line patterns can be detected with a very good signal-to-noise ratio by using this technique.

Detection of lines at any orientation is provided by the rotation of the slit with respect to the scene. The position of the straight-line target can be determined by measuring the position of the slit when a large second-derivative signal is detected. The rate of translation should be much greater than the rate of rotation so that the slit is correlated with the entire scene at each azimuth position. The slit can be rotated in steps of approximately two degrees.

Figure 94 shows a simplified block diagram of the Mod III line analyzer. The output of the slit correlator is differentiated twice, after which it is rectified and sent to a threshold detector. The edge counter counts the number of pulses that exceed the threshold for a particular azimuth position. The slit correlator can be implemented in a number of ways for high-speed slit correlation. A continuously revolving belt with a number of slits or a rotating mirror will translate a slit across a photograph at high speeds. A slit can also be generated by a high-speed sweep on a crt and can be translated quite rapidly.

This implementation will measure the number of straight-line targets at each azimuth orientation. In addition, it is believed that target width measurements are possible utilizing the width-sifter principle. The width gate accepts the output of the threshold detector and

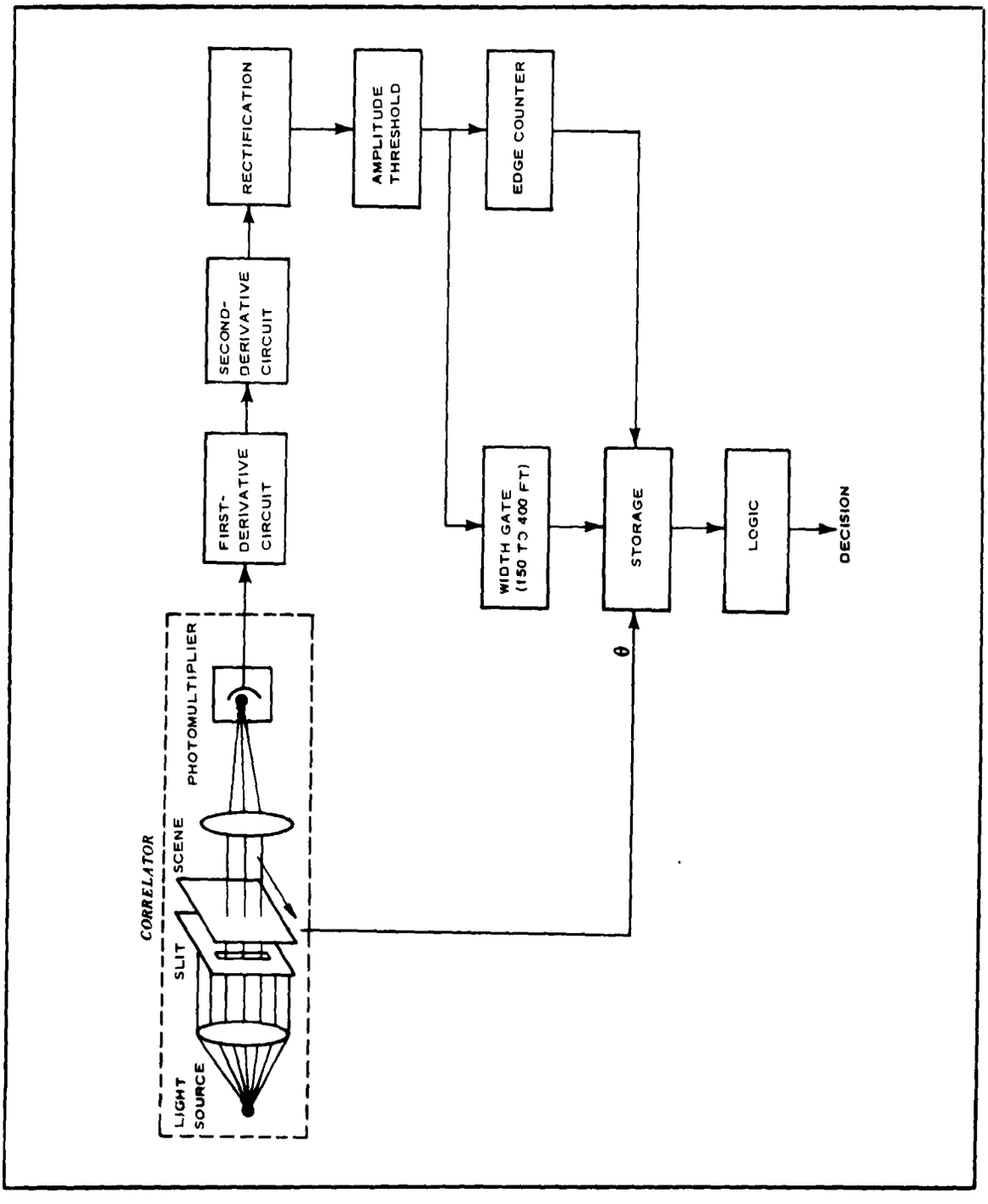

Figure 94 - Mod III Line Analyzer Block Diagram

determines the distance between successive pulses. With such a device it is possible to apply the width criteria for runways (widths that fall between 150 and 400 ft).

The feasibility of the Mod III line analyzer to detect straight lines is demonstrated in Section IV. Further work is recommended to prove the feasibility of measuring target width. As in the other line analyzers, the selection of the proper threshold is a critical operation. Any factor that causes the value of the target edge gradient to vary will affect the amplitude of the second derivative of the correlation function. These factors include exposure, processing, resolution, and atmospheric conditions.

5. PATTERN AREA DETECTOR

a. Function

The primary function of the pattern area detector is the detection of pattern areas of acceptable dimension and aspect ratio. However, the shape of the pattern is not important; in this respect the detector differs from the straight-line pattern analyzer, whose detection capability is confined to regular, straight-sided, rectangular patterns. A more important difference between the two is that the pattern area detector detects and yields a pattern area as its output, whereas the straight-line pattern analyzer detects and recognizes patterns through measurements that involve the pattern boundaries and provides the pattern's trailing boundary as its output rather than its area.

b. Description

(1) General

Detection of pattern areas is accomplished through the derivative readout of the photograph by an expanding spot in which the maximum and minimum limits of the expansion are determined by the range of dimensions of the acceptable patterns. To conserve

processing time, the point-by-point expanding-spot examination of the photograph is replaced by a two-stage hybrid scan. A first-stage conventional raster scan, as in the width-sifter, makes a one-dimensional examination of pattern widths. Whenever an acceptable one-dimensional pattern width is found, a second-stage expanding-spot scan is generated to determine the acceptability of the pattern on a two-dimensional basis.

(2) Instrumentation

The proper expansion of the crt readout spot under conditions of constant flux is obtained by defocusing. If the usual linear relationship exists between spot size and defocusing voltage, a ramp function will provide the constant expansion rate of the spot.

A proper second-derivative output signal is generated through successive time differentiation of the expanding-spot readout. A monopolarity amplifier provides an absolute-valued first derivative; modification of the amplification of each of the derivative by means of the ramp spot expansion wave form yields the required multiplication of the derivatives by the spot radius, R.

The values of the second-derivative or absolute-difference output signals are compared with two-boundary or four-boundary reference voltages to permit detection of two-boundary or four-boundary patterns. The reference voltages have been modified by the transmissivity difference information of the prior flying-spot scan to normalize the detector.

Instrumentation of the detector is shown in block form in Figure 95. The video output of the first-stage fss is processed in a modified width-sifter-type circuit so that whenever an acceptable pattern width is encountered, an acceptable pulse signal (4 in Figure 95) and a pattern width pulse (5) results whose amplitude is proportional to the width of the pattern. These two signals (4 and 5) control the generation of the ramp function defocusing

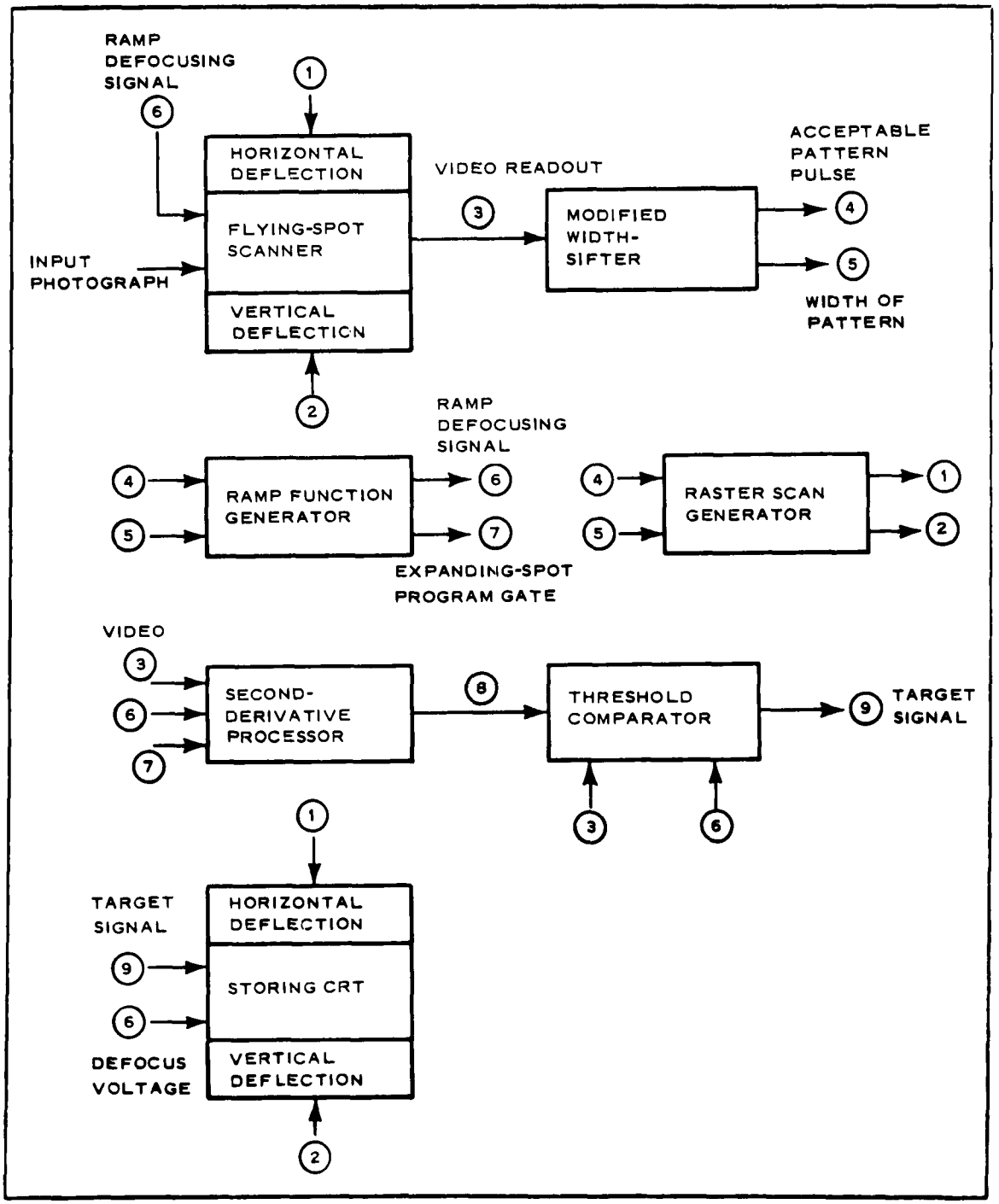

Figure 95 - Pattern Area Detector Block Diagram

signal (6) and stop the raster scan (signals 1 and 2) at the pattern centroid. When the second-derivative output signal (8) exceeds the threshold voltage, it generates a target signal (9) whose amplitude is made proportional to the square of the pattern width, which is obtained from the ramp defocusing signal (6). The variable-amplitude signal (9) inconjunction with the ramp defocus signal (6) results in the printing at the storing crt of a constant-intensity spot equal in area and position to the original target pattern.

As in the Mod II straight-line pattern analyzer, two quadrature scans of each scene are required.

c. Performance

The time required to examine the scene is of the same order as that required for the width-sifter plus that required to examine, with the individual expanding-spot scans, the possible target patterns found in the prior flying-spot scans. Thus, the detection of the irregular patterns can very probably be accomplished in real time.

The processing of the photographs (resolution, scale, and contrast) must be considered in determining the threshold voltage of the variable-spot-size scan and the reference widths of the prior flying-spot scan. Large deviations from the preset values of these photographic parameters will result in detection errors.

6. APPLICATIONS TO PATTERN RECOGNITION

a. Straight-Line Pattern Analyzers

The Mod I and Mod II straight-line pattern analyzers have similar functions. Both incorporate the width-sifter but employ different techniques for length measurement, and both are capable of the detection of straight-line patterns and the recognition of runways. In addition, the following data about the straight-line structure in an aerial photograph can be obtained:

1. Number
2. Length
3. Relative orientation
4. Quantized width
5. Spacing between parallel patterns

The Mod III analyzer differs from Mod I and Mod II in the correlation techniques used. It does not measure length, although it does give a rough indication. It is believed capable of measuring width although this has not been implemented in the laboratory. Consequently, it might recognize runways but it will detect the great majority of straight-line patterns and provide the following data about straight-line pattern structure in an aerial photograph:

1. Number
2. Relative orientation
3. Spacing between parallel patterns

The straight-line patterns that can be detected by Mod I and Mod II are roads, streets and expressways, bridges, runways, shore lines, agricultural field patterns, industrial buildings, ships, and many others that have a partial or complete straight-line structure. Mod III has essentially the same capability with the exception of industrial buildings. Here the lengths are probably not sufficient and the signal-to-noise ratio of the second-derivative signal is not large enough for detection.

The capability of these devices makes the screening of aerial photography their most likely application. One method of screening is by the number and distribution of straight-line patterns. For example, an absence of straight lines indicates a high probability of either uninhabitable waste areas, cloud cover, or water. A small number of straight lines, possibly orthogonal, would indicate a rural area; a large number of closely spaced parallel lines would indicate urban

areas. Further screening might be achieved if the width information were used.

b. Recognition of Industrial Complexes

(1) Describing Attributes

Industrial complexes are difficult to detect (1) because their describing attributes are not outstanding (the dimensions of some individual building patterns, for example, are of the same order as such background patterns as rural fields) and (2) because a common list of attributes cannot be used to describe all complexes.

The following broad attribute classes have been found to be representative of most industrial complexes:

1. Straight-sided rectangular patterns
2. Straight-sided polyrectangular patterns made up of adjoining rectangular patterns (see Figures 4 and 5, above)
3. High-frequency activity as evidenced by the presence of many narrow, parallel strips

A unique spectral energy picture for petroleum refinery oil tanks is obtained chiefly from the high (white) transmissivity of the tanks, from a tank-to-spacing duty cycle of approximately 0.5, and from the fact that the pattern of tanks is repetitive.

(2) Measurement of Attributes

The straight-sided pattern analyzer (either Mod I or Mod II) can be used to extract the acceptable straight-sided rectangular patterns. The pattern width and length criteria of the analyzer are adjusted to accommodate the widths and lengths of acceptable industrial patterns. The trailing edge of each of the detected patterns makes up the output signal and is recorded at a storage tube.

Both rectangular and polyrectangular patterns are measured and passed by the pattern area detector. The approximate areas of the detected patterns are recorded as the output signal of the detector.

The measurement of high-frequency activity, since it is of a detailed nature, is done after the above gross measurements have been made and is confined to the above detected areas.

The oil tanks, with their unique spectral energy distribution, are best extracted from their background by a suitably designed filter to be used with a coherent optical channel. The isolated oil tanks then appear in the output image plane of the coherent optical channel.

(3) Recognition of Industrial Patterns

The individual integration of the straight-edge output of the straight-line pattern analyzer and of the area output of the pattern area detector on their respective storage tubes will indicate the number of individual patterns and the area of the patterns. If the integrations are carried out over a fixed industrial size area, criteria for both the number and the area of patterns per unit search area can be established and recognition of the industrial complex becomes possible. To render the recognition more reliable, those portions of the original photograph that correspond to the detected industrial areas are tested for the existence of straight, parallel, and narrow strips that mark the high-frequency activity. This can be done with the Mod II straight-line analyzer modified to accommodate the much smaller industrial size area. A second-derivative readout will permit extraction of the narrow strips and individual pattern edges and will reinforce the presence of an industrial area.

Because of the uniqueness of the spectral energy content of the oil tanks, a sufficiently large value for the integrated output signal of the coherent optical channel will indicate the presence of

oil tanks and therefore of a petroleum refinery. The integration, as in the above pattern analyzers, is carried out over an area the size of an industrial complex.

SECTION VI - CONCLUSIONS AND RECOMMENDATIONS

1. CONCLUSIONS

a. General

The work during the program resulted in the following conclusions.

b. Photographic Examination of Pattern Attributes

The probability of airport recognition is high if the attributes of length and width are measured.

The storage tanks of the oil refineries studied had the following characteristics:

1. The majority of storage tanks have a higher reflectivity than the background.
2. A definite relationship exists between tank diameters and spacing.
3. Tanks with diameters between 5 and 40 m are certain to be present.

Industrial complexes generally have the following common attributes:

1. Rectangular or polyrectangular patterns and narrow parallel lines
2. Quadrature arrangement and close spacing of patterns, and small number of acute angles

c. Analytical Study of Correlation Techniques

Analysis showed that requirements for recognition of pattern groupings in the spatial frequency domain are as follows. Although others may exist, oil storage tanks were the only patterns found that met these requirements.

1. Repetitive pattern with duty cycle between 0.3 and 0.5
2. Pattern reflectivity higher than background

The expanding-spot scanner, conceived and analytically studied, appears promising as a means of detecting pattern areas.

d. Experimental Study of Correlation Techniques

The second derivative of the correlation function is a valid attribute for detection of straight-line patterns.

Straight-line patterns can be extracted from the background with the edge gradient and width attributes.

Pattern recognition with a rectangular slit is the only form of template correlation that appears promising.

The selection of thresholds for all the suggested systems is a problem, particularly if photographic processing and exposure are variable.

e. Systems for Detection and Recognition

Straight-line patterns can be detected with the straight-line pattern analyzers Mod I, II, and III, and runways can be recognized with Mod I and II.

Industrial Complexes can be recognized by attribute measurements of the straight-line pattern analyzers and the pattern area detector.

2. RECOMMENDATIONS

a. General

The following lines of attack are recommended as the next steps in the solution of the pattern recognition problem.

b. Laboratory Evaluation of System Designs

None of the three systems that analyze straight-line patterns exists as integrated instrumentation, although subsystems of Mod I, namely,

the width-sifter and the position-gated filter, have been designed and individually evaluated. It is recommended that Mod I of the straight-line pattern analyzers be assembled and its screening ability thoroughly evaluated with a large sample of aerial photography. Mod I is selected because of the availability of the subsystems.

It is recommended that the capability of Mod III to measure straight-line pattern width be evaluated.

The fourth system, pattern area detector, is based on the expanding-spot concept. It is recommended that this concept be breadboarded and evaluated.

c. Threshold Level Compensation

Variations in photographic exposure and processing cause undesirable fluctuations in edge gradients or those functions of edge gradients that the fixed threshold levels of the four systems are set to detect. Therefore, it is recommended that a study be made of some form of automatic threshold level compensation.

d. Target Attribute Study

It is recommended that attributes and attribute-measuring techniques be studied for those target patterns not considered in this report. Large samples of aerial photography should be studied so that specific targets can be classified according to their measurable attributes. A study of the degree to which inference is used in recognition of target classes by human operators should be included. Some important target classes may not be recognizable without the aid of certain inferences that are difficult to implement into automatic devices.

LIST OF REFERENCES

1. Contract AF30(602)-2459: Rome Air Development Center, Griffiss Air Force Base, New York, 8 March 1961.

2. Department of the Air Force: U.S. Air Force - U.S. Navy Flight Information Publication, Terminal (High Altitude): Northeast United States. 1 July 1960.

3. Jenkins, and White: Fundamental of Optics. New York, McGraw-Hill Book Co., Inc., 1957; chapters 15, 16, and 17.

4. GER-10170: Final Report, Advanced Data Correlator Study and Development (DACOR). Akron, Ohio, Goodyear Aircraft Corporation, 20 April 1961; Appendix O. SECRET

5. Davenport, and Root: Random Signals and Noise. New York, McGraw-Hill Book Co., Inc., 1958.

6. O'Neill, E. L.: Technical Note No. 133, Boston University Physical Research Laboratories, October 1957; pp 29-31.

APPENDIX A - SPECTRAL ENERGY CALCULATIONS FOR RECURRENT PULSE SEQUENCES

1. EVALUATION OF THE NONCENTRAL SPECTRAL LOOPS OR MAXIMA

The energy contained in the K^{th} ($K > 1$) positive and negative spectral loops of a recurrent sequence of N pulses, which have an amplitude of $\sqrt{A_h}$ units and a length, 2a, with a spacing between each pair of 2b units, is obtained by integrating the spectral density $\left|H_2(f)\right|^2$,

$$\left|H_2(f)\right|^2 = 4a^2 A_h \frac{\sin^2 \omega a}{(\omega a)^2} \frac{\sin^2 (N\omega)(a+b)}{\sin^2 (\omega)(a+b)} , \tag{A-1}$$

between the two spectral zeros (ω_{Ka} and ω_{Kb}) that bound the K^{th} loops and have the following values:

$$\omega_{Ka} = \pm \left(K - 1 - \frac{1}{N}\right) \frac{\pi}{a+b} , \tag{A-2}$$

$$\omega_{Kb} = \pm \left(K - 1 + \frac{1}{N}\right) \frac{\pi}{a+b} . \tag{A-3}$$

The resulting K^{th} loop energy integral, E_K, is

$$E_K = \frac{4a^2 A_h}{\pi} \int_{\left(K - 1 - \frac{1}{N}\right) \frac{\pi}{a+b}}^{\left(K - 1 + \frac{1}{N}\right) \frac{\pi}{a+b}} \left[\frac{\sin^2 \omega a}{(\omega a)^2}\right]\left[\frac{\sin^2 (N\omega)(a+b)}{\sin^2 (\omega)(a+b)}\right] d\omega . \tag{A-4}$$

The total energy of the recurrent sequences is from Equation 32

$$E_o = (2a)(N)(A_h) . \tag{A-5}$$

The percent of signal energy R_K in the positive and negative K loops is

then the ratio of Equations A-4 and A-5. After a change in variable

$$U = (\omega)(a + b) - (K - 1)(\pi) \quad , \tag{A-6}$$

this ratio becomes

$$R_K = \frac{2}{\pi} \frac{a}{a + b} \frac{1}{N} \int_{-\frac{\pi}{N}}^{+\frac{\pi}{N}} \left(\frac{\sin V}{V \sin U}\right)^2 (\sin^2 NU)(du) \quad , \tag{A-7}$$

where

$$V = \left(\frac{a}{a + b}\right)[u + (K - 1)\pi] \quad . \tag{A-8}$$

If the values of a/a + b and K are restricted so that $V < \pi$, or

$$\left(\frac{a}{a + b}\right) \times \left(K - 1 - \frac{1}{N}\right) \leq 1 \quad , \tag{A-9}$$

then the first term in the integral can be approximated as a function of u:

$$\left(\frac{\sin V}{V \sin U}\right)^2 = \left(\frac{1}{U^2}\right) \left(\sum_{i = 0}^{i = 3} a_i u^i\right)^2 \quad , \tag{A-10}$$

where the values of the coefficients are:

$$a_0 = 1 - \left[\left(\frac{a}{a + b}\right)(K - 1)\right]^2 1.648 + \left[\left(\frac{a}{a + b}\right)(K - 1)\right]^4 (0.814) \tag{A-10a}$$

$$a_1 = (1.032)\left(\frac{a}{a - b}\right)^4 (K - 1)^3 - (1.048)\left(\frac{a}{a + b}\right)^2 (K - 1) \tag{A-10b}$$

$$a_2 = \frac{a_0}{6} - 0.166\left(\frac{a}{a + b}\right)^2 + 0.495\left(\frac{a}{a + b}\right)^4 (K - 1)^2 \tag{A-10c}$$

$$a_3 = \frac{a_1}{6} + 0.105\left(\frac{a}{a + b}\right)^4 (K - 1) \tag{A-10d}$$

Substitution of the power series (A-10) permits the following solution of the integral from Equation A-7:

$$R_K \cong \left(\frac{a}{a+b}\right)\left(C_0 + \frac{C_2}{N^2} + \frac{C_4}{N^4} + \ldots\right) \quad , \tag{A-11}$$

with the following restriction upon the values a/a + b and K, namely:

$$\left(\frac{a}{a+b}\right)\left(K - 1 - \frac{1}{N}\right) \leq 1 \quad . \tag{A-9}$$

The constant "C" terms are the following functions of the power series coefficients, a_i, (Equations A-10a through A-10d):

$$C_0 = 1.85\, a_0^{\,2} \quad , \tag{A-12}$$

$$C_2 = 4a_0a_2 + 2a_1^{\,2} \quad , \tag{A-13}$$

$$C_4 = 5.59a_2^{\,2} + 11.18a_1a_3 \quad . \tag{A-14}$$

For the larger values of a/a + b and of K, an alternate approximation of the integrand of Equation A-7 is more useful. If N > 5, the value of V (Equation A-8) may be approximated by

$$V \cong \frac{a}{a+b}(K - 1) \, .$$

The solution of the integral of Equation A-7 then is

$$R_K \cong \left(\frac{a}{a+b}\right)(1.85)\frac{\sin^2\left[(\pi)\left(\frac{a}{a+b}\right)(K-1)\right]}{\left[(\pi)\frac{a}{a+b}(K-1)\right]^2} \tag{A-15}$$

for $N \geq 5$.

These two approximations (Equations A-11 and A-15), which complement each other, are used to compute the values of R_K that appear in Figure 17.

2. EVALUATION OF THE CENTRAL SPECTRAL LOOP

The energy of the central spectral loop for recurrent signals is obtained

by integrating the spectral density, $|H_2(f)|^2$, (Equation A-1) between the first two spectral zeros, $\pm[\pi/N(a - b)]$, which define the boundaries of the central loop. The integration is simplified by changing variables so that

$$u = (\omega)(a + b) \quad .$$

The percent of energy, R_1, in the first loop is then

$$R_1 = \left(\frac{2}{\pi}\right)\left(\frac{a}{a+b}\right)\left(\frac{1}{N}\right)\int_0^{\frac{\pi}{N}} \frac{\sin^2\left(U\frac{a}{a+b}\right)}{\left(U\frac{a}{a+b}\right)^2}\,\frac{\sin^2 NU}{\sin^2 U}\,dU \quad . \qquad \text{(A-16)}$$

Since U has a maximum value of π/N the integral may be simplified by approximating the trigonometric function,

$$\frac{\sin^2\left(U\frac{a}{a+b}\right)}{\left(U\frac{a}{a+b}\right)^2}\,\frac{1}{\sin^2 U} \quad ,$$

as a power series in U to give:

$$R_1 = \frac{a}{a+b}\left\{\frac{0.925 + (0.33)\left[1 - \left(\frac{a}{a+b}\right)\right]^2}{N^2} + \frac{0.078\left[1 - \left(\frac{a}{a+b}\right)^2\right]^2 + \ldots}{N^4}\right\} \quad . \qquad \text{(A-17)}$$

Values for the central loop energy, R_1, as a function of the duty cycle, a/a + b, and the number, N, of pulses in the sequences appear in Figure 17.

APPENDIX B - DERIVATION OF COHERENT CHANNEL FILTER DESIGN EQUATIONS

1. EVALUATION OF AVERAGE SIGNAL ENERGY

The input recurrent signal to be passed by the filter is in reality a distribution of signals whose one-half periods (combined one-half length of target, a, and spacing, b) lie between maximum and minimum lengths of A and B, respectively. These signals have duty cycles, a/a + b, that lie between 0.3 and 0.5. It can be seen from Figure 17 of Section III, Subsection Two, that signals within this duty cycle interval have a practically constant second spectral loop energy content.

Maximization of the signal-to-noise ratio requires that the filter band width be restricted to reject a portion, α, of the second loop energies associated with the signals that have either a maximum period or a minimum period. If the lower corner frequency ω_1 limits the passed signal energy of a maximum-period recurrent sequence, the portion, S, of the original signal energy passed by the filter becomes, from Equation A-7 of Appendix A,

$$S = \frac{2}{\pi}\left(\frac{a}{a+b}\right)\frac{1}{N}\int_{-\frac{\alpha\pi}{N}}^{+\frac{\pi}{N}}\left(\frac{\sin V}{V \sin U}\right)^2 \sin^2 NU \, dU \ , \qquad \text{(B-1)}$$

where α is the portion of the second loop energy passed by the filter.

The integrand's first term, approximated by a power series from Equation A-10, can be further simplified to yield

$$\left(\frac{\sin V}{V \sin U}\right)^2 = \frac{a_0^2}{U^2} = \frac{C_0}{1.85\,U^2} \ , \qquad \text{(B-2)}$$

where a_0 and C_0 are defined in Equations A-10a and A-12 of Appendix A. The remaining higher order terms, which are given in Equation A-10, have been neglected in the above approximation. These terms describe the additional (less than 5 percent) energy associated with the second loop when the number of pulses, N, in a given sequence is four or lower. Under these conditions,

$$S = \frac{2}{\pi}\left(\frac{a}{a+b}\right)\frac{C_0}{1.85}\int_{-\alpha\pi}^{\pi}\frac{\sin^2 NU}{(NU)^2}\,d(NU) \quad , \tag{B-3}$$

where the recurrent sequence has a maximum one-half period length of A units and

$$0 \leqq \alpha \leqq 1 \quad ,$$

$$U = \omega A - \pi \quad .$$

The integral's lower limit, $-\alpha\pi$, of the variable, $U = \omega A - \pi$, corresponds to the lower cutoff frequency, ω_1, so that

$$\omega_1 = \left(\frac{\pi}{A}\right)\left(1 - \frac{\alpha}{N}\right) \quad . \tag{B-4}$$

Because the integrand is even, the expression for S can be written as

$$S = \frac{(2C_0)}{1.85}\left(\frac{a}{a+b}\right)\left[\frac{1}{\pi}\int_0^{\pi}\frac{\sin^2 NU}{(NU)^2}\,d(NU) + \frac{1}{\pi}\int_0^{\alpha\pi}\frac{\sin^2 NU}{(NU)^2}\,d(NU)\right] \quad . \tag{B-5}$$

The values of the integrals, obtained through a power series approximation of the trigonometric terms, are given in Table B-I.

TABLE B-I - VALUE OF $\left(\frac{\sin x}{x}\right)^2$ INTEGRALS AS A FUNCTION OF α

α	0	0.1	0.25	0.375	0.5	0.625	0.75	0.9	1.0
$\frac{1}{\pi}\int_0^{\alpha\pi}\left(\frac{\sin NU}{NU}\right)^2 dNU$	0	0.099	0.234	0.323	0.386	0.425	0.449	0.460	0.462

The derivative of the signal energy with respect to the corner frequency ω_1 is also needed and becomes:

$$\frac{\partial S}{\partial \omega_1} = \frac{\partial S}{\partial(\alpha\pi)} \cdot \frac{\partial(\alpha\pi)}{\partial \omega_1}$$

$$= -(NA)\left(\frac{1}{\pi}\frac{a}{a+b} C_0\right)\left[\frac{\sin^2 \alpha\pi}{(\alpha\pi)^2}\right] . \qquad \text{(B-6)}$$

2. EVALUATION OF BACKGROUND NOISE ENERGY

The primary source of noise energy, T, is assumed to come from an ensemble of recurrent spectrums that have the same number, N, of pulses and the same duty cycle, a/a + b, as the signal spectrums but whose maximum and minimum periods lie beyond the periods of the signal spectrums. It can be noted that a filter, tuned to the second loop, will attenuate single noise pulses (since their energy is concentrated within the first or central spectral loop) as well as recurrent spectrums that have duty cycles of less than 0.3 and greater than 0.5 and therefore have less energy in the second loop.

The average second loop noise energy $< T(\omega) >$ at any frequency interval from ω to $\omega + d\omega$ is made up of the contributions of the spectrums whose periods, a + b, lie within the following range as determined by the spectral characteristics of a second loop (Equations 41 through 43 of Section III, Subsection Two) or:

$$\frac{\pi}{\omega}\left(1 - \frac{1}{N}\right) \leqq a + b \leqq \frac{\pi}{\omega}\left(1 + \frac{1}{N}\right) . \qquad \text{(B-7)}$$

A maximum entropy estimate of the probability density distribution, p(a + b), of the periods for the above recurrent spectrums when only the extreme values of the distribution are given results in a uniform distribution and a constant-valued probability function.[a] Such an entropy

[a] Goldman, Stanford: Information Theory. New York, Prentice Hall, 1953; p 130.

estimate utilizes all known information and avoids assumptions based upon information not known.[a] The second-loop contribution of each recurrent noise sequence is again based on only the first term of Equation 45 as is the case for the signal energy derivation (Equation B-3). The following expression for the average noise energy, $< T(\omega) > d\omega$, results from the summing of the contributions of the several sequences, which have periods, (a + b), that lie within the range of Equation B-6 above and are distributed in accordance with the above constant probability density function p(a + b). [The duty cycle (a/a + b) is assumed to be constant for the entire ensemble of noise sequences.] The noise energy expression is

$$< T(\omega) > d\omega = \frac{2}{\pi} \frac{a}{a+b} \frac{C_0}{1.85} \times$$

$$\left(\int_{\frac{\pi}{\omega}(1-\frac{1}{N})}^{\frac{\pi}{\omega}(1+\frac{1}{N})} \left\{ \frac{\sin [N(\omega)(a+b) - \pi]}{(N)(\omega)(a+b) - \pi} \right\}^2 (N)(a+b)[p(a+b)][d(a+b)] \right) d\omega \quad . \text{(B-8)}$$

A change in the variable

$$k = (N\omega)(a + b) - N\pi$$

permits evaluation of the above integral and provides the following value for the average energy:

$$< T(\omega) > d\omega = \left(\frac{2}{\pi} \frac{a}{a+b} \frac{C_0}{1.85} \right) \frac{[p(a+b)]\ (9.15)}{\omega^2} d\omega \quad . \qquad \text{(B-9)}$$

Finally, the total average noise energy T passed by a filter with upper and lower cutoff frequencies, ω_2 and ω_1, is:

[a] Jaynes, E. T.: "Information Theory and Statistical Mechanics," Physical Review, vol 106, no. 4, 15 May 1957, pp 620-630; and vol 108, no. 2, 15 October 1957, pp 171-190.

$$T = \int_{\omega_1}^{\omega_2} < T(\omega) > d\omega \ ; \qquad \text{(B-10)}$$

and the derivative of the noise energy with respect to the lower cutoff frequency is

$$\frac{\partial T}{\partial \omega_1} = - < T(\omega_1) > . \qquad \text{(B-11)}$$

3. LOWER CORNER FREQUENCY, ω_1, OF FILTER

The solution for the maximum signal-to-noise ratio, from Equation 18 of Section III, Subsection Three, results in

$$\frac{\left(\frac{\partial S}{\partial \omega_1}\right)}{\left(\frac{\partial T}{\partial \omega_1}\right)} = \frac{S}{T} . \qquad \text{(B-12)}$$

Substitution of the values for the above four terms from Equations B-3 and B-6 for S and $\partial S/\partial \omega_1$, and Equations B-10 and B-11 for T and $\partial T/\partial \omega_1$ yields

$$(N - \alpha_1)\left[1 - \left(\frac{N - \alpha_1}{N}\right)\left(\frac{\pi}{\omega_2 A}\right)\right]\left(\frac{\sin \alpha_1 \pi}{\alpha_1 \pi}\right)^2 =$$

$$0.462 + \frac{1}{\pi}\int_0^{\alpha_1 \pi} \left|\frac{\sin[N(\omega A - \pi]}{(N)(\omega A - \pi)}\right|^2 d[N(\omega A - \pi)] \ . \qquad \text{(B-13)}$$

The proper value of α_1, which satisfies Equation B-12, determines the optimum value of ω_1 in accordance with Equation B-4 between the two quantities.

4. UPPER CORNER FREQUENCY, ω_2, OF FILTER

Similar definitions for S and T and their respective derivatives as a function of the upper corner frequency, ω_2, permit solution of Equation 19 of Section III, Subsection Three, for the optimum value of the upper corner frequency ω_2. The required function of α_2 that results from the above substitutions is

$$\left(N + \alpha_2\right)\left[\left(\frac{\pi}{B\omega_1}\right)(1 + \alpha_2) - 1\right]\left[\frac{\sin^2(\alpha_2\pi)}{(\alpha_2\pi)^2}\right] =$$

$$0.462 + \frac{1}{\pi}\int_0^{\alpha\pi}\left\{\frac{\sin[(N)(\omega B - \pi)]}{(N)(\omega B - \pi)}\right\}^2 d[(N)(\omega B - \pi)] \quad , \qquad \text{(B-14)}$$

where B is the minimum one-half length of the signal period, i.e., the combined one-half length of the target and spacing. Finally, the relationship between the upper corner frequency, ω_2, and the value of α_2 that satisfies Equation B-14 is obtained from the high frequency definition of S as in Equation B-4, or

$$\omega_2 = \left(\frac{\pi}{B}\right)\left(1 + \frac{\alpha}{N}\right) \quad . \qquad \text{(B-15)}$$

APPENDIX C - CALCULATIONS FOR EXPANDING-SPOT OUTPUT SIGNAL AND FLUX INTEGRAL FOR TWO-LEVEL SINGLE-EDGE PATTERN

The following integral represents the portion of the expanding-spot flux, g, that is passed by a given pattern, or

$$g = \int_{\theta_L}^{\theta_h} \int_{R_h}^{R} e^{-4.5(r/R)^2} \, r \, dr \, d\theta \quad , \tag{C-1}$$

for which the problem terminology and geometry are presented in Figure 21, Section III, Subsection Four.

The solution of the inner integral with respect to r is readily obtained so that

$$g = \frac{R^2}{9} \int_{\theta_h}^{\theta_h} \left[e^{-4.5(R_h/R)^2} - e^{-4.5} \right] d\theta \quad . \tag{C-2}$$

This integral is divided into two parts for values of θ clockwise and counter-clockwise from the x axis, or

$$g = \frac{R^2}{9} \left\{ \int_0^{\theta_L} \left[e^{-4.5(R_h/R)^2} - e^{-4.5} \right] d\theta + \int_0^{\theta_h} \left[e^{-4.5(R_h'/R)^2} - e^{-4.5} \right] d\theta' \right\} \quad . \tag{C-3}$$

The various terms of the above integrals can be evaluated from the geometry of Figure 21 in terms of the input variables, the separation distance U, boundary orientation α, and the variable azimuthal angle θ. The evaluating expressions are

$$\left.\begin{aligned} \frac{R_h}{R} &= \frac{V}{\cos(\theta + \alpha)} , \\ \theta_L &= -\alpha + \cos^{-1}(V) , \end{aligned}\right\}$$

and

$$\left.\begin{aligned} \frac{R_h'}{R} &= \frac{V}{\cos(\theta - \alpha)} , \\ \theta_h &= \alpha + \cos^{-1}(V) . \end{aligned}\right\} \qquad \text{(C-4)}$$

In the above equations a normalized pattern boundary separation variable,

$$V = \frac{U \cos \alpha}{R} ,$$

is used.

Finally, the exponentials are placed in terms of a power series:

$$\left.\begin{aligned} e^{-4.5(R_h/R)^2} &= \sum_{n=0}^{n=\infty} \frac{(-4.5)^n V^{2n}}{N! \cos^{2n}(\theta + \alpha)} , \\ e^{-4.5(R_h'/R)^2} &= \sum_{n=0}^{n=\infty} \frac{(-4.5)^n V^{2n}}{N! \cos^{2n}(\theta - \alpha)} . \end{aligned}\right\} \qquad \text{(C-5)}$$

Substitution of Equations C-4 and C-5 and integration of the first, n = 0, term results in

$$g(V) = \left(\frac{R^2}{4.5}\right)(0.99 \cos^{-1} V) + \frac{R^2}{9} \sum_{n=1}^{n=\infty} \frac{(-4.5)^n V^{2n}}{N!} \times$$

$$\left[\int_0^{\cos^{-1}(V) - \alpha} \frac{d\theta}{\cos^{2n}(\theta + \alpha)} + \int_0^{\cos^{-1}(V) + \alpha} \frac{d\theta}{\cos^{2n}(\theta - \alpha)} \right] . \qquad \text{(C-6)}$$

With integration rule 281 of the Table of Integrals,[a]

$$\int \frac{dx}{\cos^{2n} x} = \frac{1}{2n-1} \frac{\sin x}{\cos^{2n-1} x} + \frac{2n-2}{2n-1} \int \frac{dx}{\cos^{2n-2} x} \quad . \qquad \text{(C-7)}$$

Evaluation of

$$2Z_{2n} = \int_0^{\cos^{-1}(V) - \alpha} \frac{d\theta}{\cos^{2n}(\theta + \alpha)} + \int_0^{\cos^{-1}(V) + \alpha} \frac{d\theta}{\cos^{2n}(\theta - \alpha)}$$

through the above integration rule (Equation C-7) results in the following recursive series:

$$Z_{2n} = \left(\frac{1}{2n-1}\right) \left\{ \frac{\sin\left[\cos^{-1}(V)\right]}{V^{2n-1}} \right\} + \left(\frac{2n-2}{2n-1}\right) (Z_{2n-2}) \quad , \qquad \text{(C-8)}$$

where

$$Z_2 = \tan(\cos^{-1} V) \quad .$$

The required value of the intersecting flux, g(V), becomes

$$g(V) = \frac{R^2}{4.5} \left[0.99 \cos^{-1}(V) + \sum_{n=1}^{n=\infty} \frac{(-4.5)^n}{N!} V^{2n} Z_{2n} \right] . \qquad \text{(C-9)}$$

[a] Pierce, B. O.: Table of Integrals. New York, Ginn and Co., 1929.